



Universitat de Girona

MANGANESE AND DICOPPER COMPLEXES FOR BIOINSPIRED OXIDATION REACTIONS: CATALYTIC AND MECHANISTIC STUDIES ON C-H AND C=C OXIDATIONS

Isaac GARCIA BOSCH

Dipòsit legal: GI-250-2012

<http://hdl.handle.net/10803/78940>

ADVERTIMENT: L'accés als continguts d'aquesta tesi doctoral i la seva utilització ha de respectar els drets de la persona autora. Pot ser utilitzada per a consulta o estudi personal, així com en activitats o materials d'investigació i docència en els termes establerts a l'art. 32 del Text Refós de la Llei de Propietat Intel·lectual (RDL 1/1996). Per altres utilitzacions es requereix l'autorització prèvia i expressa de la persona autora. En qualsevol cas, en la utilització dels seus continguts caldrà indicar de forma clara el nom i cognoms de la persona autora i el títol de la tesi doctoral. No s'autoritza la seva reproducció o altres formes d'explotació efectuades amb finalitats de lucre ni la seva comunicació pública des d'un lloc aliè al servei TDX. Tampoc s'autoritza la presentació del seu contingut en una finestra o marc aliè a TDX (framing). Aquesta reserva de drets afecta tant als continguts de la tesi com als seus resums i índexs.

**Manganese and dicopper complexes
for bioinspired oxidation reactions:
catalytic and mechanistic studies on
C-H and C=C oxidations**

PhD dissertation presented by

Isaac Garcia Bosch

Girona, November 2011. Programa de doctorat en Catàlisi Homogènia

Directed by: Dr. Miquel Costas Salgueiro and Dr. Xavi Ribas Salamaña

**In candidacy for the degree of European Doctor of
Philosophy in Chemistry**



Els sotasignants Dr. **Miquel Costas Salgueiro** i Dr. **Xavi Ribas Salamaña**, Professors Titular i Agregat respectivament, del Departament de Química de la Universitat de Girona, CERTIFIQUEM que:

La memoria que porta per títol "*Manganese and dicopper complexes for bioinspired oxidation reactions: catalytic and mechanistic studies on C-H and C=C oxidations*", recull el treball realitzat sota la nostra direcció per l'Isaac Garcia Bosch, Llicenciat en Química per la Universitat de Girona, i que constitueix la seva memòria de Tesi Doctoral per aspirar al grau de Doctor amb Menció Europea en Ciències, especialitzat en Química.

I per que així consti, signem aquest certificat el dia 23 de setembre del 2011.

Dr. Miquel Costas Salgueiro

Dr. Xavi Ribas Salamaña

Table of Contents

Abstract (p.1)

Abbreviations (p.3)

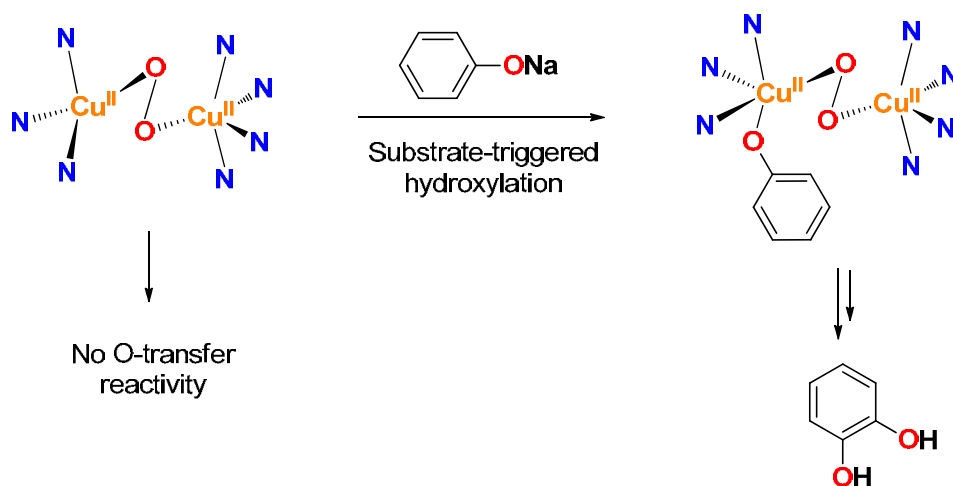
Acknowledgements (p.5)

Chapter I. General Introduction (p.7)

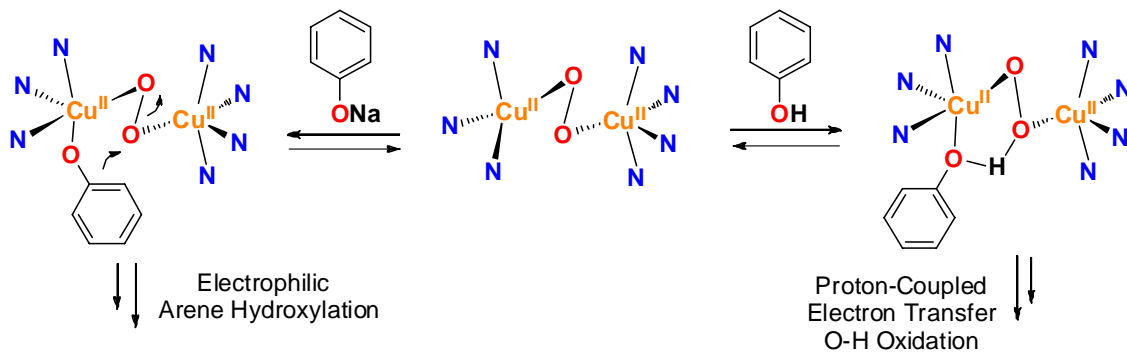
Chapter II. General Objectives (p.57)

Chapter III. O₂ Activation by an Unsymmetric Dinuclear Copper Complex (p.61)

Chapter III.1. O₂ Activation and Selective Phenolate *ortho* Hydroxylation by an Unsymmetric Dicopper μ - η^1 : η^1 -Peroxo Complex (p.63)

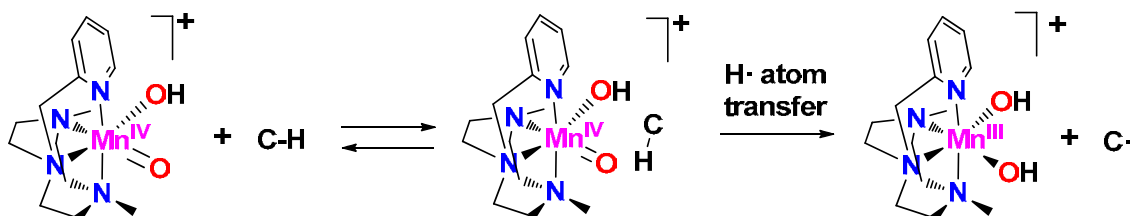


Chapter III.2. Electrophilic Arene Hydroxylation and Phenol O-H Oxidations Performed by an Unsymmetric μ - η^1 : η^1 -O₂-Peroxo-Dicopper(II) Complex. (p.111)



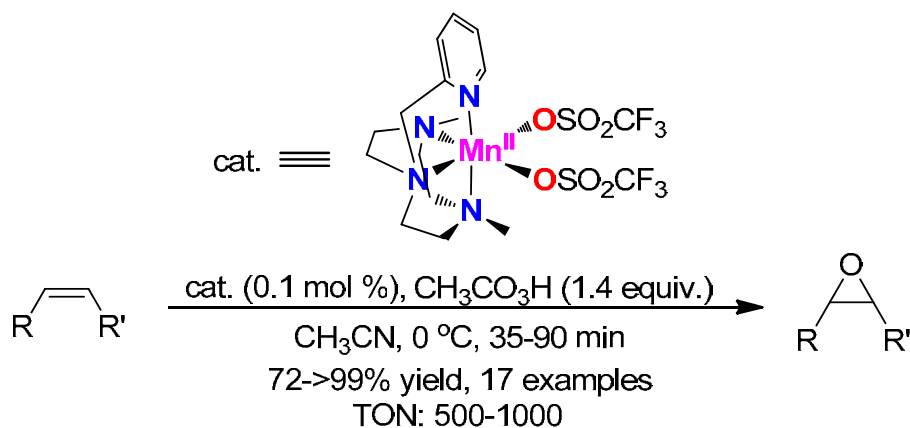
Chapter IV. Non-Porphyrinic Manganese(IV) Complexes in C-H Hydrogen Atom Transfer Reactions (p.131)

Chapter IV.1. Evidence for a Precursor Complex in C-H Hydrogen Atom Transfer Reactions Mediated by a Manganese(IV) Oxo Complex (p.133)

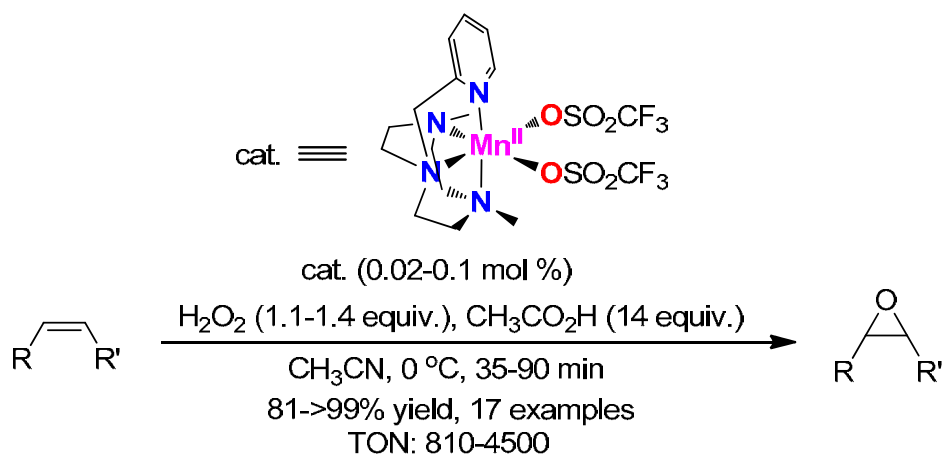


Chapter V. Alkene Epoxidation Catalyzed by Non-Porphyrinic Manganese Complexes (p.159)

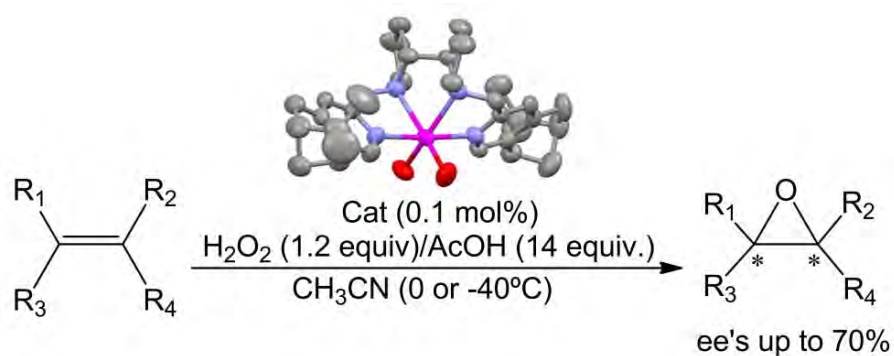
Chapter V.1. Efficient and Selective Peracetic Acid Epoxidation Catalyzed by a Robust Manganese Catalyst (p.161)



Chapter V.2. A Broad Substrate-Scope Method for Fast, Efficient and Selective Hydrogen Peroxide-Epoxidation (p.175)



Chapter V.3. Stereoselective Epoxidation of Alkenes with H₂O₂ Using Bipyrrolidine-Based Family of Manganese Complexes (p.193)



Chapter VI. Results and Discussion (p.207)

Chapter VII. Conclusions (p.245)

Abstract

Enzymes are high-weight molecules which catalyze most of the metabolic processes in living organisms. Very often, these proteins contain one or more 1st row transition metal ions in their active center (Fe, Cu, Co, Mn, Zn, etc.), and are known as metalloenzymes or metalloproteins. Among these, metalloenzymes that activate molecular oxygen and use it as terminal oxidant stand out because of the wide range of catalyzed reactions and their exquisite selectivity. In this PhD dissertation we develop low-weight synthetic bioinspired complexes that can mimic structural and/or functional features of the active center of oxygenases.

Research work is collected in Chapters III-V of this dissertation. In Chapter III, we describe a novel unsymmetric dicopper complex that activates O₂ to form a $\mu\text{-}\eta^1\text{:}\eta^1\text{-peroxo}$ dicopper, which is able to perform the *ortho* hydroxylation of phenolates mimicking the activity of Tyrosinase. Mechanistic studies reveal that the coordination event triggers the activation of the peroxide moiety to electrophilically attack the aromatic ring. In the second part of this chapter, the reaction between the unsymmetric Cu₂:O₂ complex and phenols is studied and showed to undergo a proton-coupled electron transfer to form a phenoxyl radical.

In Chapter IV, two high-valent non-porphyrinic manganese(IV) complexes are described. Their reactivity towards C-H bonds is studied. Both complexes oxidatively cleave C-H bonds, but with different mechanisms. In one hand, a manganese(IV) bis-hydroxide complex performs the oxidation of C-H in a one-step hydrogen atom transfer reaction. On the other hand, the reaction of the conjugated base manganese(IV)-oxo-hydroxo complex proceeds via a two-step mechanism with an association equilibrium between the complex and the substrate and a hydrogen atom transfer in the rate determining step.

In Chapter V we develop a new methodology for the epoxidation of olefins using manganese(II) complexes as catalysts. In the first part, we use a complex with a tetradentate ligand based on the TACN macrocycle, in combination with peracetic acid, to epoxidize alkenes with high efficiency and selectivity. In the second part, peracetic acid is replaced by hydrogen peroxide as oxidant and acetic acid as co-catalyst which allows the epoxidation of a wider range of substrates in shorter reaction times and lower catalyst loadings. In the last part of this chapter, we use the hydrogen peroxide/acetic acid conditions in combination with a novel family of manganese(II) chiral complexes containing tetradentate N-based ligands to epoxidize a broad range of alkenes with excellent yields and moderate to good enantioselectivities.

Resum

Els enzims són molècules d'elevat pes molecular que catalitzen la majoria de processos metabòlics en els éssers vius. Sovint aquestes proteïnes contenen un o diversos ions metàl·lics de la 1^a sèrie de transició en el seu centre actiu (Fe, Cu, Co, Mn, Zn, etc.), essent anomenats metal·loenzims o metal·loproteïnes. D'aquests, els metal·loenzims que activen la molècula d'oxigen i l'utilitzen com a oxidant ressalten per la varietat de reaccions catalitzades i la seva exquisida selectivitat. En aquesta tesi doctoral, desenvolupem complexos de baix pes molecular que puguin mimetitzar estructural i/o funcionalment els centres actius de les oxigenases. Per això, aquests complexos es consideren bioinspirats.

Els Capítols III-V recullen els resultats de la investigació d'aquesta tesi. En el Capítol III, es descriu un nou complex asimètric dinuclear de coure que activa O₂ formant un centre $\mu\text{-}\eta^1\text{:}\eta^1\text{-}$ peroxo dicoure capaç de dur a terme la *orto*-hidroxilació de fenolats mimetitzant la activitat de la tirosinasa. Estudis del mecanisme de reacció revelen que la coordinació del fenolat produeix l'activació del peròxid que ataca electrofílicament l'anell benzílic. En la segona part d'aquest capítol, s'estudia la reacció del complex asimètric amb fenols. L'estudi mostra que la reacció ocorre via transferència d'electró acoblada a protó per formar un radical fenoxil.

En el Capítol IV, dos nous complexos de manganès(IV) no-porfirínics són descrits. La seva reactivitat en front enllaços C-H és analitzada, i les dues espècies de manganès(IV) mostren diferent comportament. El complex manganès(IV) bis-hidròxid reacciona en un únic pas mitjançant una transferència d'hidrogen. En canvi, el complex manganès(IV)-oxo-hidroxo oxida enllaços C-H a través d'un mecanisme de dos etapes, on un primer equilibri d'associació complex/substrat és seguit per una segona etapa on la transferència d'hidrogen ocorre.

En el Capítol V es desenvolupa una nova metodologia per a l'epoxidació d'olefines utilitzant complexos de manganès(II) com a catalitzadors. En una primera part, s'utilitza un complex que conté un lligand triazaciclonoà, combinat amb àcid peracètic per epoxidar alguns de manera molt eficient i selectiva. En una segona part, l'àcid peracètic és substituït per peròxid d'hidrogen com a oxidant i àcid acètic com a co-catalitzador permetent l'epoxidació d'una sèrie més àmplia de substrats en temps de reacció més curts i quantitats de catalitzador més petites. En la última part d'aquest capítol s'utilitzen les condicions de catàlisi amb peròxid d'hidrogen i àcid acètic combinades amb una nova família de complexos de manganès(II) quirals amb lligands N-tetradentats per epoxidar un ampli rang d'olefines amb excel·lents rendiment i bona estereoselectivitat.

Abbreviations

AcOEt: Ethyl acetate
AcOH: Acetic acid
AcOOH: Peracetic acid
ATP: adenosine triphosphate
Asp: Asparagine
BDE: bond dissociation energy
BPBP: *N,N'*-bis(2-pyridylmethyl)-2,2'-bipyrrolidine
BPMCP: *N,N'*-dimethyl-*N,N'*-bis(2-pyridylmethyl-2-(4-*tert*-butylphenyl))cyclohexane-*trans*-1,2-diamine
Bu: butyl
bipy: 2,2'-bipyridine
ca.: around
cat.: catalyst
cal: calorie
CO: catechol oxidase
conv.: conversion
CV: cyclic voltammetry
DFT: density functional theory
ee: enantiomeric excess
eq.: equilibrium
equiv.: equivalents
EPR: electron paramagnetic resonance
ESI-MS: ElectroSpray Ionization Mass Spectroscopy
Et₂O: diethyl ether
FT-IR: Fourier Transform Infrared Spectroscopy
GC: Gas Chromatography
His: histidine
Ile: isoleucine
J: Joule
K: Kelvin degrees
K.I.E.: kinetic isotopic effect
HAT: hydrogen atom transfer
Hc: hemocyanin
HPLC/MS: high performance liquid chromatography/ mass spectrometry
L: ligand
LO: lipoxygenase
M: metal
MCP: *N,N'*-dimethyl-*N,N'*-bis(2-pyridylmethyl)cyclohexane-*trans*-1,2-diamine
MndD: manganese-dependent catechol dioxygenase
MW: molecular weight
n.d.: not determined
NMR: Nuclear Magnetic Resonance
OEC: oxygen evolving center

OTf: trifluoromethanesulfonate anion
PCET: proton-coupled electron transfer
pMMO: particulate methane monooxygenase
PhOH: phenol
PhONa: sodium phenolate
PT-ET: proton transfer-electron transfer
PyTACN: 1-(2-pyridyl)-4,7-dimethyl-1,4,7-triazacyclononane
rRAMAN: resonance raman
r.d.s.: rate determining step
SCE: saturated calomel electrode
SHE: standard hydrogen electrode
SOD: superoxide dismutase
TACN: 1,4,7-triazacyclononane
(TBP)₈(Cz): (4-*tert*-butylphenyl)₈(corrolazine)
tBu: *tert*-butyl
TFA: trifluoroacetic acid
THF: tetrahydrofuran
TON: turnover number
TS: transition state
Tyr: tyrosinase
unc.: uncoupled
UV-Vis: ultraviolet-visible

Acknowledgements

This work would not have been possible without the following collaborations:

- Serveis tècnics de Recerca from Universitat de Girona for technical support.
- Dr. Alfons Polo from Universitat de Girona for the help in the synthesis of bypirrolidine synthons and his useful pieces of advice in asymmetric catalysis.
- Prof. Dr. Kenneth Karlin from Johns Hopkins University (Maryland, USA) for hosting a scientific visit within the context of the $\text{Cu}_2\text{:O}_2$ chemistry.
- Dr. Wesley R. Browne from University of Groningen for hosting a scientific visit within the context of the non-porphyrinic manganese(IV) chemistry.
- Dr. Jonathan R. Frisch and Prof. Dr. Lawrence Que from the University of Minnesota for the rRaman measurements of the $\text{Cu}_2\text{:O}_2$ described complexes.
- Dr. Ilaria Gamba and Prof. Dr. Luigi Casella from the University of Pavia for the HPLC/MS analyses.
- Dr. Miquel Torrent-Sucarrat, Dr. Mireia Güell and Dr. Josep M. Luis from the Institut de Química Computacional (UdG) for the DFT calculations on the unsymmetric $\text{Cu}_2\text{:O}_2$ system.
- Dr. Clyde W. Cady and Dr. Stenbjörn Styring from the Uppsala University for the EPR measurements.
- MICINN of Spain for financial support through projects CTQ2006-05367 and CTQ2009-08464, and MICINN for PhD-FPI Grant BES-2007-15456. Generalitat de Catalunya for project SGR-637. European Research Foundation for ERC-2009-Starting Grant 239910.

Chapter I

General Introduction

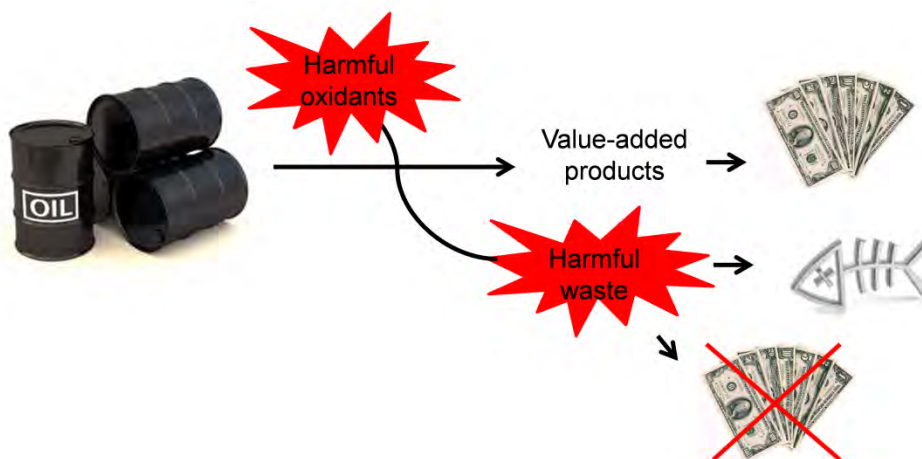
Table of Contents

I.1. Bioinspired approaches to selective oxidation reactions.....	11
I.1.1. Oxidation in modern chemistry: the bioinspired approach.....	11
I.1.2. Role of molecular dioxygen in biological systems.....	12
I.1.3. Bioinorganic chemistry. Model systems.....	13
I.2. O₂ activation by copper systems.....	15
I.2.1. Copper in biological systems.....	15
I.2.2. Copper metalloenzymes in O ₂ activation.....	15
I.2.3. Hemocyanin and tyrosinase.....	17
I.2.4. O ₂ activation by biomimetic copper systems.....	18
<i>I.2.4.1. Cu₂:O₂ intermediate complexes.....</i>	<i>18</i>
<i>I.2.4.2. Tyrosinase-like reactivity by Cu₂:O₂ in model system: ortho-hydroxylation of phenolic substrates</i>	<i>21</i>
<i>I.2.4.3. Oxidation of phenols via phenoxyl radical formation by Cu₂:O₂ model systems..</i>	<i>23</i>
I.2.5. Unsymmetric copper-metal (metal = Cu, Fe, Zn, other species) for O ₂ activation ...	25
<i>1.2.5.1. Formation of unsymmetric complexes by reaction between M-O₂ complexes with M' reduced species.....</i>	<i>28</i>
<i>1.2.5.2. Formation of unsymmetric complexes by reaction between LMM'L' complexes with molecular oxygen.....</i>	<i>30</i>
I.3. Oxidation reactions mediated by manganese systems.....	35
I.3.1. Manganese in biological systems. Fe/Mn dualism.....	35
I.3.2. Manganese metalloproteins in O ₂ metabolism.....	35
I.3.3. High-valent manganese bioinspired systems.....	38
I.3.4. Oxidation catalysis mediated by manganese systems.....	42
I.4. References.....	51

I.1. Bioinspired approaches to selective oxidation reactions

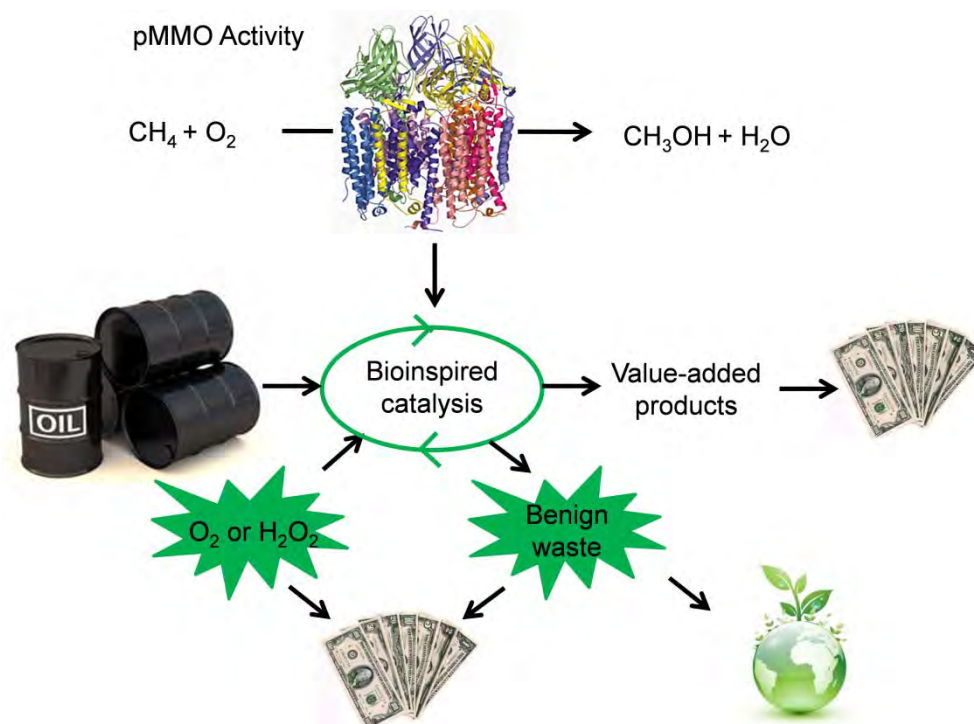
I.1.1. Oxidations in modern chemistry: the bioinspired approach.

The functionalization of hydrocarbons is a non-solved issue in modern chemistry. These transformations have special interest due to the relative abundance of hydrocarbons in nature, making them a reserve to obtain useful chemical derivatives.^{1,2} One of the most pursued reactions in industry is the oxidation of C-H and C=C bonds. The oxidation of these bonds affords very versatile intermediates subsequently used in the synthesis of value-added chemical products. However, most of these oxidative processes are not catalytic and make use of stoichiometric oxidants such as nitric acid, chromic acid and its derivatives, alkyl hydroperoxides, permanganate, osmium tetroxide or organic peracids.^{3,4} These oxidants generate several environmentally harmful by-products in stoichiometric quantities (Scheme 1). Therefore, the innovation and improvement of new synthetic routes to obtain these compounds under “greener” conditions is a challenging task for chemists in the coming years.



Scheme 1. Oxidation of oil-derivatives by stoichiometric harmful oxidants.

Enzymes constitute a paradigmatic case of “green catalysts”. They efficiently catalyze most of the organic transformations occurring in living systems under mild conditions, making use of 1st row metals such as Fe, Mn, Ni, Cu, Zn combined with non-toxic oxidants such as O₂ or H₂O₂ to oxidize a wide range of molecules, usually in a very selective manner. Thus, we can take inspiration from the enzymatic activity to develop new “green” catalytic systems based on 1st row metal ions which ideally will oxidize a wide array of organic molecules using cheap and environmentally benign oxidants (O₂ and/or H₂O₂) (Scheme 2).



Scheme 2. Bioinspired approach for the oxidation of oil-derivatives.

I.1.2. Role of molecular dioxygen in biological systems.

Life based on dioxygen appeared 2.5 billion years ago with the spread of organisms capable to use solar energy to form carbon-carbon bonds. The increase in the atmospheric O_2 concentrations promoted the appearance of eukaryotic organisms (about 1.5 billion years ago), which underwent the oxidation of glucose to CO_2 and water to obtain energy in the ATP form, closing the O_2 cycle.⁵

In parallel, aerobic organisms developed the capacity to convert molecular oxygen into highly oxidizing species which were used in the catalytic synthesis of biomolecules. The general reaction of this process implies the dioxygen O-O bond cleavage and the formation of C-O and O-H bonds. Despite being very favorable in terms of thermodynamics, the reactivity of O_2 with organic matter is kinetically unfavorable. This is due to the electronic structure of O_2 , where the six valence electrons conform a triplet ground state ($S=1$) leading to a spin-forbidden reaction with the majority of organic molecules ($S=0$). This electronic feature determined the expansion of life in an O_2 based atmosphere. In order to surpass the inherent reactivity of molecular oxygen in its triplet ground state, living systems generate more reactive species such as superoxide (O_2^- , $S = 1/2$) or peroxide (O_2^{2-} , $S = 0$) using metalloenzymes. Majorly, enzymes contain one or more metal centers (Fe, Cu, Mn, Ni, Zn) that usually activate dioxygen by

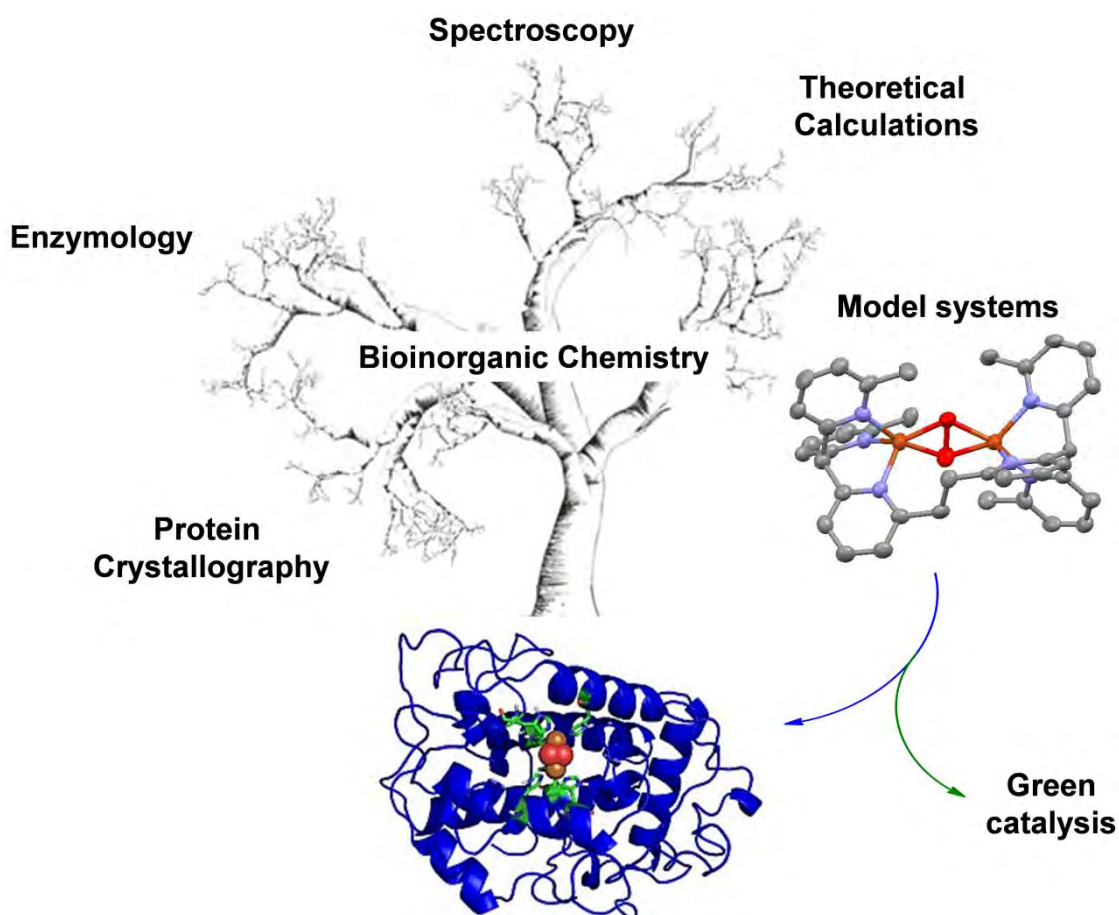
forming metal-oxygen species. The electron source for the O₂ activation is diverse: metal itself suffering an oxidation, co-substrates or electron-supplier cofactors.⁶

All these O₂-activating reactions are extremely regulated giving rise to very specific oxidative processes. Little anomalies of these enzymatic routes are believed to induce very hazardous diseases where free O₂⁻ or O₂²⁻ result in cellular dysfunction or death. Therefore, understanding the reaction mechanisms involved in these oxidative transformations would provide treasured information that would have applications in the development of new pharmaceuticals or in development of catalysts for synthetically relevant oxidative reactions.

I.1.3. Bioinorganic chemistry. Model systems.

It is currently understood that enzymes regulate most of the chemical processes in cells. It has also been established that one third of these enzymes contains at least one metal center in their structure. These enzymes are called metalloenzymes or metalloproteins and they can be understood as bio-catalysts. The exquisite richness of active center geometries and oxidation states of the different metals permit their involvement in many different processes, usually with high specificity. They participate in biochemical processes such as electron transport, oxygen transport, redox processes, hydrolysis or biosynthesis.^{6,7}

Over the last decades numerous advances have been achieved in the elucidation of the structure and function of metalloenzymes. This research field arises from the contribution of different disciplines and methodologies such as protein crystallography, spectroscopy, site-directed mutagenesis, mechanistic enzymology or theoretical calculations (Scheme 3). Another approach sought by the bioinorganic chemistry community is the development of low-weight model systems that reproduce structural, spectroscopic and/or chemical features. This methodology bypasses the direct study of metalloproteins which often entails sophisticated and challenging isolation and purification processes. From the study of these bioinspired systems we can extract structural and spectroscopic information and also mechanistic details that can help in the understanding of the in-vivo processes. Furthermore, these complexes can be used as catalysts for the synthesis of organic molecules ideally providing efficient, selective and sustainable activity.⁸



Scheme 3. Bioinorganic chemistry approaches. Model systems and their applications.

The aim of this thesis is the study of model systems for the activation of O_2 and use of its reduced forms (H_2O_2) for their application in oxidative catalysis. Predominantly, the work is focused on the development of bioinspired unsymmetric dicopper systems and mononuclear manganese complexes.

I.2. O₂ activation by copper systems.

I.2.1. Copper in biological systems.

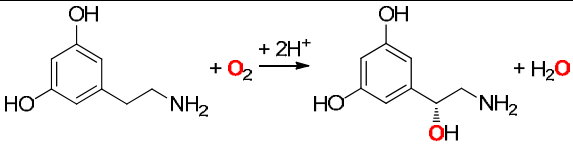
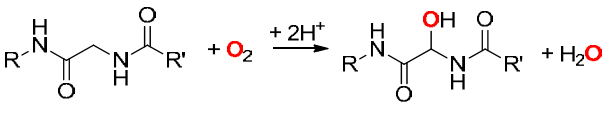
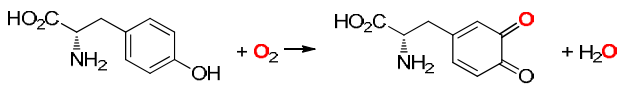
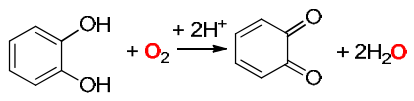
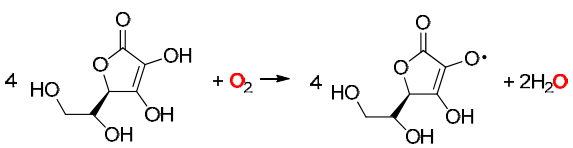
Since early 20th century, it is known that copper is essential for life. Considered as an oligoelement (trace amounts), it is present in most living organisms. Copper is found in metalloenzyme active centers in mononuclear, non-coupled and coupled multinuclear configurations. It is also found sharing the active site with other metals like iron or zinc.⁹

The characteristic oxidation states of copper found in nature are Cu(I) and Cu(II). Despite Cu(III) has been proposed as a very reactive intermediate in some biological reactions,¹⁰ its occurrence has so far not been demonstrated. The rich redox chemistry of the Cu(I)/Cu(II) couple makes copper a very versatile metal for multiple biological functions. Among them, it stands out its function in electron transfer and O₂ activation and transport.¹¹⁻¹⁴

I.2.2. Copper metalloenzymes in O₂ activation.

Some of the most important copper-containing proteins for O₂ activation are summarized in Table 1, where the number of metal ions and the reaction catalyzed is depicted.^{15,16} The variety of copper reactivity is reflected by its multiple functions, acting as oxidase, mono- and di-oxygenase, O₂-carrier or dismutase. Furthermore, there is no direct link between the reactivity and the number of copper atoms present in the active center. For example, the enzymes which contain two coupled copper ions like hemocyanin, tyrosinase and catechol oxidase act as O₂ carrier, monooxygenase + oxidase and oxidase, respectively.

Table 1. Copper proteins involved in dioxygen activation.^{15,16}

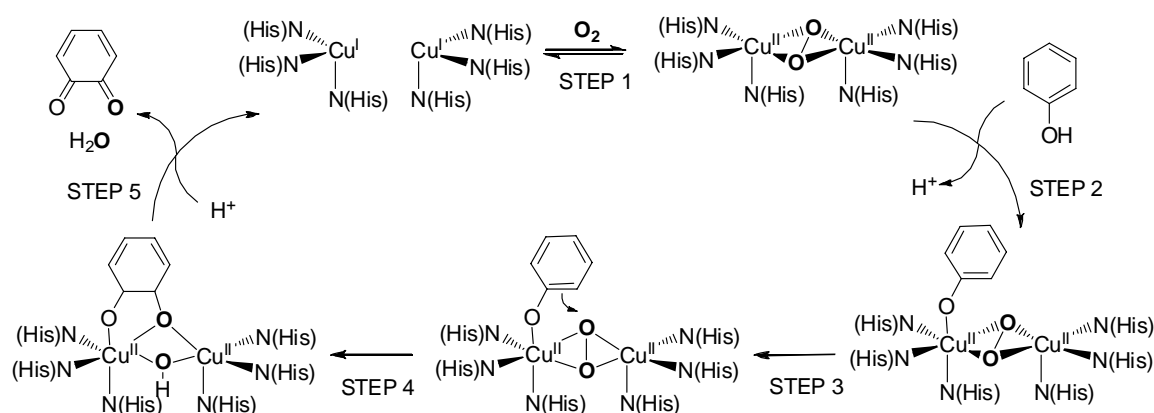
Protein	Metal ions	Reaction catalyzed
Amine oxidase	1 Cu	$RCH_2NH_2 + O_2 + H^+ \longrightarrow RCHO + NH_3 + 1/2H_2O_2$
Galactose oxidase	1 Cu	$RCH_2OH + O_2 \longrightarrow RCHO + H_2O_2$
Glyoxal	1 Cu	$RCHO + O_2 + 2H^+ \longrightarrow RCOOH + 1/2H_2O_2$
Quercetin 2,3-dioxygenase	1 Cu	Oxidative ring opening of quercetin
Dopamine- β -monooxygenase	2 Cu (unc.)	
Peptidylglycine α -hydroxylating monooxygenase	2 Cu (unc.)	
Hemocyanin	2 Cu	$deoxyHc[Cu^I Cu^I] + O_2 \rightleftharpoons oxyHc[Cu^{II}-O_2^{2-}-Cu^{II}]$
Tyrosinase	2 Cu	
Catechol oxidase	2 Cu	
Laccase	3 Cu	$4 HO-C_6H_4-OH + O_2 \longrightarrow 4 HO-C_6H_4-O\cdot + 2H_2O$
Ascorbate oxidase	3 Cu	
Ceruloplasmin	3 Cu	$4 Fe^{2+} + O_2 + 4H^+ \longrightarrow 4 Fe^{3+} + 2H_2O$
Fet3	3 Cu	$4 Fe^{2+} + O_2 + 4H^+ \longrightarrow 4 Fe^{3+} + 2H_2O$
Phenoxazinone synthase	3 Cu	Oxidative coupling of aminophenols
Cytochrome c oxidase	1 Cu + 1 Fe	$O_2 + 4e^- + 4H^+ \longrightarrow 2H_2O$
Superoxide dismutase	1 Cu + 1 Zn	$2O_2^- + 2H^+ \longrightarrow O_2 + H_2O_2$
Particulated methane monooxygenase	Unclear	$CH_4 + O_2 + 2H^+ \longrightarrow CH_3OH + H_2O$
Ammonia monooxygenase	Unclear	$NH_3 + O_2 + 2H^+ \longrightarrow NH_2OH + 2H_2O$

I.2.3. Hemocyanin and tyrosinase.

Hemocyanin is found in some mollusks and arthropods acting as oxygen carrier, likewise hemoglobin in mammals. On the other hand, tyrosinase catalyzes the oxidation of phenols to *ortho*-catechols and *ortho*-quinones. Despite the different reactivity shown, both metalloenzymes share an almost isostructural active center: in their reduced form, two Cu(I) centers are bound to three histidine residues in a trigonal planar distorted coordination geometry. The reversible reaction with O₂ gives rise to the formation of a Cu(II)-O₂²⁻-Cu(II) center, where the O₂ has suffered a 2e⁻ reduction, 1e⁻ coming from each Cu(I). The peroxide binds in a μ-η²:η²-O₂ fashion, where each Cu(II) is coordinated in a distorted square-pyramidal geometry.^{17,18}

Therefore, a question arises from analyzing the structure and reactivity of Tyr and Hc: which is the factor that controls their different reactivity while sharing an identical active center? A plausible response was found in the detailed study of the protein chain: while in tyrosinase a specific channel conferred by the tertiary structure of the polypeptide chain orientates the substrate to the active center, in hemocyanin a protein domain acts as stopper, avoiding the access of organic moieties to the metal centers. This idea was also corroborated by a piece of work from Itoh and coworkers where the treatment of hemocyanin with urea provided tyrosinase-like reactivity to the O₂-carrier: urea disrupted the quaternary structure of the protein, rendering the active site accessible to phenolic substrates. This experiment points out the critical role played by the tridimensional polypeptide structure.¹⁹

Mechanistic studies on the tyrosinase reactivity have led to the proposal of a five-step mechanism (Scheme 4).^{20,21}



Scheme 4. Proposed mechanism for the oxidation of phenols catalyzed by tyrosinase.^{20,21}

In the first step, the reduced form of tyrosinase binds reversibly O_2 by a $2e^-$ process forming a $\mu-\eta^2:\eta^2-O_2^{2-}-Cu^{II}_2$ moiety, a reaction found in hemocyanin as well. Their different behavior is observed in the second step, where the oxygenated form of the tyrosinase is capable of binding a phenolate to one of the copper centers (Cu_A). It is proposed that the phenol molecule is deprotonated by one yet unidentified amino acid residue, previous to the coordination event. However, this question has not been clarified so far. The binding of the phenolate triggers the rotation of the peroxide moiety in the third step, orientating one of the oxygen towards the arene ring. In the fourth step, the *ortho*-phenolic position suffers an electrophilic attack by the Cu(II)-peroxo center, and the O-O bond is cleaved. Closing the cycle, in the fifth step the quinone oxidation product is released in an oxidase type of reaction together with water, regenerating the reduced form of the metalloenzyme.

1.2.4. O_2 activation by biomimetic copper systems.

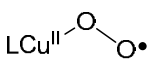
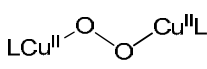
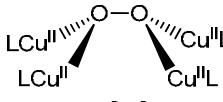
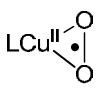
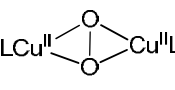
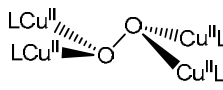
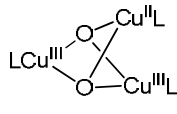
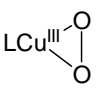
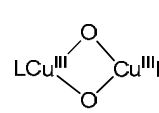
The relevance of copper in biological processes has fueled the development of novel strategies to understand the mechanistic details in which its subtle chemistry occurs. Among them, the synthesis of bioinspired complexes has brought major advances over the last decades because of improvement in synthetic, spectroscopic and kinetic techniques. It has to be noted that the use of anhydrous and anaerobic conditions, the development of Raman spectroscopy and stop-flow UV-vis measurements has allowed the synthesis of Cu(I) complexes and the study of their reactivity with O_2 . The aim of their study is not just obtaining mechanistic details relevant for the understanding of processes in-vivo, but their potential use in synthetic catalysis.

Most of the model systems developed have been conceived as mono- and dinuclear Cu(I) compounds, which react with O_2 forming numerous copper- O_2 species (Table 2). Remarkably, most of the copper- O_2 complexes generated are thermally unstable thus considered as “intermediate species”.¹⁶

1.2.4.1. $Cu_2:O_2$ intermediate complexes.

Focusing on $Cu_2:O_2$ species, they have been designed following two different strategies. On one hand, the reaction of mononuclear LCu^I complexes with O_2 forms LCu^{II} -superoxo species which are usually rapidly trapped by another LCu^I unit to form the $LCu-(O_2)-CuL$ moiety. On the other hand, the design of a dinucleating ligand which binds two copper metals allows the formation of a $Cu_2:O_2$ intermediate directly. All the $Cu_2:O_2$ complexes can be classified in three different families. Furthermore, each type of $Cu_2:O_2$ has its own spectroscopic features and its characteristic reactivity in front of external substrates.^{15,16}

Table 2. Copper-oxygen species formed by the reaction of copper(I) complexes and O₂.^{15,16}

	Cu:O ₂	Cu ₂ :O ₂	Cu ₃ :O ₂	Cu ₄ :O ₂
Cu ^{II}	 superoxo η ¹ end-on (^{ES})	 <i>trans</i> -μ-η ¹ :η ¹ -peroxo end-on (^{TP})		 <i>cis</i> -μ ₄ -η ² :η ² -peroxo
	 superoxo η ² side-on (^{SS})	 μ-η ² :η ² -peroxo side-on (^{SP})		 <i>trans</i> -μ ₄ -η ² :η ² -peroxo
Cu ^{II} /Cu ^{III}			 bis(μ ₃ -oxo) (^T)	
Cu ^{III}	 superoxo η ² side-on (^{MP})	 bis(μ-oxo) (^O)		

***Trans*-μ-η¹-η¹-peroxo-dicopper(II) (**^{TP}**):**

The first crystal structure of a Cu₂:O₂ species was determined 20 years ago by Karlin and co-workers using the tetradentate tmpa ligand (Figure 1).²² Complex [Cu^{II}₂(μ-η¹:η¹-O₂)(tmpa)₂]²⁺ shows a peroxo moiety bridging the two Cu^{II} centers in an *end-on* fashion. Each copper center presents a distorted trigonal-bipyramidal coordination geometry with the copper metals separated by 4.36 Å. Since then, only another crystal structure of a *trans*-μ-η¹-η¹-peroxo-dicopper(II) has been published.²³

Despite the biological relevance of **^{TP}** moiety has not been demonstrated so far, its stability and reactivity make its study very interesting. Usually, Cu(I) complexes with tetradentate ligands promote the formation of the *trans*-peroxo intermediates with distinctive spectroscopic features. About the reactivity of these complexes, it has generally determined that *trans*-μ-η¹-η¹-peroxo-copper(II) have a nucleophilic character. For example, they react with strong acids to promote the release of the peroxide moiety as H₂O₂. Moreover, when triphenylphosphine is used as substrate, the formation of Cu^I-PPh₃ is achieved with no formation of O=PPh₃.^{15,24}

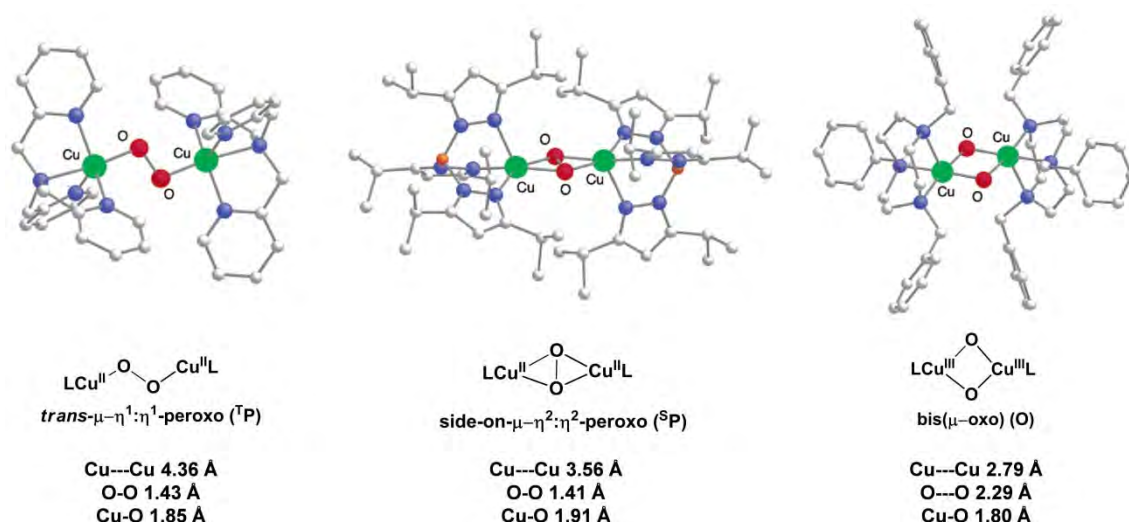


Figure 1. X-Ray structures of ^TP, ^SP and O complexes ($\text{Cu}_2\text{:O}_2$).^{22,25,26}

Side-on-μ-η²:η²-peroxo-dicopper(II) (^SP):

A milestone example of the importance of the model systems in bioinorganic chemistry is the characterization of a side-on peroxo dicopper complex by Kitajima and co-workers.²⁵ The crystal structure of the complex $[\text{Cu}^{\text{II}}_2(\text{HB}(3,5\text{-iPr}_2\text{pz})_3)_2(\mu\text{-}\eta^2\text{:}\eta^2\text{-O}_2)]$ shows a peroxide moiety bridging the two metal centers in a side-on fashion. Curiously, when the spectroscopic features of the complex were analyzed, it was found that they fitted well with the natural system tyrosinase (See Table 3). By analogy, the authors predicted the structure of the *oxy*-tyrosinase as a μ-η²:η²-peroxo copper(II) complex, which was later corroborated by the X-ray structure of the enzyme.¹⁸ The copper(II) centers, which are separated by 3.56 Å, are coordinated in a distorted square-pyramidal geometry.

Side-on peroxo-copper(II) complexes can be defined as electrophilic reagents, performing the oxidation of several substrates such as hydrogen atom abstraction from C-H and O-H bonds and oxo-transfers to PPh_3 or thioanisole.^{15,27} In a few examples, tyrosinase-like reactivity, that is the *ortho*-hydroxylation of phenolic substrates, is also observed (See Section I.2.4.2).

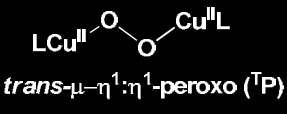
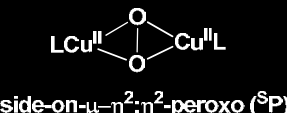
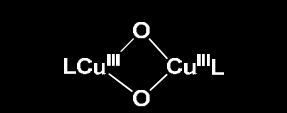
Bis-(μ-oxo)-dicopper(III) (O):

The first example of a bis-(μ-oxo)- Cu^{III}_2 complex was reported fifteen years ago by Tolman and co-workers.²⁶ The crystal structure of the complex $[\text{Cu}^{\text{III}}_2(\mu\text{-O})_2(\text{Bz}_3\text{TACN})_2]^{2+}$ shows short Cu-Cu and Cu-O distances (2.79 Å and 1.80 Å, respectively) where the copper(III) is held in a distorted square-pyramidal geometry. Since then, different cases have been described with similar spectroscopic features: two intense UV-Vis characteristic absorptions at *ca.* 300 nm and 400

nm, and a Cu-O vibration at *ca.* 600 cm⁻¹ determined by rRaman spectroscopy. Another major contribution from Tolman's group was the demonstration of an equilibrium between the side-on peroxo dicopper(II) and bis-(μ-oxo)-dicopper(III) isomers.²⁸ Due to the impact in technological and academic fields, the effect of solvent, counteranion, and ligand shape in the equilibrium have been studied in several key papers.^{29,30}

Although the relevance of bis-(μ-oxo)-Cu^{III}₂ species have not been demonstrated in natural systems so far, its reactivity in oxidative reactions has been studied. Like in side-on peroxo-copper(II) species, the bis-(μ-oxo)-Cu^{III} intermediate shows an electrophilic character reacting with C-H, O-H, N-H and S-H bonds to abstract the hydrogen atom, or reacting with PPh₃ or thioanisole to form O=PPh₃ and Ph-S(O)-Me, respectively.¹⁵

Table 3. Spectroscopic features and reactivity for Cu₂:O₂ complexes.^{15,16}

Cu ₂ :O ₂	Spectroscopic features	Reactivity
 <i>trans-μ-η¹:η¹-peroxo (TP)</i>	UV-Vis: <i>ca.</i> λ = 530 nm (ε = 10000 M ⁻¹ cm ⁻¹), λ = 600 nm (shoulder). rR: <i>ca.</i> ν(O-O) = 830 cm ⁻¹ (Δ[¹⁸ O ₂] ≈ 45 cm ⁻¹), ν(Cu-O) = 555 cm ⁻¹ (Δ[¹⁸ O ₂] ≈ 24 cm ⁻¹)	Nucleophilic character
 <i>side-on-μ-η²:η²-peroxo (SP)</i>	UV-Vis: <i>ca.</i> λ = 340 nm (ε = 21000 M ⁻¹ cm ⁻¹), λ = 540 nm (ε = 840 M ⁻¹ cm ⁻¹). rR: <i>ca.</i> ν(O-O) = 745 cm ⁻¹ (Δ[¹⁸ O ₂] ≈ 40 cm ⁻¹)	Electrophilic character
 <i>bis(μ-oxo) (O)</i>	UV-Vis: <i>ca.</i> λ = 300 nm (ε = 20000 M ⁻¹ cm ⁻¹), λ = 400 nm (ε = 25000 M ⁻¹ cm ⁻¹). rR: <i>ca.</i> ν(Cu-O) = 600 cm ⁻¹ (Δ[¹⁸ O ₂] ≈ 25 cm ⁻¹)	Electrophilic character

1.2.4.2. Tyrosinase-like reactivity by Cu₂:O₂ in model systems: *ortho*-hydroxylation of phenolic substrates.

Although an important number of Cu₂:O₂ species have been synthesized over the last decades, only a few selected examples are able to effect the *ortho*-hydroxylation of phenolic substrates like in tyrosinase. Despite the first example of tyrosinase-like reactivity was reported in 2001, Karlin and co-workers have observed the intramolecular aromatic hydroxylation performed by complex [Cu^{II}₂(μ-η²:η²-O₂)(XYL-H)]²⁺ in the early 1980s (Figure 2).³¹ Casella and co-workers reported the first example of oxidation of sodium phenolates using a *meta*-xylyl linked

dinuclear copper-peroxo complex $[\text{Cu}^{\text{II}}_2(\mu\text{-}\eta^2\text{:}\eta^2\text{-O}_2)(\text{MeL66})]^{2+}$.^{32,33} Hammett analysis using *p*-substituted phenolates revealed that the *ortho*-hydroxylation occurred via electrophilic attack of the peroxide moiety to the aromatic ring likewise in tyrosinase. The oxidation of external phenolic substrates was also reported by Itoh and co-workers, where a side-on peroxo-copper(II) complex $[\text{Cu}^{\text{II}}_2(\text{O}_2)(\text{L}^{\text{Py}2})_2]^{2+}$ reacted with lithium phenolates to form the corresponding catechol products.³⁴

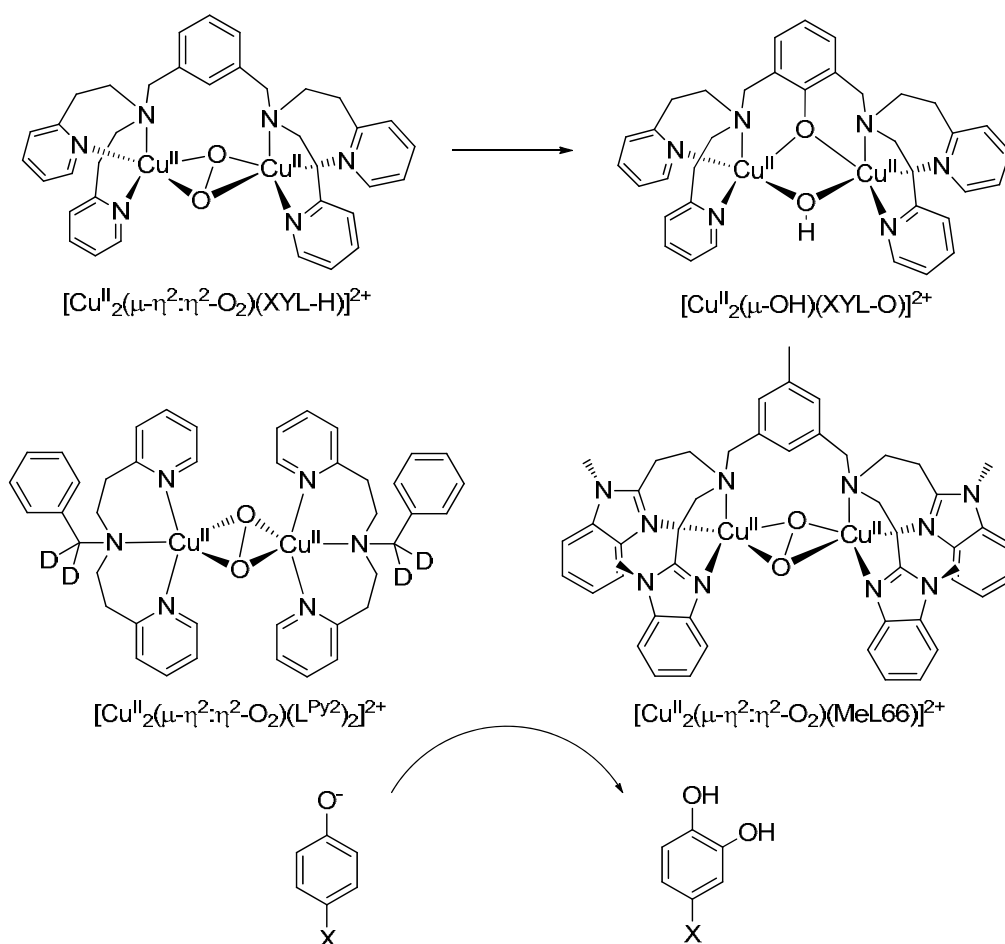


Figure 2. Selected ^5P complexes capable of performing aromatic hydroxylation.^{31,32,34}

A landmark contribution was reported by Mirica *et al.* in 2005.¹⁰ The proposal of a new mechanism for the *ortho*-hydroxylation of phenols by $\text{Cu}_2\text{:O}_2$ systems was described. The use of a bidentate ligand combined with copper(I) led to the formation of a *side-on* peroxo-copper(II) complex $[\text{Cu}^{\text{II}}_2(\mu\text{-}\eta^2\text{:}\eta^2\text{-O}_2)(\text{DBED})_2]^{2+}$ when reacting with O_2 at low temperatures ($-120\text{ }^\circ\text{C}$). Strikingly, the coordination of the phenolate to one of the copper centers triggered the O-O cleavage and a phenolate- $\text{Cu}^{\text{III}}_2(\mu\text{-O})_2$ species was characterized. Therefore, the O-O cleavage occurred prior to the electrophilic attack to the phenolate moiety (Figure 3). This discovery contradicted the stipulated idea that the peroxo-copper(II) species is the true reactive species in the hydroxylation of phenols opening the door to the relevance of the Cu^{III} -

bis(μ -oxo) species in natural systems. Direct evidences of the involvement of bis(μ -oxo)-dicopper(III) species in phenolate hydroxylation were also reported by Company *et al.* in 2008, where a *meta*-xylyl linked Cu(III)-(μ -O)₂ complex $[\text{Cu}^{\text{III}}(\mu\text{-O})_2(m\text{-XYL}^{\text{MeAN}})]^{2+}$ reacted with phenolates forming the corresponding catechols (Figure 3).³⁵

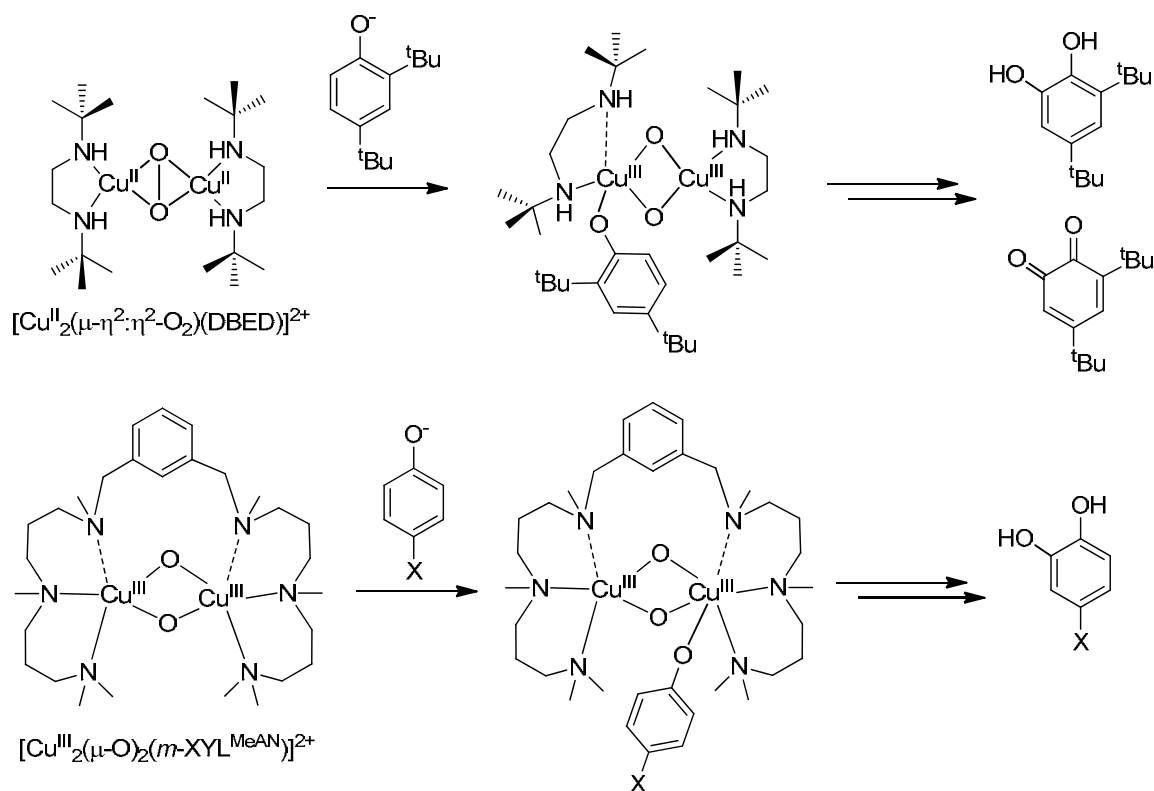


Figure 3. Selected bis(μ -oxo)₂ dicopper(III) species responsible of the *ortho*-hydroxylation of external phenolates.^{10,35}

Very recently, Tuczek and co-workers have reported the first examples of a catalytic tyrosinase model system reactivity. The authors described a mononuclear Cu^I complex using a N₂-bidentate ligand which reacts with O₂ to form a $\mu\text{-}\eta^2\text{-}\eta^2\text{-peroxo}$ -dicopper(II) complex.³⁶ The use of triethylamine is crucial because acts as a base to deprotonate the phenol and also it acts as reductant species to regenerate the Cu(I) complex in the last catalytic step. The system is capable to perform 18 catalytic cycles before its decomposition.

1.2.4.3. Oxidation of phenols via phenoxyl radical formation by Cu₂:O₂ complexes.

As described in the previous lines, the *ortho*-hydroxylation of phenolates performed by selected Cu₂:O₂ model systems, mimicking the tyrosinase activity, requires the introduction of the substrate as a deprotonated species. This supports the mechanism proposed for the

tyrosinase activity, where the phenolic substrate is deprotonated before its coordination to the Cu_A center.

Itoh and co-workers described the reactivity of the side-on peroxo complex $[\text{Cu}^{\text{II}}_2(\mu\text{-}\eta^2\text{:}\eta^2\text{-O}_2)(\text{L}^{\text{Py}2})_2]^{2+}$ and the bis-(μ -oxo) complex $[\text{Cu}^{\text{III}}_2(\mu\text{-O})_2(\text{L}^{\text{Py}1})_2]^{2+}$ towards phenols to proceed via a proton-coupled electron transfer (PCET).³⁷ This $1\text{e}^-/1\text{H}^+$ process generates a phenoxyl radical moiety, which can be coupled with another radical to form a C-C biphenol coupling product (Figure 4).

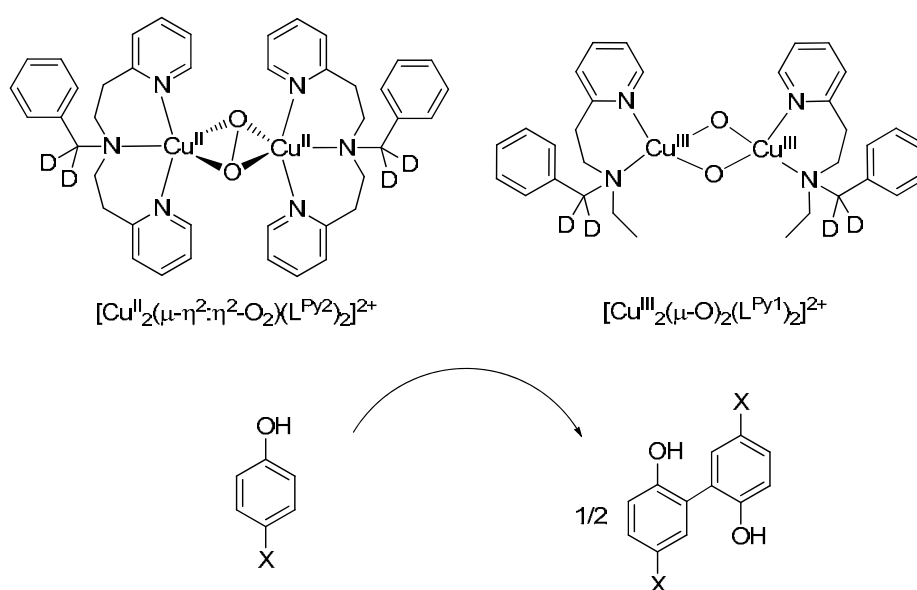


Figure 4. Oxidation of phenols performed by selected $\text{Cu}_2\text{:O}_2$ complexes.³⁷

The reactivity of $\text{Cu}_2\text{:O}_2$ complexes against phenols and phenolates was also reported by Stack and coworkers.³⁸ The use of a series of guanidine/amine ligands to generate different bis-(μ -oxo) copper(III) cores allowed the authors to establish some electronic and steric factors that could explain the different reactivity observed (Figure 5). Firstly, the use of a sterically hindered ligand ^1L made complex $[\text{Cu}^{\text{III}}(\mu\text{-O})_2(^1\text{L})_2]^{2+}$ unreactive towards both 2,4-di-*tert*-butylphenol and sodium 2,4-di-*tert*-butylphenolate. When one of the guanidine substituents was replaced by an aliphatic amine as in ligand ^2L , the resulting complex $[\text{Cu}^{\text{III}}(\mu\text{-O})_2(^2\text{L})_2]^{2+}$ reacted with 2,4-di-*tert*-butylphenol and sodium 2,4-di-*tert*-butylphenolate to generate the C-C coupling and catechol products, respectively. Finally, the substitution of a second guanidine moiety with another aliphatic amine (^3L) to produce the complex $[\text{Cu}^{\text{III}}(\mu\text{-O})_2(^3\text{L})_2]^{2+}$ induced the formation of C-C coupling product exclusively when reacted with both 2,4-di-*tert*-butylphenol and sodium 2,4-di-*tert*-butylphenolate. This reactivity towards sodium 2,4-di-*tert*-butylphenolate to generate the C-C coupling product was explained by the higher redox

potential of the $[\text{Cu}^{\text{III}}(\text{O})_2(^3\text{L})_2]^{2+}$, which favored an electron-transfer path generating the phenoxy radical over the *ortho*-hydroxylation of the phenolate.

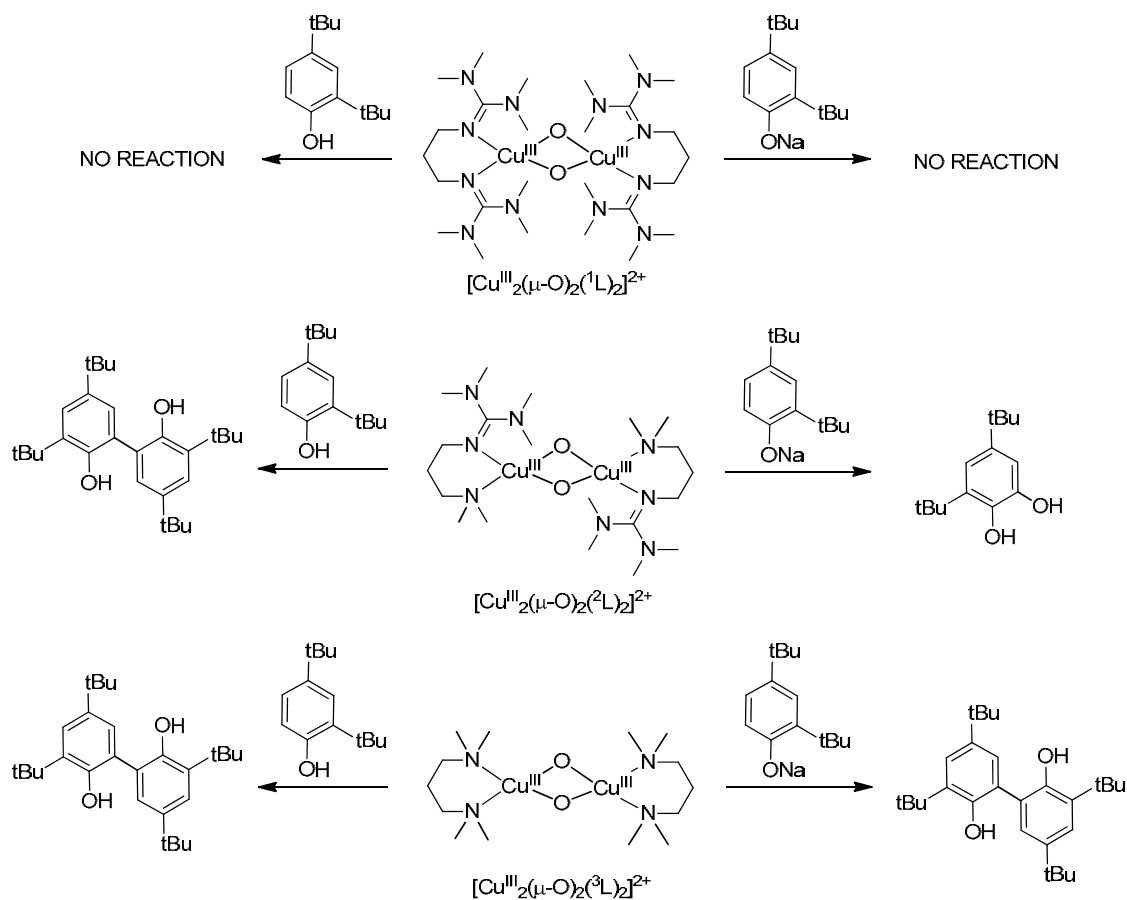


Figure 5. Reactivity toward phenolic substrates shown by a family of bis(μ -oxo) dicopper(III) complexes.³⁸

1.2.5. Unsymmetric copper-metal (metal = Cu, Fe, Zn, other species) for O_2 activation.

A number of enzymes use a dimetallic site in order to bind and activate O_2 .^{39,40} This activation involves reduction of the O_2 molecule to reactive species such as superoxides, peroxides, or metal-oxo species. In most of the cases where two metal centers participate synergistically in the binding and activation of O_2 , the two metal sites are not equivalent. This lack of equivalence can have a different nature: (a) the metals may be different, such as for example cytochrome *c* oxidases, where a heme-copper binuclear site performs the 4e- reduction of O_2 , as the last step in the cellular respiration,^{41,42} and Cu-Zn superoxide dismutases,⁴³ where O_2 disproportionation is mediated by an heterometallic CuZn center (Figure 6); (b) asymmetry may also arise from a distinct coordination environment. This is the case of dopamine- β -hydroxylase (D β H),^{44,45} peptidylglycine- α -hydroxylating monooxygenase (PHM)^{46,47} and also tyrosinase (Tyr).^{18,21} In the first two cases, the first coordination environment of the two

copper ions is different (Figure 6). In the case of Tyr, differences in the second coordination sphere render the two metal ions unequivalent.¹⁸

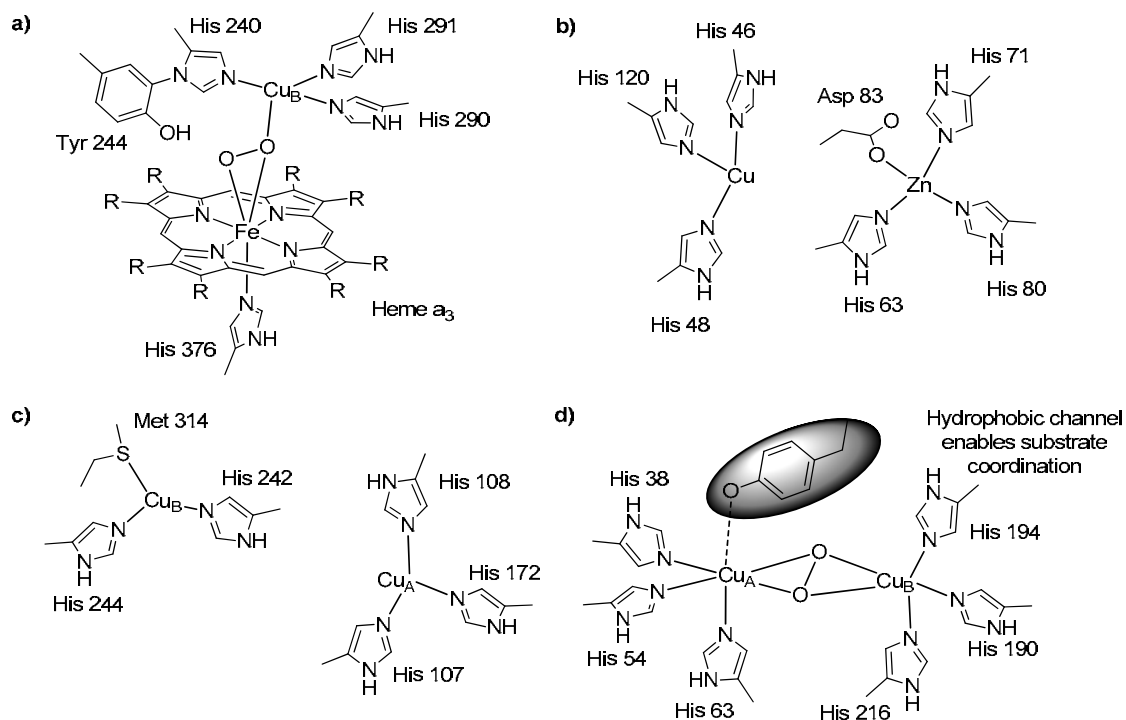


Figure 6. Active centers of: a) cytochrome *c* oxidase (CcO); b) CuZn superoxide dismutase (CuZn-SOD); c) peptidylglycine- α -hydroxylating monooxygenase (PHM); and d) Tyrosinase (Tyr).

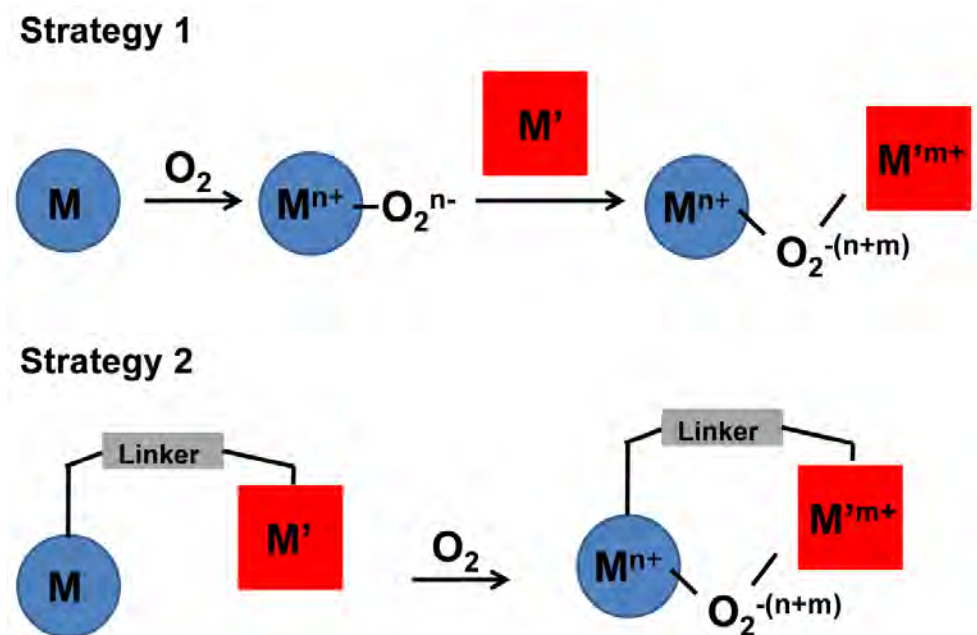
Because of the biological relevance of O_2 -binding and activation reactions at transition metal ions, and also the potential technological interest that these reactions can have in the field of selective oxidation catalysis, the O_2 -chemistry of transition metal coordination complexes has been extensively investigated, with particular emphasis placed in biologically relevant first row transition metal ions.^{14-16,48-53}

The immense majority of the biomimetic synthetic dinuclear complexes developed so far contain metal ions with the same coordination geometry, and symmetric binding modes are adopted by the O_2 molecule when interacting with the complex.^{14-16,49-54} Exploration of O_2 -activation at unsymmetric and heterometallic sites remains much less explored. Study of O_2 -binding and activation at unsymmetric dimetal cores is interesting because it can lead to fundamental understanding of enzymatic O_2 -binding activation reactions, but in addition these studies offer to create novel species exhibiting alternative reactivity patterns to that of symmetric species. Such novel oxidation chemistry may also lead to the development of catalytic processes exhibiting hitherto selectivities.

Preparation of unsymmetric $[(LM)(LM')O_2]$ species (L stands for ligand and M for transition metal) is inherently more complicated than symmetric analogues. The most common methodology employed for preparing symmetric M_2O_2 species involves reaction of O_2 with mononuclear LM synthons, resulting in the spontaneous self-assembly of the dimetallic- O_2 core, but this methodology is unsuitable for unsymmetric systems because of the possible formation of mixtures of products. In order to address this problem, two main strategies have been pursued (Scheme 5):

Strategy I. Reaction between a preformed $LM-O_2$ synthon with a reduced metal complex M' , to form a $LM-O_2-M'L'$ species. In this case, the challenge resides in finding complexes that preclude the formation of $LM-O_2-ML$ species. This is generally accomplished by using sterically very demanding ligands.

Strategy II. The design of ligands which hold two different binding sites, with distinct coordination environments for the two metals (scheme 5). In this case, the preparation of the unsymmetric ligand usually constitutes a more significant synthetic challenge. Nevertheless, in the case of heterometallic complexes, the most challenging aspect is to accomplish a site selective metal binding, and to avoid formation of mixtures.



Scheme 5. Two main strategies used in the development of unsymmetric complexes for the activation of O_2 .

1.2.5.1. Formation of unsymmetric complexes by reaction between $M-O_2$ complexes with M' reduced species.

Inspired by pioneer works of van Koten⁵⁵ and Carpenter⁵⁶, Tolman and co-workers used an isolable $LCuO_2$ complex, where L stands for a sterically bulky β -diketiminate ligand, to synthesize unsymmetric $LCu^{III}-(\mu-O)_2-Cu^{III}L'$ complexes by reaction with a second mononuclear LCu^I synthon (Figure 7).⁵⁷ A key aspect to develop this strategy was the use of a bulky β -diketiminate ligand, which allowed the isolation of the $[H(Me_2L^{iPr2})Cu^{III}(\eta^2-O_2)]$ and $[H(Me_2L^{Me2})Cu^{III}(\eta^2-O_2)]$ complexes. The bulky nature of the β -diketiminate ligand prevented the formation of symmetric $LCu^{III}-(\mu-O)_2-Cu^{III}L$ species. In addition, its anionic character likely contributed to stabilize the copper(III) oxidation state. Once the monomeric moiety was isolated, it was used as building block to generate unsymmetric $[H(Me_2L^{iPr2})Cu^{III}-(\mu-O)_2-Cu^{III}L']$ ($L' = H(Me_2L^{iPr2})$, Me_3TACN , $TMPDA$) species by reaction with a second $L'Cu^I$ complex (Figure 7, top). Moreover, the $[H(Me_2L^{iPr2})Cu^{III}(\eta^2-O_2)]$ moiety was combined with other metal complexes to generate heterometallic complexes containing $[Cu^{III}-(\mu-O)_2-Ni^{III}]$ ⁵⁸ and $[Cu^{III}-(\mu-O)_2-Ge^{IV}]$ cores.⁵⁹ Likewise, $[(PPh_3)_2M^{II}(\eta^2-O_2)]$ ($M = Pt, Pd$) could be isolated and subsequently were used to obtain $[(PPh_3)_2M^{II}-(\mu-O)_2-Cu^{III}H(Me_2L^{Me2})]$ ($M = Pt; M = Pd$) complexes (Figure 7, bottom).⁶⁰ Furthermore, the use of $[(PPh_3)_2M^{II}(\eta^2-O_2)]$ allowed the synthesis of $[(PPh_3)_2M^{II}-(\mu-O)_2-Cu^{III}(iPr_3TACN)]$ ($M = Pt; M = Pd$), for which the $LCu^{III}(\eta^2-O_2)$ moiety was not isolable because it underwent fast dimerization.

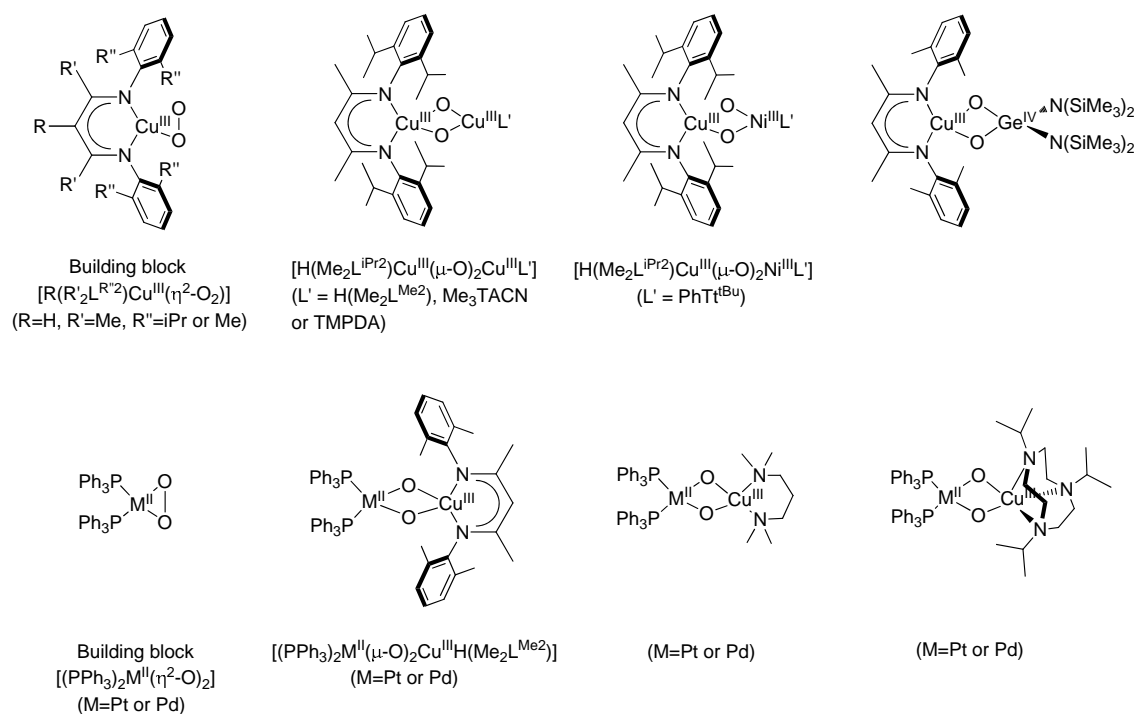


Figure 7. Several examples of heterometallic $Cu-(\mu-O)_2-M$ complexes.

Access to this set of complexes allowed comparison between the reactivity of symmetric and unsymmetric complexes in front of exogenous substrates (Figure 8). $[(PPh_3)_2Pt^{II}-(\mu-O)_2-Cu^{III}H(Me_2L^{Me_2})]$ acts as a nucleophile in front of substrates such as $[NH_4](PF_6)$ (weak acid) or CO_2 , while symmetric complex $[H(Me_2L^{Me_2})_2Cu^{III}]_2-(\mu-O)_2$ showed no reaction with these substrates. The symmetric $Cu^{III}_2-(\mu-O)_2$ complex does not oxidize substrates such as 9,10-dihydroanthracene (9,10-DHA), thioanisole or 1-decene, which in the first two cases usually undergo electrophilic oxidations by $Cu^{III}_2-(\mu-O)_2$ cores. The authors suggested that the low reactivity performed by the symmetric $Cu^{III}_2-(\mu-O)_2$ core could be due to the inhibition of substrate approach by the bulky β -diketiminato, or because the anionic character of one of the ligands quench the electrophilicity of the Cu_2O_2 core. When the complexes were tested in the oxidation of 2,4-di-*tert*-butylphenol another interesting behavior was found: while the homometallic complex was not able to oxidize the phenol, the heterometallic complex reacted abstracting the hydrogen atom to form the C-C coupling product. It was proposed that the higher basicity of the unsymmetric $Pt^{II}-(\mu-O)_2-Cu^{III}$ allowed the deprotonation of the substrate which preceded the electron transfer from the bound phenolate to the copper center.

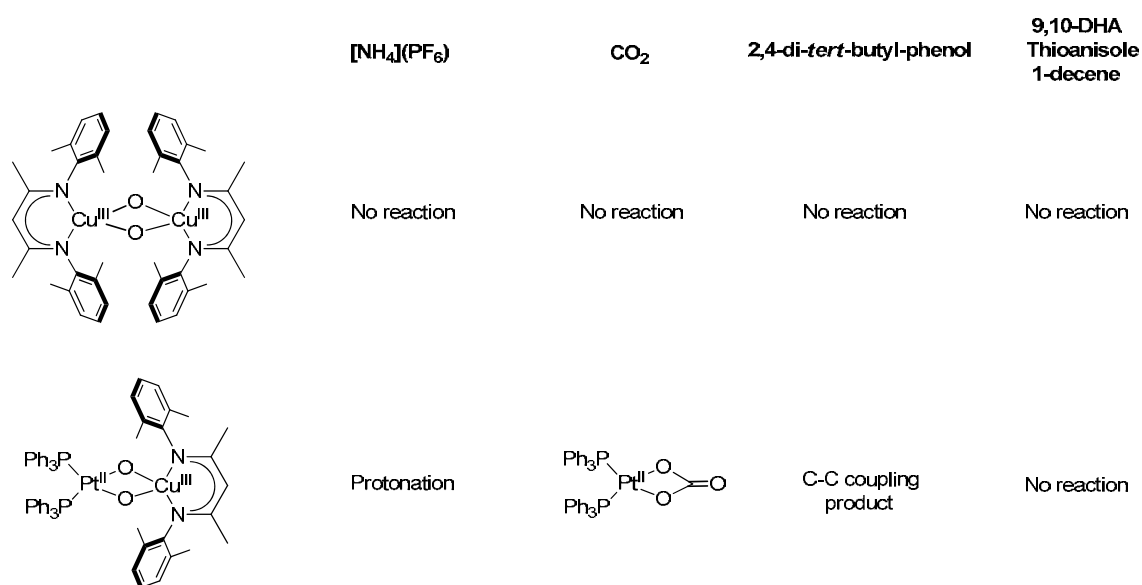


Figure 8. Reactivity of heterometallic $[(PPh_3)_2Pt^{II}-(\mu-O)_2-Cu^{II}H(Me_2L^{Me_2})]$ complex in comparison with its homometallic symmetric analog $[H(Me_2L^{Me_2})_2Cu^{III}]_2-(\mu-O)_2$.

Very recently, Tolman's group prepared a new mononuclear anionic copper(II) that led to the formation of an end-on superoxide complex by reaction with KO_2 . This superoxide complex is supported by a sterically hindered pyridinedicarboxamide ligand, where the metal adopts a tetragonal coordination geometry. Superoxide complex can be then used as building block for the synthesis of other unsymmetric complexes,⁶¹ as illustrated by reaction with

$[\text{Cu}^{\text{I}}(\text{tmpa})(\text{CH}_3\text{CN})](\text{CF}_3\text{SO}_3)$ to yield a dicopper complex exhibiting an unsymmetric $\text{Cu}_2^{\text{II}}(\mu-\eta^1:\eta^1\text{-O}_2)$ core (Figure 9).

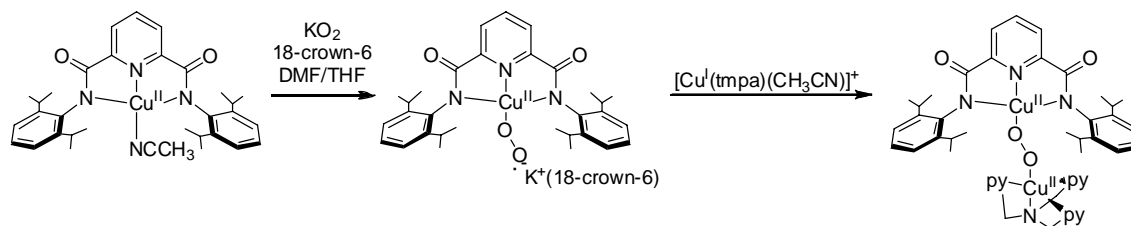


Figure 9. Schematic diagram for the synthesis of an unsymmetric Cu_2O_2 complex with a $\text{Cu}_2^{\text{II}}(\mu-\eta^1:\eta^1\text{-O}_2)$ core assembled from reaction of a $\text{LCu}^{\text{II}}\text{O}_2$ complex and a second $\text{L}'\text{Cu}^{\text{I}}$.

1.2.5.2. Formation of unsymmetric complexes by reaction between $\text{LMM}'\text{L}'$ complexes with molecular oxygen.

A different strategy to build unsymmetric complexes is based on the design of ligands which possess two different coordination environments (Scheme 5). A prototypical example is a set of model complexes that have been prepared and studied as models for the cytochrome *c* oxidase enzyme.^{14,62} In this case, one of the two sites is a porphyrinic complex, while the second one contains a non-porphyrinic, N-based ligand covalently linked by a spacer. Unsymmetric complexes are relatively common in the literature, but only few reports describe the formation of well-defined M_2O_2 species from O_2 binding-activation reactions.

Pioneer work developed by Karlin and co-workers, comprised four different unsymmetric xylyl-type of ligands, each of which was used to synthesize the corresponding dicopper(II) complex.⁶³⁻⁶⁵ A rich chemistry was observed when the complexes were exposed to molecular oxygen (Figure 10). In first place, when $[\text{Cu}_2^{\text{I}}(\text{UN})]^{2+}$ reacted with O_2 at low temperatures, a side-on Cu_2 -peroxo complex $[\text{Cu}_2^{\text{II}}(\mu-\eta^2:\eta^2\text{-O}_2)(\text{UN})]^{2+}$ was obtained, which subsequently underwent aryl oxidation of the UN ligand to generate a hydroxyl bridged dicopper complex. Related behavior was also observed for the analogous $[\text{Cu}_2^{\text{I}}(\text{UN}_2)]^{2+}$ complex. In second place, $[\text{Cu}_2^{\text{I}}(\text{UN-OH})]^{2+}$ (Figure 10) reacted with O_2 at $-80\text{ }^\circ\text{C}$ to form $[\text{Cu}_2^{\text{II}}(\mu\text{-OOH})(\text{UN-O})]^{2+}$ (a hydroperoxo-dicopper(II) complex). Thirdly, the oxygenation of the related $[\text{Cu}_2^{\text{I}}(\text{UN-O}^-)]^+$ complex gave the corresponding $[\text{Cu}_2^{\text{II}}(\text{O}_2^{2-})(\text{UN-O}^-)]^+$. Interestingly, the latter complex undergoes a $1e^-$ oxidation reaction to produce an unsymmetric superoxo-dicopper(II) complex. This complex was also obtained by initial chemical oxidation of the $[\text{Cu}_2^{\text{I}}(\text{UN-O}^-)]^+$ precursor with $[\text{Fe}(\text{Cp})_2]^+$, to form a mixed-valence copper(I)-copper(II) complex, followed by exposition

to molecular O_2 . Finally, the hydroperoxo-dicopper(II) complex was also prepared by protonation of $[Cu^II_2(O_2^{2-})(UN-O^-)]^+$.

The oxidation ability of complexes $[Cu^II_2(O_2^{2-})(UN-O^-)]^+$ and $[Cu^II_2(\mu-OOH)(UN-O)]^{2+}$ was studied using PPh_3 as substrate. The peroxy-dicopper(II) complex does not effect its oxidation to phosphine oxide, but instead, PPh_3 coordinates the metal extruding O_2 and forming the corresponding $[Cu^I_2(UN-O^-)(PPh_3)_2]^+$ complex. This reactivity is consistent with a species exhibiting nucleophilic character. Also consistent with this character, the reaction of $[Cu^II_2(O_2)(UN-O^-)]^+$ with an excess of protons quantitatively produces H_2O_2 . On the other hand, the hydroperoxo-dicopper(II) complex readily oxidizes PPh_3 to quantitatively form $O=PPh_3$ and $[Cu^II_2(OH)(UN-O)]^{2+}$. This reaction can be understood as an electrophilic oxygen atom transfer to the substrate, and evidences fundamental differences of reactivity between copper-peroxide and copper-hydroperoxide complexes.

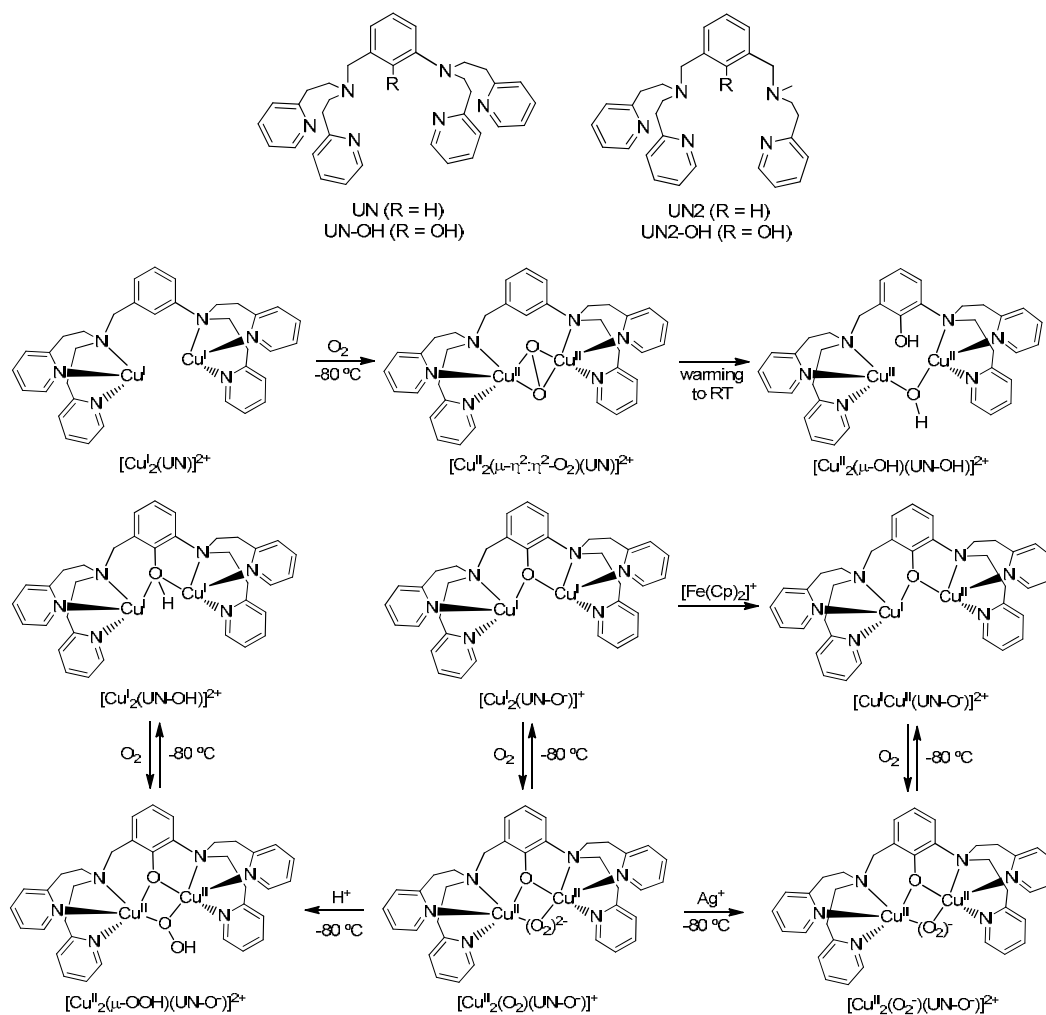


Figure 10. Unsymmetric xylyl-bridged dicopper complexes described by Karlin and co-workers.

Superoxide dismutases catalyze a very fast two step disproportionation of the superoxide (O_2^-) anion to molecular oxygen and hydrogen peroxide.⁴³ The heterometallic active site of the copper and zinc dependent form of superoxide dismutase (CuZn-SOD) also constitutes an attractive target for synthetic bioinorganic chemistry. Fukuzumi and co-workers provided an interesting model by designing an heterometallic Cu^{II}-Zn^{II} complex with a bridging imidazolate ring (Figure 11).^{66,67} The analogous homometallic Cu^{II}₂ complex was also synthesized. The SOD activity of both complexes was tested, and the heterometallic complex showed a higher activity than the dicopper complex. Indeed, the activity of the latter complex constitutes the highest reported to date for a dinuclear complex. Furthermore, when complexes react with H_2O_2/NEt_3 at low temperatures, a metastable Cu^{II}(OOH)Zn^{II} species could be spectroscopically characterized. Such species is considered an intermediate during the CuZn-SOD activity. Corresponding Cu^{II}₂(OOH)₂ species could be also characterized when the homometallic species was reacted in a similar manner.

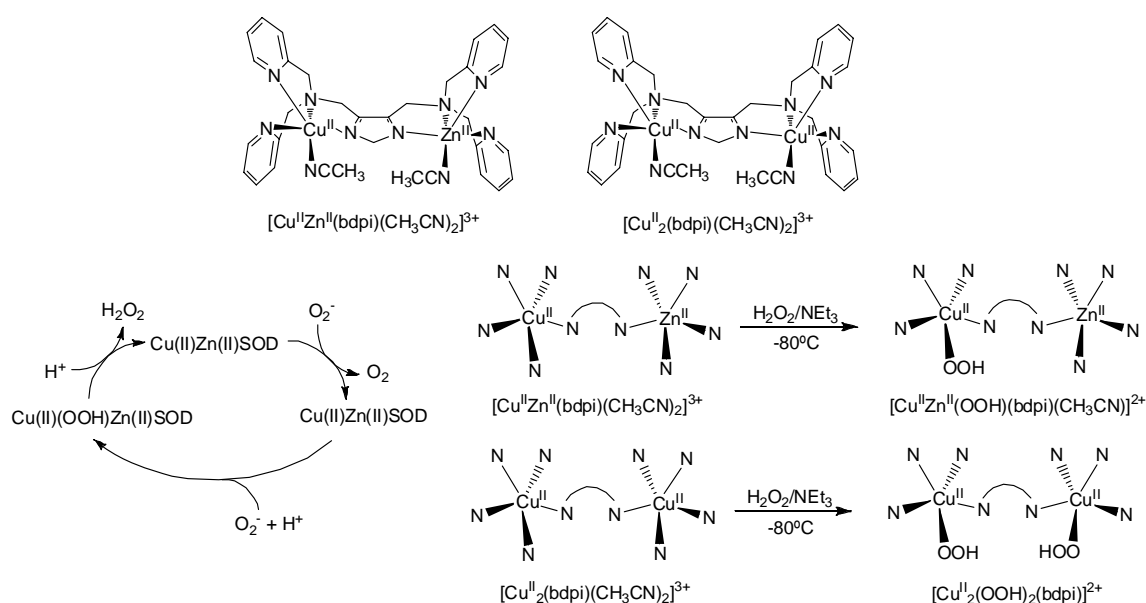


Figure 11. Schematic diagram of heterometallic Cu-Zn and homometallic Cu complexes (top). SOD activity in CuZn-SOD (bottom left), and reaction of heterometallic Cu-Zn and homometallic Cu complexes with H_2O_2 at low temperature (bottom right).

Itoh and co-workers synthesized a pentapyridine molecule that acted as an unsymmetric dinucleating ligand for copper ions (Figure 12).⁶⁸ The reaction of the corresponding dicopper(I) complex with O_2 at low temperatures in acetone resulted in the formation of a Cu^I₂- O_2 species, which the authors described as the first example of a Cu^I(μ - η^1 : η^2 - O_2)Cu^I complex. The reactivity of this novel Cu₂O₂ intermediate was studied in some prototypical reactions of

peroxodicopper cores. When it was treated with $\text{CF}_3\text{SO}_3\text{H}$, the complex underwent protonation, releasing H_2O_2 , which suggests that the Cu_2O_2 unit can exhibit a nucleophilic character against protons. However, when the complex was reacted with substrates such PPh_3 , PhSMe or 2,4-di-*tert*butylphenol, products resulting from electrophilic oxidation reactions were observed. This strange behavior was explained by the chameleonic character of the unsymmetric $\text{Cu}^{\text{II}}(\mu\text{-}\eta^1\text{:}\eta^2\text{-O}_2)\text{Cu}^{\text{II}}$ intermediate, which could exhibit nucleophilic reactivity against good electrophiles, likewise the majority of $\text{Cu}^{\text{II}}(\mu\text{-}\eta^1\text{:}\eta^2\text{-O}_2)\text{Cu}^{\text{II}}$ complexes, but it could also engage in electrophilic oxygen atom transfer reactions against oxophilic substrates, as commonly observed in $\text{Cu}^{\text{II}}(\mu\text{-}\eta^2\text{:}\eta^2\text{-O}_2)\text{Cu}^{\text{II}}$ centers.¹⁵

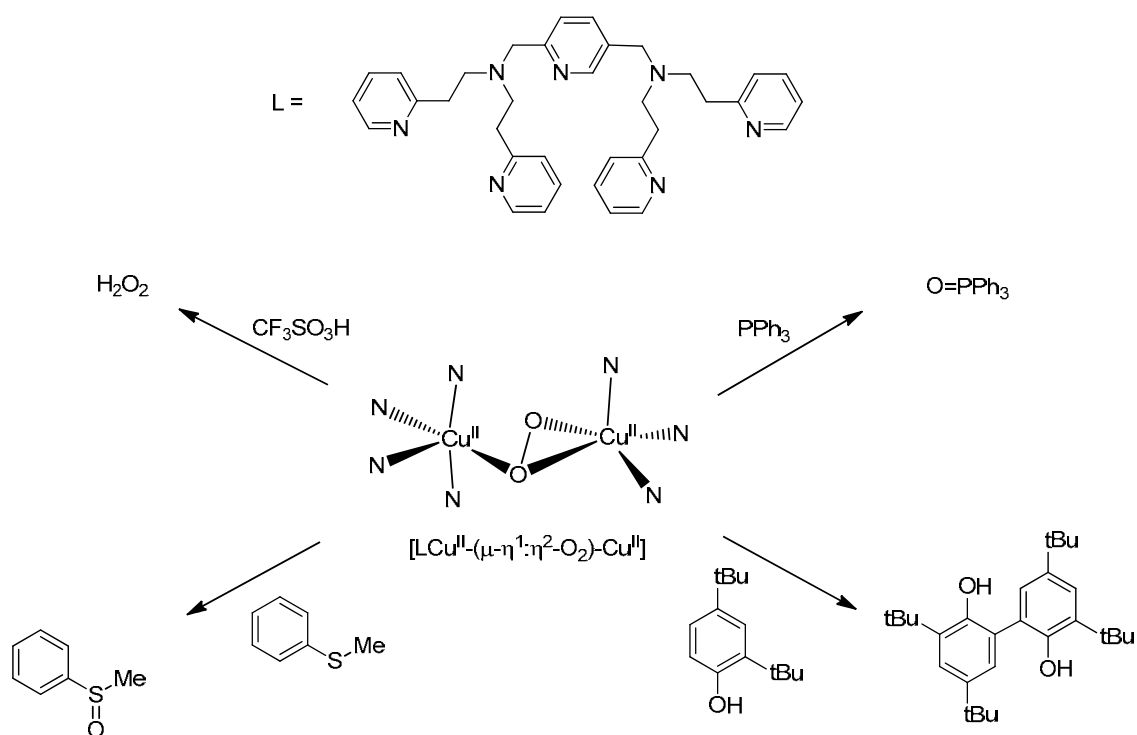


Figure 12. Pentapyridine ligand described by Itoh (top), and reactivity of the corresponding $\text{Cu}^{\text{II}}(\mu\text{-}\eta^1\text{:}\eta^2\text{-O}_2)\text{Cu}^{\text{II}}$ complex.

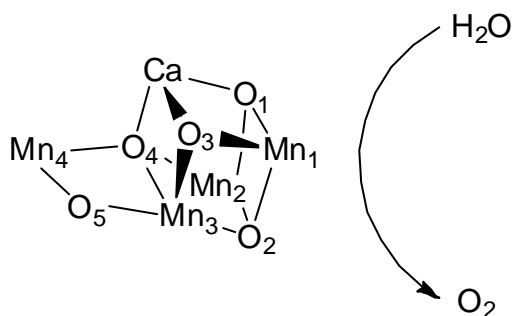
I.3. Oxidation reactions mediated by manganese systems.

I.3.1. Manganese in biological systems. Fe/Mn dualism.

Manganese plays two major roles in biological systems. On one hand, manganese(II) ions act as Lewis acids like Ca^{II} , Mg^{II} or Zn^{II} . On the other hand, the rich redox chemistry of manganese, which in living systems can be found in Mn^{II} , Mn^{III} , and Mn^{IV} forms, is used by a large number of enzymes including oxidoreductases, transferases, hydrolases, oxygenases, lyases, isomerases, ligases, lectins, integrins and the oxygen evolving center of photosystem II.⁶⁹⁻⁷²

Although iron is the most widespread metal found in metalloenzymes, in specific cases manganese forms isostructural active centers to Fe, and that shows an analogous reactivity.

Nature has taken advantage of the rich redox chemistry of manganese to use it in different oxidative catalytic transformations. One of the most studied for its relevance is the photosystem II, where it has been proposed that a $\text{Mn}^{\text{V}}(\text{O})$ or a $\text{Mn}^{\text{IV}}(\text{O})$ -organic radical is the active species in the oxygen evolving center (OEC), oxidizing H_2O to form O_2 (Scheme 6).^{73,74}



Scheme 6. Proposed Mn_4CaO_5 cluster in the oxygen evolving center (OEC).^{73,74}

I.3.2. Manganese metalloproteins in O_2 metabolism.

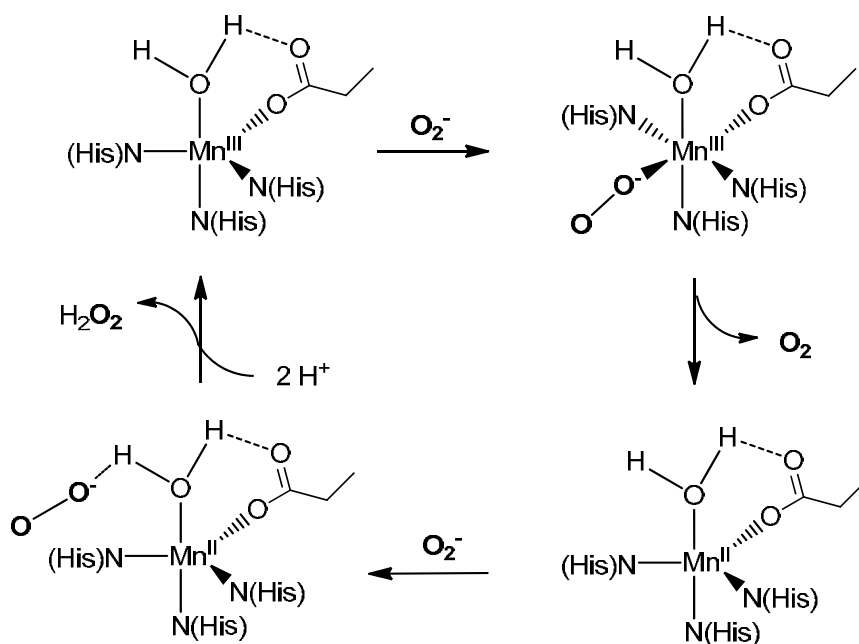
In the following paragraphs a summary of some of the most relevant Mn-based enzymes involved in O_2 metabolism is described.

Manganese superoxide dismutase (Mn-SOD):

Manganese superoxide dismutase (Mn-SOD) is one of the most extended manganese-containing metalloenzymes, which can be found in both eukaryotic and prokaryotic cells. In eukaryotic cells is found in mitochondria. Despite the existence of Fe-SOD in prokaryotic systems, the Mn-SOD is one rare example where manganese is preferred in natural systems over iron.⁷ X-Ray crystal structures reveal that both enzymes contain an isostructural active

center, with three histidines, one aspartate and a water molecule bound to the metal center ($M = \text{Mn}^{\text{III}}, \text{Fe}^{\text{III}}$) adopting a distorted trigonal bipyramidal coordination geometry.⁷⁵ Even with these similarities, generally the substitution of Mn by Fe or Fe by Mn results in the loss of activity of the SOD enzyme. Different exceptions to this rule are so-called “cambialistic” SOD, that are active with both Fe and Mn ions.⁷

The catalytic reaction performed by Mn-SOD can be understood as a two-step process (Scheme 7). In a first step, a superoxide moiety (O_2^-) coordinates to the manganese(III) center, transferring one electron via an inner-sphere process forming the molecular dioxygen (O_2) and a manganese(II) center. In a second step, another superoxide molecule is docked by hydrogen bonding interactions to the water ligand bound to the manganese(II) center, and a proton-coupled electron transfer occurs forming a free hydroperoxide moiety which is liberated as H_2O_2 , restoring the initial manganese(III) center.



Scheme 7. Proposed catalytic cycle in manganese-superoxide dismutase (Mn-SOD).⁷⁵

Manganese catechol dioxygenase (MndD):

Catechol dioxygenases catalyze the degradation of catechols via extradiol C-C cleavage as part of the route for the synthesis of fatty acids. Like in superoxide dismutases, iron and manganese dependent catechol dioxygenases exist, and they share a common active site where the metal is held in a 2-histidine-1-carboxylate facial triad.⁷⁶ In some cases, like in 3,4-dihydroxyphenylacetate 2,3-dioxygenases there is a clear dependence in the metal ion bound to the active center.⁷⁷ However, it has been demonstrated that exchange of the metal ions

doesn't affect the activity of the homoprotocatechate 2,3-dioxygenase.⁷⁸ Despite little is known about the reaction mechanism, it has been demonstrated that the catechol moiety binds to the metal center before its oxidation (Figure 13).

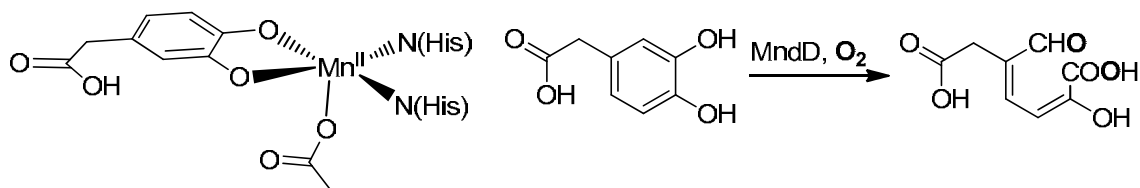
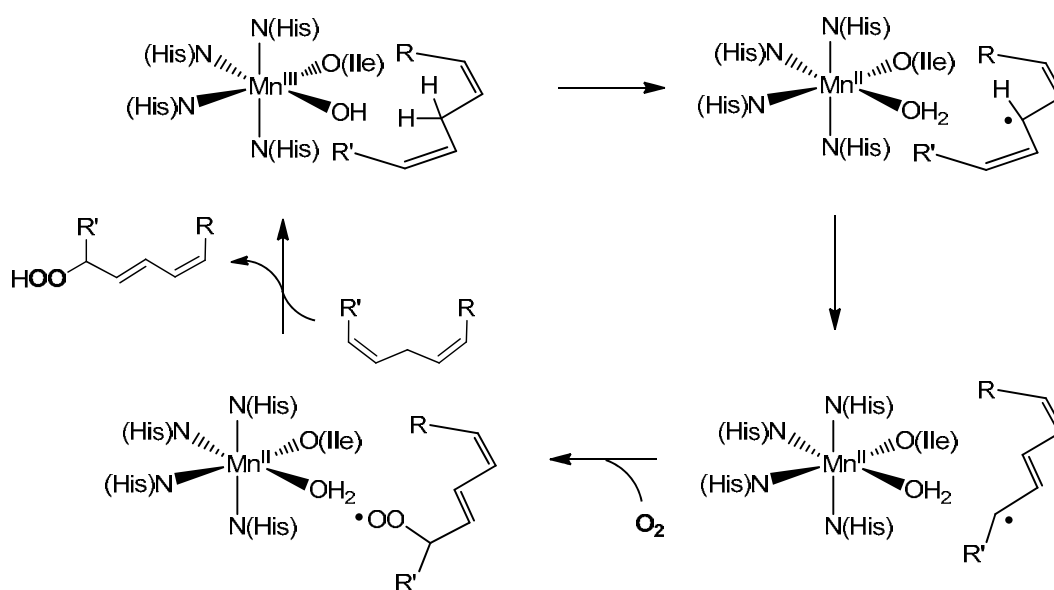


Figure 13. Active center and reaction catalyzed by manganese catechol dioxygenase (MndD).⁷⁶⁻

78

Manganese lipoxygenases (Mn-LO)

Ten years ago the first manganese-based lipoxygenase was discovered by Su and Oliw.⁷⁹ Their biological function consists of catalyzing the peroxidation of linoleic and linolenic acids.



Scheme 8. Proposed catalytic cycle for the manganese lipoxygenase (Mn-LO).⁸⁰

Despite Fe-LO have been studied in more detail, a similar mechanistic scenario is proposed for the Mn-LO enzyme (Scheme 8).⁸⁰ In the active form, a manganese(III) center is coordinated to four histidines, one oxygen from another isoleucine residue and a hydroxide moiety. In a first catalytic step, a hydrogen abstraction is carried out by the Mn^{III}-OH center to generate an allylic radical, which rearranges in a second catalytic step, and subsequently reacts with molecular oxygen in the third step. The organic peroxy radical formed is capable of abstracting

a hydrogen atom from the $\text{Mn}^{\text{II}}\text{-OH}_2$ center, regenerating the $\text{Mn}^{\text{III}}\text{-OH}$ complex and releasing the alkyl peroxide product.

I.3.3. High-valent manganese complexes in bioinspired oxidations.

Systems which hold manganese centers with high oxidation states have been widely studied over the last decades. The comparison of manganese systems with their iron analogs has also attracted the attention of different authors, trying to shed light into the Fe/Mn duality found in nature.^{81,82} One of the systems that has attracted more attention is the development of manganese complexes in high oxidation states using porphyrinic or pseudo-porphyrinic ligands because the analogous iron complexes are model systems for the cytochrome P450. In light of this, several research groups have synthesized and characterized families of $\text{Mn}(\text{IV},\text{V})(\text{O})\text{-L}$ complexes (L = porphyrins, corrolazine or salen ligands, see Figure 14).⁸²⁻⁸⁶ Furthermore, these complexes have been widely studied in several oxidative transformations such as C-H oxidations, sulfide oxidations and epoxidations.

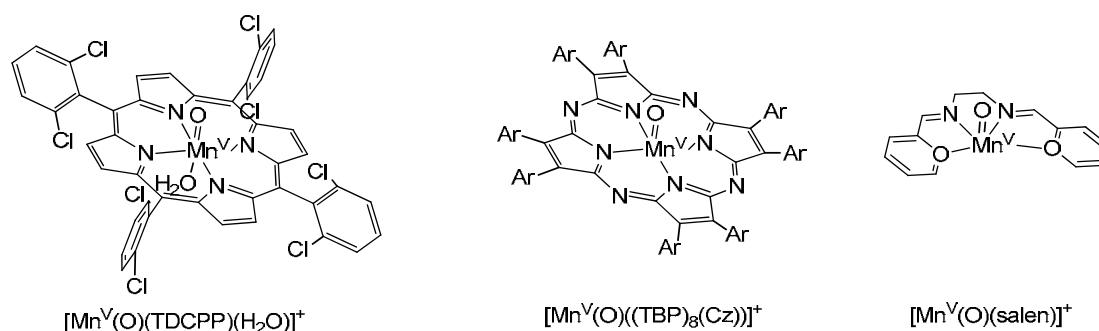


Figure 14. Porphyrinic and pseudo-porphyrinic manganese(V)-oxo complexes.⁸²⁻⁸⁶

One of the landmarks in the synthesis of non-porphyrinic manganese complexes in high oxidation states is the work by Weighardt *et al.* in late 1980s,⁸⁷ with the synthesis and characterization of a dinuclear manganese(IV) $[\text{Mn}_2(\mu\text{-O})_3(\text{Me}_3\text{TACN})_2](\text{PF}_6)_2$ which has been widely used in several catalytic oxidations or as bleaching agent combined with H_2O_2 (see section I.3.4).⁸⁸ Shortly later, Pecoraro and co-workers synthesized a dinuclear manganese(IV) complex bridged with two oxo anions.⁸⁹ Both complexes were understood as structural models for the OEC (Figure 15).

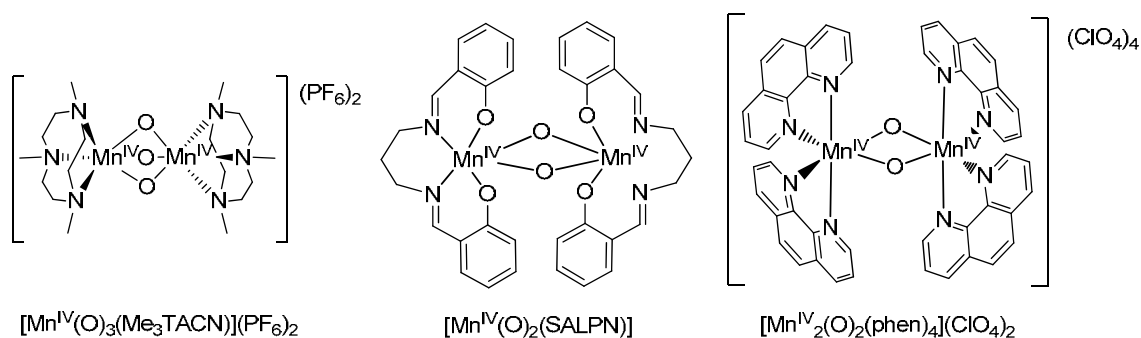
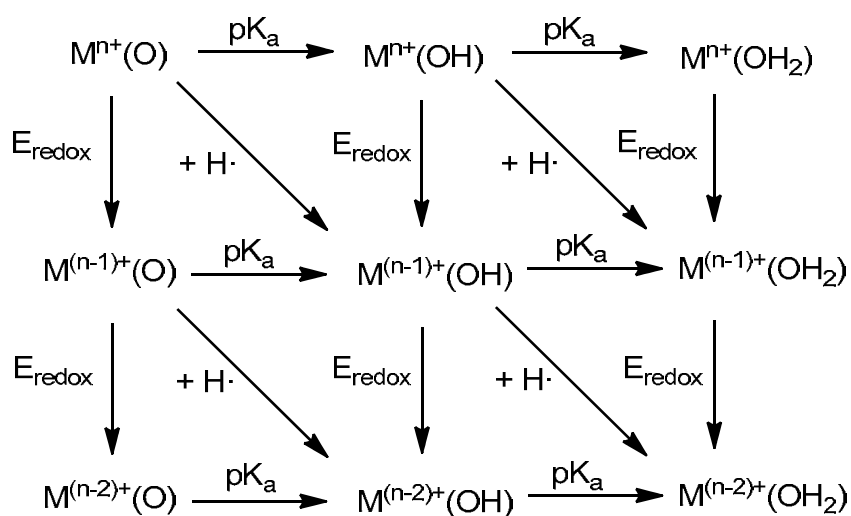


Figure 15. First examples of high valent manganese(IV)-oxo complexes^{87,89,90}

Mayer and coworkers took advantage of the versatility of the dimeric species $[\text{Mn}(\text{O})(\text{phen})_2]_2$ species, which can be isolated in different oxidation and protonation states, to study their reactivity towards C-H bonds. Over the years, Mayer has developed a groundbreaking methodology that permits to predict the reactivity of metal-oxo complexes in the hydrogen atom abstraction through the study of the basicity and redox properties of the species involved (Scheme 9).⁹⁰⁻⁹³ This thermodynamic approximation has been applied in several metal-oxo species, including manganese, iron, ruthenium and vanadium.



Scheme 9. Thermodynamic approximation for the hydrogen atom abstraction performed by metal-oxo(hydroxo) complexes.

It has to be noticed that the synthesis of mononuclear manganese-oxo complexes in high oxidation states is difficult because of its tendency of forming polynuclear species. Stack and coworkers designed a bioinspired manganese(III)-hydroxo complex that reproduced the activity of the manganese-lipoxygenase (Mn-LO) (Figure 16).⁹⁴ Following the approach of Mayer, the authors calculated the energy for a hydrogen atom abstraction through the redox and acid/base properties of the $\text{Mn}^{\text{III}}\text{-OH}$ complex.

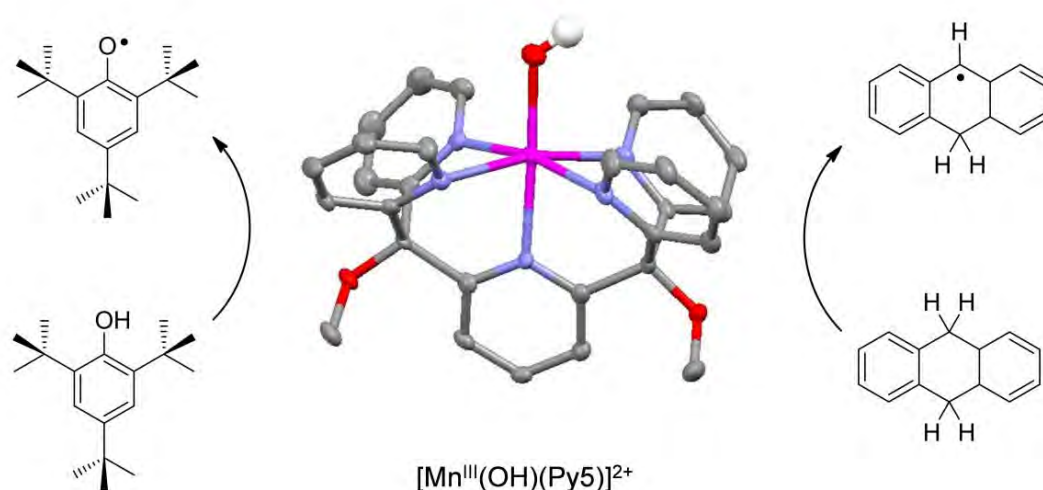


Figure 16. Manganese(III)-hydroxo complex as functional model for manganese lipoxygenase (Mn-LO).⁹⁴

Borovik and co-workers have designed an anionic tripodal tris-aminato ligand to generate iron and manganese-oxo species by direct reaction with O_2 .⁹⁵⁻⁹⁸ The ligand provides a cavity that prevents dimerization of the complex and stabilizes the oxo moiety which is stabilized by hydrogen bonding with the amido groups (Figure 17). The synthesis of the analogue iron/manganese-(hydroxo) complexes allowed direct comparison of their relative reactivity towards C-H bonds.⁹⁹ In the case of manganese, an intriguing behavior was observed when the $\text{LMn}^{\text{III}}(\text{O})$ and $\text{LMn}^{\text{IV}}(\text{O})$ ($\text{L} = \text{H}_3\text{buea}$) complexes were tested in the oxidation of dihydroanthracene.¹⁰⁰ When the thermodynamic force for the hydrogen atom abstraction was calculated for both complexes, the $\text{LMn}^{\text{IV}}(\text{O})$ moiety gave a higher value (89 kcal/mol) over the $\text{LMn}^{\text{III}}(\text{O})$ system (77 kcal/mol). Despite this difference, complex $\text{LMn}^{\text{III}}(\text{O})$ performed the oxidation of C-H bonds 20 times faster than the $\text{LMn}^{\text{IV}}(\text{O})$ analog, contradicting the thermodynamic preference. Noticing that the redox potentials of the species were negative (a typical value for reducing species), they carried out mechanistic studies in order to explain this counterintuitive behavior. The kinetic isotopic effects and kinetic values led to a proposal of a distinct mechanistic scenario for the high valent manganese species: while $\text{LMn}^{\text{IV}}(\text{O})$ abstracted hydrogen in a PCET (proton-coupled electron transfer) step, the $\text{LMn}^{\text{III}}(\text{O})$ acted in a two-step process initiated with a first deprotonation of the substrate followed by electron transfer. This switch in the mechanism was explained in terms of basicity of the Mn-oxo complexes, having the $\text{LMn}^{\text{III}}(\text{O})$ a pK_a value ten times higher than the $\text{LMn}^{\text{IV}}(\text{O})$. Furthermore, they proposed that kinetic factors have to be taken into account in the understanding of these oxidations.

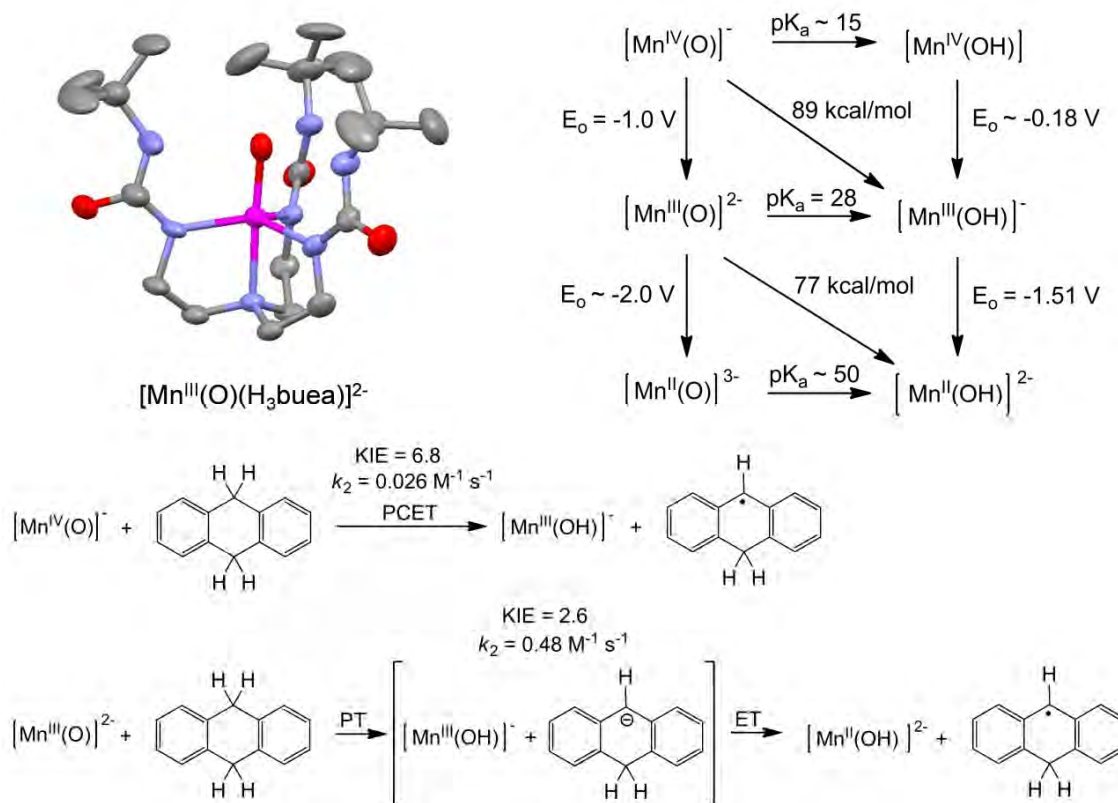


Figure 17. Manganese(oxo) complexes developed by Borovik and co-workers and their reactivity towards C-H bonds.^{97,100}

Busch and co-workers were able to isolate a manganese(IV) bis-hydroxide moiety using a macrocyclic ligand (Me₂EBC), which provided a steric protection to the metal center thus avoiding the formation of dimeric products (Figure 18).¹⁰¹ Like in Borovik's case, the reactivity towards C-H bonds was explained based on the thermodynamic parameters. In their system, the prediction that the manganese(oxo)(hydroxo) complex had a major energetic gain in the hydrogen abstraction reaction was also confirmed by kinetic measurements.^{102,103} The linear correlation between reaction rates and the BDE of the tested substrates allowed the authors to propose a bimolecular hydrogen transfer (HAT). Kinetic isotopic effect (KIE_{H/D} = 3.3) also supported the proposed mechanism.

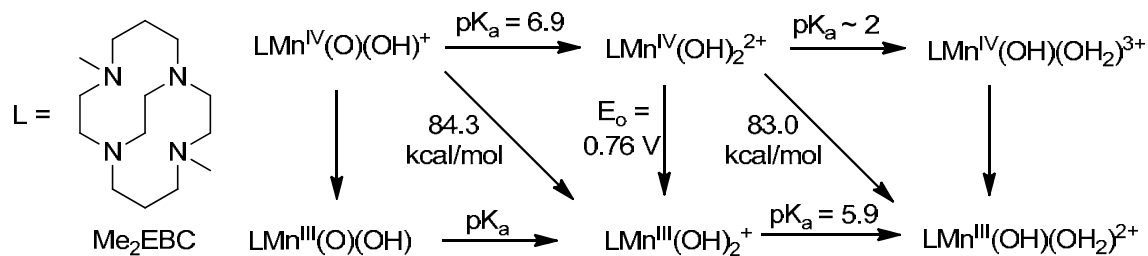


Figure 18. Manganese(IV) complexes developed by Busch and co-workers and thermodynamic values for predicting the reactivity towards C-H bonds.¹⁰¹⁻¹⁰³

Very recently, Nam and co-workers have reported the generation of a mononuclear manganese(IV)-oxo system by the reaction of the respective manganese(II) complex with cerium(IV) as electron source and water.¹⁰⁴ Despite no crystal structure is reported, DFT calculations and rRaman spectroscopy ($\nu(\text{Mn}-\text{O}) = 676 \text{ cm}^{-1}$, $\Delta[^{18}\text{O}] = 31 \text{ cm}^{-1}$) supported a Mn^{IV} -oxo formulation. The authors confirmed the hydrogen atom transfer mechanism for substrates with low bond dissociation energies (such as dihydroanthracene or 1,4-cyclohexadiene). Interestingly, the manganese-oxo complex was able to perform the hydroxylation of anthracene via electrophilic attack of the oxo ligand towards the arene (Figure 19).

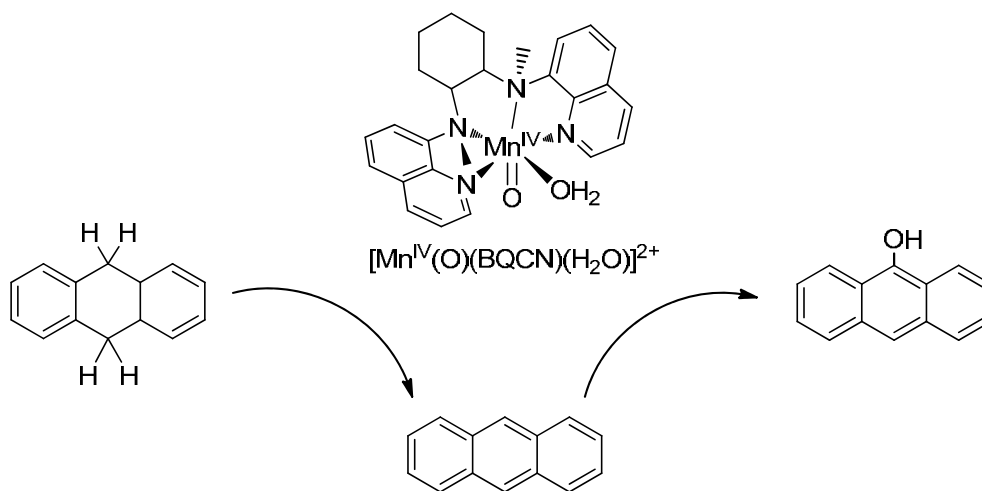


Figure 19. Manganese-oxo complex developed by Nam and co-workers and its reactivity towards external substrates.¹⁰⁴

I.3.4. Oxidation catalysis mediated by manganese systems.

Manganese has emerged during the last two decades as a very active transition metal ion for oxidation catalysis. It has been used in the epoxidation and *cis*-dihydroxylation of alkenes, the oxidation of sulfoxides, and the oxidation and desaturation of C-H bonds. One of the pioneer

examples of the application of a manganese complex in oxidation catalysis was the report by Hage *et al.* describing the use of $[\text{Mn}_2(\mu\text{-O})_3(\text{Me}_3\text{TACN})_2](\text{PF}_6)_2$ as bleaching agent and alkene epoxidation catalyst using hydrogen peroxide as oxidant.⁸⁸ Following this precedent, Feringa and co-workers reported the use of $[\text{Mn}^{\text{IV}}_2(\mu\text{-O})_3(\text{Me}_3\text{TACN})_2](\text{PF}_6)_2$ as a *cis*-dihydroxylation catalyst.¹⁰⁵ In a first approach, the authors used H_2O_2 as oxidant, and different carboxylic acids as co-catalysts (Figure 20). The use of carboxylic acids not only suppressed the inherent catalase activity of the complex but also provided the tuning of the selectivity toward *cis*-dihydroxylation versus epoxidation: when $\text{Cl}_3\text{CCO}_2\text{H}$ was used as co-catalyst, a ratio of *cis*-diol/epoxide = 1.8 was observed, and with 2,6-dichlorobenzoic acid the ratio was 7. Interestingly, using salicylic acid as additive this ratio was reversed, and epoxide was the major product (diol/epoxide ratio = 0.09). This methodology was extended to a series of alkenes: despite good yields and selectivity towards *cis*-dihydroxylation was observed for electron-rich aliphatic substrates such as cyclooctene, *cis*-2-heptene or *trans*-2-heptene, the system failed to elicit selective *cis*-dihydroxylation of aromatic substrates such as styrene, where the epoxide was mainly obtained. In addition, electron-poor substrates such as dimethylmaleate and dimethylfumarate were also unsuitable for the system.

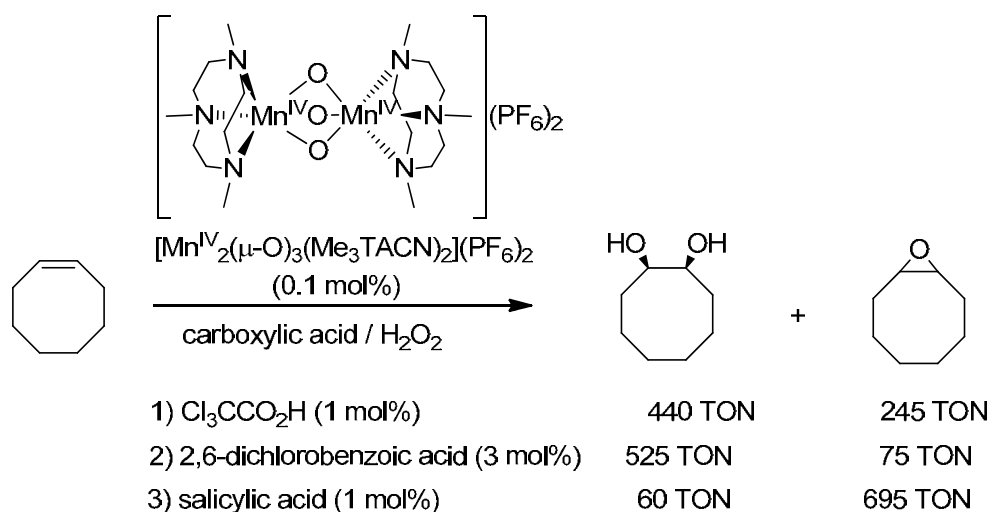


Figure 20. Epoxidation/*cis*-dihydroxylation performed by $[\text{Mn}^{\text{IV}}_2(\mu\text{-O})_3(\text{Me}_3\text{TACN})_2](\text{PF}_6)_2$ in the presence of different co-catalysts and hydrogen peroxide.¹⁰⁵

A seminal contribution to this field was made by Stack and co-workers in 2003, by describing the use of a mononuclear manganese complex $[\text{Mn}^{\text{II}}(\text{CF}_3\text{SO}_3)_2((R,R)\text{-mcp})]$, where mcp is a linear N-based tetradentate ligand, as a very active epoxidation catalyst (Figure 21).¹⁰⁶ This complex, in combination with peracetic acid, rapidly catalyzes the epoxidation of olefins. The

reactions were carried out using 0.1 mol% of catalyst, 1.2 equiv. of $\text{CH}_3\text{CO}_3\text{H}$ using CH_3CN as solvent. Epoxidation of a wide range of alkenes was achieved in excellent yields: cyclooctene (99%), *cis*-2-heptene (99%), 1-heptene (95%), 2-cyclohexen-1-one (97%) or *cis*- β -methylstyrene (90%). Furthermore, the system showed excellent chemoselectivity in the epoxidation of dienes such as *R*-carvone where the exclusive oxidation of one of the alkenes was achieved. The same authors tested a wide range of N-based ligands, combined with a manganese salt, as catalysts for the oxidation of 1-octene.¹⁰⁷ By using peracetic acid immobilized in a resin, the strong acidity of commercial peracetic acid could be avoided, and simple systems such as $[\text{Mn}^{\text{II}}(\text{CF}_3\text{SO}_3)_2(\text{bipy})_2]$ were found to catalyze the epoxidation of 1-octene under low catalyst loadings (0.1 mol%), providing excellent conversion (99%) and yield (94%).

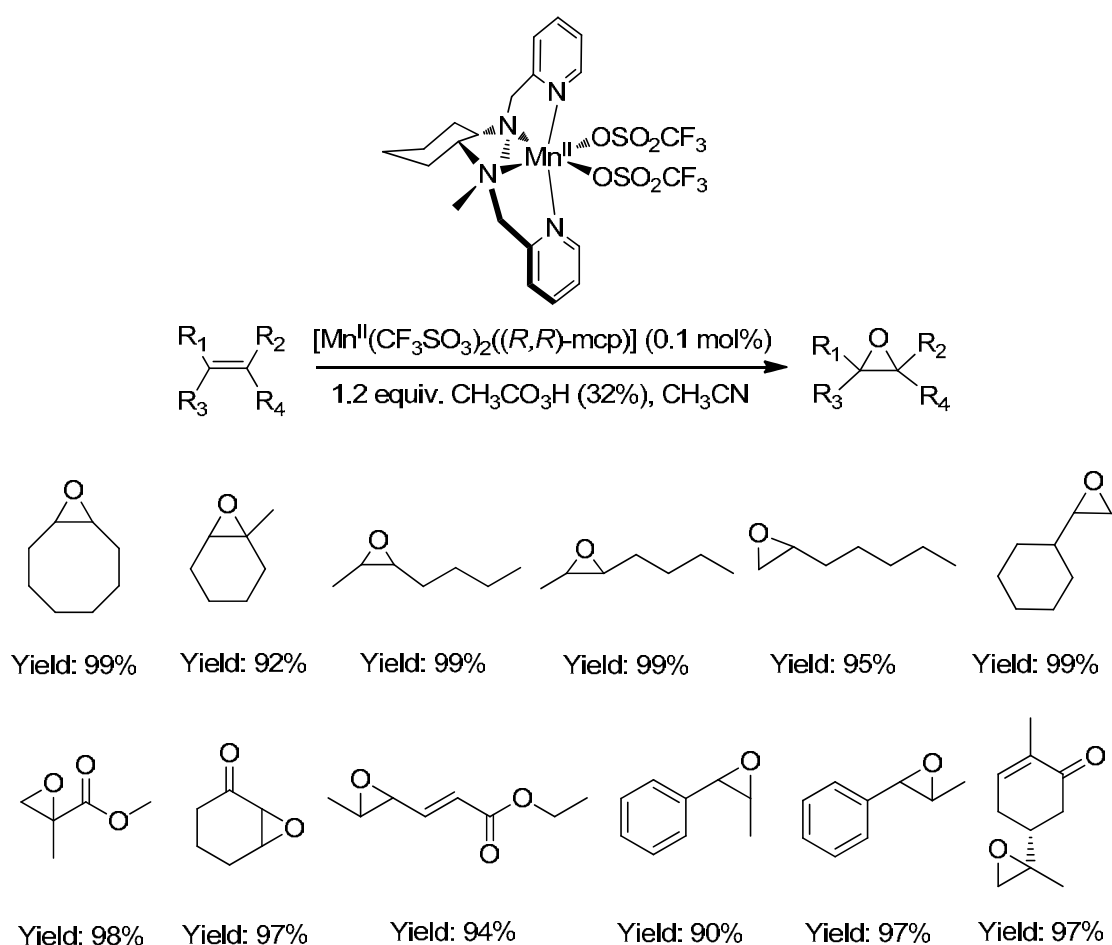


Figure 21. Stack's manganese-based system for the epoxidation of alkenes with $\text{CH}_3\text{CO}_3\text{H}$.¹⁰⁶

Following in this precedent, several manganese complexes containing nitrogen based ligands have been studied as epoxidation catalysts (Figure 22).¹⁰⁸⁻¹¹³ In Table 4, a summary of state of the art catalytic systems used in the epoxidation of 1-octene is described.

Catalytic asymmetric epoxidation of alkenes was pioneered by Jacobsen *et al.* and Katsuki *et al.* in the 90s by employing Mn-salen complexes.^{114,115} Although excellent enantioselectivities were observed, these systems have room for improvement in aspects such as catalyst loadings, substrate scope and oxidants used. Because of that, more robust catalysts that could rely on the use of H₂O₂ continue to be a very attractive target. With this interest in mind, Gómez *et al.* designed two novel chiral ligands based on the (*R,R*)-mcp system by fusing a pinene ring in the 4,5-positions of the pyridine (Figure 23).¹¹⁶ The resulting diastereoisomeric ligands (*S,S,R*)-mcpp and (*R,R,R*)-mcpp were used to prepare the corresponding Mn^{II}-complexes. Complexes were studied in the asymmetric epoxidation of styrene, with Λ -[Mn(CF₃SO₃)₂((*S,S,R*)-mcpp)] complex achieving the highest stereoselectivity (46% ee) (Table 5). Complex Λ -[Mn(CF₃SO₃)₂((*S,S,R*)-mcpp)] (0.5 mol%) was subsequently used in the epoxidation of different alkenes using peracetic acid (2 equiv.) as oxidant. Despite the good conversions (80-100%) and yields (60-100%) achieved, the stereoselectivity was moderate (ee. 40-50%). Xia and Sun *et al.* modified the (*R,R*)-mcp ligand introducing aryl groups at the pseudobenzyl methylenic groups (*R,R,R,R*-bpmcp), which in turn represented an extra element of chirality, closer to the chiral center (Figure 23).¹¹⁷ The authors obtained good to excellent enantioselectivities in the epoxidation of α - β -enones (70-90%), but moderate stereoselectivities (30-50%) were accomplished for other substrates (Table 5). Another approach was pioneered by Watkinson and co-workers, using chiral ligands derived from the bipyridine moiety ((*S*)-L4 and (*S*)-L5, Figure 23) which was also used by other groups ((*R*)-L6, Figure 23).^{118,119}

Very recently, Talsi and co-workers synthesized the chiral complex [Mn(CF₃SO₃)₂((*S,S*)-bpbp)] (Figure 23),¹²⁰ which catalyzed alkene epoxidation using the H₂O₂/AcOH conditions early described by Garcia-Bosch *et al.* (see Chapter V.2.). Remarkable stereoselectivities were obtained for electron-deficient substrates such as *trans*-chalcone (78% ee) or 2,2-dimethyl-2H-1-benzopyran-6-carbonitrile (76% ee), but low selectivity was achieved for substrates such as styrene (39% ee), 1,2-dihydronaphthalene (27% ee) and *trans*-stilbene (8% ee) (Table 5).

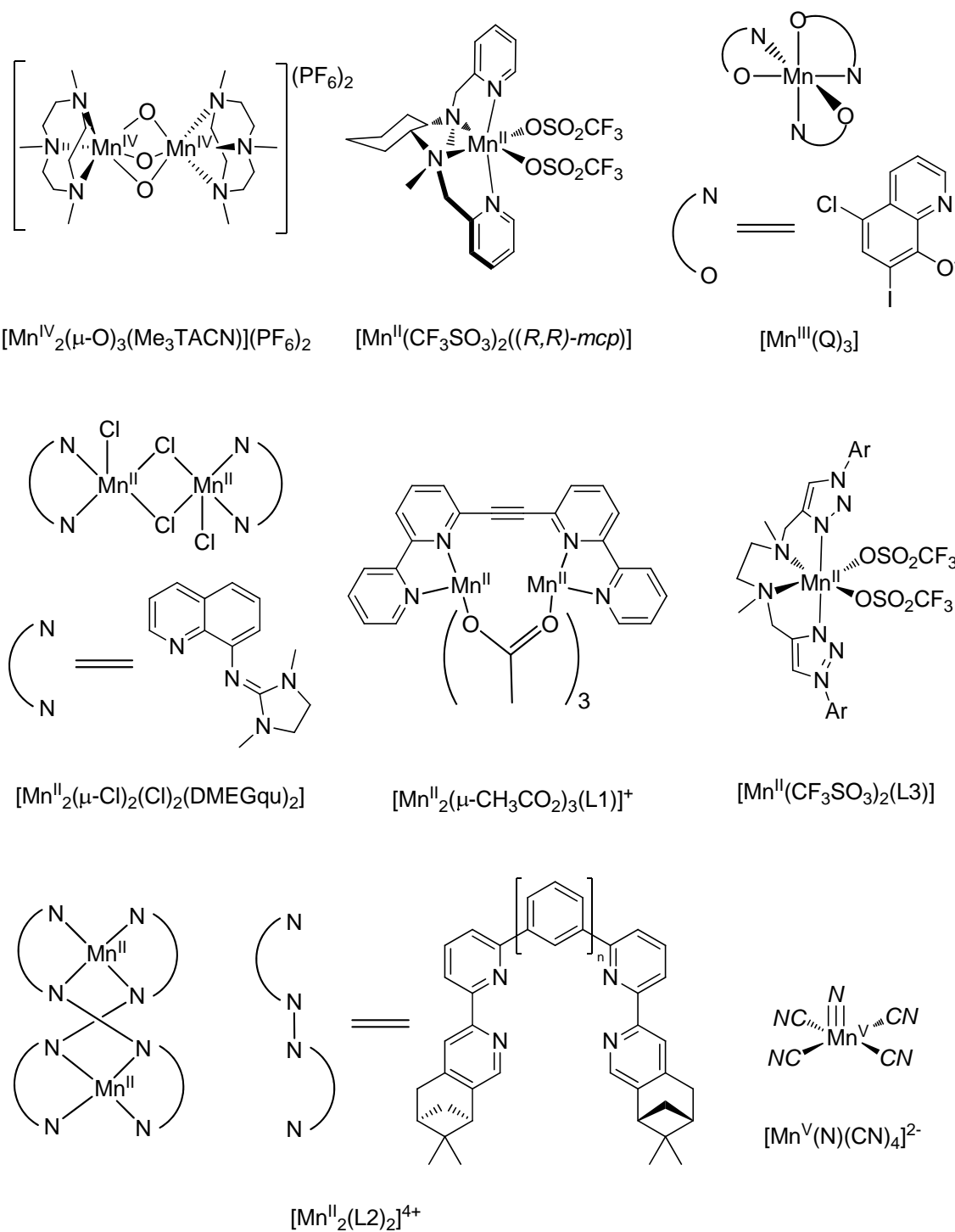
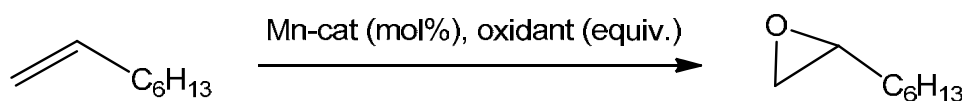


Figure 22. Selected manganese complexes for the epoxidation of alkenes.

Table 4. Comparison of manganese catalysts (see Figure 22) in the epoxidation of 1-octene.

System	Cat. (%)	Oxidant (equiv.)	Conv. (%)	Yield (%)	T.O.N.	Ref.
$[\text{Mn}^{\text{IV}}_2(\mu\text{-O})_3(\text{Me}_3\text{TACN})_2](\text{PF}_6)_2$	1	H_2O_2 (100)	99 ^a	99 ^a	99 ^a	88
$[\text{Mn}^{\text{II}}(\text{CF}_3\text{SO}_3)_2((R,R)\text{-mcp})]$	0.1	$\text{CH}_3\text{CO}_3\text{H}$ (1.2)	95 ^b	89 ^b	890 ^b	106
$[\text{Mn}^{\text{II}}(\text{CF}_3\text{SO}_3)_2(\text{bipy})_2]$	0.1	$\text{CH}_3\text{CO}_3\text{H}^{\text{c}}$ (1.2)	99	94	940	107
$[\text{Mn}^{\text{III}}(\text{Q})_3]$	2	H_2O_2 (1.5)	95	93	47	112
$[\text{Mn}^{\text{II}}_2(\mu\text{-Cl})_2(\text{Cl})_2(\text{DMEGqu})_2]$	0.1	$\text{CH}_3\text{CO}_3\text{H}$ (2.0)	85	62	620	113
$[\text{Mn}^{\text{II}}_2(\mu\text{-CH}_3\text{CO}_2)_3(\text{L1})]^+$	3.3	$\text{CH}_3\text{CO}_3\text{H}$ (2.0)	91	91	28	111
$[\text{Mn}^{\text{II}}_2(\text{L2})_2]^{4+}$	1	$\text{CH}_3\text{CO}_3\text{H}$ (2.0)	100 ^d	99 ^d	99 ^d	108
$[\text{Mn}^{\text{II}}(\text{CF}_3\text{SO}_3)_2(\text{L3})]$	0.5	$\text{CH}_3\text{CO}_3\text{H}$ (2.0)	-	93 ^e	465 ^e	110
$[\text{Mn}^{\text{V}}(\text{N})(\text{CN})_4]^{2-}$	1	H_2O_2 (2.5)	98	74	74	109

a) Oxidation of styrene. ^{b)} Oxidation of 1-heptene. ^{c)} $\text{CH}_3\text{CO}_3\text{H}$ in strongly acidic resins ^{d)} Oxidation of 1-pentene. ^{e)} Oxidation of 1-decene.

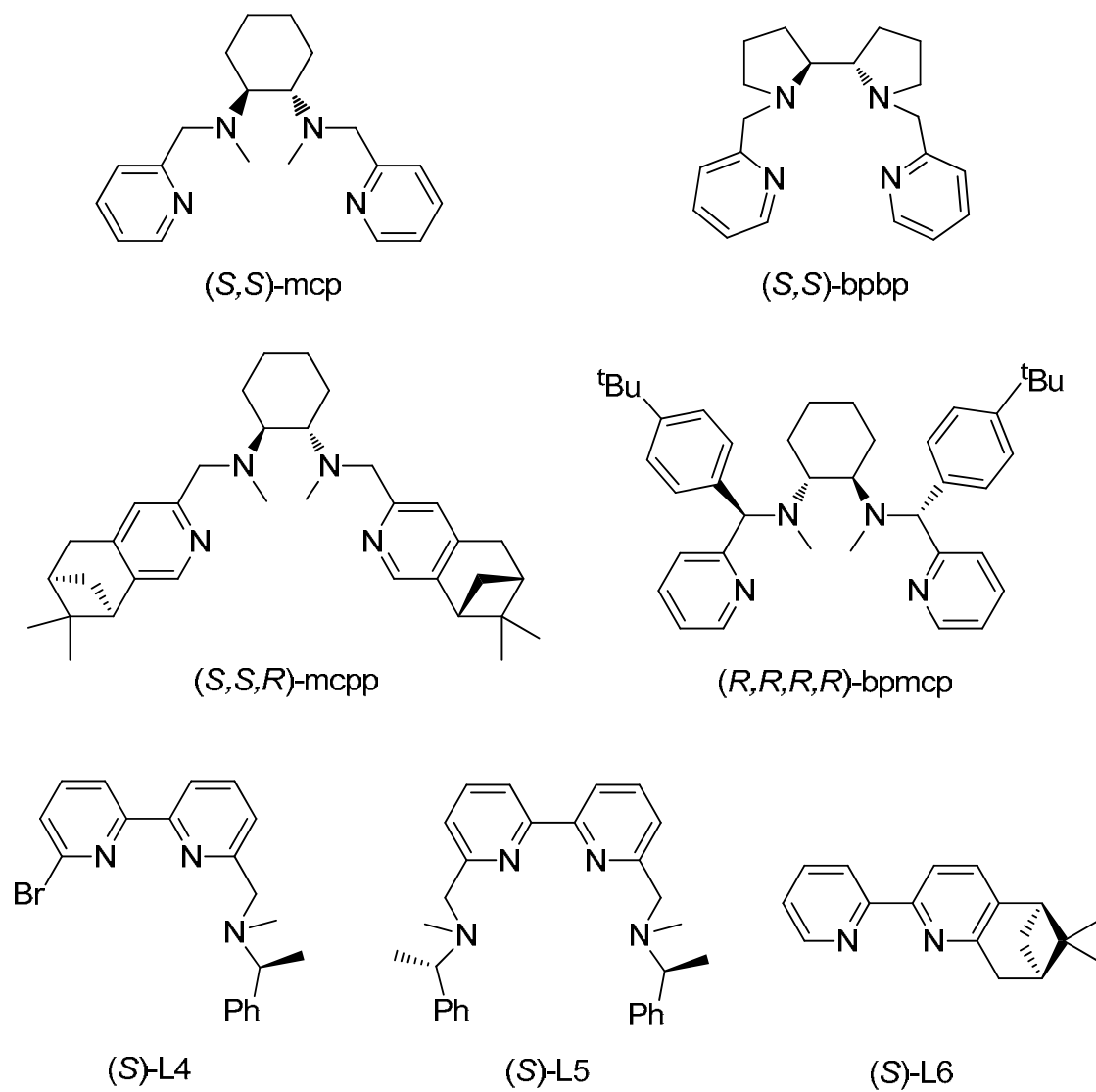
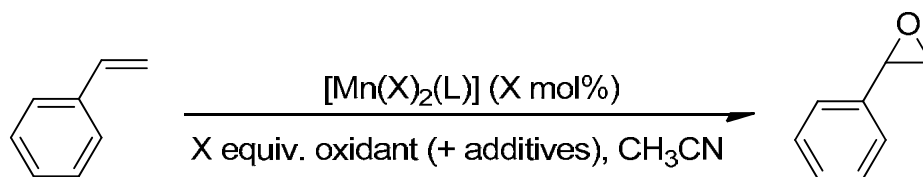


Figure 23. Chiral ligands for the stereoselective epoxidation of alkenes with the corresponding Mn-complexes.

Table 5. Comparison of manganese catalysts (see Figure 23) in the stereoselective epoxidation of styrene.

System	Cat. (%)	Oxidant (equiv.)	Conv. (%)	Yield (%)	Ee (%)	Ref.
$[\text{Mn}(\text{CF}_3\text{SO}_3)_2(\text{S},\text{S})\text{-mcp}]$	1	H ₂ O ₂ (1.1)	100	98	35	121
$[\text{Mn}(\text{CF}_3\text{SO}_3)_2(\text{S},\text{S})\text{-mcp}]$	1	H ₂ O ₂ (2.0)	100 ^a	95 ^a	72 ^a	121
$[\text{Mn}(\text{CF}_3\text{SO}_3)_2(\text{S},\text{S})\text{-bpbp}]$	0.1	H ₂ O ₂ (1.3)	84	84	39	120
$[\text{Mn}(\text{CF}_3\text{SO}_3)_2(\text{S},\text{S})\text{-bpbp}]$	0.1	H ₂ O ₂ (1.3)	97 ^b	97 ^b	78 ^b	120
$[\text{Mn}(\text{CF}_3\text{SO}_3)_2(\text{S},\text{S},\text{R})\text{-mcpp}]$	0.5	CH ₃ CO ₃ H (2.0)	99	78	46	116
$[\text{Mn}(\text{CF}_3\text{SO}_3)_2(\text{R},\text{R},\text{R},\text{R})\text{-bpmcp}]$	1	H ₂ O ₂ (6.0)	-	85	43	117
$[\text{Mn}(\text{CF}_3\text{SO}_3)_2(\text{R},\text{R},\text{R},\text{R})\text{-bpmcp}]$	1	H ₂ O ₂ (6.0)	-	91 ^b	78 ^b	117
$[\text{Mn}(\text{S})\text{-L4}]^{2+}$	0.1	CH ₃ CO ₃ H (2.0)	50	15	0	118
$[\text{Mn}(\text{S})\text{-L5}]^{2+}$	1	CH ₃ CO ₃ H (2.0)	89	43	21	118
$[\text{Mn}(\text{R})\text{-L6}]^{2+}$	1	CH ₃ CO ₃ H (2.0)	100	65	10	119

a) Epoxidation of 2,2-dimethyl-2H-1-benzopyran-6-carbonitrile. b) Epoxidation of *trans*-chalcone.

Regarding the reaction mechanism, it has been proposed that manganese-based epoxidation catalysis occurs via three possible mechanisms: i) direct oxo transfer from a high valent manganese species, ii) peroxy radical pathway and iii) Lewis acid concerted mechanism. Busch and co-workers have demonstrated that their complex $[\text{Mn}(\text{Cl})_2(\text{Me}_2\text{-EBC})]$ proceeded via oxidation of the complex by H_2O_2 to form the manganese(IV)-oxo complex which then activates another hydrogen peroxide unit generating a manganese(IV)-oxo-hydroperoxo responsible of the oxo-transfer to the alkene (figure 24).¹²² Other authors have also proposed the concerted mechanism as the most feasible pathway for the alkene oxidation.^{121,123}

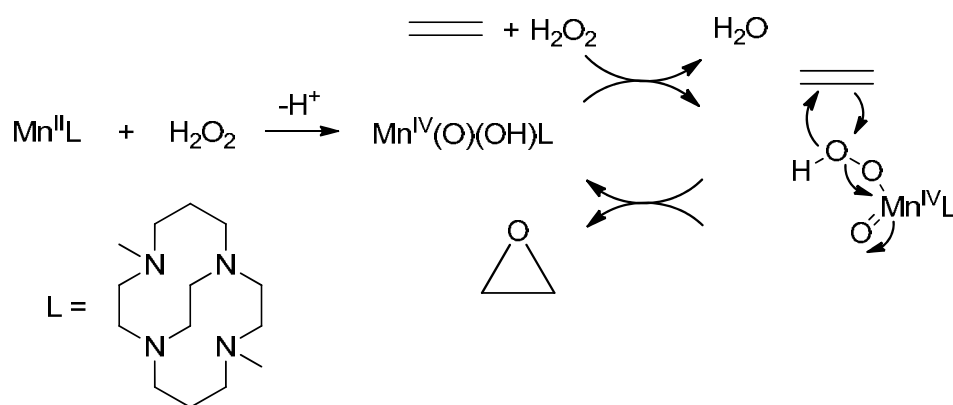


Figure 24. Lewis-acid activation mechanism proposed for the epoxidation of alkenes.¹²²

I.4. References.

- (1) *Modern oxidation Methods*; (Ed.: J.-E. Bäckvall), Wiley-VCH: Weinheim, 2004.
- (2) Sheldon, R. A.; Kochi, J. K. *Metal-Catalyzed Oxidation of Organic Compounds*; Academic: New York, 1981.
- (3) March, J. *Advanced Organic Chemistry*; 3rd ed. New York, 1985.
- (4) Schröder, M. *Chem. Rev.* **1980**, *80*, 187-213.
- (5) Semenza, G. L. *Science* **2007**, *318*, 62-64.
- (6) Holm, R. H.; Kennepohl, P.; Solomon, E. I. *Chem. Rev.* **1996**, *96*, 2239-2314.
- (7) Bertini, I.; Gray, H. B.; Stiefel, E. I.; Valentine, J. S. *Biological Inorganic Chemistry. Structure & Reactivity*; University Science Books, 2007.
- (8) Bertini, I.; Gray, H. B.; Lippard, S. J.; Valentine, J. S. *Bioinorganic Chemistry*; University Science Books, 1994.
- (9) Lippard, S. J.; Berg, J. M. *Principles of Bioinorganic Chemistry*; University Science Books: Mill Valley, CA, 1994.
- (10) Mirica, L. M.; Vance, M.; Rudd, D. J.; Hedman, B.; Hodgson, K. O.; Solomon, E. I.; Stack, T. D. P. *Science* **2005**, *308*, 1890-1892.
- (11) Solomon, E. I.; Szilagy, R. K.; George, S. D.; Basumallick, L. *Chem. Rev.* **2004**, *104*, 419-458.
- (12) Solomon, E. I.; Sundaram, U. M.; Machonkin, T. E. *Chem. Rev.* **1996**, *96*, 2563-2605.
- (13) Ferguson-Miller, S.; Babcock, G. T. *Chem. Rev.* **1996**, *96*, 2889-2907.
- (14) Kim, E.; Chufan, E. E.; Kamaraj, K.; Karlin, K. D. *Chem. Rev.* **2004**, *104*, 1077-1134.
- (15) Lewis, E. A.; Tolman, W. B. *Chem. Rev.* **2004**, *114*, 1047-1076.
- (16) Mirica, L. M.; Ottenwaelder, X.; Stack, T. D. P. *Chem. Rev.* **2004**, *114*, 1013-1046.
- (17) Cuff, M. E.; Miller, K. I.; Holde, K. E. v.; Hendrickson, W. A. *J. Mol. Biol.* **1998**, *278*, 855-870.
- (18) Matoba, Y.; Kumagai, T.; Yamamoto, A.; Yoshitsu, H.; Sugiyama, M. *J. Biol. Chem.* **2006**, *281*, 8981-8990.
- (19) Morioka, C.; Tachi, Y.; Suzuki, S.; Itoh, S. *J. Am. Chem. Soc.* **2006**, *128*, 6788-6789.
- (20) Decker, H.; Dillinger, R.; Tuzcek, F. *Angew. Chem. Int. Ed.* **2000**, *39*, 1591-1595.
- (21) Decker, H.; Schweikardt, T.; Tuzcek, F. *Angew. Chem. Int. Ed.* **2006**, *45*, 4546-4550.
- (22) Tyeklár, Z.; Jacobson, R. R.; Wei, N.; Murthy, N. N.; Zubieta, J.; Karlin, K. D. *J. Am. Chem. Soc.* **1993**, *115*, 2677-2689.
- (23) Wurtele, C.; Sander, O.; Lutz, V.; Waitz, T.; Tuzcek, F.; Schindler, S. *J. Am. Chem. Soc.* **2009**, *131*, 7544-7545.
- (24) Paul, P. P.; Tyeklár, Z.; Jacobson, R. R.; Karlin, K. D. *J. Am. Chem. Soc.* **1991**, *113*, 5322-5332.

- (25) Kitajima, N.; Fujisawa, K.; Moro-oka, Y. *J. Am. Chem. Soc.* **1989**, *111*, 8975-8976.
- (26) Halfen, J. A.; Mahapatra, S.; Wilkinson, E. C.; Kaderli, S.; Young, V. G., Jr.; Que, L., Jr.; Zuberbühler, A. D.; Tolman, W. B. *Science* **1996**, *271*, 1397-1400.
- (27) Matsumoto, T.; Ohkubo, K.; Honda, K.; Yazawa, A.; Furutachi, H.; Fujinami, S.; Shunichi Fukuzumi; Suzuki, M. *J. Am. Chem. Soc.* **2009**, *131*, 9258-9267.
- (28) Tolman, W. B. *Acc. Chem. Res.* **1997**, *30*, 227-237.
- (29) Ottenwaelder, X.; Rudd, D. J.; Corbett, M. C.; Hodgson, K. O.; Hedman, B.; Stack, T. D. P. *J. Am. Chem. Soc.* **2006**, *128*, 9268-9269.
- (30) Mahapatra, S.; Young, V. G., Jr.; Kaderli, S.; Zuberbühler, A. D.; Tolman, W. B. *Angew. Chem. Int. Ed.* **1997**, *36*, 130-133.
- (31) Karlin, K. D.; Dahlstrom, P. L.; Cozzette, S. N.; Scensny, P. M.; Zubieta, J. *J. Chem. Soc., Chem. Commun.* **1981**, 881-882.
- (32) Palavicini, S.; Granata, A.; Monzani, E.; Casella, L. *J. Am. Chem. Soc.* **2005**, *127*, 18031-18036.
- (33) Casella, L.; Monzani, E.; Gullotti, M.; Cavagnino, D.; Cerina, G.; Santagostini, L.; Ugo, R. *Inorg. Chem.* **1996**, *35*, 7516-7525.
- (34) Itoh, S.; Kumei, H.; Taki, M.; Nagatomo, S.; Kitagawa, T.; Fukuzumi, S. *J. Am. Chem. Soc.* **2001**, *123*, 6708-6709.
- (35) Company, A.; Palavicini, S.; Garcia-Bosch, I.; Mas-Ballesté, R.; Que, L., Jr.; Rybak-Akimova, E. V.; Casella, L.; Ribas, X.; Costas, M. *Chem. Eur. J.* **2008**, *14*, 3535-3538.
- (36) Rolff, M.; Schottenheim, J.; Peters, G.; Tuczek, F. *Angew. Chem. Int. Ed.* **2010**, *49*, 6438 – 6442.
- (37) Osako, T.; Ohkubo, K.; Taki, M.; Tachi, Y.; Fukuzumi, S.; Itoh, S. *J. Am. Chem. Soc.* **2003**, *125*, 11027-11033.
- (38) Herres-Pawlis, S.; Verma, P.; Haase, R.; Kang, P.; Lyons, C. T.; Wasinger, E. C.; Flrke, U.; Henkel, G.; Stack, T. D. P. *J. Am. Chem. Soc.* **2009**, *131*, 1154-1169.
- (39) Solomon, E. I.; Chen, P.; Metz, M.; Lee, S.-K.; Palmer, A. E. *Angew. Chem. Int. Ed.* **2001**, *40*, 4570-4590.
- (40) Sazinsky, M. H.; Lippard, S. J. *Acc. Chem. Res.* **2006**, *39*, 558-566.
- (41) Kaila, V. R. I.; Verkhovsky, M. I.; Wikström, M. *Chem. Rev.* **2010**, *110*, 7062-7081.
- (42) Gennis, R.; Ferguson-Miller, S. *Science* **1995**, *269*, 1063-1064.
- (43) Tainer, J. A.; Getzoff, E. D.; Beem, K. M.; Richardson, J. S.; Richardson, D. C. *J. Mol. Biol.* **1982**, *160*, 181-217.
- (44) Blackburn, N. J.; Pettingill, T. M.; Seagraves, K. S.; Shigeta, R. T. *J. Biol. Chem.* **1990**, *265*, 15383-15386.

- (45) Klinman, J. P. *Chem. Rev.* **1996**, *96*, 2541-2561.
- (46) Chen, P.; Solomon, E. I. *PNAS* **2004**, *101*, 13105-13110.
- (47) Prigge, S. T.; Kolhekar, A. S.; Eipper, B. A.; Mains, R. E.; Amzel, L. M. *Science* **1997**, *278*, 1300-1305.
- (48) Schindler, S. *Eur. J. Inorg. Chem.* **2000**, 2311-2326.
- (49) Rolffe, M.; Schottenheim, J.; Decker, H.; Tuzcek, F. *Chem. Soc. Rev.* **2011**, *40*, 4077-4098.
- (50) Costas, M.; Mehn, M. P.; Jensen, M. P.; Que, L., Jr. *Chem. Rev.* **2004**, *104*, 939-986.
- (51) Friedle, S.; Reisner, E.; Lippard, S. J. *Chem. Soc. Rev.* **2010**, *39*, 2768-2779.
- (52) Battaini, G.; Granata, A.; Monzani, E.; Gullotti, M.; Casella, L. *Adv. Inorg. Chem.* **2006**, *58*, 185-233.
- (53) Kieber-Emmons, M. T.; Riordan, C. G. *Acc. Chem. Res.* **2007**, *40*, 618-625.
- (54) Gavrilova, A. L.; Bosnich, B. *Chem. Rev.* **2004**, *104*, 349-384.
- (55) Alsters, P. L.; Boersma, J.; Koten, G. v. *Organometallics* **1993**, *12*, 1629-1638.
- (56) Litz, K. E.; Holl, M. M. B.; Kampf, J. W.; Carpenter, G. B. *Inorg. Chem.* **1998**, *37*, 6461-6469.
- (57) Aboeella, N. W.; Lewis, E. A.; Reynolds, A. M.; Brennessel, W. W.; Cramer, C. J.; Tolman, W. B. *J. Am. Chem. Soc.* **2002**, *124*, 10660-10661.
- (58) Aboeella, N. W.; York, J. T.; Reynolds, A. M.; Fujita, K.; Kinsinger, C. R.; Cramer, C. J.; Riordan, C. G.; Tolman, W. B. *Chem. Commun.* **2004**, *15*, 1716-1717.
- (59) York, J. T.; Jr., V. G. Y.; Tolman, W. B. *Inorg. Chem.* **2006**, *45*, 4191-4198.
- (60) York, J. T.; Llobet, A.; Cramer, C. J.; Tolman, W. B. *J. Am. Chem. Soc.* **2007**, *129*, 7990-7999.
- (61) J. Donoghue, P.; Gupta, A. K.; Boyce, D. W.; Cramer, C. J.; Tolman, W. B. *J. Am. Chem. Soc.* **2010**, *132*, 15869-15871.
- (62) Chishiro, T.; Shimazaki, Y.; Tani, F.; Tachi, Y.; Naruta, Y.; Karasawa, S.; Hayami, S.; Maeda, Y. *Angew Chem. Int. Ed.* **2003**, *42*, 2788-2791.
- (63) Mahroof-Tahir, M.; Karlin, K. D. *J. Am. Chem. Soc.* **1992**, *114*, 7599-7601.
- (64) Nasir, M. S.; Karlin, K. D.; McGowty, D.; Zubieta, J. *J. Am. Chem. Soc.* **1991**, *113*, 698-700.
- (65) Murthy, N. N.; Mahroof-Tahir, M.; Karlin, K. D. *Inorg. Chem.* **2001**, *40*, 628-635.
- (66) Ohtsu, H.; Shimazaki, Y.; Odani, A.; Yamauchi, O.; Mori, W.; Itoh, S.; Fukuzumi, S. *J. Am. Chem. Soc.* **2000**, *122*, 5733-5741.
- (67) Ohtsu, H.; Itoh, S.; Nagatomo, S.; Kitagawa, T.; Ogo, S.; Watanabe, Y.; Fukuzumi, S. *Chem. Commun.* **2000**, 1051-1052.
- (68) Tachi, Y.; Aita, K.; Teramae, S.; Tani, F.; Naruta, Y.; Fukuzumi, S.; Itoh, S. *Inorg. Chem.* **2004**, *43*, 4558-4560.
- (69) Wu, A. J.; Penner-Hahn, J. E.; Pecoraro, V. L. *Chem. Rev.* **2004**, *104*, 903-938.
- (70) Yachandra, V. K.; Sauer, K.; Klein, M. P. *Chem. Rev.* **1996**, *96*, 2927-2950.

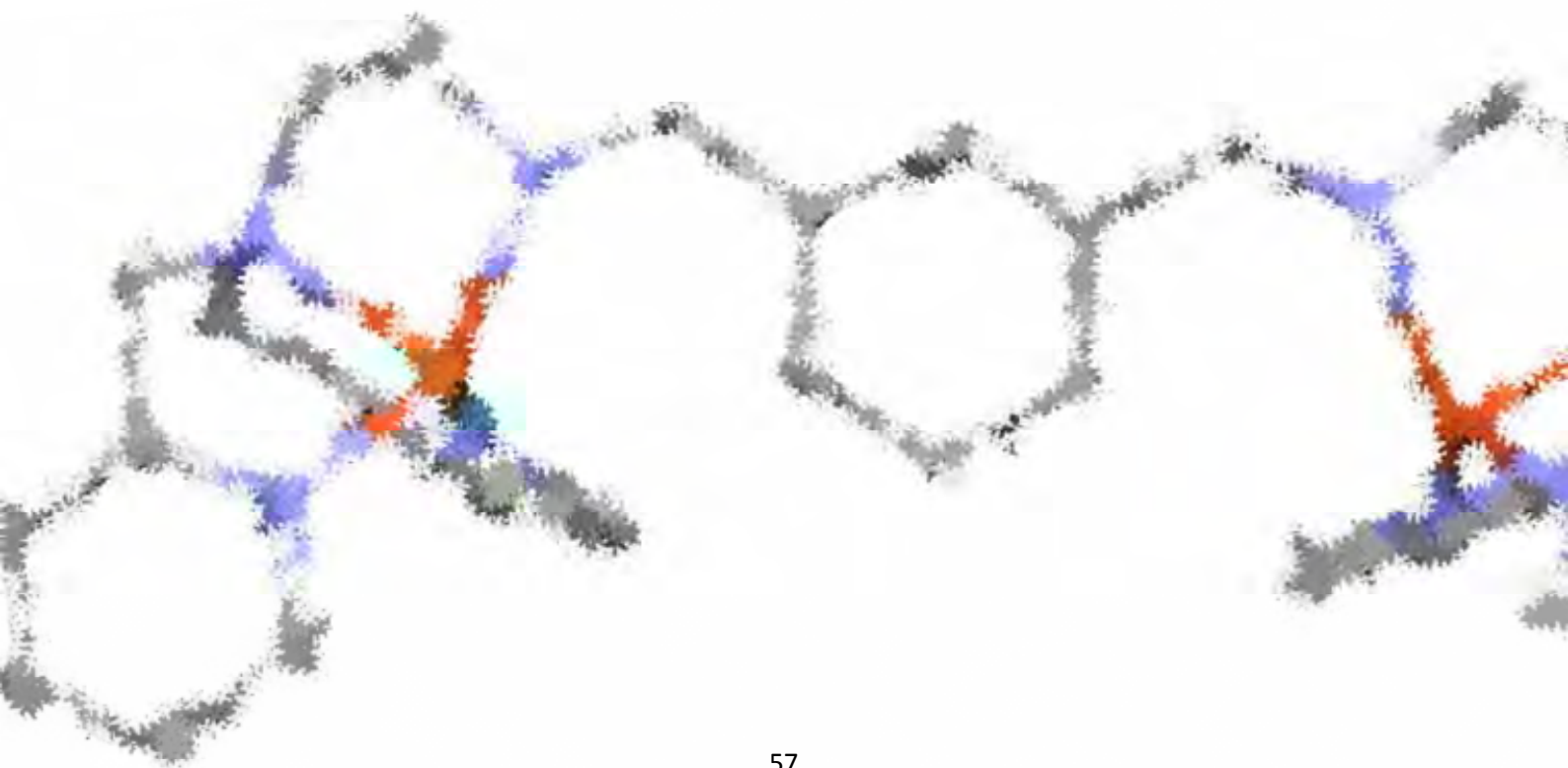
- (71) Wilcox, D. E. *Chem. Rev.* **1996**, *96*, 2435-2458.
- (72) Cotton, F. A.; Wilkinson, G.; Murillo, C. A.; Bochmann, M. *Advanced Inorganic Chemistry*; John Wiley & Sons, 1999.
- (73) Umena, Y.; Kawakami, K.; Shen, J.-R.; Kamiya, N. *Nature* **2011**, *473*, 55-60.
- (74) Yano, J.; Kern, J.; Sauer, K.; Latimer, M. J.; Pushkar, Y.; Biesiadka, J.; Loll, B.; Saenger, W.; Messinger, J.; Zouni, A.; Yachandra, V. K. *Science* **2006**, *314*, 821-825.
- (75) Sundaramoorthy, M.; Kishi, K.; Gold, M. H.; Poulos, T. L. *J. Biol. Chem.* **1994**, *269*, 32759-32767.
- (76) Whiting, A. K.; Boldt, Y. R.; Hendrich, M. P.; Wackett, L. P.; Que, L., Jr. *Biochemistry* **1996**, *35*, 160-170.
- (77) Boldt, Y. R.; Whiting, A. K.; Wagner, M. L.; Sadowsky, M. J.; Que, L., Jr. *Biochemistry* **1997**, *36*, 2147-2153.
- (78) Emerson, J. P.; Kovaleva, E. G.; Farquhar, E. R.; Lipscomb, J. D.; Que, L., Jr. *Proc. Natl. Acad. Sci. USA* **2008**, *105*, 7347-7352.
- (79) Su, C.; Oliw, E. H. *J. Biol. Chem.* **1998**, *273*, 13072-13079.
- (80) Su, C.; Sahlin, M.; Oliw, E. H. *J. Biol. Chem.* **2000**, *275*, 18830-18835.
- (81) Nam, W.; Goh, Y. M.; Lee, Y. J.; Lim, M. H.; Kim, C. *Inorg. Chem.* **1999**, *38*, 3238-3240.
- (82) Song, W. J.; Seo, M. S.; George, S. D.; Ohta, T.; Song, R.; Kang, M.-J.; Tosha, T.; Kitagawa, T.; Solomon, E. I.; Nam, W. *J. Am. Chem. Soc.* **2007**, *129*, 1268-1277.
- (83) Groves, J. T.; Lee, J.; Marla, S. S. *J. Am. Chem. Soc.* **1997**, *119*, 6269-9273.
- (84) Feichtinger, D.; Plattner, D. A. *Angew. Chem. Int. Ed. Engl.* **1997**, *36*, 1718-1719.
- (85) Kurahashi, T.; Kikuchi, A.; Shiro, Y.; Hada, M.; Fujii, H. *Inorg. Chem.* **2010**, *49*, 6664-6672.
- (86) Mandimutsira, B. S.; Ramdhanie, B.; Todd, R. C.; Wang, H.; Zareba, A. A.; Czernuszewicz, R. S.; Goldberg, D. P. *J. Am. Chem. Soc.* **2002**, *124*, 15170-15171.
- (87) Belal, A. A.; Chaudhuri, P.; Fallis, I.; Farrugia, L. J.; Hartung, R.; MacDonald, N. M.; Nuber, B.; Peacock, R. D.; Weiss, J.; Weighardt, K. *Inorg. Chem.* **1991**, *30*, 4397-4402.
- (88) Hage, R.; Iburg, J. E.; Kerschner, J.; Koek, J. H.; Lempers, E. L. M.; Martens, R. J.; Racherla, U. S.; Russell, S. W.; Swarthoff, T.; Vliet, M. R. P. v.; Warnaar, J. B.; Wolf, L. v. d.; Krijnen, B. *Nature* **1994**, *369*, 637-639
- (89) Larson, E. J.; Pecoraro, V. L. *J. Am. Chem. Soc.* **1991**, *113*, 3810-3818.
- (90) Larsen, A. S.; Wang, K.; Lockwood, M. A.; Rice, G. L.; Won, T.-J.; Lovell, S.; Sadílek, M.; Tureek, F.; Mayer, J. M. *J. Am. Chem. Soc.* **2002**, *124*, 10112-10123.
- (91) Lockwood, M. A.; Wang, K.; Mayer, J. M. *J. Am. Chem. Soc.* **1999**, *121*, 11894-11895.
- (92) Roth, J. P.; Yoder, J. C.; Won, T.-J.; Mayer, J. M. *Science* **2001**, *294*, 2524-2526.
- (93) Warren, J. J.; Tronic, T. A.; Mayer, J. M. *Chem. Rev.* **2010**, *110*, 6961-7001.

- (94) Goldsmith, C. R.; Cole, A. P.; Stack, T. D. P. *J. Am. Chem. Soc.* **2005**, *127*, 9904-9912.
- (95) MacBeth, C. E.; Golombek, A. P.; Young, V. G., Jr.; Yang, C.; Kuczera, K.; Hendrich, M. P.; Borovik, A. S. *Science* **2000**, *289*, 938-941.
- (96) Shirin, Z.; Hammes, B. S.; Young, V. G., Jr.; Borovik, A. S. *J. Am. Chem. Soc.* **2000**, *122*, 1836-1837.
- (97) Parsell, T. H.; Behan, R. K.; Green, M. T.; Hendrich, M. P.; Borovik, A. S. *J. Am. Chem. Soc.* **2006**, *128*, 8728-8729.
- (98) Lacy, D. C.; Gupta, R.; Stone, K. L.; Greaves, J.; Ziller, J. W.; Hendrich, M. P.; Borovik, A. S. *J. Am. Chem. Soc.* **2010**, *132*, 12188-12190.
- (99) Gupta, R.; Borovik, A. S. *J. Am. Chem. Soc.* **2003**, *125*, 13234-13242.
- (100) Parsell, T. H.; Yang, M.-Y.; Borovik, A. S. *J. Am. Chem. Soc.* **2009**, *131*, 2762-2763.
- (101) Yin, G.; McCormick, J. M.; Buchalova, M.; Danby, A. M.; Rodgers, K.; Day, V. W.; Smith, K.; Perkins, C. M.; Kitko, D.; Carter, J. D.; Scheper, W. M.; Busch, D. H. *Inorg. Chem.* **2006**, *45*, 8052-8061.
- (102) Yin, G.; Danby, A. M.; Kitko, D.; Carter, J. D.; Scheper, W. M.; Busch, D. H. *J. Am. Chem. Soc.* **2008**, *130*, 16245-16253.
- (103) Yin, G.; Danby, A. M.; Kitko, D.; Carter, J. D.; Scheper, W. M.; Busch, D. H. *J. Am. Chem. Soc.* **2007**, *129*, 1512-1513.
- (104) Sawant, S. C.; Wu, X.; Cho, J.; Cho, K.-B.; Kim, S. H.; Seo, M. S.; Lee, Y.-M.; Kubo, M.; Ogura, T.; Shaik, S.; Nam, W. *Angew. Chem. Int. Ed.* **2010**, *49*, 8190-8194.
- (105) Boer, J. W. d.; Brinksma, J.; Browne, W. R.; Meetsma, A.; Alsters, P. L.; Hage, R.; Feringa, B. L. *J. Am. Chem. Soc.* **2005**, *127*, 7990-7991.
- (106) Murphy, A.; Dubois, G.; Stack, T. D. P. *J. Am. Chem. Soc.* **2003**, *125*, 5250-5251.
- (107) Murphy, A.; Pace, A.; Stack, T. D. P. *Org. Lett.* **2004**, *6*, 3119-3122.
- (108) Sham, K.-C.; Weung, H.-L.; Yiu, S.-M.; Lau, T.-C.; Kwong, H.-L. *Dalton Trans.* **2010**, *39*, 9469-9471.
- (109) Kwong, H.-K.; Lo, P.-K.; Lau, K.-C.; Lau, T.-C. *Chem. Commun.* **2011**, *47*, 4273-4275.
- (110) Hao, E.; Wang, Z.; Jiao, L.; Wang, S. *Dalton Trans.* **2010**, *39*, 2660-2666.
- (111) Madhu, V.; Ekambaram, B.; Shimon, L. J. W.; Diskin, Y.; Leitun, G.; Neumann, R. *Dalton Trans.* **2010**, *39*, 7266-7275.
- (112) Zhong, S.; Fu, Z.; Tan, Y.; Xie, Q.; Xie, F.; Zhou, X. g.; Ye, Z.; Peng, G.; Yin, D. *Adv. Synth. Catal.* **2008**, *350*, 802-806.
- (113) Wortmann, R.; Flörke, U.; Sarkar, B.; Umamaheshwari, V.; Gescheidt, G.; Herres-Pawlis, S.; Henkel, G. *Eur. J. Inorg. Chem.* **2011**, 121-130.

- (114) Zhang, W.; Loebach, J. L.; Wilson, S. R.; Jacobsen, E. N. *J. Am. Chem. Soc.* **1990**, *112*, 2801-2803.
- (115) Katsuki, T. *Coord. Chem. Rev.* **1995**, *140*, 189-214.
- (116) Gómez, L.; Garcia-Bosch, I.; Company, A.; Sala, X.; Fontrodona, X.; Ribas, X.; Costas, M. *Dalton Trans.* **2007**, 5539-5545.
- (117) Wu, M.; Wang, B.; Wang, S.; Xia, C.; Sun, W. *Org. Lett.* **2009**, *11*, 3622-3625.
- (118) Ilyashenko, G.; Sale, D.; Montevalli, M.; Watkinson, M. *J. Mol. Catal. A: Chem.* **2008**, *296*, 1-8.
- (119) Rich, J.; Rodriguez, M.; Romero, I.; Vaquer, L.; Sala, X.; Llobet, A.; Corbella, M.; Collomb, M. N.; Fontrodona, X. *Dalton Trans.* **2009**, 8117-8126.
- (120) Ottenbacher, R. V.; Bryliakov, K. P.; Talsi, E. P. *Adv. Synth. Catal.* **2011**, *353*, 885-889.
- (121) Ottenbacher, R. V.; Bryliakov, K. P.; Talsi, E. P. *Inorg. Chem.* **2010**, *49*, 8620-8628.
- (122) Yin, G.; Buchalova, M.; Danby, A. M.; Perkins, C. M.; Kitko, D.; Carter, J. D.; Scheper, W. M.; Busch, D. H. *J. Am. Chem. Soc.* **2005**, *127*, 17170-17171.
- (123) Lee, S. H.; Xu, L.; Byeong Kwon Park; Mironov, Y. V.; Kim, S. H.; Song, Y. J.; Kim, C.; Kim, Y.; Kim, S.-J. *Chem. Eur. J.* **2010**, *16*, 4678 - 4685.

Chapter II

General Objectives

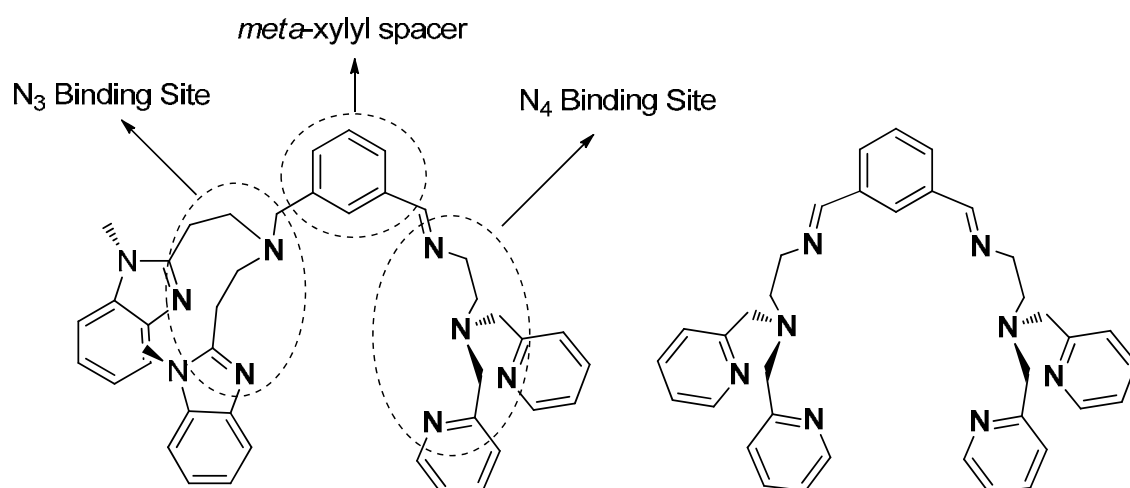


II. General Objectives.

Over the last decades, bioinorganic chemistry has tried to understand how natural systems were able to mediate selective oxidative transformations. This knowledge not only has importance in understanding biological systems but also in technological applications like selective oxidation reactions to form value-added chemicals. With this purpose, the use of model systems that structurally and functionally reproduce a metalloenzyme have been widely explored. In this context, low molecular weight systems with copper, iron, manganese, nickel or zinc (predominant metals in the active centers of metalloproteins) have been used in the understanding of the principles by which oxidation reactions take place in living systems.

In this thesis we benefit from the model chemistry approach to develop copper and manganese systems for the activation of oxygen or for the use of reduced forms of oxygen. Furthermore, these complexes will be used in catalysis of oxidation.

In the first part of the dissertation (Chapter III), we will center our attention in the development of dicopper complexes inspired in the active center of the type III copper proteins (Tyr, Hc). In light of this, we foresee the use of dinucleating ligands with two coordination sites which are connected by a *meta*-xylyl moiety. In order to understand the importance of asymmetry in dinuclear copper complexes, we planned the synthesis of an asymmetric ligand with two different coordination sites and its symmetric analog (Scheme 1).



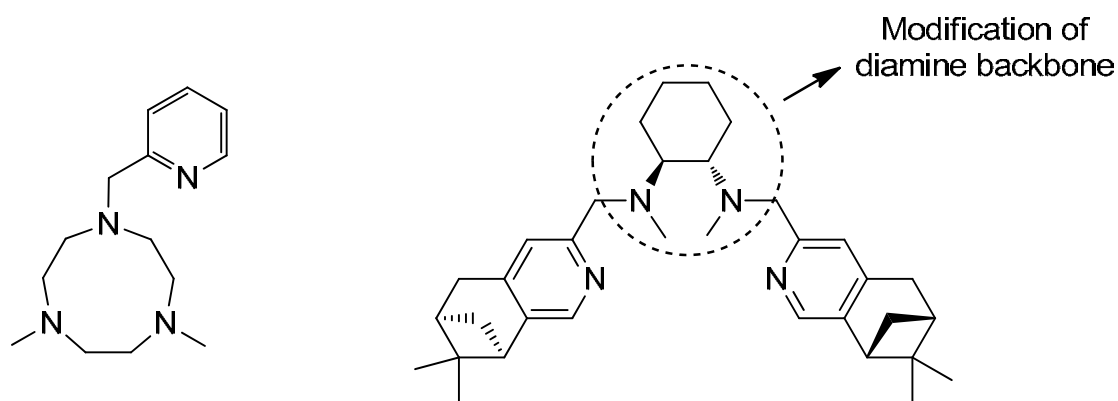
Scheme 1. Design of two-unequivalent sites dinucleating ligand and its symmetrical analog.

After the synthesis of dicopper(I) complexes, we will inspect their reactivity towards O_2 where the generation of intermediate species will be examined in detail. Then, the features and reactivity of the new $Cu_2:O_2$ species will be compared, in particular the ability of the

intermediate species to reproduce bioinspired oxidations such as the *ortho*-hydroxylation of phenolic substrates.

In the second part of this thesis, we will put our efforts in the development of mononuclear manganese systems as oxidation catalysts. For this purpose, we envision the use of a tetracoordinating ligand, which is derived from the Me₃TACN by fusing a pyridine ring to its structure (Scheme 2). On one hand, we will synthesize the corresponding manganese complex in high oxidation states studying its spectroscopic and chemical properties (Chapter IV). Moreover, the reaction of the high-valent manganese species towards C-H bonds will be mechanistically studied in detail. On the other hand, the corresponding manganese(II) complex will be tested in the epoxidation of alkenes with environmentally benign oxidants such as hydrogen peroxide or peracetic acid (Chapter V.1 and Chapter V.2).

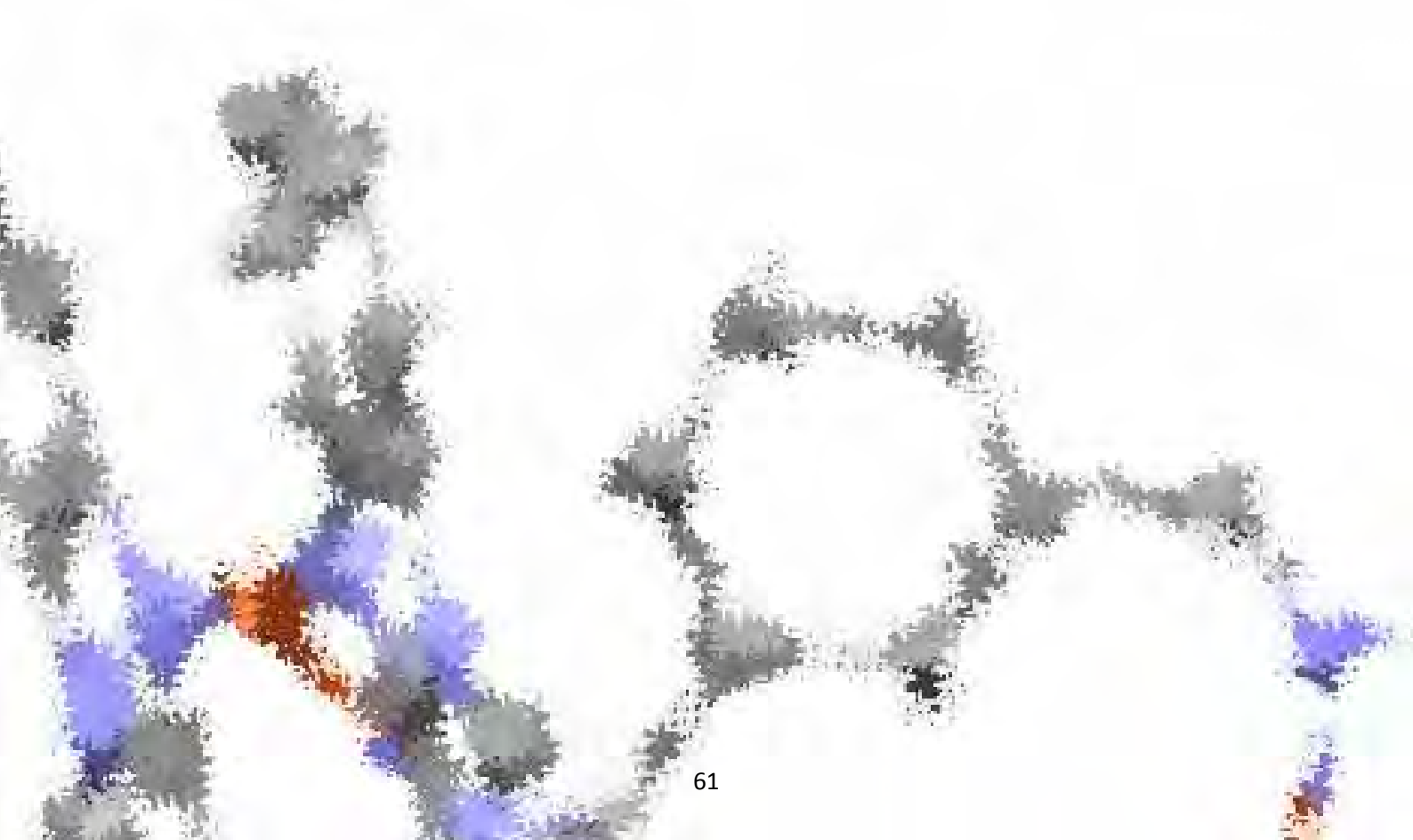
Finally, we aim to design chiral mononuclear manganese complexes based in the mcpp precedent (Scheme 2), which will be used in stereoselective alkene epoxidations under mild conditions, a reaction of special technological interest (Chapter V.3).



Scheme 2. Ligands used in the synthesis of mononuclear manganese complexes.

Chapter III

O₂ Activation by an Unsymmetric Dinuclear Copper Complex



Chapter III.1

O₂ Activation and Selective Phenolate *ortho* Hydroxylation by an Unsymmetric Dicopper μ - η^1 : η^1 - Peroxido Complex

Garcia-Bosch, I.; Company, A.; Frisch, J. R.; Torrent-Sucarrat, M.; Cardellach, M.; Gamba, I.; Güell, M.; Casella, L.; Que, L.; Ribas, X.; Luis, J. M.; Costas, M. *Angew. Chem. Int. Ed.* **2010**, *49*, 2406-2409.

Isaac Garcia-Bosch, Anna Company, Jonathan R. Frisch, Miquel Torrent-Sucarrat, Mar Cardellach, Ilaria Gamba, Mireia Güell, Luigi Casella, Lawrence Que Jr., Xavi Ribas, Josep M. Luis, Miquel Costas. "O₂ Activation and Selective Phenolate *ortho* Hydroxylation by an Unsymmetric Dicopper μ - η^1 : η^1 -Peroxido Complex". *Angewandte Chemie International Edition*. Vol. 49, issue 13 (March 2010) : p. 2406-2409
Copyright © 2010 WILEY-VCH Verlag GmbH & Co. KGaA

<http://dx.doi.org/10.1002/anie.200906749>

<http://onlinelibrary.wiley.com/doi/10.1002/anie.200906749/abstract>

Abstract

Unusual reactivity: A novel unsymmetric dicopper complex gives rise to the unsymmetric species 1-O₂ having a μ - η^1 : η^1 -O₂ binding mode and reactivity patterns not previously observed for symmetric analogues. It is unreactive in oxygen atom transfer reactions, but it can selectively bind phenolate and mediate its *ortho* hydroxylation, thereby demonstrating a conceptually different tyrosinase model with exquisite selectivity.

Keywords

- bioinorganic chemistry;
- dioxygen ligands;
- O—O activation;
- oxidation



Supporting information:

Detailed facts of importance to specialist readers are published as "Supporting Information". Such documents are peer-reviewed, but not copy-edited or typeset. They are made available as submitted by the authors.

http://onlinelibrary.wiley.com/store/10.1002/anie.200906749/asset/supinfo/anie_200906749_sm_miscellaneous_information.pdf?v=1&s=f3c0b5a8b6c90312c20a5abe5af5298af261333f

Please note: Wiley-Blackwell are not responsible for the content or functionality of any supporting materials supplied by the authors. Any queries (other than missing material) should be directed to the corresponding author for the article.

Supporting Information

© Wiley-VCH 2010

69451 Weinheim, Germany

**O₂ Activation and Selective Phenolate *ortho* Hydroxylation by an
Unsymmetric Dicopper μ - η^1 : η^1 -Peroxido Complex****

*Isaac Garcia-Bosch, Anna Company, Jonathan R. Frisch, Miquel Torrent-Sucarrat,
Mar Cardellach, Ilaria Gamba, Mireia Güell, Luigi Casella,* Lawrence Que, Jr.,* Xavi Ribas,*
Josep M. Luis,* and Miquel Costas**

anie_200906749_sm_miscellaneous_information.pdf

Contents

1. Physical Methods	S2
2. Materials	S2
3. Synthesis of ligands and complexes	S2
4. Generation of the intermediates and characterization	S7
5. Intermediates reactivity	S10
6. Computational details	S20
7. References	S39

1. Physical Methods

IR spectra were taken in a Mattson-Galaxy Satellite FT-IR spectrophotometer using a MKII Golden Gate single reflection ATR system. UV-vis spectroscopy was performed on a Cary 50 Scan (Varian) UV-vis spectrophotometer with 1 cm quartz cells. The low temperature control was performed with a cryostat from Unisoku Scientific Instruments, Japan. Elemental analyses were performed using a CHNS-O EA-1108 elemental analyzer from Fisons. NMR spectra were taken on Bruker DPX200 and DPX400 spectrometers using standard conditions. Resonance Raman spectra were collected on an Acton AM-506 spectrometer (1200 groove grating) using a Kaiser Optical holographic super-notch filters with a Princeton Instruments liquid-N₂-cooled (LN-1100PB) CCD detector with a 4 cm⁻¹ spectral resolution. The 488 nm laser excitation line was obtained with a Spectra Physics BeamLok 2065-7S argon ion laser. The Raman frequencies were referenced to indene. Solutions of **1O**₂ in acetone (1 mM) were prepared in a schlenk flask and were exposed to pure O₂ at -90°C. The resulting dark solutions were frozen within 20-30 seconds at 77 K on a gold-plated copper cold finger in thermal contact with a Dewar containing liquid N₂. Solutions of **2O**₂ in acetone (1 mM) were prepared in a NMR tube and were exposed to pure O₂ at -90°C. The resulting dark solutions were frozen within 20-30 seconds at 77 K in the NMR tube by placing it in a Dewar containing liquid N₂. No photobleaching was observed upon repeated scans. Baseline corrections (polynomial fits) were carried out using Grams/32 Spectral Notebase Version 4.04 (Galactic). All HPLC-MS spectra were obtained on a Micromass ZQ mass spectrometer in electrospray positive ionization (ESI+) mode in-line with a Waters® 2795 HPLC system (separation module, Alliance™) and a Waters® Dual Absorbance Detector.

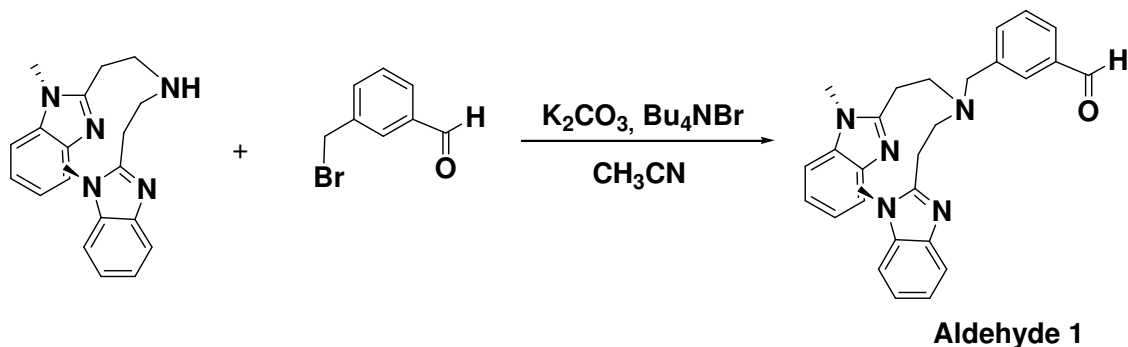
2. Materials

Reagents and solvents used were of commercially available reagent quality unless otherwise stated. Solvents were purchased from SDS and Scharlab. Acetonitrile and diethyl ether were purified and dried by passing through an activated alumina purification system (MBraun SPS-800) and anhydrous acetone was purchased from Across Organics (99.8 % extra dry, water < 50 ppm) and stored into the glove box. Preparation and handling of air-sensitive materials were carried out in a N₂ drybox (MBraun) with O₂ and H₂O concentrations < 1 ppm.

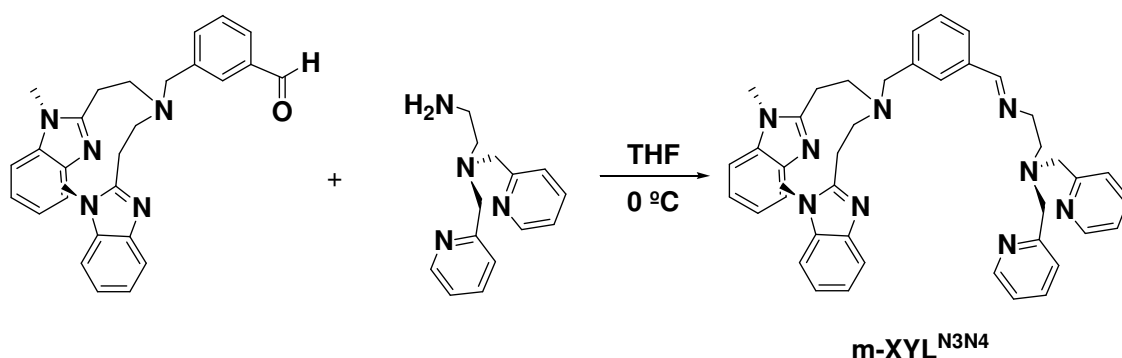
3. Synthesis of ligands and complexes

Caution: Perchlorate salts are all potentially explosive and should be handled with care.

m-(Bromomethyl)benzaldehyde was synthesized and purified as previously reported.¹ *N,N*-Bis(2-pyridylmethyl)ethylenediamine,² *N,N'*-bis[2-(1'-methyl-2'-benzimidazolyl)ethyl]amine³ and $\text{Cu}(\text{CH}_3\text{CN})_4\text{X}$, X = ClO_4 , CF_3SO_3 and PF_6 were prepared as described in the literature.^{4, 5} Sodium *p*-X-phenolate (X= F, Me, H, Cl, MeO, CN, NO_2 , CO_2Me) were prepared as earlier described.⁶

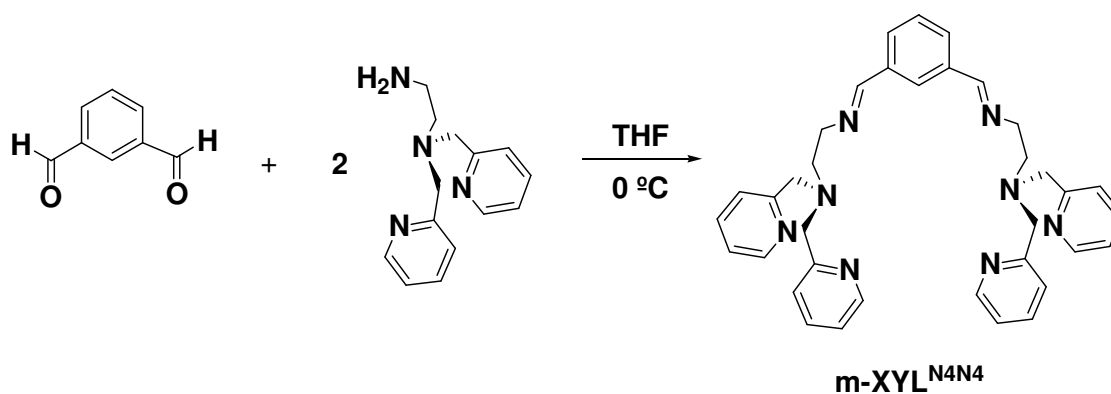


3.1 Synthesis of aldehyde 1: 3-(Bromomethyl)benzaldehyde (0.29 g, 1.5 mmol) and *N,N'*-bis[2-(1'-methyl-2'-benzimidazolyl)ethyl]amine (0.5 g, 1.5 mmol) were dissolved in CH_3CN (30 mL). K_2CO_3 (0.30 g, 2.1 mmol) and a small amount of Bu_4NBr (5 mg, 16 μmol s) were added directly as solids to the resulting mixture which was then refluxed under N_2 for 14 hours. After that time, the mixture was cooled down to room temperature, and the solvent was removed under reduced pressure. The resulting white solid was treated with H_2O (15 mL) and extracted with CH_2Cl_2 (4x15 mL). The combined organic phases were dried over MgSO_4 , filtered and the solvent was removed under reduced pressure to obtain 0.53 g of the desired product (1.2 mmol, 80%) as a brown oil. Anal. Calcd for $\text{C}_{28}\text{H}_{29}\text{N}_5\text{O}$: C, 74.47; N, 15.51; H, 6.47 %. Found: C, 74.22; N, 15.60; H, 6.31 %. FT-IR: $\nu = 1692 \text{ cm}^{-1}$ (C=O). $^1\text{H-NMR}$ (400 MHz, CDCl_3 , 300K) δ , ppm: 9.74 (s, 1H, CHO), 7.68 - 7.18 (m, 12H, Ar-H), 3.85 (s, 2H, Ar- CH_2 -NR), 3.55 (s, 6H, N- CH_3), 3.20 (m, 4H, N- CH_2 - CH_2), 3.00 (m, 4H, N- CH_2 - CH_2).

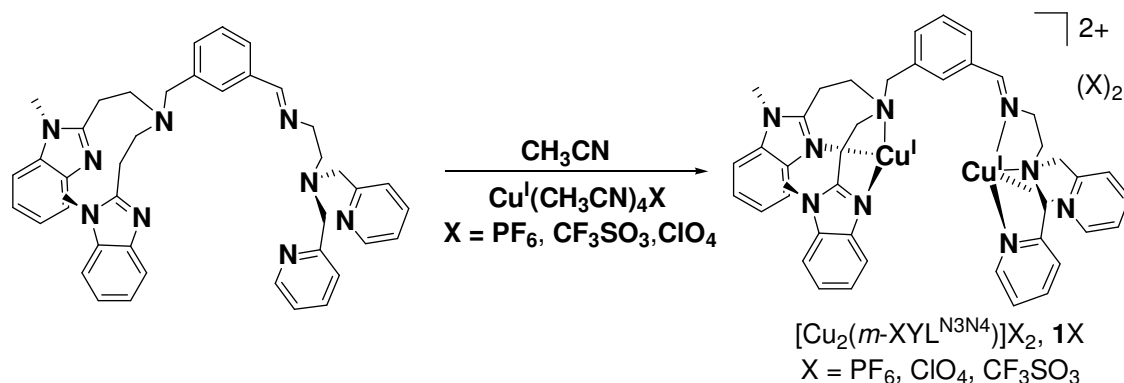


3.2 Synthesis of m-XYL^{N3N4}: *N,N*-Bis(2-pyridylmethyl)ethylenediamine (0.16 g, 0.64 mmol) was dissolved in THF (5 mL) and cooled in an ice bath at 0 °C. A solution of aldehyde 1 (0.3 g, 0.64 mmol) in THF (10 mL) was added dropwise under vigorous stirring. The mixture was left

to attain room temperature and it was stirred for further 5 hours. Then, the solvent was removed under reduced pressure and the resultant product was dried under vacuum to obtain 0.36 g of *m*-XYL^{N3N4} (0.54 mmol, 84 %) as an orange oil. Anal. Calcd for C₄₂H₄₅N₉·H₂O: C, 72.70; N, 18.17; H, 6.83 %. Found: C, 72.71; N, 17.48; H, 7.40 %. FT-IR: ν = 1644 (C=N), 1472, 1440 (C=C)_{arom} cm⁻¹. ¹H-NMR (400 MHz, CDCl₃, 300K) δ , ppm (**Figure S1**): 8.49 (m, 3H, pyH α + CH=N), 8.03 (s, 1H, Ar-H), 7.69-7.40 (m, 8H, Ar-H + pyH β + pyH γ), 7.25-7.05 (m, 9H, Ar-H + pyH β), 3.93 (s, 4H, py-CH₂), 3.82 (m, 2H, C=N-CH₂), 3.73 (m, 2H, Ar-CH₂), 3.51 (s, 6H, N-CH₃), 3.17 (m, 4H, N-CH₂-CH₂), 3.05 (m, 6H, N-CH₂-CH₂ + C=N-CH₂-CH₂). ¹³C-RMN: (100 MHz, CDCl₃, 300K) δ , ppm 161.89, 159.78, 158.78, 153.59, 148.98, 142.47, 139.89, 136.74, 136.41, 136.28, 130.93, 128.26, 123.15, 122.80, 122.13, 121.99, 121.88, 118.97, 109.00, 67.97, 60.70, 59.43, 54.84, 51.88, 29.66, 25.98. ESI-MS (m/z): 698.4 [M+Na]⁺ (100), 676.4 [M+H]⁺ (3).



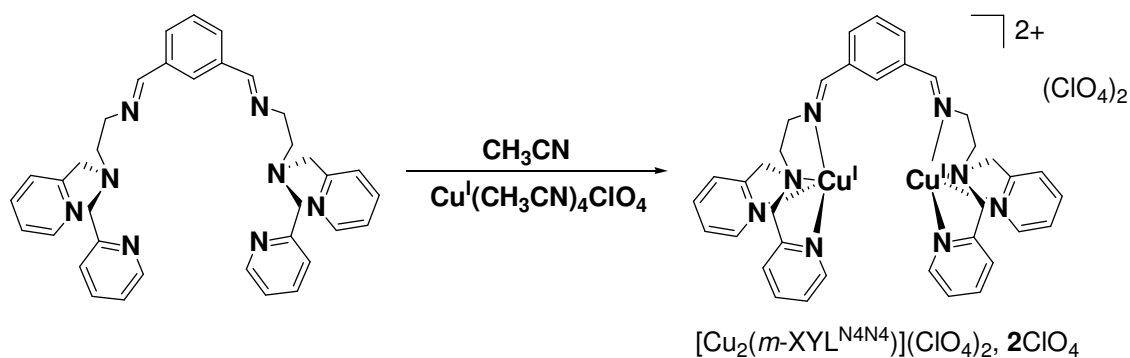
3.3 Synthesis of *m*-XYL^{N4N4}. 1.21 g of *N,N*-Bis(2-pyridylmethyl)ethylenediamine (4.99 mmols) were placed in a 50 mL round bottom flask and dissolved in THF (10 mL). The mixture was cooled in an ice bath and a solution of 0.29 g of isophthalaldehyde (2.06 mmols) in THF (13 mL) was added dropwise to the vigorously stirred solution of the amine. The mixture was allowed to warm up to room temperature and left under stirring during 15 hours. At this point, the solvent was removed under vacuum to obtain the product as a yellow-orange oil (1.19 g, 2.04 mmols, 99%). Anal. Calcd for C₃₆H₃₈N₈: C, 74.20; N, 19.23; H, 6.57 %. Found: C, 73.95; N, 19.20; H, 6.70 %. FT-IR: ν = 2837 (C-H)_{sp³}, 1645 (C=N), 1590, 1433 (pyr) cm⁻¹. ¹H-RMN (400 MHz, CDCl₃, 300 K) δ , ppm (**Figure S1**): 8.52 (d, J = 5.5Hz, 4H, pyH α), 8.30 (s, 2H, CH=N), 8.03 (s, 1H, Ar-H), 7.79 – 7.75 (d, J = 7.2 Hz, 2H, Ar-H), 7.58 – 7.49 (m, 9H, Ar-H + pyH γ + pyH β), 7.13 – 7.08 (t, J = 5.5 Hz, 4H, pyH β), 3.94 (s, 8H, N-CH₂-py), 3.82 – 3.74 (t, J = 6.4 Hz, 4H, CH=N-CH₂), 3.01 – 2.95 (t, J = 6.4 Hz, 4H, CH=N-CH₂-CH₂). ¹³C-RMN (50 MHz, CDCl₃, 300K) δ , ppm: 161.22, 159.71, 158.74, 148.92, 136.66, 129.83, 123.06, 122.80, 122.23, 121.86, 60.69, 59.60, 54.79. ESI-MS (m/z): 583.3 [M+H]⁺ (100), 601.4 [M+H₂O+H]⁺ (70).



3.4 Synthesis of $[\text{Cu}_2(m\text{-XYL}^{\text{N}3\text{N}4})](\text{CF}_3\text{SO}_3)_2$ (1CF₃SO₃**):** $m\text{-XYL}^{\text{N}3\text{N}4}$ (50 mg, 73 μmol) was dissolved in CH_3CN (1 mL) and $[\text{Cu}(\text{CH}_3\text{CN})_4]\text{CF}_3\text{SO}_3$ (55 mg, 146 μmol) was added directly as a solid into the vigorously stirred solution, generating a deep orange-red solution. After 30 min, the resulting solution was filtered through Celite©. Slow diethyl ether diffusion afforded the desired compound as orange crystals suitable for X-Ray diffraction (60 mg, 54 μmol , 75%). Anal. Calcd for $\text{C}_{44}\text{H}_{45}\text{N}_9\text{Cu}_2\text{F}_6\text{O}_6\text{S}_2 \cdot 2\text{H}_2\text{O}$: C, 47.22; N, 11.26; H, 4.23; S, 5.73 %. Found: C, 47.03; N, 11.27; H, 4.38; S, 5.11 %. FT-IR: $\nu = 1636$ (C=N), 1481, 1455 (C=C)_{arom}, 1257, 1224, 1148, 1030, 634 (CF_3SO_3) cm^{-1} . $^1\text{H-NMR}$ (400 MHz, CD_3CN , 300K) δ , ppm (**Figure S1**): 8.52 (d, 2H, $J = 4$ Hz, αHpy), 8.03 – 7.80 (m, 6H, CH=N + Ar-H), 7.55-7.35 (m, 13H, Ar-H + pyH β + pyH γ), 4.11 (s, 4H, py-CH₂), 4.06 (s, 2H, Ar-CH₂), 3.86 (m, 8H, N-CH₃ + CH=N-CH₂), 3.32 (m, 8H, N-CH₂-CH₂), 3.05 (t, 2H, $J = 2$ Hz, CH=N-CH₂-CH₂).

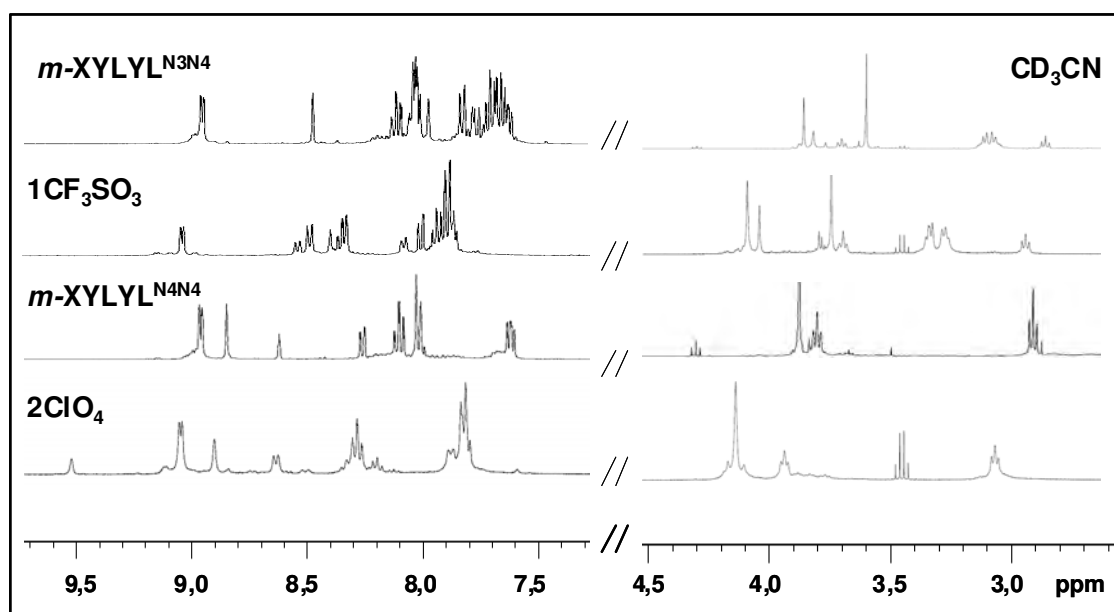
3.5 Synthesis of $[\text{Cu}_2(m\text{-XYL}^{\text{N}3\text{N}4})](\text{ClO}_4)_2$ (1ClO₄**):** This compound was synthesized in analogous manner to complex **1CF₃SO₃** (42 mg, 42 μmol , 60%). Anal. Calcd for $\text{C}_{42}\text{H}_{45}\text{N}_9\text{Cu}_2\text{Cl}_2\text{O}_8 \cdot 2\text{H}_2\text{O}$: C, 48.60; N, 12.15; H, 4.76 %. Found: C, 48.35; N, 12.65; H, 4.90 %. FT-IR: $\nu = 1636$ (C=N), 1481, 1455 (C=C)_{arom}, 1075, 621 (ClO_4) cm^{-1} .

3.6 Synthesis of $[\text{Cu}_2(m\text{-XYL}^{\text{N}3\text{N}4})](\text{PF}_6)_2$ (1PF₆**):** This compound was synthesized in analogous manner to complex **1CF₃SO₃** (52 mg, 48 μmol , 66%). Anal. Calcd for $\text{C}_{42}\text{H}_{45}\text{N}_9\text{Cu}_2\text{P}_2\text{F}_{12} \cdot 2\text{H}_2\text{O}$: C, 44.68; N, 11.17; H, 4.37 %. Found: C, 44.80; N, 11.22; H, 4.10 %. FT-IR: $\nu = 1636$ (C=N), 1481, 1455 (C=C)_{arom}, 750, 655 cm^{-1} .



3.7 Synthesis of $[\text{Cu}_2(m\text{-XYL}^{\text{N}4\text{N}4})](\text{ClO}_4)_2 (2\text{ClO}_4)$: $m\text{-XYL}^{\text{N}4\text{N}4}$ (30 mg, 50 μmol) was dissolved in CH_3CN (1 mL) and $[\text{Cu}(\text{CH}_3\text{CN})_4]\text{ClO}_4$ (34 mg, 100 μmol) was added directly as a solid into the vigorously stirred solution, generating a deep orange-red solution. After 30 min, the resulting solution was filtered through Celite©. Slow diethyl ether diffusion afforded the desired compound as an orange solid which was dried under vacuum (40 mg, 44 μmol , 88%). Anal. Calcd for $\text{C}_{36}\text{H}_{38}\text{N}_8\text{Cu}_2\text{Cl}_2\text{O}_8 \cdot 2\text{H}_2\text{O}$: C, 45.77; N, 11.86; H, 4.48 %. Found: C, 45.67; N, 12.39; H, 4.31 %. FT-IR: $\nu = 1602$ (C=N), 1433 (C=C)_{arom}, 1076, 620 (ClO_4) cm^{-1} . $^1\text{H-NMR}$ (400 MHz, CD_3CN , 300K) δ , ppm (**Figure S1**): 9.02 (s, 1H, Ar-H), 8.54 (d, 4H, $J = 4.0$ Hz, pyH α), 8.43 (s, 2H, CH=N), 8.17 (d, $J = 7.4$ Hz, 2H, Ar-H), 7.86-7.70 (m, 5H, Ar-H + pyH γ), 7.39 (d, $J = 7.4$ Hz, 8H, pyH β + pyH β'), 4.14 (s, 8H, N-CH₂-py), 3.94 (t, $J = 5.4$ Hz, 4H, CH=N-CH₂), 3.05 (t, 4H, $J = 5.4$ Hz, CH=N-CH₂-CH₂).

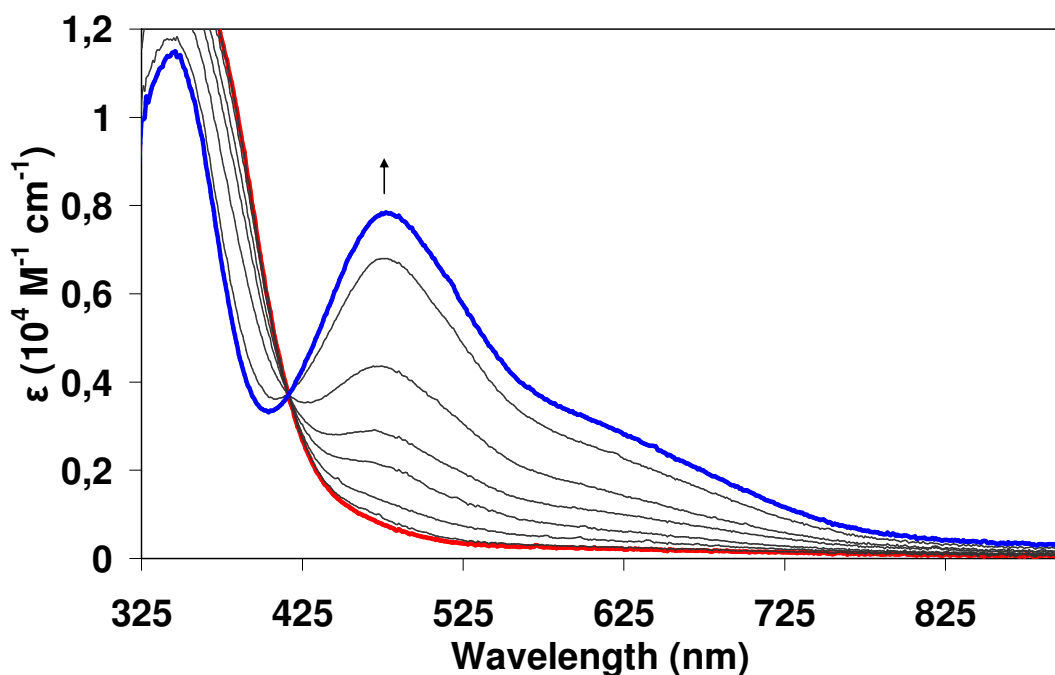
Figure S1. $^1\text{H-NMR}$ characterization of $m\text{-XYL}^{\text{N}3\text{N}4}$, $m\text{-XYL}^{\text{N}4\text{N}4}$, $1\text{CF}_3\text{SO}_3$, and 2ClO_4 .



4. Generation of intermediates and characterization.

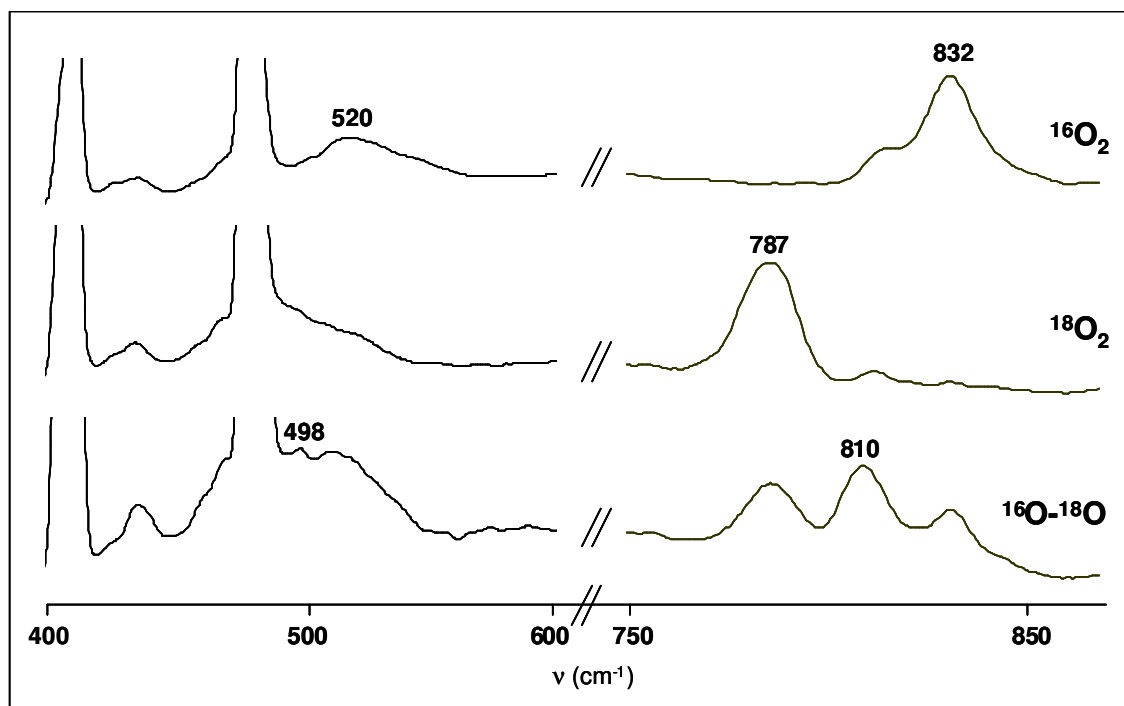
4.1 Generation of $[\text{Cu}_2(m\text{-XYL}^{N3N4})(\text{O}_2)]^{2+}$ (1O_2) monitored by UV-vis Spectroscopy: A solution of $1\text{CF}_3\text{SO}_3$ (0.18 mM) in anhydrous acetone was placed in a low temperature UV-vis cell into the drybox, which was subsequently capped with a septum. The cell was taken out of the box, placed in the Unisoku cryostat of the UV-vis spectrophotometer, and cooled to 183K. After reaching thermal equilibrium an UV-vis spectrum of the starting $1\text{CF}_3\text{SO}_3$ complex was recorded. Dioxygen gas was injected into the cell with a balloon and a needle through the septum causing immediate reaction: the solution changed from yellow to red-brown ($\lambda_{\text{max}} = 478$ nm, $\epsilon = 7700 \text{ M}^{-1}\text{cm}^{-1}$) (**Figure S2**).

Figure S2. UV-Vis spectra of the generation of 1O_2 ($[1\text{CF}_3\text{SO}_3] = 0.18$ mM in acetone at -90 °C).



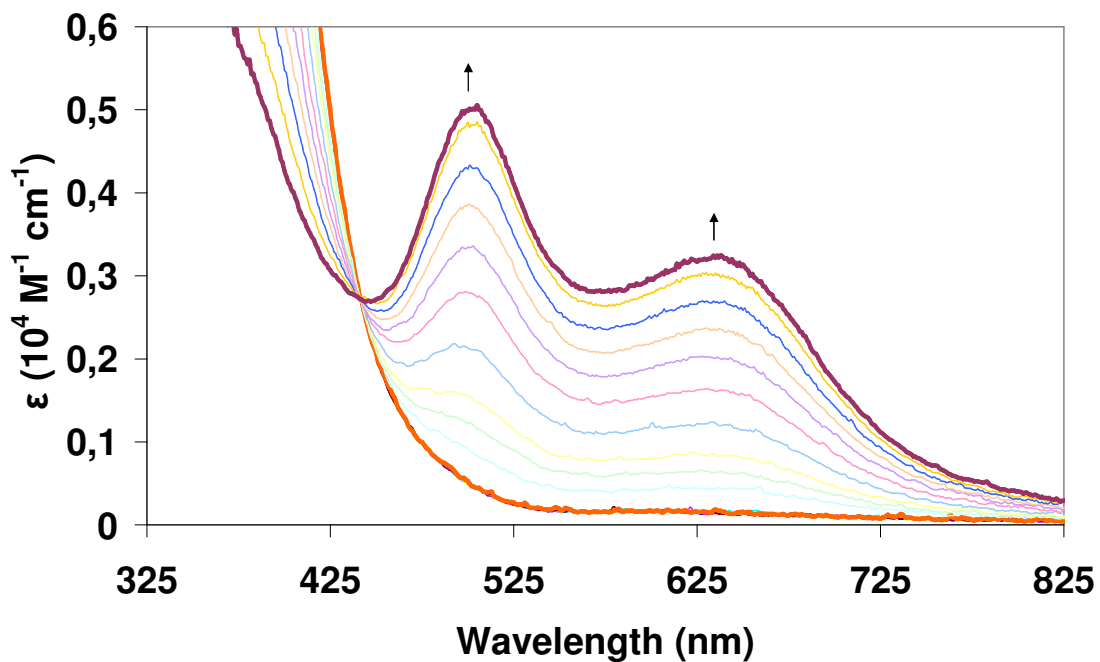
4.2 Characterization of $[\text{Cu}_2(m\text{-XYL}^{N3N4})(\text{O}_2)]^{2+}$ (1O_2) by rRaman Spectroscopy:

Figure S3. Resonance Raman spectra ($\lambda_{\text{ex}} = 488 \text{ nm}$) of 1O_2 .



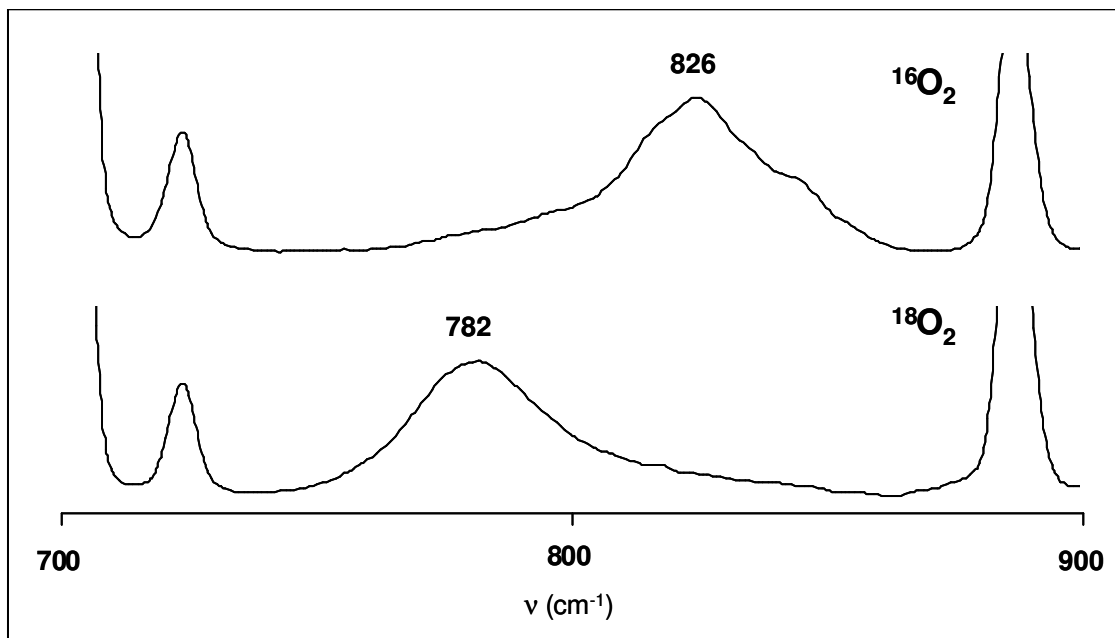
4.3 Generation of $[\text{Cu}_2(m\text{-XYL}^{N_4N_4})(\text{O}_2)]^{2+}$ (2O_2) monitored by UV-vis Spectroscopy: In the glovebox, a solution of 2ClO_4 (0.18 mM) in anhydrous acetone was placed into a low temperature UV-vis cell which was subsequently capped with a septum. The cell was taken out of the box and placed in the Unisoku cryostat of the UV-vis spectrophotometer, cooled to 183K. After reaching thermal equilibrium an UV-vis spectrum of the starting 2ClO_4 complex was recorded. Dioxygen gas was injected to the cell with a balloon and a needle through the septum causing immediate reaction: the solution changed from yellow to purple ($\lambda_{\text{max}} = 500 \text{ nm}$, $\epsilon = 5000 \text{ M}^{-1}\text{cm}^{-1}$). (**Figure S4**)

Figure S4. UV-Vis spectra of the generation of $2O_2$ ($[2ClO_4] = 0.18$ mM in acetone at $-90^\circ C$).



4.4 Characterization of $[Cu_2(m-XYL^{N4N4})(O_2)]^{2+}$ ($2O_2$) by *rRaman* Spectroscopy:

Figure S5. Resonance Raman spectra ($\lambda_{ex} = 488$ nm) of $2O_2$.



5. Intermediates reactivity.

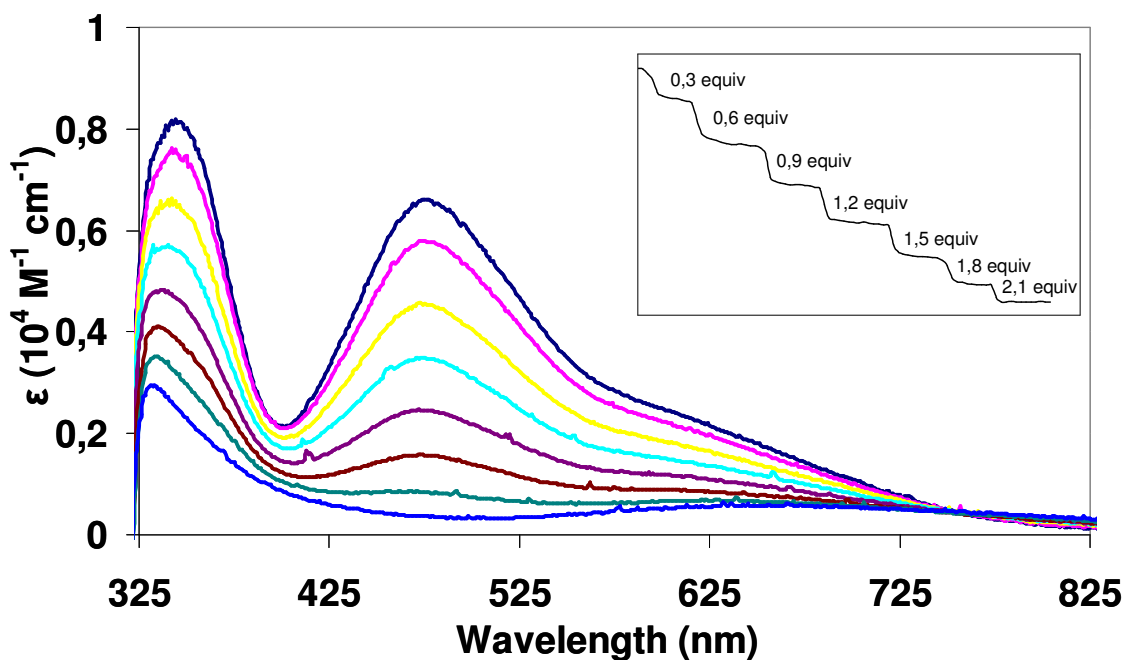
5.1 Reaction of $1O_2$ with TFA (H^+). Quantitative determination of H_2O_2 by the Peroxotitanyl

Method. 3 mg of $1CF_3SO_3$ were dissolved in anhydrous acetone (10 mL) in a flask with a stirbar in the glovebox, which was then capped with a septum. The flask was taken out of the box and cooled to 183 K. Dioxygen gas was injected to the flask with a balloon and a needle through the septum causing immediate formation of $1O_2$. After 5 minutes, the excess of dioxygen was removed by N_2 /vacuum cycles. Then, 1 mL of a solution of trifluoroacetic acid (2 equiv.) in acetone (prepared by diluting 0.43 mL of TFA in 10 mL of anhydrous acetone) was added. The solution color immediately changed from deep red brown to green. The solution was removed from the cold bath and 10 mL of distilled water were added. H_2O_2 was determined spectrophotometrically at 408 nm upon addition of 1 mL of titanium(IV) oxysulfate in sulfuric acid to 10 mL of the crude solution. The yield of H_2O_2 was determined by correlation with a calibration curve. The resulting yield was 99% of H_2O_2 .

5.2 Reaction of $1O_2$ with H^+ monitored by UV-vis Spectroscopy, titration:

2.2 mg of $1CF_3SO_3$ were dissolved in anhydrous acetone (10 mL) in a flask with a stirbar in the glovebox, which was then capped with a septum. Then, the flask was taken out of the box and cooled to 183 K. Dioxygen gas was injected to the flask with a balloon and a needle through the septum causing immediate reaction and formation of $1O_2$ ($[1O_2] = 0.13$ mM). Then, 10 μ L of a solution of trifluoroacetic acid (TFA) in acetone (0.3 equiv.) (prepared by diluting 1.4 μ L of TFA in 1 mL of anhydrous acetone) were added, and the UV-vis spectra recorded. Subsequent additions of 0.3 equiv. of TFA were done until no changes were observed in the UV-vis spectrum (**Figure S6**).

Figure S6. UV-Vis spectra of the titration reaction of **1O₂** with TFA. Inset, normalized modification of the absorbance at $\lambda_{\text{max}} = 478$ nm during titration with TFA (0.3-2.1 equiv.).

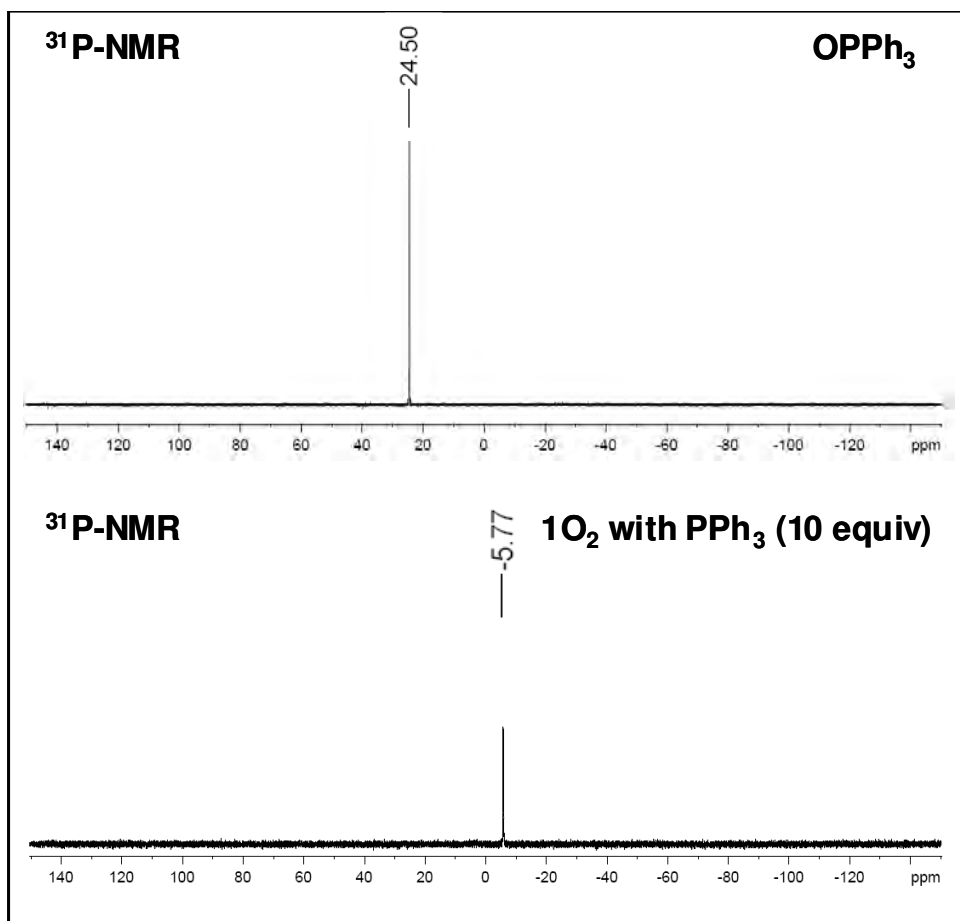


5.3 Reaction of **1O₂ with thioanisole, styrene, triphenylmethane, and ferrocene monitored by UV-vis Spectroscopy:** **1O₂** was generated as described above. Then, 0.1 mL of an acetone solution containing 10 equiv. of substrate (thioanisole, styrene, triphenylmethane or ferrocene) was added. No changes in the absorption feature at 476 nm were observed over 30 minutes in any case. The resulting crude was analyzed by GC and only the starting substrates were detected.

5.4 Reaction of **1O₂ with PPh₃ monitored by UV-vis Spectroscopy:** **1O₂** was generated as described above. Then 0.4 mL of a solution of PPh₃ (1.1 mg of PPh₃ solved in anhydrous acetone, 10 equiv.) was added. UV-Vis monitoring of the reaction indicated rapid bleaching of the spectral features associated to **1O₂** and formation of a pale yellow solution. Analysis of the resulting product was obtained as follows; 5 mg of **1CF₃SO₃** were dissolved in anhydrous acetone (20 mL) in a flask with a stirbar in the glovebox, which was subsequently capped with a septum, and taken out of the box. Then, the solution was cooled at 183 K and dioxygen was bubbled. After 5 minutes, the excess of dioxygen was removed by N₂/vacuum cycles and 0.5 mL of a solution of PPh₃ in acetone (10 equiv., 0.12 mg PPh₃ in 5 mL of anhydrous acetone) were added. The solution color rapidly changed from deep red brown to pale yellow. Then, the solvent was removed and the resulting solid was dissolved in CD₃CN into the glovebox. ³¹P-NMR analysis showed a single signal assigned to PPh₃ (-4.4 ppm). No signal corresponding to OPPh₃ (29.5 ppm) was observed, indicating that triphenylphosphine oxide is not formed. ¹H-

NMR (200 MHz, CD₃CN, 300K) δ , ppm: 8.42 (d, $J = 4$ Hz, 2H, α Hpy), 7.88 – 7.12 (m, Ar-H), 4.15 (s, 4H, py-CH₂), 3.76 (s, 2H, Ar-CH₂), 3.65 (m, 5H, CH=N-CH₂-CH₂, N-CH₃), 3.08 (m, 10H, CH=N-CH₂-CH₂, N-CH₂-CH₂). The ¹H-RMN spectra is identical to that prepared by combining 1CF₃SO₃ with PPh₃ (10 equiv.) in CD₃CN. (Figure S7)

Figure S7. ³¹P-NMR of the reaction of **1O₂** with 10 equiv. of PPh₃ (bottom). Comparison with ³¹P-NMR of pure OPPh₃.



5.5 Reaction of **1O₂ with sodium *p*-Cl-phenolate monitored by UV-vis Spectroscopy:** **1O₂** was generated as described above. Then, 0.1 mL of a solution of sodium *p*-Cl-phenolate (3, 10 or 20 equiv.) in acetone were added. UV-vis monitoring of the reaction indicated immediate formation of a new species **3^{Cl}** ($\epsilon = 6000 \text{ M}^{-1} \text{ cm}^{-1}$, $\lambda_{\text{max}} = 472 \text{ nm}$) that was very unstable and decayed rapidly, to form a final green solution (Figure S8). Decay rate of **3^{Cl}** is independent of sodium *p*-Cl-phenolate concentration, from 3 to 20 equiv. (Figure S9).

Figure S8. Generation of 3^{Cl} . $[1O_2] = 0.18$ mM in acetone at -90 °C.

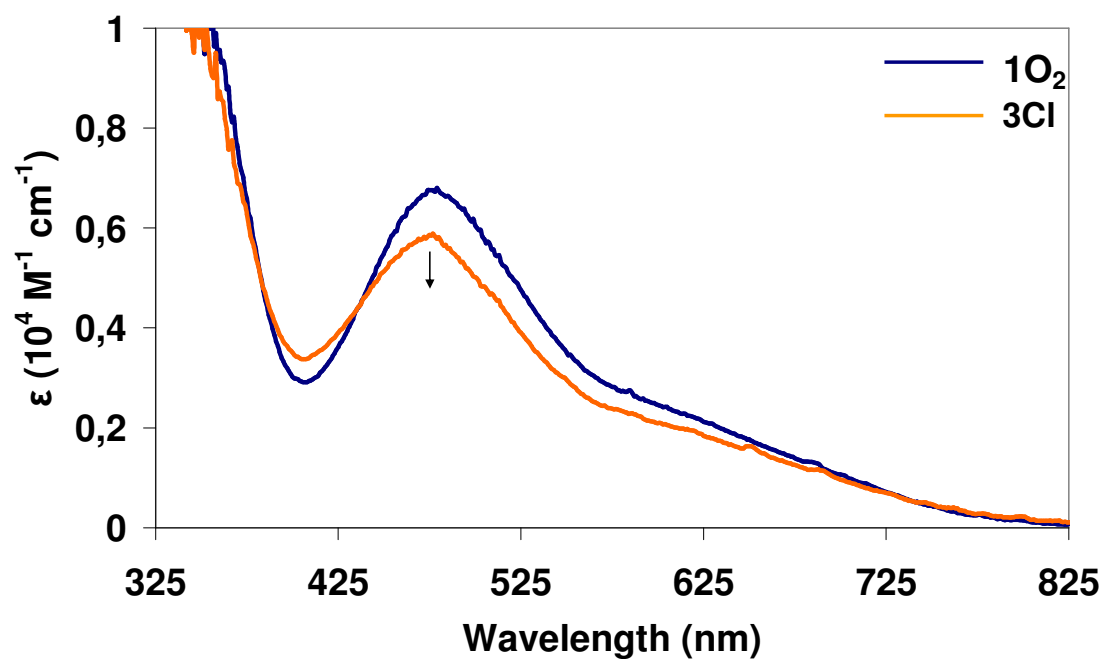
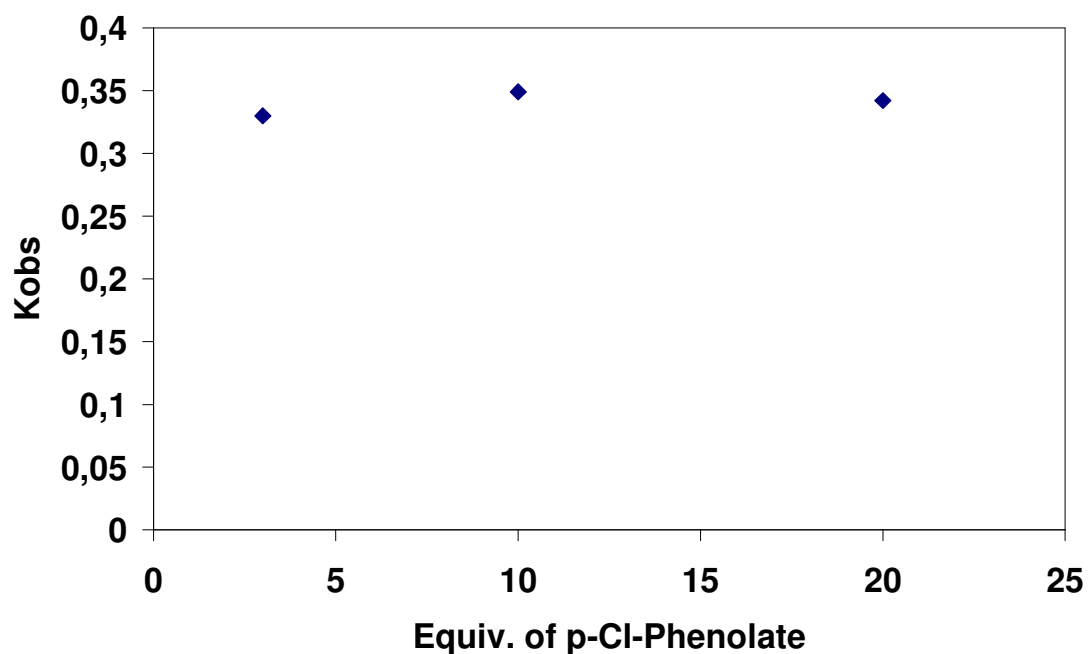


Figure S9. Dependence between k_{obs} and the equivalents of added substrate in the reaction of $1O_2$ with sodium *p*-Cl-phenolate



5.6 Reaction of $1O_2$ with sodium *p*-Cl-Phenolate. Quantitative determination of *p*-Cl-catechol by HPLC analysis.

Calibration: The quantification of the catechol was performed by HPLC analysis by an internal standard method. A mixture of known amounts of *p*-Cl-phenol, *p*-CN-phenol, and *p*-

Cl-catechol (30 μ L of 1mM solution in methanol for each compound) was initially analyzed. A sample of 100 μ L of this mixture was injected in to the HPLC apparatus (Jasco MD-1510 instrument with diode array detection) using a C18 RP (4.6 x 250 mm) column to obtain the relative response of the instrument at the retention times of the compounds. The reading wavelengths and the retention times are as follows: *p*-Cl-catechol: 285 nm, 22.4 min; *p*-CN-phenol: 247 nm, 26.2 min; *p*-Cl-phenol: 281 nm, 33.5 nm.

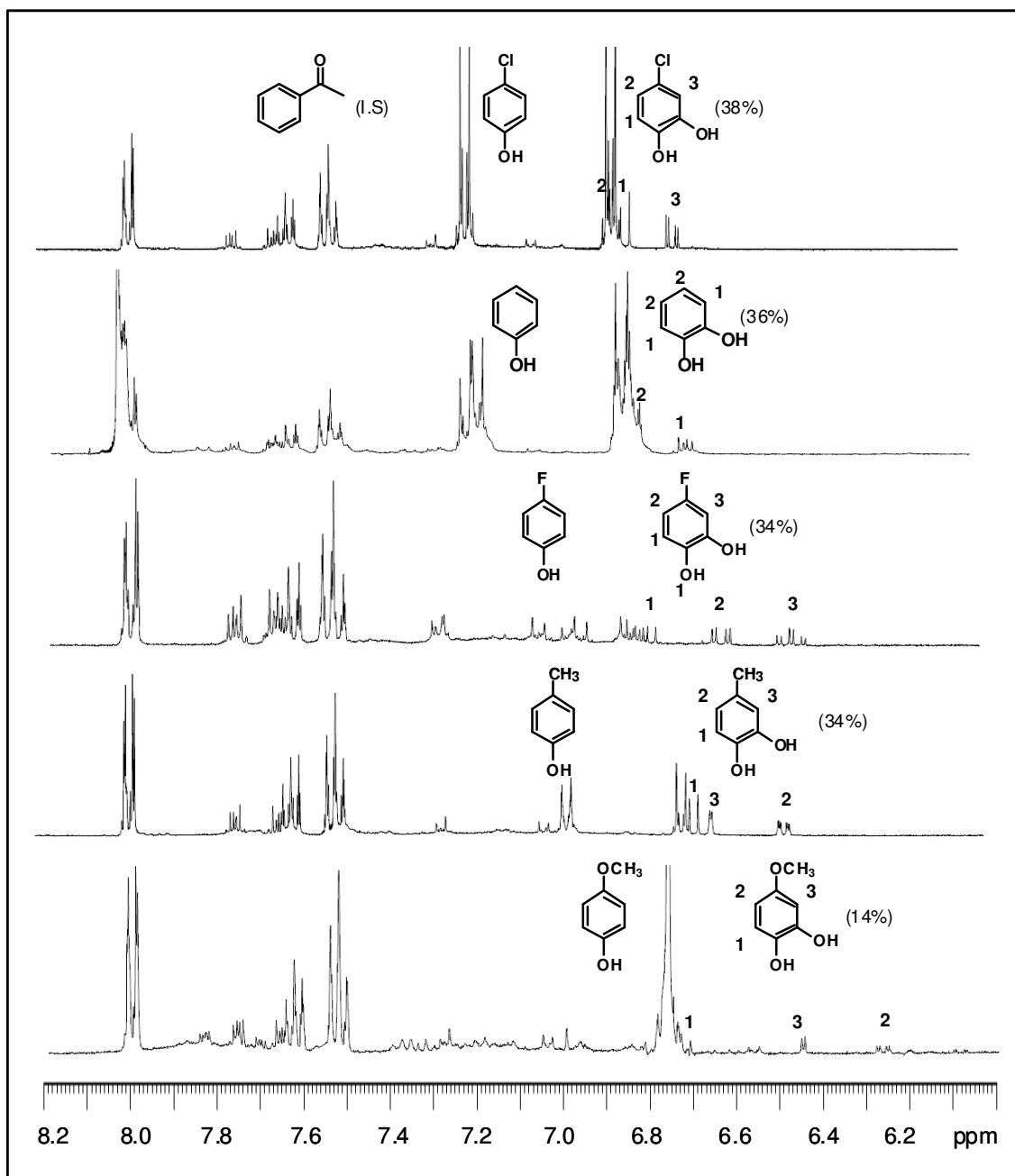
Preparation of reaction samples: 3 mg of ICF_3SO_3 were dissolved in anhydrous acetone (10 mL) in a flask equipped with a stirbar into the glovebox, and it was capped with a septum. Then, the solution was cooled at 183 K, and exposed to dioxygen with a needle connected to an O_2 -filled balloon. After 5 minutes, the excess of dioxygen was removed by N_2 /vacuum cycles. At this point, 1 mL of a solution of sodium *p*-Cl-phenolate (3 equiv.) in acetone (4.1 mg of sodium *p*-Cl-phenolate in 1 mL of anhydrous acetone) was added. The solution rapidly changed from red brown to green. The solution was removed from the cold bath and 3 mL of HCl 0.5 M were added and the solution became blue. Then acetone was removed from the mixture under reduced pressure and the resulting aqueous solution was extracted with CH_2Cl_2 (3 x 10 mL). The organic fraction was dried over MgSO_4 , filtered and the solvent was removed under vacuum.

Analysis of the reaction samples: The dried samples from the reaction mixtures were dissolved in 200 μ L of methanol. To 140 μ L of this solution a known amount (60 μ L of 1 mM solution in methanol) of *p*-CN-phenol was added as internal standard. Then, 100 μ L of the resulting solution was injected into the HPLC column (C18 RP, 4.6x250 mm). The elution mixture was 9/1 water/acetonitrile solution, the flow rate was 1 mL/min. The same procedure was followed with the samples from the reactions carried out using 3 and 10 equivalents of *p*-Cl-phenol. Analysis of the data gave 19% yield of *p*-Cl-catechol for the sample from 10 equivalents reaction, and 39% yield for the sample from the 3 equivalents reaction.

5.7 Reaction of IO_2 with sodium *p*-X-phenolates (X= Cl, H, F, Me, MeO). Quantitative determination of *p*-X-catechols by $^1\text{H-NMR}$: 6 mg of ICF_3SO_3 were dissolved in anhydrous acetone (20 mL) in a flask equipped with a stirbar into the glovebox, and it was capped with a septum. Then, the solution was cooled at 183 K, and exposed to dioxygen with a needle connected to an O_2 -filled balloon. After 5 minutes, the excess of dioxygen was removed by N_2 /vacuum cycles. Then, 1 mL of a solution of sodium *p*-X-phenolate (3 equiv.) in anhydrous acetone was added. The solution rapidly changed from red brown to green. The solution was removed from the cold bath and 3 mL of HCl 0.5 M were added and the solution became blue. Then acetone was removed from the mixture under reduced pressure and the resulting aqueous solution was extracted with CH_2Cl_2 (3 x 10 mL). The organic fraction was dried over MgSO_4 ,

filtered and the solvent was removed by vacuum. The resultant crude was dissolved in acetone- d_6 and 1 equiv. of acetophenone was added to the solution as internal standard. The quantification of the products was done by $^1\text{H-NMR}$ comparing the signals of the acetophenone with the resulting *p*-*X*-catechols. ($^1\text{H-NMR}$ spectra are shown in **Figure S10**)

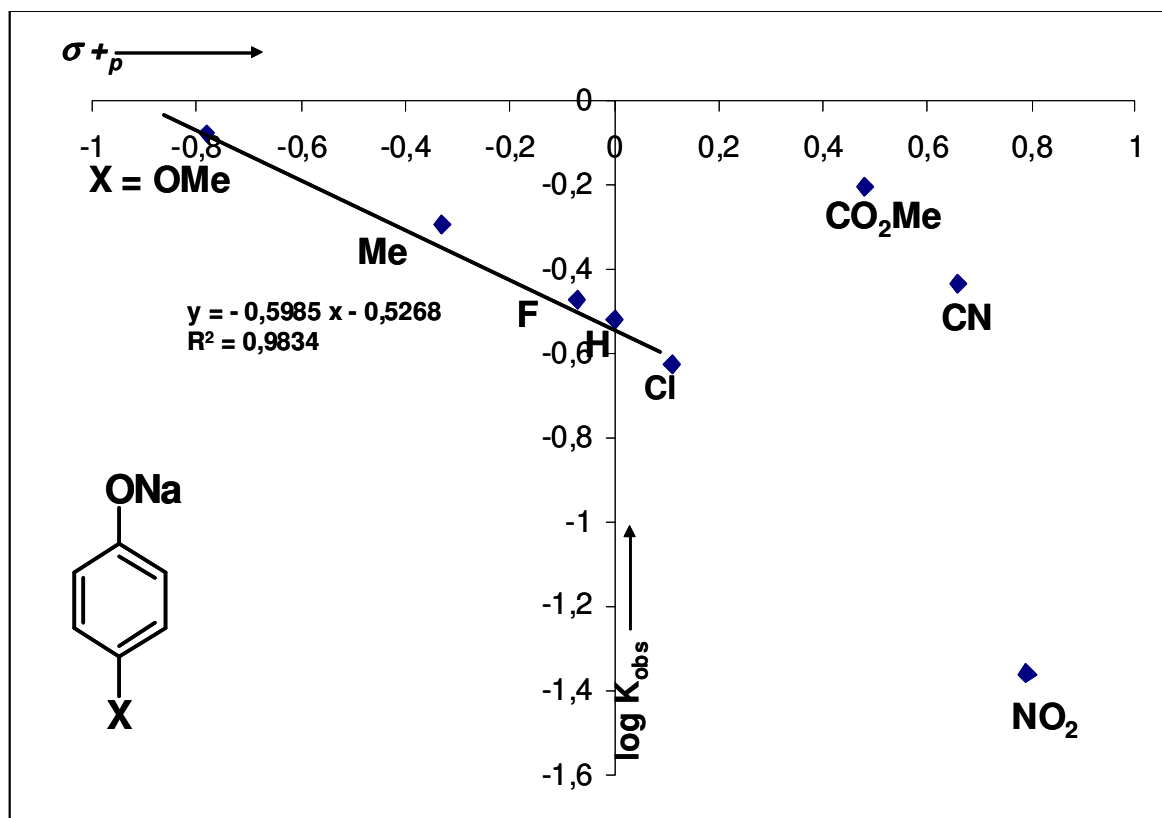
Figure S10. Quantification of *p*-*X*-catechols by $^1\text{H-NMR}$.



5.8 Reaction of IO_2 with sodium *p*-*X*-phenolates ($X = \text{NO}_2, \text{CN}, \text{CO}_2\text{Me}, \text{Cl}, \text{H}, \text{F}, \text{Me}, \text{MeO}$) monitored by UV-Vis. Determination of the Hammett constant ρ 3^X intermediates were generated at low temperature in a UV-Vis cell as described above at 183K ($[\text{complex}] = 0.18 \text{ mM}$). After complete accumulation of the intermediate ($\epsilon = 7700 \text{ M}^{-1} \text{ cm}^{-1}$), 150 μL of an

acetone solution containing 10 equiv. of sodium *p*-X-phenolate was added. UV-vis monitoring of the reaction indicated immediate formation of new species 3^X (when X = OMe, Me, F, H and Cl). UV-Vis decay of these new intermediate species was fitted to a first order rate constant. The observed decay rate constants were plotted against the corresponding Hammett parameter (σ^+) (Figure S11), obtaining a ρ value of -0.6 ($R^2 = 0.98$).

Figure S11. Hammett plot corresponding to the decay of intermediates 3^X .



5.9 Reaction of $2O_2$ with TFA (H^+). Quantitative determination of H_2O_2 by Peroxotitanyl

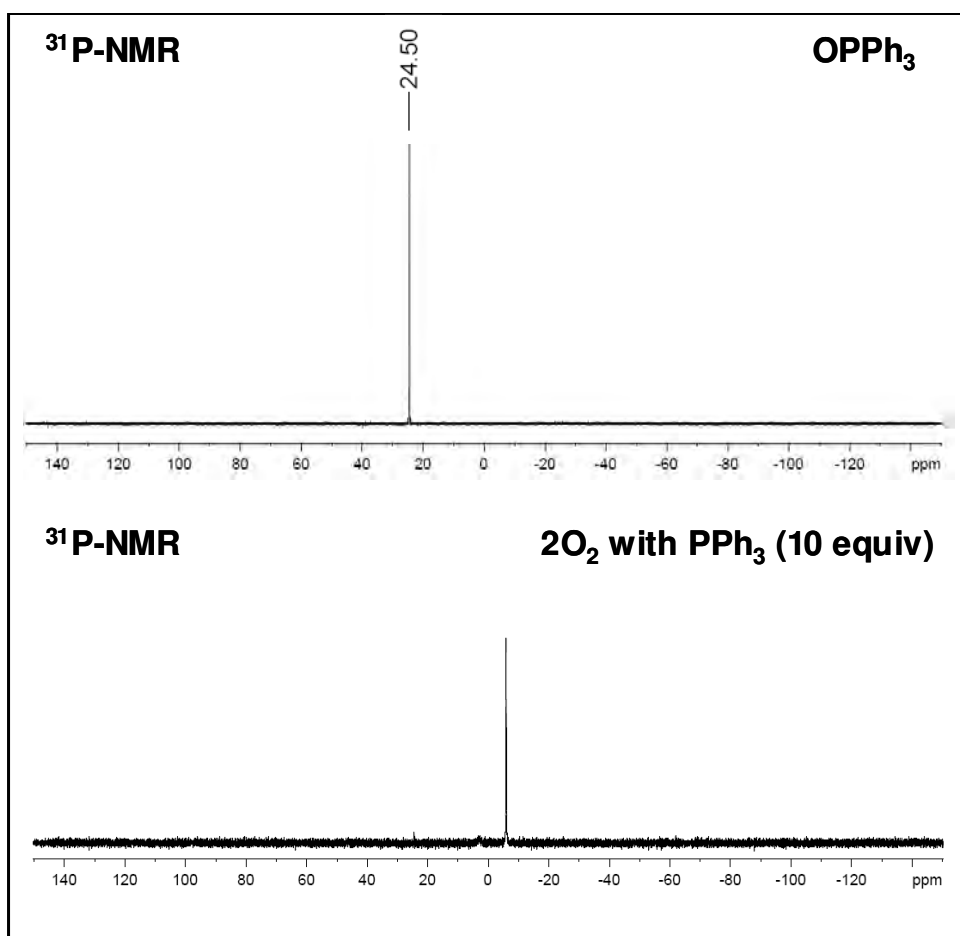
Method. 3 mg of $2ClO_4$ were dissolved in anhydrous acetone (10 mL) in a flask with a stirbar in the glovebox, which was then capped with a septum. Then, the flask was taken out of the box and cooled to 183 K. Dioxygen gas was injected to the flask with a balloon and a needle through the septum causing immediate reaction. After 5 minutes, the excess of dioxygen was removed by several N_2 /vacuum cycles. Then, 0.1 mL of a solution of trifluoroacetic acid (2 equiv.) in acetone (prepared by diluting 0.52 mL of TFA in 10 mL of anhydrous acetone) was added. The solution color immediately changed from purple to green. The solution was removed from the cold bath and 10 mL of distilled water were added. H_2O_2 was determined spectrophotometrically at 408 nm upon addition of 1 mL of titanium(IV) oxysulfate in sulfuric acid to 10 mL of the crude solution. The yield of H_2O_2 was determined by correlation with a

calibration curve made in the same mixture of the reaction. The resulting yield was 99% of H₂O₂.

5.10 Reaction of 2O₂ with thioanisole, styrene, triphenylmethane, and ferrocene monitored by UV-vis Spectroscopy: 2O₂ was generated as described above. Then, 0.1 mL of a solution containing 10 equiv. of substrate (thioanisole, styrene, triphenylmethane or ferrocene) was added. No changes in the absorption feature at 500 nm were observed over 30 minutes in any case. The resulting crude was analyzed by GC and only the starting substrates were detected.

5.11 Reaction of 2O₂ with PPh₃ monitored by UV-vis Spectroscopy. 2O₂ was generated as described above. Then 0.4 mL of a solution of PPh₃ (1.1 mg of PPh₃ dissolved in anhydrous acetone, 10 equiv.) was added. UV-Vis monitoring of the reaction indicated rapid bleaching of the spectral features associated to 2O₂ and formation of a pale yellow solution. Analysis of the resulting product was obtained as follows: in the glovebox, 5 mg of 2ClO₄ were dissolved in anhydrous acetone (20 mL) in a flask equipped with a stirbar, which was subsequently capped with a septum, and taken out of the box. Then, the solution was cooled at 183 K and dioxygen was bubbled. After 5 minutes, the excess of dioxygen was removed by N₂/vacuum cycles and 0.5 mL of a solution of PPh₃ in acetone (10 equiv., 0.10 mg PPh₃ in 5 mL of anhydrous acetone) was added. The solution color rapidly changed from deep red brown to pale yellow. Then, the solvent was removed and the resulting solid was dissolved in CD₃CN into the glovebox. ³¹P-NMR analysis showed a single signal assigned to PPh₃ (-4.4 ppm). No signal corresponding to OPPh₃ (29.5 ppm) was observed, indicating that triphenylphosphine oxide was not formed (**Figure S12**).

Figure S12. ^{31}P -NMR of the reaction of 2O_2 with 10 equiv. of PPh_3 (bottom). Comparison with ^{31}P -NMR of pure OPPh_3 .



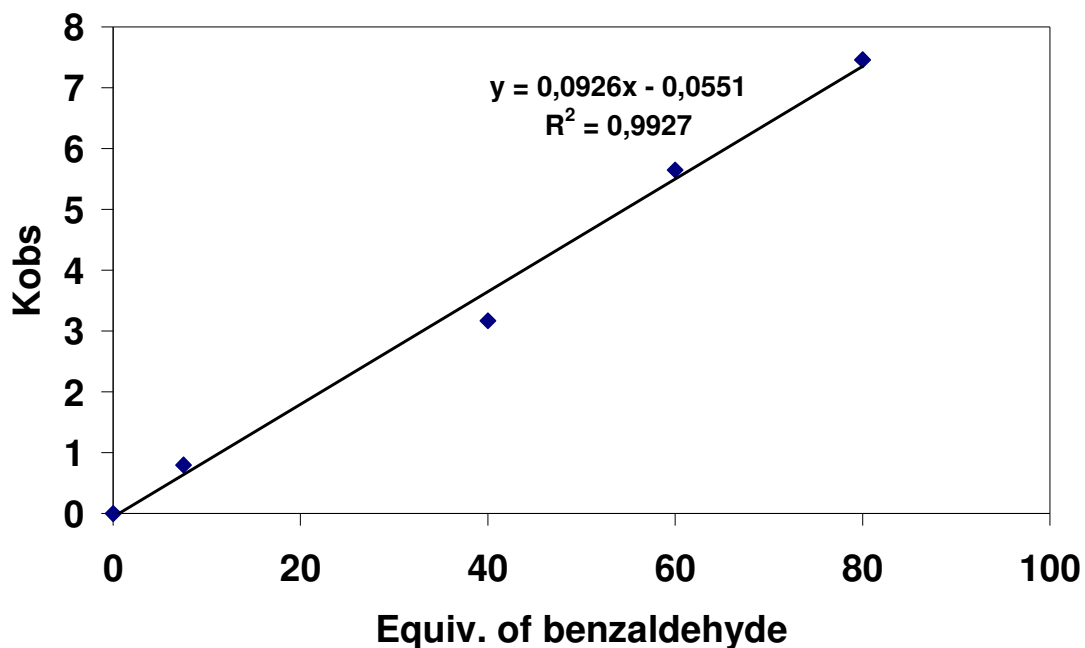
5.12 Reaction of 2O_2 with benzaldehyde. Quantitative determination of benzoic acid by GC.

In a glovebox, 6 mg of 2ClO_4 were dissolved in anhydrous acetone (5 mL) in a flask equipped with a stirbar, which was then capped with a septum. Then, the flask was taken out of the box and cooled to 183 K. Dioxygen gas was injected to the flask with a balloon and a needle through the septum causing immediate formation of 2O_2 . After 5 minutes, the excess of dioxygen was removed by N_2 /vacuum cycles. Then, 14 μL of benzaldehyde (20 equiv.) were added. The solution color changed from purple to green in a few minutes. The solution was removed from the cold bath and 0.1 mL of HCl 0.6 M were added. The resulting solution was extracted with CH_2Cl_2 (3x15 mL). The organic layers were dried under vacuum and dissolved in 1 mL of AcOEt. Then, an internal standard (biphenyl) was added to the solution, which was analyzed by GC. The quantification of the benzoic acid formed was done by comparison with a calibration curve. (Yield: 99%).

5.13 Reaction of 2O_2 with different amounts of benzaldehyde monitored by UV-Vis. 2O_2 was generated in a UV-Vis cell as described above ([complex]=0.18 mM). Then, a solution of benzaldehyde in anhydrous acetone was added. The reactions were monitored by following the

decay of the band at 500 nm in the UV-Vis spectra and fitted to single exponential functions, affording k_{obs} . **Figure S13** shows the lineal dependence between benzaldehyde concentration and k_{obs} .

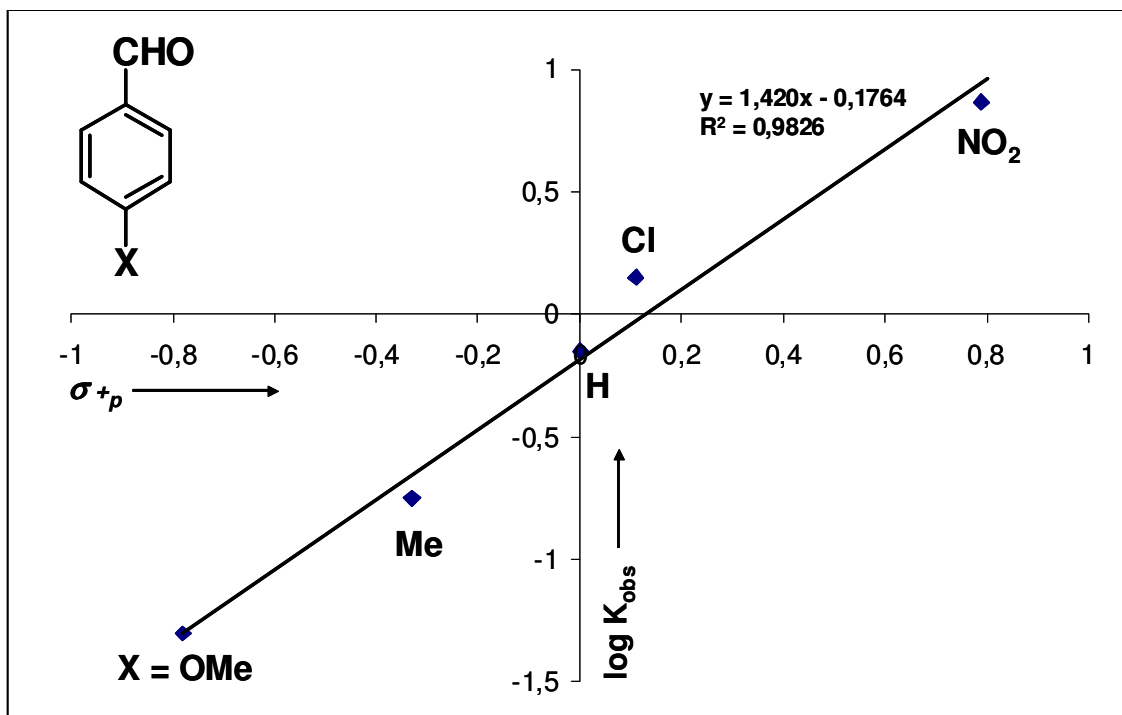
Figure S13. Reaction of 2O_2 with benzaldehyde. Dependence of k_{obs} vs the amount of added benzaldehyde.



5.14 Reaction of 2O_2 with p-X-benzaldehydes (NO_2 , Cl, H, Me, MeO) monitored by UV-Vis.

Determination of the Hammet constant ρ . 2O_2 was generated in a UV-Vis cell as described above ($[\text{complex}] = 0.18 \text{ mM}$). Then, a solution containing 10 equiv. of p-X-benzaldehyde in anhydrous acetone was added. The reaction was followed by the decay of the band at 500 nm and was fitted to a single exponential decay. Decay rates were plotted against σ_p^+ Hammet values (**Figure S14**), obtaining a ρ value of 1.42 ($R^2 = 0.98$).

Figure S14. Hammett plot of the reaction of 2O_2 with p-X-benzaldehydes.



6. Computational Details

Figures S15-S20 show the optimized structures studied in this work calculated at the B3LYP level of theory in junction of the SDD basis set and associated ECP for Cu, 6-311G(d) basis set for the atoms bond to Cu, and 6-31G basis set for the other atoms.

Figure S15: Structure of $trans\text{-Cu}^{\text{II}}_2(\mu\text{-}\eta^1:\eta^1\text{-O}_2)\text{-(1O}_2\text{)}$ calculated at the B3LYP level of theory in junction of the SDD basis set and associated ECP for Cu, 6-311G(d) basis set for the atoms bond to Cu, and 6-31G basis set for the other atoms.

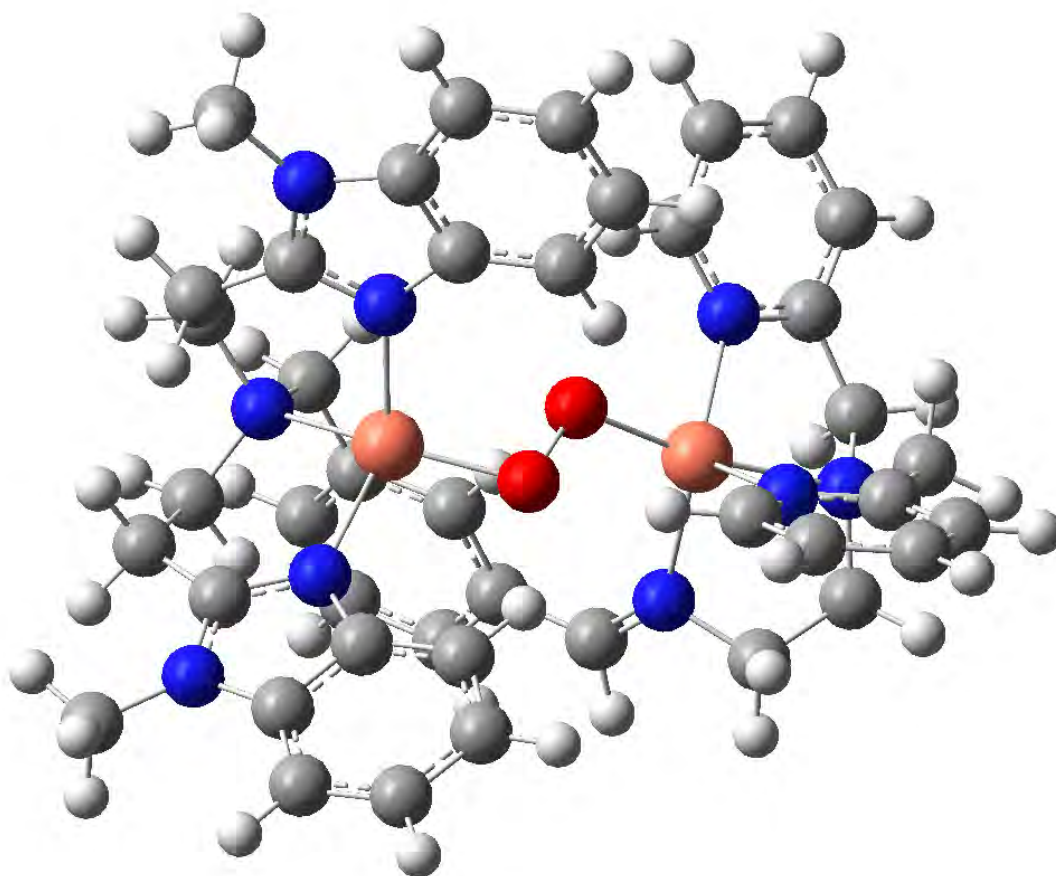


Figure S16: Structure of $(\text{Cu}^{\text{III}}_2(\mu\text{-O})_2)\text{-1O}_2$ calculated at the B3LYP level of theory in junction of the SDD basis set and associated ECP for Cu, 6-311G(d) basis set for the atoms bond to Cu, and 6-31G basis set for the other atoms.

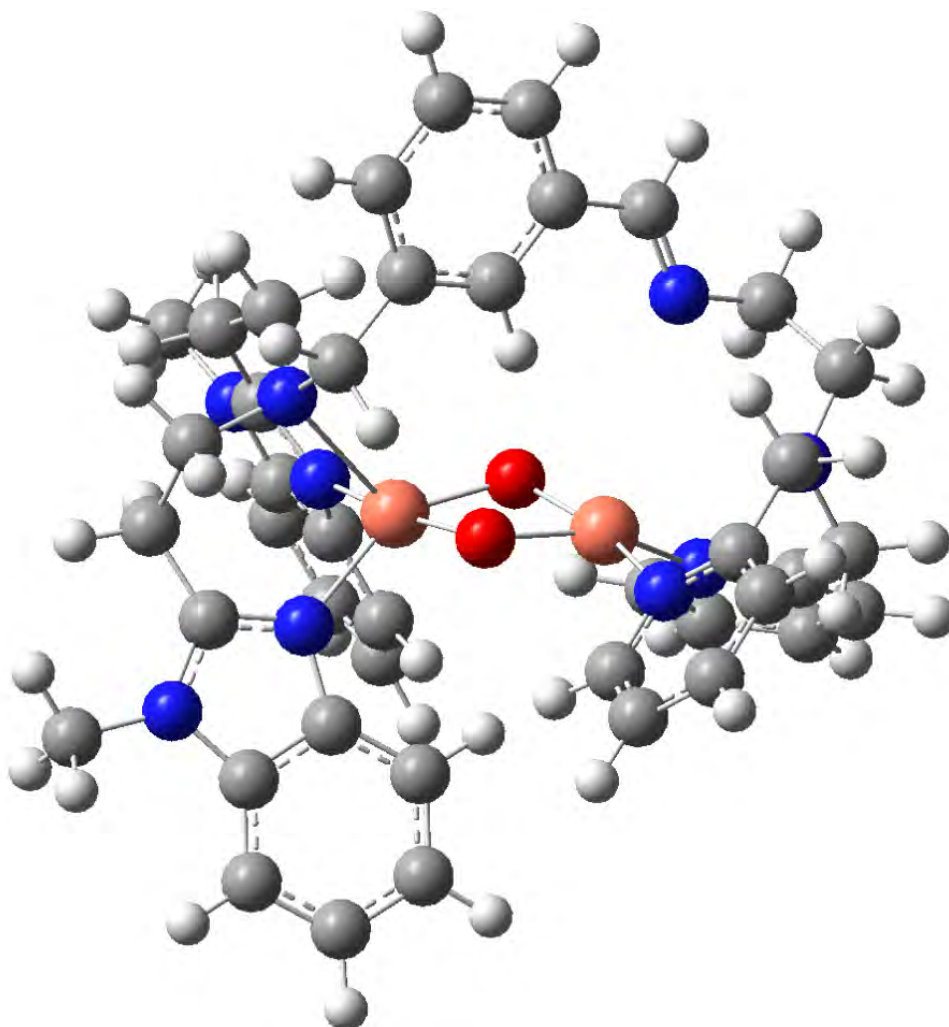


Figure S17: Structure of $\text{Cu}^{\text{II}}_2(\mu\text{-}\eta^1:\eta^2\text{-O}_2)\text{-}(\mathbf{1O}_2)$ calculated at the B3LYP level of theory in junction of the SDD basis set and associated ECP for Cu, 6-311G(d) basis set for the atoms bond to Cu, and 6-31G basis set for the other atoms.

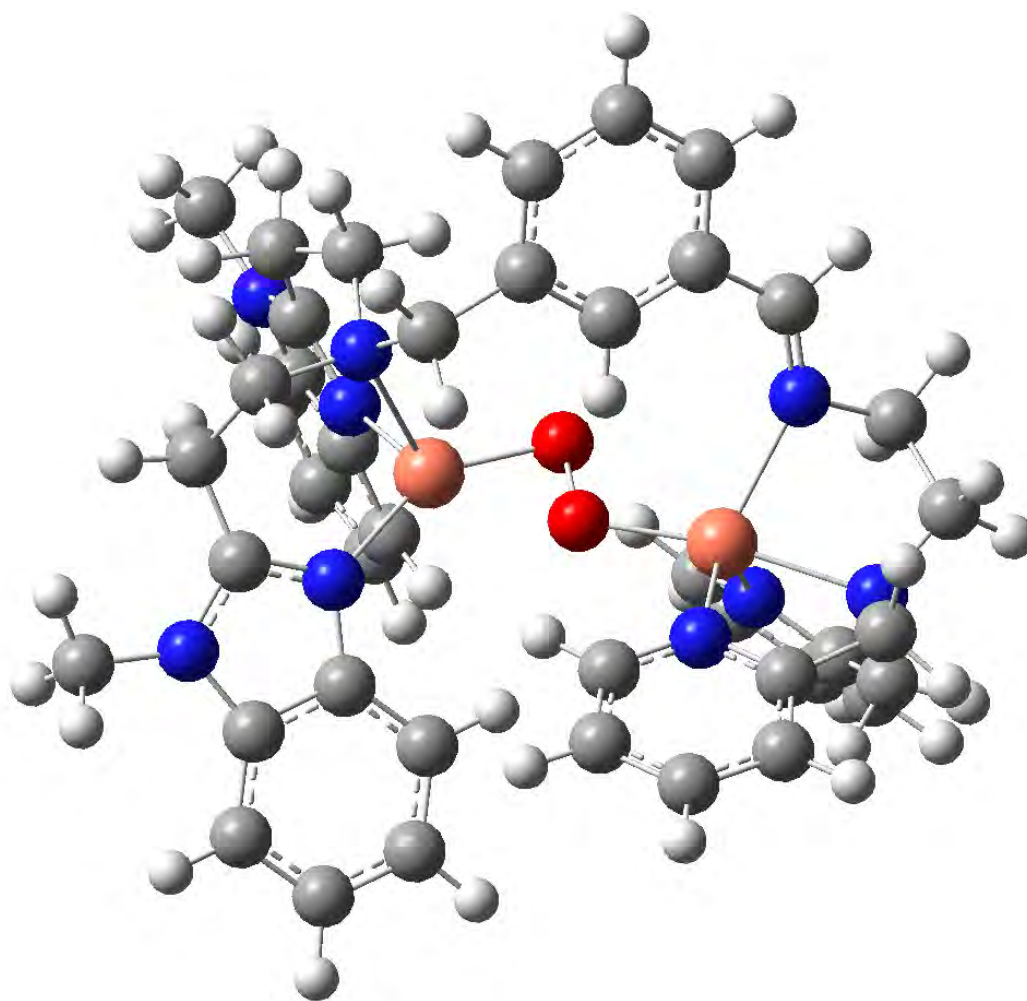


Figure S18: Structure of the $[\text{Cu}^{\text{II}}_2-(\mu-\eta^1:\eta^1-\text{O}_2)(4\text{-Me-PhO})]_3^{\text{Me}}$ species calculated at the B3LYP level of theory in junction of the SDD basis set and associated ECP for Cu, 6-311G(d) basis set for the atoms bond to Cu, and 6-31G basis set for the other atoms.

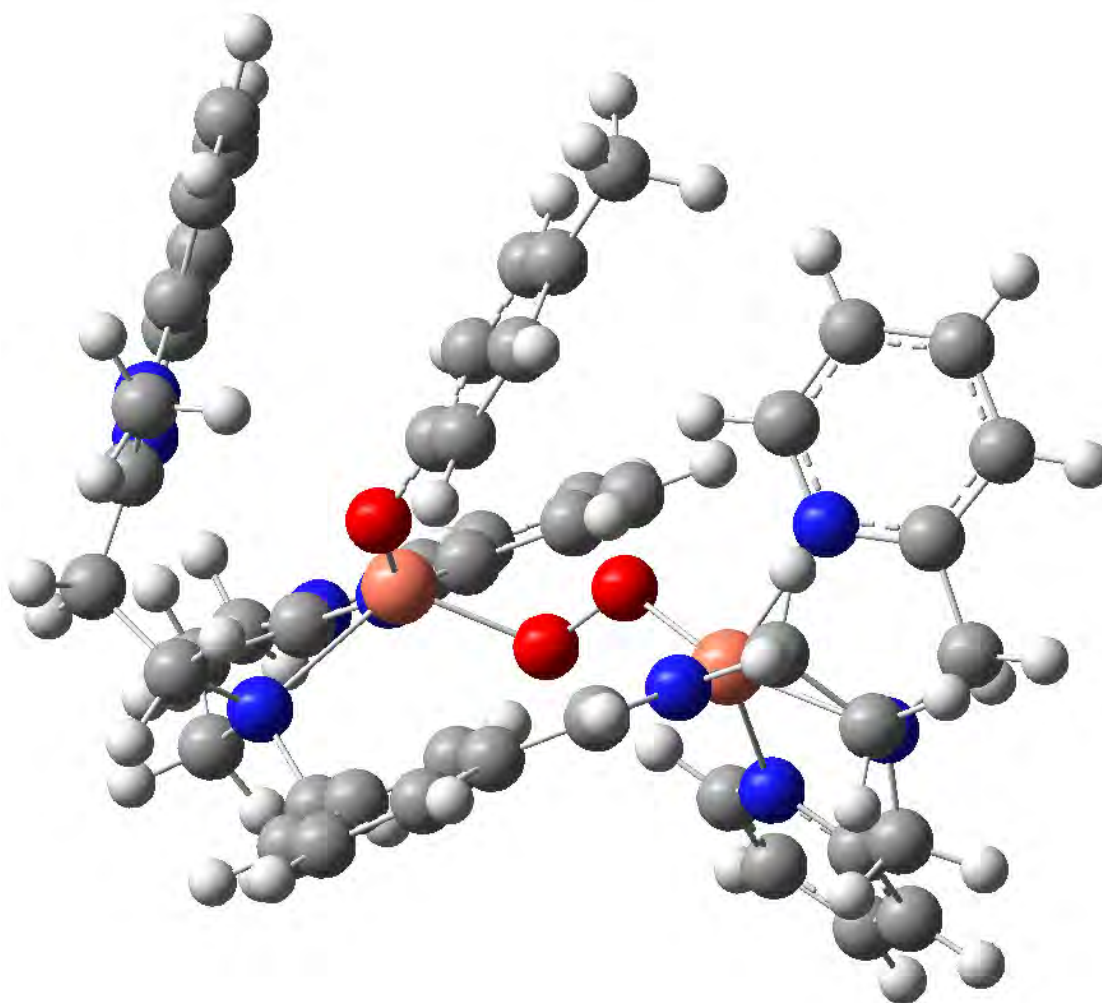


Figure S19: Structure of 3^{Me} (TS) calculated at the B3LYP level of theory in junction of the SDD basis set and associated ECP for Cu, 6-311G(d) basis set for the atoms bond to Cu, and 6-31G basis set for the other atoms.

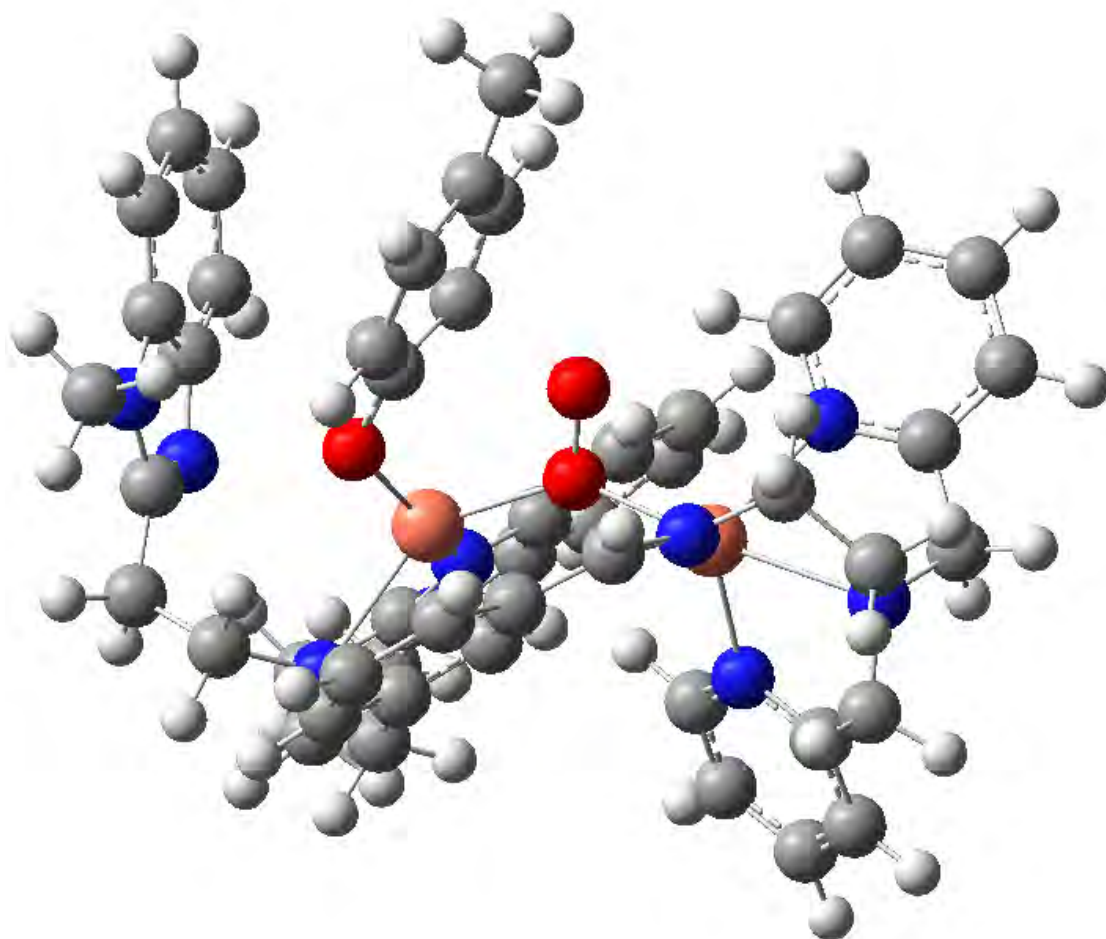


Figure S20: Structure of the phenolate hydroxylated species 3^{Me} (**Prod**) calculated at the B3LYP level of theory in junction of the SDD basis set and associated ECP for Cu, 6-311G(d) basis set for the atoms bond to Cu, and 6-31G basis set for the other atoms.

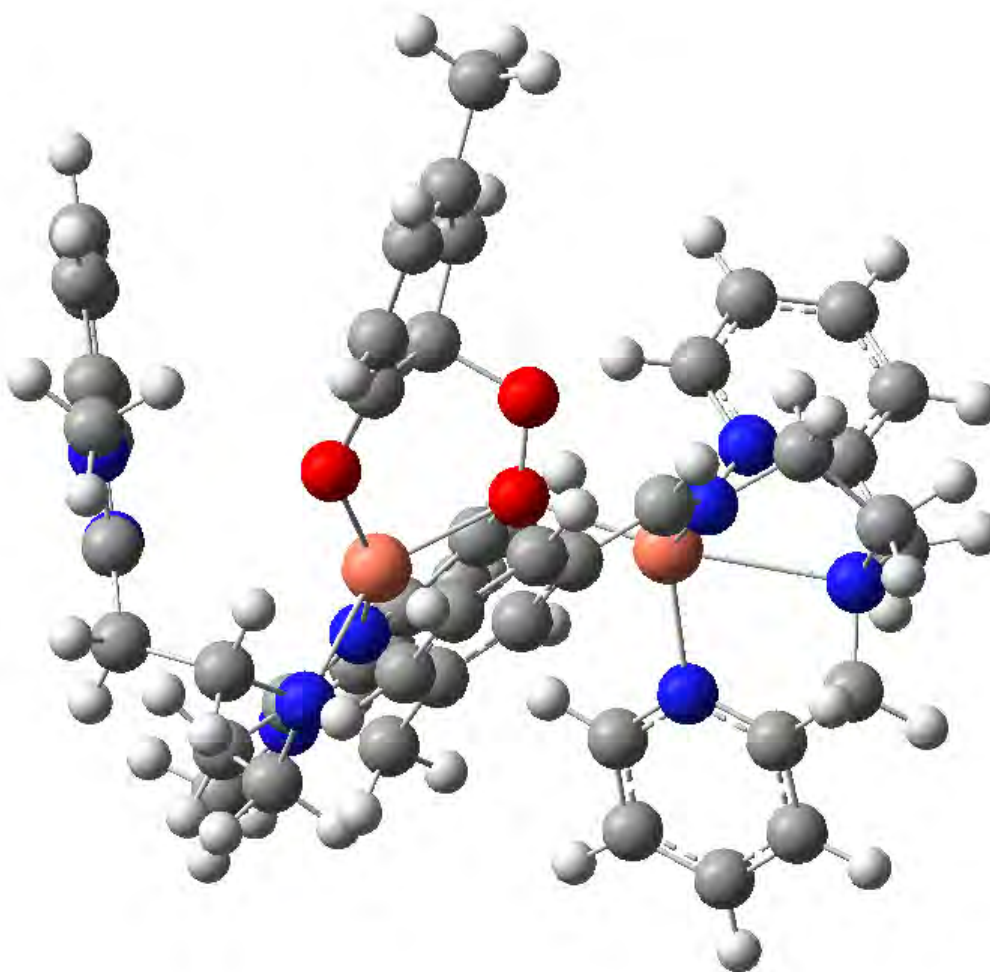


Table S1: Energies, enthalpies, and free energies (in kcal/mol) calculated for different isomeric forms of **1O₂**

	ΔE^a	ΔE^b	$\Delta H(298^\circ\text{K})^c$	$\Delta G(298^\circ\text{K})^c$
B3LYP				
<i>trans</i> -Cu ^{II} ₂ (μ - η^1 : η^1 -O ₂)-(1O ₂)	0.00	0.00	0.00	0.00
(Cu ^{III} ₂ (μ -O) ₂)-1O ₂	38.34	34.50	34.45	36.83
Cu ^{II} ₂ (μ - η^1 : η^2 -O ₂)-(1O ₂)	0.92	-0.38	-0.43	1.23
BLYP				
<i>trans</i> -Cu ^{II} ₂ (μ - η^1 : η^1 -O ₂)-(1O ₂)	0.00	0.00	0.00	0.00
(Cu ^{III} ₂ (μ -O) ₂)-1O ₂	23.16	21.19	21.14	23.52
Cu ^{II} ₂ (μ - η^1 : η^2 -O ₂)-(1O ₂)	1.97	0.16	0.11	1.77
OPBE				
<i>trans</i> -Cu ^{II} ₂ (μ - η^1 : η^1 -O ₂)-(1O ₂)	0.00	0.00	0.00	0.00
(Cu ^{III} ₂ (μ -O) ₂)-1O ₂	34.57	28.07	28.03	30.41
Cu ^{II} ₂ (μ - η^1 : η^2 -O ₂)-(1O ₂)	1.01	-1.41	-1.46	0.20

^a Energies computed at the B3LYP, BLYP, and OPBE levels in junction of the SDD basis set and associated ECP for Cu, 6-311G(d) basis set for the atoms bond to Cu, and 6-31G basis set for the other atoms. The geometries were optimized at the B3LYP level in junction of the SDD basis set and associated ECP for Cu, 6-311G(d) basis set for the atoms bond to Cu, and 6-31G basis set for the other atoms.

^b Energies computed at the B3LYP, BLYP, and OPBE levels in junction of the cc-pVTZ basis set for Cu and the atoms bond to Cu, and cc-pVDZ basis set for the other atoms. The geometries were optimized at the B3LYP level in junction of the SDD basis set and associated ECP for Cu, 6-311G(d) basis set for the atoms bond to Cu and 6-31G basis set for the other atoms.

^c Energies computed at the B3LYP, BLYP, and OPBE levels in junction of the cc-pVTZ basis set for Cu and the atoms bond to Cu and cc-pVDZ basis set for the other atoms. The equilibrium geometries, zero-point energies, thermal corrections, and entropy were calculated at the B3LYP level in junction of the SDD basis set and associated ECP for Cu, 6-311G(d) basis set for the atoms bond to Cu, and 6-31G basis set for the other atoms.

Table S2: Energies, enthalpies, and free energies (in kcal/mol) calculated for 3^{Me} , $3^{\text{Me}}(\text{TS})$, and oxygenation product.

	ΔE^{a}	ΔE^{b}	$\Delta H(298^{\circ}\text{K})^{\text{c}}$	$\Delta G(298^{\circ}\text{K})^{\text{c}}$
B3LYP				
3^{Me}	0.00	0.00	0.00	0.00
$3^{\text{Me}}(\text{TS})$	19.09	15.18	13.97	14.71
$3^{\text{Me}}(\text{Prod})$	15.74	7.53	7.16	7.82
BLYP				
3^{Me}	0.00	0.00	0.00	0.00
$3^{\text{Me}}(\text{TS})$	15.16	12.32	11.10	11.85
$3^{\text{Me}}(\text{Prod})$	17.62	11.15	10.77	11.43
OPBE				
3^{Me}	0.00	0.00	0.00	0.00
$3^{\text{Me}}(\text{TS})$	13.13	12.58	11.36	12.11
$3^{\text{Me}}(\text{Prod})$	13.73	9.06	8.69	9.35

^a Energies computed at the B3LYP, BLYP, and OPBE levels in junction of the SDD basis set and associated ECP for Cu, 6-311G(d) basis set for the atoms bond to Cu, and 6-31G basis set for the other atoms. The geometries were optimized at the B3LYP level in junction of the SDD basis set and associated ECP for Cu, 6-311G(d) basis set for the atoms bond to Cu, and 6-31G basis set for the other atoms.

^b Energies computed at the B3LYP, BLYP, and OPBE levels in junction of the cc-pVTZ basis set for Cu and the atoms bond to Cu and cc-pVDZ basis set for the other atoms. The geometries were optimized at the B3LYP level in junction of the SDD basis set and associated ECP for Cu, 6-311G(d) basis set for the atoms bond to Cu, and 6-31G basis set for the other atoms.

^c Energies computed at the B3LYP, BLYP, and OPBE levels in junction of the cc-pVTZ basis set for Cu and the atoms bond to Cu and cc-pVDZ basis set for the other atoms. The equilibrium geometries, zero-point energies, thermal corrections, and entropy were calculated at at the B3LYP level in junction of the SDD basis set and associated ECP for Cu, 6-311G(d) basis set for the atoms bond to Cu, and 6-31G basis set for the other atoms.

Tables S3-S8 show the optimized Cartesian xyz coordinates in Ångstroms for all structures studied in this work at the B3LYP level of theory in junction of the SDD basis set and associated ECP for Cu, 6-311G(d) basis set for the atoms bond to Cu, and 6-31G basis set for the other atoms.

Table S3: Optimized Cartesian xyz coordinates of the *trans*-Cu^{II}₂(μ - η^1 : η^1 -O₂)-(1O₂) structure at the B3LYP level of theory in junction of the SDD basis set and associated ECP for Cu, 6-311G(d) basis set for the atoms bond to Cu, and 6-31G basis set for the other atoms.

Cu	-1.703856	0.124497	-0.348747
N	-1.867609	2.182638	-0.438780
C	-2.987417	2.720986	-0.923074
Cu	2.558994	-0.455658	-0.024044
N	-3.072399	4.065527	-0.636656
C	-4.138288	5.018559	-0.958092
H	-4.606937	5.382163	-0.039038
H	-4.902078	4.546286	-1.573648
H	-3.723596	5.867639	-1.508160
N	-2.680252	-0.216791	-2.248420
C	-1.922382	4.405445	0.085847
N	-2.989664	-1.074127	0.708530
C	-1.499004	5.623339	0.627311
H	-2.084212	6.530773	0.534038
N	-4.946245	-1.977729	1.324942
C	-0.279235	5.617434	1.303515
H	0.088682	6.537821	1.742927
N	2.292735	-2.594432	-0.109421
C	0.484623	4.435065	1.428676
H	1.427118	4.475418	1.964418
N	4.641035	-1.096605	0.169573
C	0.057771	3.223207	0.885945
H	0.642899	2.317282	0.961375
C	-1.169531	3.215518	0.206227
N	3.454305	0.808218	-1.405815
N	2.954469	0.031964	2.047656
C	-4.018154	1.938176	-1.676653
H	-4.640844	1.379290	-0.969819
C	-3.406738	1.008566	-2.746588
H	-4.196379	0.687697	-3.440658
H	-2.691692	1.599083	-3.326261
C	-3.600749	-1.401385	-2.183314
H	-2.979093	-2.278583	-2.000380
H	-4.075550	-1.529520	-3.168412
C	-4.706306	-1.371097	-1.117583
H	-5.369244	-0.506684	-1.249244
H	-5.334927	-2.247476	-1.317221
C	-4.200033	-1.454166	0.292501
C	-6.309767	-2.513525	1.274352
H	-6.825554	-2.153253	0.384528
H	-6.863995	-2.167269	2.149630
H	-6.299791	-3.607781	1.268506
C	-4.150940	-1.943310	2.475854
C	-4.396745	-2.352848	3.790329
H	-5.339354	-2.794580	4.091568
C	-3.361027	-2.171386	4.706528
H	-3.505820	-2.474315	5.737365
C	-2.125546	-1.604857	4.318713
H	-1.347041	-1.487338	5.064592
C	-1.886508	-1.199323	3.006715
H	-0.940715	-0.775230	2.697634
C	-2.921790	-1.372896	2.077632

C	-1.591014	-0.516028	-3.285036
H	-0.887767	0.320127	-3.226875
H	-2.060369	-0.494453	-4.279263
C	-0.870775	-1.836440	-3.103170
C	0.092446	-1.992962	-2.098668
H	0.366871	-1.151214	-1.471069
C	0.714004	-3.239890	-1.893790
C	0.376423	-4.328003	-2.724272
H	0.845729	-5.294501	-2.566295
C	-0.545767	-4.164562	-3.758901
H	-0.784058	-4.996046	-4.412259
C	-1.168375	-2.926317	-3.944434
H	-1.892540	-2.806743	-4.745132
C	1.700128	-3.476954	-0.837113
H	1.942585	-4.535084	-0.679917
C	3.273255	-3.083610	0.879975
H	2.976976	-2.704715	1.863048
H	3.294258	-4.180334	0.930687
C	4.670790	-2.562886	0.497241
H	5.379590	-2.759615	1.309778
H	5.023895	-3.109776	-0.382095
C	5.268484	-0.788041	-1.150429
H	4.998157	-1.596923	-1.838582
H	6.365132	-0.770438	-1.083139
C	4.741586	0.519944	-1.708153
C	5.507566	1.358321	-2.521782
H	6.539437	1.109610	-2.742619
C	4.922759	2.518255	-3.041783
H	5.497846	3.183650	-3.675625
C	3.592718	2.810020	-2.722431
H	3.110182	3.704389	-3.096819
C	2.891403	1.932320	-1.894334
H	1.866080	2.112037	-1.591200
C	5.231653	-0.256422	1.252488
H	5.479108	0.718574	0.814003
H	6.171330	-0.693417	1.616748
C	4.259518	-0.029293	2.393337
C	4.687679	0.187519	3.706018
H	5.740733	0.121246	3.955925
C	3.737441	0.499151	4.684242
H	4.044289	0.673131	5.709426
C	2.390554	0.584613	4.317581
H	1.627163	0.833247	5.044725
C	2.037787	0.339646	2.988783
H	1.012426	0.386306	2.638700
H	-4.695694	2.617527	-2.202329
O	-0.116147	-0.088269	0.666236
O	0.867162	0.400230	-0.219378

Table S4: Optimized Cartesian xyz coordinates of the $(\text{Cu}^{\text{III}}(\mu\text{-O})_2)\text{-IO}_2$ structure at the B3LYP level of theory in junction of the SDD basis set and associated ECP for Cu, 6-311G(d) basis set for the atoms bond to Cu, and 6-31G basis set for the other atoms.

Cu	1.060469	0.227042	-0.118548
N	2.357666	-0.834999	-1.256511
C	3.464186	-0.389994	-1.855920
Cu	-1.699827	-0.577982	0.059128
N	4.057278	-1.386679	-2.598268
C	5.290948	-1.328866	-3.391446
H	6.129446	-1.761672	-2.838101
H	5.527590	-0.299033	-3.655196
H	5.144931	-1.888393	-4.317708

N	1.801012	2.322868	-1.304431
C	3.288644	-2.545775	-2.436860
N	2.371627	0.614646	1.275340
C	3.451162	-3.845306	-2.928252
H	4.277286	-4.117794	-3.574317
N	3.704080	1.587980	2.774712
C	2.506390	-4.792554	-2.534194
H	2.597652	-5.813033	-2.887806
N	-3.241602	2.244440	0.995271
C	1.442916	-4.453168	-1.667877
H	0.743322	-5.225182	-1.366654
N	-4.507687	-0.246535	0.481414
C	1.285846	-3.154393	-1.183589
H	0.481783	-2.903467	-0.501728
C	2.218993	-2.187640	-1.586708
N	-2.762351	-1.245844	-1.514261
N	-2.406328	-1.647694	1.683996
C	3.999846	0.995908	-1.700346
H	4.305130	1.131819	-0.659926
C	3.014476	2.098299	-2.150883
H	3.568582	3.045215	-2.257442
H	2.666681	1.824611	-3.151352
C	2.037437	3.330260	-0.231292
H	1.091060	3.467278	0.293021
H	2.300644	4.303349	-0.677875
C	3.128504	3.014690	0.802334
H	4.122857	3.041224	0.331995
H	3.124372	3.859306	1.502300
C	3.011588	1.746393	1.596077
C	4.515617	2.603757	3.457872
H	5.110445	3.166781	2.736771
H	5.201092	2.102382	4.140974
H	3.885204	3.291128	4.029548
C	3.491928	0.282326	3.231647
C	3.958627	-0.403337	4.358369
H	4.587104	0.069715	5.103423
C	3.583125	-1.740059	4.484154
H	3.929059	-2.310017	5.338719
C	2.773203	-2.371603	3.513284
H	2.527819	-3.420905	3.634227
C	2.301567	-1.679921	2.398403
H	1.703309	-2.176203	1.644439
C	2.659804	-0.329969	2.270482
C	0.717086	2.829188	-2.267648
H	0.270485	1.929506	-2.703475
H	1.214485	3.386736	-3.072823
C	-0.346945	3.727185	-1.677738
C	-1.274064	3.229098	-0.761103
H	-1.247308	2.188448	-0.466934
C	-2.231393	4.070722	-0.169833
C	-2.271101	5.430239	-0.520692
H	-3.005502	6.088095	-0.065420
C	-1.368053	5.932250	-1.463294
H	-1.406362	6.977887	-1.747951
C	-0.407315	5.089246	-2.032756
H	0.297638	5.491399	-2.754728
C	-3.156724	3.509155	0.827971
H	-3.744789	4.224298	1.420593
C	-4.119627	1.710897	2.026168
H	-3.490538	1.160281	2.737459
H	-4.661753	2.491046	2.585396
C	-5.137028	0.740003	1.400599

H	-5.659869	0.210806	2.205387
H	-5.898620	1.313979	0.854862
C	-4.785466	0.053116	-0.926981
H	-4.480942	1.094109	-1.094152
H	-5.858200	-0.014693	-1.177728
C	-4.013027	-0.844806	-1.863641
C	-4.578787	-1.248318	-3.080024
H	-5.580185	-0.917470	-3.328835
C	-3.861489	-2.068567	-3.951016
H	-4.295413	-2.384190	-4.892894
C	-2.578708	-2.478902	-3.578057
H	-1.982227	-3.121692	-4.213223
C	-2.063505	-2.041888	-2.361365
H	-1.060271	-2.306362	-2.058750
C	-4.732453	-1.642966	0.873450
H	-4.661866	-2.288122	-0.009705
H	-5.732367	-1.812027	1.300078
C	-3.680980	-2.072679	1.876839
C	-4.016698	-2.869875	2.976164
H	-5.045452	-3.186693	3.104268
C	-3.036536	-3.233627	3.901921
H	-3.288830	-3.847897	4.758830
C	-1.733694	-2.768427	3.709818
H	-0.940538	-2.998772	4.410268
C	-1.460118	-1.979009	2.594391
H	-0.475344	-1.565359	2.422345
H	4.907068	1.113034	-2.299172
O	-0.367923	0.163210	1.041112
O	-0.382358	-0.140708	-1.127265

Table S5: Optimized Cartesian xyz coordinates of the $\text{Cu}^{\text{II}}(\mu\text{-}\eta^1\text{-}\eta^2\text{-O}_2)\text{-(1O}_2\text{)}$ structure at the B3LYP level of theory in junction of the SDD basis set and associated ECP for Cu, 6-311G(d) basis set for the atoms bond to Cu, and 6-31G basis set for the other atoms.

Cu	-1.380721	-0.101643	-0.183701
N	-2.036363	1.645194	-0.890365
C	-3.134618	1.792291	-1.632132
Cu	2.619145	-0.239774	0.158230
N	-3.402737	3.124864	-1.864451
C	-4.525380	3.720991	-2.596101
H	-5.293258	4.079252	-1.904063
H	-4.967998	2.993667	-3.275590
H	-4.159531	4.560726	-3.190843
N	-2.209213	-1.270823	-2.148357
C	-2.415470	3.870922	-1.206819
N	-2.960635	-0.777557	0.899276
C	-2.210805	5.249251	-1.084618
H	-2.872594	5.974830	-1.542825
N	-4.711392	-1.930165	1.681705
C	-1.113437	5.657004	-0.325046
H	-0.921655	6.716439	-0.198149
N	3.083847	-2.379090	0.135552
C	-0.253423	4.720369	0.292791
H	0.580172	5.083631	0.883869
N	4.758805	-0.138063	0.454309
C	-0.460648	3.346716	0.166558
H	0.192607	2.622381	0.640345
C	-1.559662	2.927346	-0.597223
N	3.083381	1.152743	-1.296942
N	2.689502	0.173845	2.240951
C	-3.973481	0.645600	-2.102981
H	-4.469781	0.204407	-1.233697

C	-3.189394	-0.423209	-2.903860
H	-3.912840	-1.072611	-3.422934
H	-2.630355	0.103741	-3.683468
C	-2.833601	-2.525928	-1.624953
H	-2.051656	-3.064916	-1.085752
H	-3.144955	-3.158533	-2.473732
C	-4.065922	-2.392847	-0.712556
H	-4.898503	-1.926868	-1.258999
H	-4.394107	-3.421390	-0.519168
C	-3.876416	-1.700233	0.605812
C	-5.828836	-2.876095	1.762734
H	-6.265586	-3.033360	0.776207
H	-6.602148	-2.457348	2.409414
H	-5.503556	-3.837021	2.173373
C	-4.283349	-1.108811	2.730675
C	-4.749865	-0.935523	4.038167
H	-5.588003	-1.497922	4.432543
C	-4.081452	0.002586	4.825018
H	-4.412671	0.171962	5.843302
C	-2.984395	0.740472	4.324195
H	-2.502738	1.468125	4.968051
C	-2.519490	0.557588	3.022727
H	-1.681828	1.126438	2.635331
C	-3.182337	-0.384798	2.223638
C	-1.140602	-1.653152	-3.165985
H	-0.575423	-0.736233	-3.363186
H	-1.645793	-1.938786	-4.101967
C	-0.199896	-2.775851	-2.778432
C	0.826214	-2.563151	-1.852818
H	0.937920	-1.589238	-1.397478
C	1.687137	-3.612174	-1.481530
C	1.528143	-4.881783	-2.074567
H	2.189084	-5.696376	-1.793321
C	0.528686	-5.093197	-3.024619
H	0.417627	-6.065348	-3.491149
C	-0.332640	-4.046776	-3.370697
H	-1.110206	-4.217611	-4.109486
C	2.737017	-3.460181	-0.475915
H	3.262025	-4.391758	-0.231895
C	4.158698	-2.489799	1.139936
H	3.730521	-2.254703	2.119374
H	4.571459	-3.506328	1.190934
C	5.288909	-1.505850	0.794210
H	6.001095	-1.442210	1.625275
H	5.833400	-1.887636	-0.073698
C	5.345003	0.398278	-0.809552
H	5.502085	-0.449590	-1.485286
H	6.327184	0.857853	-0.633757
C	4.405414	1.373138	-1.488668
C	4.864913	2.392220	-2.327045
H	5.929493	2.551563	-2.455859
C	3.934533	3.193880	-2.995579
H	4.268656	3.989173	-3.652065
C	2.570502	2.955503	-2.799344
H	1.819177	3.558083	-3.294252
C	2.184113	1.929442	-1.937361
H	1.143156	1.712381	-1.734315
C	4.924316	0.836712	1.576998
H	4.778185	1.841716	1.160589
H	5.945405	0.795289	1.979387
C	3.897960	0.605846	2.667568
C	4.153266	0.864670	4.016069

H	5.133461	1.202747	4.333018
C	3.123511	0.677708	4.945610
H	3.296887	0.869246	5.998547
C	1.876030	0.232302	4.497341
H	1.058502	0.067552	5.188467
C	1.695356	-0.013464	3.134055
H	0.760888	-0.379248	2.719365
H	-4.771199	1.009576	-2.756707
O	0.011050	-1.021793	0.696453
O	0.717589	-0.019381	-0.050335

Table S6: Optimized Cartesian xyz coordinates of the 3^{Me} structure at the B3LYP level of theory in junction of the SDD basis set and associated ECP for Cu, 6-311G(d) basis set for the atoms bond to Cu, and 6-31G basis set for the other atoms.

Cu	1.429978	0.562216	0.408805
N	2.141752	2.260204	-0.359650
C	3.200358	2.933826	0.086272
Cu	-3.040783	0.086101	0.125095
N	3.497577	3.998294	-0.743934
C	4.607523	4.945057	-0.647155
H	5.433227	4.650134	-1.302671
H	4.972959	4.999896	0.377827
H	4.257958	5.938637	-0.937902
N	2.351525	0.955791	2.499433
C	2.566166	3.986910	-1.789460
N	5.038381	-0.197304	0.092953
C	2.409451	4.815254	-2.904926
H	3.076320	5.646521	-3.103881
N	4.490985	-2.303643	0.689326
C	1.353598	4.515688	-3.767224
H	1.197141	5.129188	-4.647969
N	-3.248708	-1.563009	1.547446
C	0.490044	3.425673	-3.519621
H	-0.316578	3.224400	-4.216641
N	-5.337402	-0.079652	0.271159
C	0.650287	2.601218	-2.405045
H	-0.018975	1.774010	-2.206410
C	1.709883	2.893097	-1.533381
N	-3.600037	2.095625	0.427564
N	-3.566280	-0.844548	-1.731703
C	3.998905	2.553292	1.290821
H	4.636155	1.708507	0.996467
C	3.147769	2.226131	2.536538
H	3.805202	2.218141	3.421373
H	2.438282	3.047593	2.681635
C	3.102594	-0.216324	3.055621
H	2.463856	-1.086353	2.895195
H	3.224001	-0.066868	4.142986
C	4.518660	-0.510026	2.505506
H	5.165145	0.363791	2.623724
H	4.937116	-1.270675	3.178284
C	4.657987	-0.982129	1.087811
C	4.010027	-3.434025	1.475620
H	4.109210	-3.216355	2.540013
H	4.611889	-4.319388	1.250995
H	2.959449	-3.641791	1.252022
C	4.768437	-2.345277	-0.677066
C	4.762492	-3.388486	-1.608564
H	4.487200	-4.401609	-1.337421
C	5.119095	-3.066087	-2.919415
H	5.129301	-3.846287	-3.673356

C	5.467392	-1.746459	-3.287356
H	5.742240	-1.540569	-4.316587
C	5.469173	-0.710795	-2.352968
H	5.743772	0.301268	-2.629524
C	5.112548	-1.016608	-1.031658
C	1.133625	1.210787	3.378486
H	0.520175	1.938807	2.839271
H	1.485233	1.690916	4.306710
C	0.282961	0.016340	3.773212
C	-0.762317	-0.442452	2.958275
H	-0.929588	0.025557	1.995685
C	-1.572504	-1.516323	3.376241
C	-1.313587	-2.140223	4.615019
H	-1.931025	-2.974924	4.934879
C	-0.287442	-1.679902	5.437184
H	-0.104491	-2.148497	6.397926
C	0.496631	-0.600733	5.020624
H	1.281662	-0.229095	5.672545
C	-2.706971	-2.040878	2.613088
H	-3.139737	-2.949747	3.052537
C	-4.422739	-2.292637	1.030160
H	-4.183750	-2.655613	0.026507
H	-4.668060	-3.164314	1.654369
C	-5.640756	-1.350465	0.987702
H	-6.492550	-1.868329	0.524357
H	-5.926755	-1.110671	2.016714
C	-5.770493	1.136983	0.999549
H	-5.649397	0.936828	2.070277
H	-6.834202	1.367175	0.831770
C	-4.912723	2.339480	0.643881
C	-5.438918	3.633681	0.599201
H	-6.498174	3.794485	0.767973
C	-4.582526	4.707335	0.334504
H	-4.968744	5.719934	0.294603
C	-3.226640	4.449799	0.116255
H	-2.530222	5.251505	-0.098047
C	-2.772271	3.129365	0.164120
H	-1.733152	2.860737	-0.002575
C	-5.799869	-0.077077	-1.137914
H	-5.815108	0.967274	-1.476306
H	-6.830574	-0.456543	-1.219506
C	-4.876022	-0.857050	-2.058033
C	-5.341391	-1.494488	-3.211863
H	-6.400699	-1.495282	-3.445240
C	-4.419744	-2.124165	-4.055478
H	-4.756385	-2.625903	-4.956129
C	-3.063845	-2.099194	-3.716527
H	-2.317516	-2.577959	-4.338281
C	-2.675006	-1.450170	-2.541568
H	-1.639380	-1.405875	-2.223255
H	4.665929	3.375229	1.570280
O	-1.247401	0.319655	-0.542839
O	-0.421634	1.160003	0.154944
O	1.398233	-1.288492	0.659004
C	0.915712	-2.182493	-0.218727
C	0.215133	-3.320837	0.252568
C	1.137549	-2.080653	-1.612736
C	-0.232961	-4.304390	-0.630498
H	0.046935	-3.412424	1.320880
C	0.682842	-3.072666	-2.484841
H	1.704677	-1.235373	-1.991001
C	-0.012822	-4.203338	-2.017929

H	-0.752413	-5.175961	-0.238094
H	0.895484	-2.980874	-3.547436
C	-0.508594	-5.271378	-2.968922
H	-0.383816	-6.275753	-2.547801
H	-1.577879	-5.152402	-3.197928
H	0.033634	-5.241051	-3.920284

Table S7: Optimized Cartesian xyz coordinates of the 3^{Me} (TS) transition state structure at the B3LYP level of theory in junction of the SDD basis set and associated ECP for Cu, 6-311G(d) basis set for the atoms bond to Cu, and 6-31G basis set for the other atoms.

Cu	-1.252322	0.370059	-0.422888
N	-1.317913	2.313331	0.038398
C	-2.134739	3.187395	-0.548401
Cu	2.682806	-0.263432	-0.112828
N	-2.110360	4.411662	0.098403
C	-2.914975	5.596864	-0.198107
H	-3.901889	5.535629	0.271584
H	-3.039005	5.716736	-1.275482
H	-2.396163	6.478991	0.181011
N	-2.067885	0.666718	-2.606008
C	-1.227090	4.296709	1.178024
N	-4.807222	0.839412	-0.003406
C	-0.830952	5.203233	2.166851
H	-1.222553	6.213131	2.214779
N	-5.058354	-1.387087	-0.272676
C	0.089807	4.745332	3.110870
H	0.419813	5.415402	3.897417
N	3.027260	-2.209869	-0.955676
C	0.593179	3.426092	3.067798
H	1.303779	3.107999	3.823296
N	5.148592	-0.374239	-0.513454
C	0.193822	2.524063	2.081025
H	0.575326	1.512046	2.024789
C	-0.730945	2.974431	1.127493
N	3.097891	1.478776	-1.156656
N	3.649257	-0.256936	1.867721
C	-3.048389	2.882491	-1.691681
H	-3.904420	2.343383	-1.265282
C	-2.407359	2.103152	-2.859686
H	-3.073880	2.175450	-3.735489
H	-1.477714	2.612227	-3.134790
C	-3.201063	-0.257540	-2.940914
H	-2.877037	-1.255073	-2.640493
H	-3.330837	-0.252258	-4.038903
C	-4.602855	0.025877	-2.347002
H	-4.932068	1.036198	-2.603666
H	-5.284440	-0.643941	-2.888115
C	-4.801785	-0.157068	-0.871644
C	-5.081365	-2.708719	-0.886482
H	-5.238291	-2.619351	-1.962447
H	-5.908102	-3.291371	-0.470276
H	-4.140649	-3.238936	-0.708496
C	-5.204164	-1.141315	1.092425
C	-5.458378	-1.983481	2.179909
H	-5.571298	-3.056052	2.065134
C	-5.560247	-1.379945	3.435417
H	-5.759124	-1.996506	4.305752

C	-5.412052	0.016214	3.597882
H	-5.503011	0.444419	4.590565
C	-5.157362	0.849357	2.508180
H	-5.050121	1.921749	2.628372
C	-5.049126	0.260199	1.240432
C	-0.921132	0.331227	-3.537821
H	-0.114542	1.027607	-3.289692
H	-1.239708	0.549468	-4.572670
C	-0.376097	-1.083707	-3.481880
C	0.677189	-1.390693	-2.613550
H	1.055245	-0.635056	-1.935710
C	1.254356	-2.672965	-2.591101
C	0.746541	-3.665124	-3.452383
H	1.187679	-4.657981	-3.448196
C	-0.302150	-3.370982	-4.325802
H	-0.677813	-4.133514	-4.999701
C	-0.851495	-2.084553	-4.349624
H	-1.644355	-1.853883	-5.054869
C	2.410902	-3.009336	-1.751923
H	2.772305	-4.039688	-1.869682
C	4.238949	-2.709574	-0.290572
H	4.070649	-2.669882	0.789946
H	4.462782	-3.751106	-0.567484
C	5.444564	-1.813328	-0.668713
H	6.309153	-2.100540	-0.053421
H	5.714098	-2.015633	-1.711855
C	5.243791	0.426600	-1.740333
H	4.936562	-0.216318	-2.573763
H	6.273288	0.761787	-1.957032
C	4.322497	1.637592	-1.716001
C	4.717581	2.851341	-2.290192
H	5.709844	2.943354	-2.718416
C	3.831509	3.931544	-2.300373
H	4.123373	4.879699	-2.738275
C	2.569513	3.764543	-1.724320
H	1.851744	4.575691	-1.694142
C	2.245506	2.527859	-1.163851
H	1.283584	2.358848	-0.695739
C	5.733725	0.263803	0.669090
H	5.691225	1.350516	0.516312
H	6.799074	0.004438	0.795514
C	4.982869	-0.054777	1.955176
C	5.658675	-0.082636	3.181480
H	6.732522	0.069993	3.208986
C	4.938276	-0.309074	4.356455
H	5.443015	-0.332608	5.316217
C	3.558877	-0.514993	4.265470
H	2.959176	-0.705030	5.147906
C	2.957509	-0.488046	3.005502
H	1.898522	-0.679567	2.865884
H	-3.436692	3.817237	-2.110004
O	0.653418	-1.288558	1.170241
O	0.610044	-0.145069	0.407128
O	-1.924168	-1.433337	-0.361881
C	-1.471615	-2.300206	0.479540
C	-1.293974	-3.678999	0.116794
C	-1.050014	-1.888260	1.805312
C	-0.886098	-4.594696	1.054184
H	-1.521321	-3.969585	-0.903295
C	-0.713499	-2.890879	2.773052
H	-1.385662	-0.913221	2.145227
C	-0.594540	-4.215326	2.415689

H	-0.790237	-5.642156	0.779954
H	-0.523232	-2.583948	3.796862
C	-0.202691	-5.282849	3.409075
H	-0.983994	-6.048202	3.503624
H	0.713758	-5.800671	3.096626
H	-0.026505	-4.859855	4.402340

Table S8: Optimized Cartesian xyz coordinates of the **3^{Me}(Prod)** structure at the B3LYP level of theory in junction of the SDD basis set and associated ECP for Cu, 6-311G(d) basis set for the atoms bond to Cu, and 6-31G basis set for the other atoms.

Cu	-1.185987	0.421204	-0.422026
N	-1.173432	2.376814	0.036431
C	-1.936770	3.291621	-0.556176
Cu	2.632098	-0.370570	-0.143074
N	-1.846938	4.517729	0.084576
C	-2.585158	5.742898	-0.219843
H	-3.577514	5.735503	0.242514
H	-2.694907	5.867048	-1.298441
H	-2.023195	6.597259	0.161493
N	-2.009351	0.750030	-2.609111
C	-0.971582	4.359158	1.165231
N	-4.677598	1.059158	0.018448
C	-0.519676	5.245563	2.148571
H	-0.852622	6.276450	2.194606
N	-5.161721	-1.122634	-0.296068
C	0.380591	4.739937	3.088451
H	0.752790	5.393730	3.869949
N	2.942402	-2.322613	-0.926771
C	0.811947	3.395097	3.046747
H	1.511914	3.042303	3.796879
N	5.169091	-0.583947	-0.512232
C	0.356195	2.513097	2.066338
H	0.680043	1.480250	2.006030
C	-0.550160	3.011072	1.119695
N	3.175382	1.346926	-1.180555
N	3.631066	-0.345314	1.838782
C	-2.857196	3.029994	-1.704436
H	-3.743585	2.542803	-1.280157
C	-2.250544	2.207185	-2.862183
H	-2.897168	2.323312	-3.748628
H	-1.285204	2.653880	-3.121376
C	-3.206490	-0.088251	-2.948443
H	-2.954810	-1.111014	-2.663728
H	-3.339236	-0.060621	-4.046061
C	-4.584714	0.283499	-2.345994
H	-4.841563	1.318118	-2.586730
H	-5.313121	-0.327179	-2.895442
C	-4.788614	0.090453	-0.872455
C	-5.362170	-2.415822	-0.936298
H	-5.396866	-2.296275	-2.019432
H	-6.311727	-2.850325	-0.608864
H	-4.548753	-3.104193	-0.685675
C	-5.261112	-0.895864	1.076237
C	-5.581727	-1.735097	2.148341
H	-5.813173	-2.785682	2.009388
C	-5.592515	-1.157365	3.420298
H	-5.838748	-1.771593	4.280141
C	-5.293561	0.210548	3.611999
H	-5.317286	0.619816	4.616460
C	-4.975541	1.041018	2.536763

H	-4.750753	2.091978	2.680632
C	-4.956997	0.477559	1.253132
C	-0.892806	0.335342	-3.544743
H	-0.047496	0.992009	-3.319517
H	-1.208805	0.546002	-4.582185
C	-0.424654	-1.104582	-3.453396
C	0.623789	-1.438591	-2.588892
H	1.060856	-0.679838	-1.949765
C	1.130188	-2.749565	-2.526460
C	0.554808	-3.741195	-3.344906
H	0.941145	-4.756104	-3.311221
C	-0.488386	-3.419974	-4.215731
H	-0.913766	-4.183612	-4.858278
C	-0.967521	-2.106930	-4.278907
H	-1.756203	-1.857418	-4.982527
C	2.279089	-3.117985	-1.689795
H	2.586058	-4.168920	-1.775484
C	4.132275	-2.861457	-0.253371
H	3.970501	-2.786834	0.826151
H	4.304885	-3.919249	-0.505268
C	5.379806	-2.034817	-0.654850
H	6.233998	-2.365711	-0.045855
H	5.625489	-2.263172	-1.698662
C	5.282871	0.204767	-1.742572
H	4.937834	-0.429024	-2.568252
H	6.322906	0.495682	-1.974961
C	4.416077	1.455297	-1.717230
C	4.878766	2.655871	-2.268878
H	5.881822	2.704290	-2.678905
C	4.047196	3.778452	-2.280714
H	4.392496	4.716612	-2.701005
C	2.768523	3.664662	-1.729578
H	2.089151	4.508408	-1.701323
C	2.376137	2.437644	-1.192021
H	1.396917	2.310917	-0.746747
C	5.767382	0.033480	0.670340
H	5.810713	1.117033	0.496235
H	6.807862	-0.299828	0.830789
C	4.969084	-0.197499	1.948430
C	5.616758	-0.199882	3.191162
H	6.695567	-0.092271	3.236905
C	4.862783	-0.341552	4.357684
H	5.345243	-0.343328	5.329161
C	3.477333	-0.491066	4.243725
H	2.851054	-0.613974	5.119727
C	2.906980	-0.493941	2.969495
H	1.844441	-0.641549	2.817421
H	-3.189008	3.981386	-2.134046
O	0.524780	-1.572884	1.183964
O	0.595841	-0.289461	0.511326
O	-2.052252	-1.373560	-0.337572
C	-1.625369	-2.273201	0.440318
C	-1.743228	-3.678738	0.122354
C	-0.869163	-1.879108	1.679749
C	-1.444702	-4.617462	1.064290
H	-2.116230	-3.947670	-0.860132
C	-0.711720	-2.963332	2.692370
H	-1.263861	-0.947794	2.102135
C	-0.956373	-4.264817	2.399230
H	-1.580220	-5.672184	0.839454
H	-0.339338	-2.676294	3.670894
C	-0.758610	-5.377751	3.399869

H	-1.697681	-5.913098	3.590849
H	-0.037888	-6.118526	3.029515
H	-0.388522	-4.995915	4.355317

7. References

1. Wagner, W. R.; Johnson, E. T.; Lidsley, J. S., *Tetrahedron* **1997**, *53*, 6755-6790.
2. Schatz, M.; Leibold, M.; Foxon, S. P.; Weitzer, M.; Heinemann, F. W.; Hampel, F.; Walter, O.; Schindler, S., *Dalton Trans.* **2003**, 1480-1487.
3. Casella, L.; Gullotti, M.; Radaelli, R.; Di Gennaro, P., *J. Chem. Soc., Chem. Comm.* **1991**, 1611-1612.
4. Kubas, G. J., *Inorg. Synth.* **1979**, *19*, 90-92.
5. Kubas, G. J., *Inorg. Synth.* **1990**, *28*, 68-72.
6. Company, A.; Palavacini, S.; Garcia-Bosch, I.; Mas-Ballesté, R.; Que Jr., L.; Rybak-Akimova, E. V.; Casella, L.; Ribas, X.; Costas, M., *Chem. Eur. J.* **2008**, *14*, 3535-3538.
7. LaRue, T. A.; Blakley, E. R., *Anal. Chim. Acta.* **1964**, *31*, 400-403.
8. Becke, A. D., *J. Chem. Phys.* **1993**, *98*, 5648-5652.
9. Lee, C.; Yang, W.; Parr, R. G., *Phys. Rev. B* **1988**, *37*, 785-789.
10. Hehre, W. J.; Radom, L.; Schleyer, P. v. R.; Pople, J. A., *Ab Initio Molecular Orbital Theory*. Wiley: New York, 1986.
11. Dolg, M.; Wedig, U.; Stoll, H.; Preuss, H. J., *Chem. Phys.* **1987**, *86*, 866-872.

Chapter III.2

Electrophilic Arene Hydroxylation and Phenol O-H Oxidations Performed by an Unsymmetric μ - $\eta^1:\eta^1$ -O₂-Peroxo-Dicopper(II) Complex.

Garcia-Bosch, I.; Ribas, X.; Costas, M. Accepted in *Chem. Eur. J.* DOI: 10.1002/chem.201102372

Electrophilic Arene Hydroxylation and Phenol O-H Oxidations Performed by an Unsymmetric μ - η^1 : η^1 -O₂-Peroxo-Dicopper(II) Complex.

Isaac Garcia-Bosch, Xavi Ribas,* Miquel Costas*

Dedication.

Abstract: Reactions of the unsymmetric dicopper(II) peroxide complex $[\text{Cu}^{\text{II}}_2(\mu\text{-}\eta^1\text{:}\eta^1\text{-O}_2)(m\text{-XYL}^{\text{N}3\text{N}4})]^{2+}$ (**1O₂**), against phenolates and phenols are described. **1O₂** reacts with *p*-X-PhONa (X = MeO, Cl, H, Me) at -90 °C performing Tyrosinase-like *ortho*-hydroxylation of the aromatic ring and forming corresponding catechol products. Mechanistic studies demonstrate that reactions occur via initial reversible formation of metastable association complexes $[\text{Cu}^{\text{II}}_2(\mu\text{-}\eta^1\text{:}\eta^1\text{-O}_2)(p\text{-X-PhO})(m\text{-XYL}^{\text{N}3\text{N}4})]^{2+}$ (**1O₂•X-PhO**) that then undergo *ortho*-hydroxylation of the aromatic ring by the peroxide moiety. **1O₂** also reacts with 4-X-substituted phenols *p*-X-PhOH (X = MeO, Me, F, H, Cl) and with 2,4-di-*tert*-butylphenol at -90 °C causing rapid

decay of **1O₂** and afford biphenol coupling products, indicative that reactions occur via formation of phenoxyl radicals than then undergo radical C-C coupling. Spectroscopic UV-vis monitoring and kinetic analysis show that reactions occur via reversible formation of ground state association complexes $[\text{Cu}^{\text{II}}_2(\mu\text{-}\eta^1\text{:}\eta^1\text{-O}_2)(X\text{-PhOH})(m\text{-XYL}^{\text{N}3\text{N}4})]^{2+}$ (**1O₂•X-PhOH**) that then evolve via an irreversible rate determining step. Mechanistic studies indicate that **1O₂** reacts with phenols via initial phenol binding to the Cu₂O₂ core, followed by a proton coupled electron transfer (PCET) in the rate determining step. Results disclosed in this work provide experimental evidence that the unsymmetric **1O₂** complex can mediate electrophilic arene hydroxylation and PCET

reactions commonly associated to electrophilic Cu₂O₂ cores, and strongly suggest that the ability to form substrate•Cu₂O₂ association complexes may provide paths to overcome the inherent reactivity of the O₂-binding mode. This work provides experimental evidence that the presence of a H⁺ completely determines the fate of the association complex $[\text{Cu}^{\text{II}}_2(\mu\text{-}\eta^1\text{:}\eta^1\text{-O}_2)(X\text{-PhO(H)})(m\text{-XYL}^{\text{N}3\text{N}4})]^{2+}$ between a PCET and an arene hydroxylation reaction, and may provide clues to understand enzymatic reactions at dicopper sites.

Keywords: O₂-activation • unsymmetric complexes • arene hydroxylation • HAT • PCET

Introduction

Multicopper proteins that bind and activate O₂ play important roles in a number of biological processes.^[1-5] Among them, proteins where O₂ binding and activation takes place at a dicopper site include Hemocyanin (Hc), which acts as O₂-carrier in arthropods and mollusks,^[6-8] Tyrosinase (Tyr) which catalyzes 4e- oxidation of tyrosine to dopaquinone, in the first step of melanine biosynthesis,^[9] catechol oxidase (CO), that carries out the 2e- oxidation of catechols to quinones,^[10] and particulated methane monooxygenase (pMMO)

which catalyzes methane oxidation to methanol.^[11] Irrespective of their function, this group of proteins shares a N-rich active site, and except for pMMO, in the absence of O₂, each copper ion is three coordinate to histidine residues in the reduced Cu(I) state. The identity of the species formed in pMMO after reaction with O₂ remains unknown,^[11] but in Tyr, CO and Hc, O₂-binding results in the formation of a common Cu^{II}₂(μ - η^2 : η^2 -O₂) species.^[9, 10, 12] From this step, chemistry diverges, depending on the specific protein. The chemical reasons that underlay the different reactivity from an apparently common Cu₂O₂ species remain a matter of intense study in enzymology and synthetic model chemistry.^[4, 13] It has been shown that one of the factors that modulate the diverse chemistry is substrate accessibility to the active site.^[14-17] Other factors such as asymmetry between the two copper coordination sites, and specific substrate orientation at the Cu₂O₂ core can be also important.^[13, 18] For instance, crystallographic analyses show that the oxygenated form of tyrosinase (oxyTyr) binds a molecule of the phenolic substrate in one of the copper centers,^[9] triggering the rotation of the peroxo core and orientating the *ortho*-phenolic position which suffers an electrophilic attack by the Cu₂-O₂ center (Scheme 1).^[9, 15, 19]

[a] I. Garcia-Bosch, Dr. X. Ribas, Dr. M. Costas,*
QBIS Group, Departament de Química
Universitat de Girona
Campus de Montilivi, E-17071 Girona, Catalonia (Spain)
E-mail: miquel.costas@udg.edu

Supporting information for this article is available on the WWW under
<http://www.chemeurj.org/> or from the author.

Supporting Information

for

Electrophilic Arene Hydroxylation and Phenol O-H Oxidations Performed by an Unsymmetric μ - η^1 : η^1 -O₂-Peroxo-Dicopper(II) Complex.

Isaac Garcia-Bosch, Xavi Ribas* and Miquel Costas*

^a*Departament de Química, Campus de Montilivi, Universitat de Girona, E-17071
Girona, Spain.*

Contents

1. Physical Methods.....	S2
2. Materials.....	S2
3. Reactivity of complexes 1O ₂ and 2O ₂ towards sodium <i>p</i> -phenolates	S2
4. Reactivity of complexes 1O ₂ and 2O ₂ towards phenols.....	S4
5. References.....	S7

1. Physical Methods

UV-vis spectroscopy was performed on a Cary 50 Scan (Varian) UV-vis spectrophotometer with 1 cm quartz cells. The low temperature control was performed with a cryostat from Unisoku Scientific Instruments, Japan. Elemental analyses were performed using a CHNS-O EA-1108 elemental analyzer from Fisons. NMR spectra were taken on Bruker Bruker DPX400 spectrometer using standard conditions. All HPLC-MS were obtained on a HPLC Agilent 1200 (G1354A) connected to a Detector Diode Array Agilent Series 1200 (G1315B) and a Mass Detector Agilent Series G6100AA.

2. Materials

Reagents and solvents used were of commercially available reagent quality unless otherwise stated. Solvents were purchased from SDS and Scharlab. Preparation and handling of air-sensitive materials were carried out in a N₂ drybox (MBraun) with O₂ and H₂O concentrations < 1 ppm. All phenols used were commercially available. Phenolates were synthesized as previously described.^[1] Complex [Cu^I₂(*m*-XYL^{N³N⁴)}]²⁺ (**1**) and complex [Cu^I₂(*m*-XYL^{N⁴N⁴)}]²⁺ (**2**) were synthesized as previously described.^[2]

3. Reactivity of complexes **1O₂** and **2O₂** towards sodium *p*-phenolates.

3.1 Reactivity of complexes **1O₂** and **2O₂** towards sodium *p*-phenolates. Products analysis.

Analysis of the products obtained from the reaction of complex **1O₂** with phenolates was previously described.^[2] The results obtained for the *ortho*-hydroxylation of different phenols are shown in Table S1. Complex **2O₂** is unable to perform the oxidation of phenolates.

Table S1. Quantification of catechol formed in the oxidation of phenolates by **1O₂**.

Substrate	<i>p</i> -catechol yield (%) ^[a]
<i>p</i> -MeO-phenolate	14%
2,4-di- <i>tert</i> -butyl-phenolate	0%
<i>p</i> -Me-phenolate	34%
<i>p</i> -F-phenolate	34%
Phenolate	36%
<i>p</i> -Cl-phenolate	38%

<i>p</i> -CN-phenolate	0%
<i>p</i> -CO ₂ Me-phenolate	0%
<i>p</i> -NO ₂ -phenolate	0%

[a] 3 equiv. of sodium phenolate were used. Yield is based on mols of complex **1O₂** used.

3.2 Reactivity of complexes **1O₂** and **2O₂** towards sodium *p*-phenolates. Kinetic analysis.

In a typical experiment, 3 mL of a solution of complex **1** or **2** ([0.1 mM]) in anhydrous acetone was prepared under anaerobic conditions and was placed in a special UV-vis cell (1cm path length) with the appropriate design of the cryostat-UV-vis system. The solution was cooled to the desired temperature (178-203 K) and complex **1O₂** or **2O₂** was generated by injection of O₂ using a filled balloon. After full accumulation of **1O₂** or **2O₂**, 0.2 mL of an anhydrous acetone solution prepared under anaerobic conditions and containing the corresponding equivalents of the desired sodium phenolate were injected. The decay of the **1O₂** or **2O₂** UV-vis features was recorded until no significant changes in the spectra were observed.

For complex **1O₂**, the obtained decays were fitted to single exponential decays. For all the phenolates studied, the k_{obs} values calculated show a saturation behavior with increase on [*p*-X-phenolate]. The curves observed can be fitted using a mathematic model (Equations 1 and 2) consisting in a pre-equilibrium prior to the rate determining step (Figure S1).

$$k_{obs} = \frac{k_2 K_{eq} [Subs.]}{1 + K_{eq} [Subs.]} \quad (\text{Equation 1})$$

$$\frac{1}{k_{obs}} = \frac{1}{k_2 K_{eq}} \frac{1}{[Subs.]} + \frac{1}{k_2} \quad (\text{Equation 2})$$

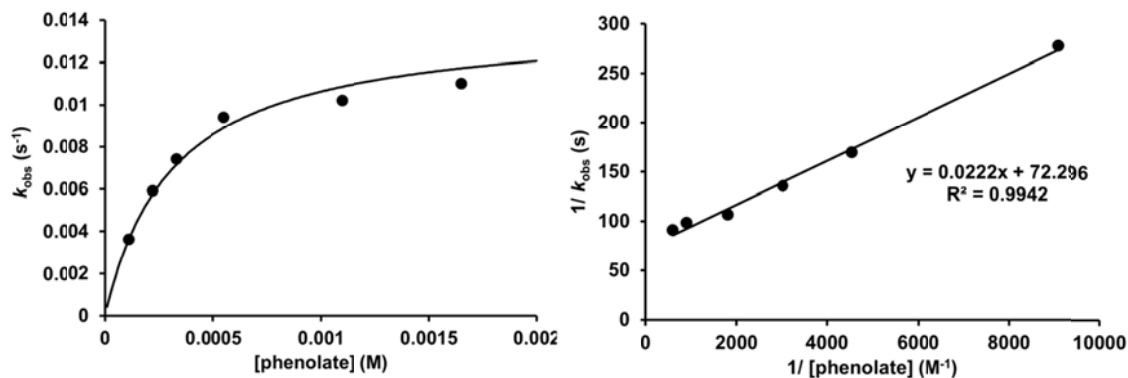


Figure S1. Left: Plot of k_{obs} vs. [phenolate]. Right: Plot of $1/k_{obs}$ vs. $1/[phenolate]$.

The reaction of complex $1O_2$, with sodium phenolate was analyzed in a range of temperatures in order to obtain the thermodynamic parameters for the pre-equilibrium process and activation parameters for the *r.d.s.* The different k_{obs} at different concentrations and at different temperatures are plotted in Figure S2.

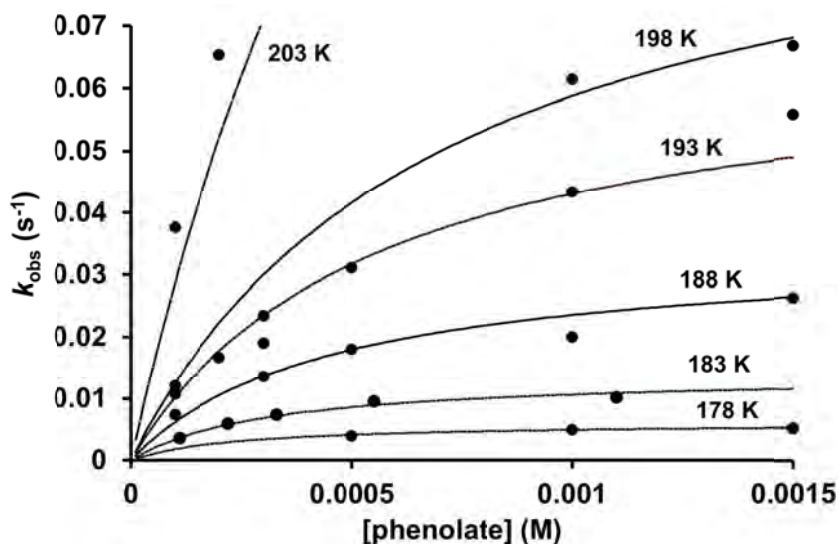


Figure S2. k_{obs} for reaction of complex $1O_2$ with sodium phenolate at different temperatures.

The kinetic isotope effect (K.I.E) was determined for the reaction of $1O_2$ with sodium phenolates by using phenolate- d_5 . k_{obs} at different substrate concentration are plotted in Figure S3.

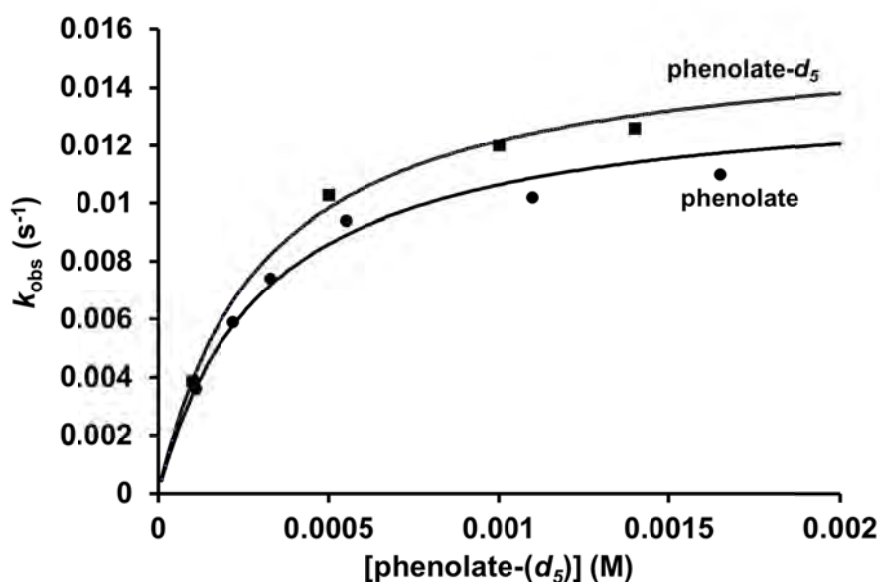


Figure S3. k_{obs} for reaction of complex $1O_2$ with sodium phenolate and sodium phenolate- d_5 .

4. Reactivity of complexes $1O_2$ and $2O_2$ towards phenols.

4.1 Reactivity of complexes $1O_2$ and $2O_2$ towards phenols. Products analysis.

Analysis of the products obtained from the reaction of $1O_2$ with phenols was performed by 1H -NMR in acetone- d_6 using acetophenone as internal standard. In a typical experiment, complex $1O_2$ or $2O_2$ was generated at -90 °C bubbling molecular O_2 through a solution of **1** previously prepared under anaerobic conditions ($[1O_2]$, $[2O_2]$ = 0.1 mM). Then, the excess of O_2 was removed by several vacuum / N_2 cycles and a solution containing 10-100 equiv. of phenol was added. The reaction was quenched by 3 ml of HCl 0.5 M and the acetone is removed from the mixture under reduced pressure. The resulting aqueous phase was extracted using CH_2Cl_2 (3 x 10 mL). The organic fraction was dried over $MgSO_4$ and the solvent removed under reduced pressure. The resultant product was solved with acetone- d_6 and analyzed by 1H -NMR using mesitylene as internal standard. The presence of C-C coupled products was confirmed by HPLC-MS.

Table S2. Quantification of C-C coupling products in the oxidation of phenols by $1O_2$.

Substrate	C-C coupling product (%) ^[a]
2,4-di- <i>tert</i> -butyl-phenol ^[b]	50%
<i>p</i> -Me-phenol ^[b]	30%
<i>p</i> -F-phenol ^[c]	28%

[a] Yield is based on mols of complex $1O_2$ used. [b] 10 equiv. of phenol were used. [c] 100 equiv. of *p*-F-phenol were used.

4.2 Reactivity of complexes $1O_2$ and $2O_2$ towards phenols. Kinetic analysis.

In a typical experiment, 3 mL of a solution of complex **1** or **2** ([0.1 mM]) in anhydrous acetone was prepared under anaerobic conditions and was placed in a special UV-vis cell (1cm path length) with the appropriate design of the cryostat-UV-vis system. The solution was cooled to the desired temperature (183-203 K) and complex $1O_2$ or $2O_2$ was generated by injection of O_2 using a filled balloon. After full accumulation of $1O_2$ or $2O_2$, 0.2 mL of an anhydrous acetone solution prepared under anaerobic conditions and containing the corresponding equivalents of the desired phenol were injected. The decay of the $1O_2$ or $2O_2$ UV-vis features was recorded until no significant changes in the spectra were observed. The injection of the desired phenol causes a shift in the UV-vis band, and it is dependent on the electronic nature of the phenol (Figure S4).

For complex $1O_2$, the obtained decays were fitted to single exponential decays. As in the phenolates, the k_{obs} values calculated show a saturation behavior with an increase on [phenols].

the curves observed can be fitted using a mathematic model consisting in a pre-equilibrium prior to the rate determining step (Figure S1). For poor-electron *p*-phenols (X= CO₂Me, CN, NO₂), the coordination of the phenol was observed but no decay on the UV-vis features was observed.

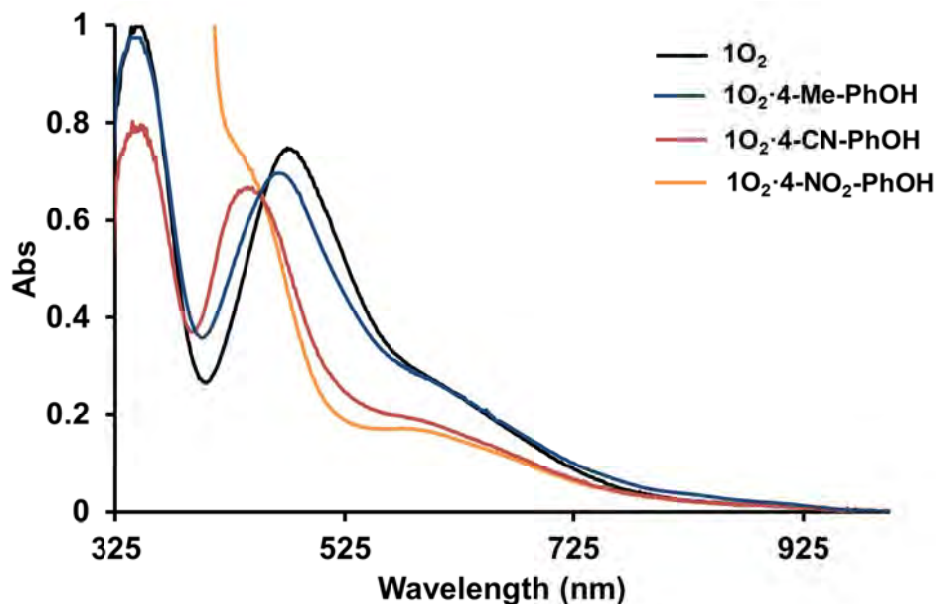


Figure S4. UV-vis of the reaction with different phenols (150 equiv. of phenol were used).

The reaction of complex **1O₂**, with phenol was analyzed in a range of temperatures in order to obtain the thermodynamic parameters for the pre-equilibrium process and activation parameters for the *r.d.s*. The different k_{obs} at different concentrations and at different temperatures are plotted in Figure S5. The different $K_{eq(OH)}$ and $k_{2(OH)}$ were used to build Van't Hoff and Eyring plots (Figure S6).

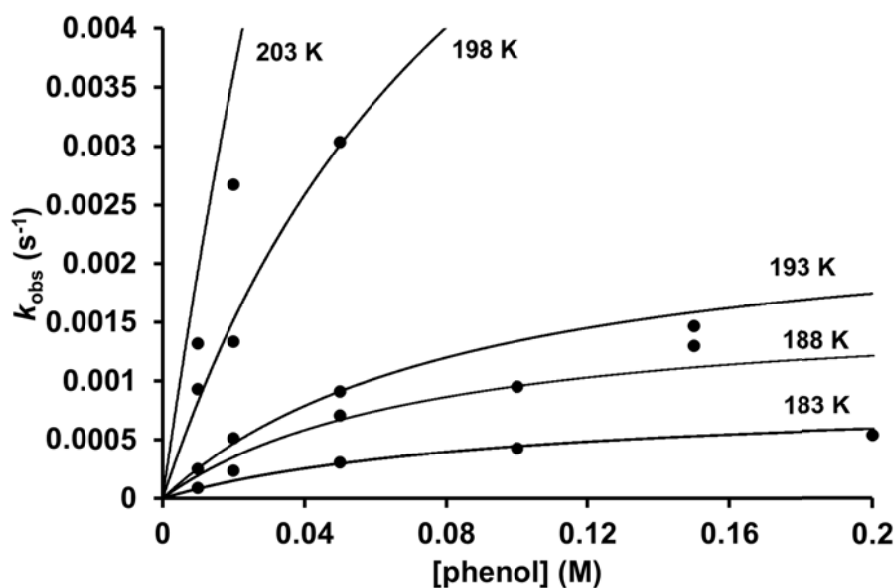


Figure S5. k_{obs} for reaction of complex $\mathbf{1O}_2$ with phenol at different temperatures.

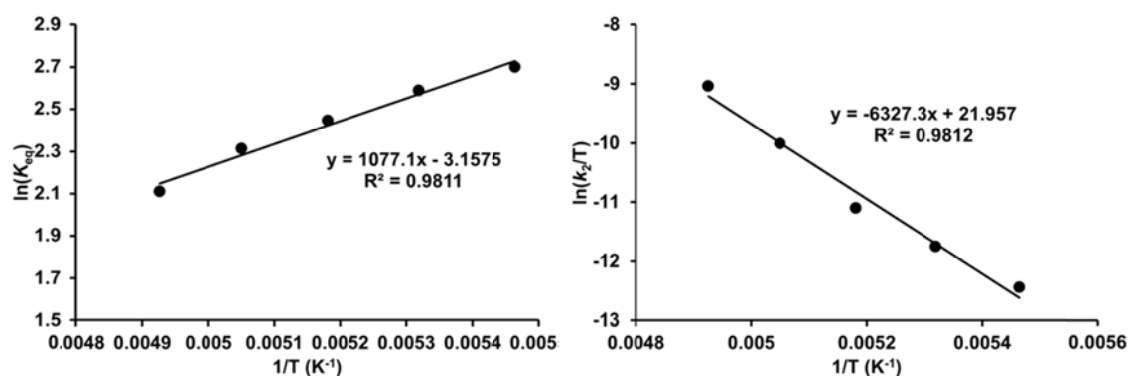


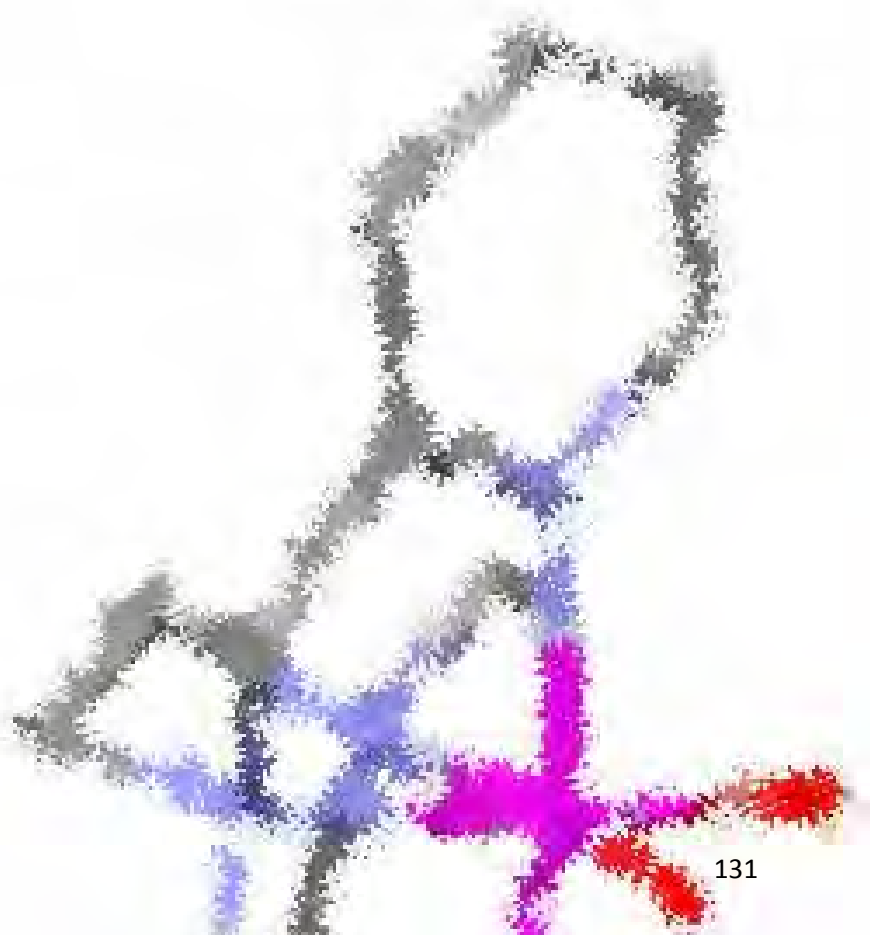
Figure S6. Van't Hoff and Eyring plots for the reaction of $\mathbf{1O}_2$ towards phenols.

5. References

- [1] A. Company, S. Palavicini, I. Garcia-Bosch, R. Mas-Ballesté, L. Que, Jr., E. V. Rybak-Akimova, L. Casella, X. Ribas, M. Costas, *Chem. Eur. J.* **2008**, *14*, 3535-3538.
- [2] I. Garcia-Bosch, A. Company, J. R. Frisch, M. Torrent-Sucarrat, M. Cardellach, I. Gamba, M. Guell, L. Casella, L. Que, X. Ribas, J. M. Luis, M. Costas, *Angew. Chem. Int. Ed.* **2009**, *49*, 2406-2409.

Chapter IV

**Non-Porphyrinic Manganese(IV)
Complexes in C-H Hydrogen Atom
Transfer Reactions.**



Chapter IV.1

Evidence for a Precursor Complex in C-H Hydrogen Atom Transfer Reactions Mediated by a Manganese(IV) Oxo Complex.

Garcia-Bosch, I.; Company, A.; Cady, C. W.; Styring, S.; Browne, W. R.; Ribas, X.; Costas, M. *Angew. Chem. Int. Ed.* **2011**, *50*, 5648-5653.

Isaac Garcia-Bosch, Anna Company, Clyde W. Cady, Stenbjörn Styring, Wesley R. Browne, Xavi Ribas, Miquel Costas. "Evidence for a Precursor Complex in C-H Hydrogen Atom Transfer Reactions Mediated by a Manganese(IV) Oxo Complex". *Angewandte Chemie International Edition*. Vol. 50, issue 25 (June 2011) : p. 5648-5653
Copyright © 2011 WILEY-VCH Verlag GmbH & Co. KGaA

Article first published online: 14 APR 2011

<http://dx.doi.org/10.1002/anie.201100907>

<http://onlinelibrary.wiley.com/doi/10.1002/anie.201100907/abstract>

Abstract:

HAT trick: $[\text{Mn}^{\text{IV}}(\text{OH})_2(\text{H,MePytacn})]^{2+}$ (**A**) and $[\text{Mn}^{\text{IV}}(\text{O})(\text{OH})(\text{H,MePytacn})]^+$ (**B**) differ in their reactions with C—H bonds: compound **A** engages in typical single-step hydrogen atom transfer (HAT) reactions, whereas **B** first forms a substrate–**B** encounter complex (**C**; see scheme). This equilibrium alters the relative C—H reactivity from that expected from C—H bond dissociation energies.

Keywords

- C—H activation;
- hydrogen atom transfer;
- kinetics;
- manganese;
- metal oxo compounds

Supporting information:

Detailed facts of importance to specialist readers are published as "Supporting Information". Such documents are peer-reviewed, but not copy-edited or typeset. They are made available as submitted by the authors.

http://onlinelibrary.wiley.com/store/10.1002/anie.201100907/asset/supinfo/anie_201100907_sm_miscellaneous_information.pdf?v=1&s=20840568dbac4499d7935fadf93aa5f6e4024e80

Please note: Wiley-Blackwell are not responsible for the content or functionality of any supporting materials supplied by the authors. Any queries (other than missing material) should be directed to the corresponding author for the article.

Supporting Information

© Wiley-VCH 2011

69451 Weinheim, Germany

Evidence for a Precursor Complex in C–H Hydrogen Atom Transfer Reactions Mediated by a Manganese(IV) Oxo Complex**

*Isaac Garcia-Bosch, Anna Company, Clyde W. Cady, Stenbjörn Styring, Wesley R. Browne, Xavi Ribas, and Miquel Costas**

anie_201100907_sm_miscellaneous_information.pdf

Contents

1. Physical Methods.....	S1
2. Materials.....	S2
3. Synthesis and generation of complexes 2 and 3	S2
4. Characterization of complexes 2 and 3	S3
5. Complexes reactivity towards C-H bonds.....	S9
6. References.....	S16

1. Physical Methods

UV-vis spectroscopy was performed on a Cary 50 Scan (Varian) UV-vis spectrophotometer with 1 cm quartz cells. The low temperature control was performed with a cryostat from Unisoku Scientific Instruments, Japan. Elemental analyses were performed using a CHNS-O EA-1108 elemental analyzer from Fisons. NMR spectra were taken on Bruker Bruker DPX400 spectrometer using standard conditions. All HPLC-MS were obtained on a HPLC Agilent 1200 (G1354A) connected to a Detector Diode Array Agilent Serie 1200 (G1315B) and a Mass Detector Agilent

Serie G6100AA. Raman spectra were recorded using a fiber optic equipped dispersive Raman spectrometer (785 nm, Perkin Elmer RamanFlex). Electrochemical measurements were carried out on a model 630B Electrochemical Workstation (CH Instruments). Complex concentrations were typically 1mM using different solvent mixtures which contained 0.1M tetrabutylammonium hexafluorophosphate. A Teflon-shrouded glassy carbon working electrode and a SCE reference electrode were employed. Cyclic voltammograms were obtained at sweep rates between 100mV s⁻¹ and 1 V s⁻¹.

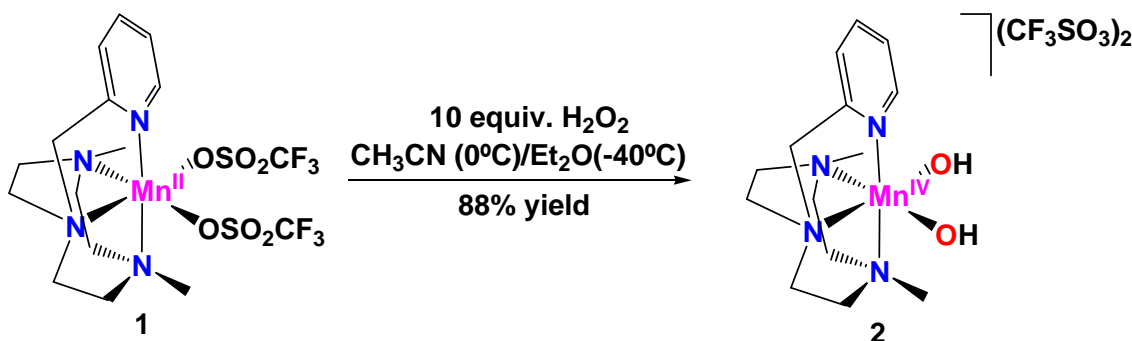
2. Materials

Reagents and solvents used were of commercially available reagent quality unless otherwise stated. Solvents were purchased from SDS and Scharlab. Preparation and handling of air-sensitive materials were carried out in a N₂ drybox (MBraun) with O₂ and H₂O concentrations < 1 ppm. Xanthene-d₂ and DHA-d₄ were synthesized as described somewhere else.¹

3. Synthesis and generation of complexes 2 and 3

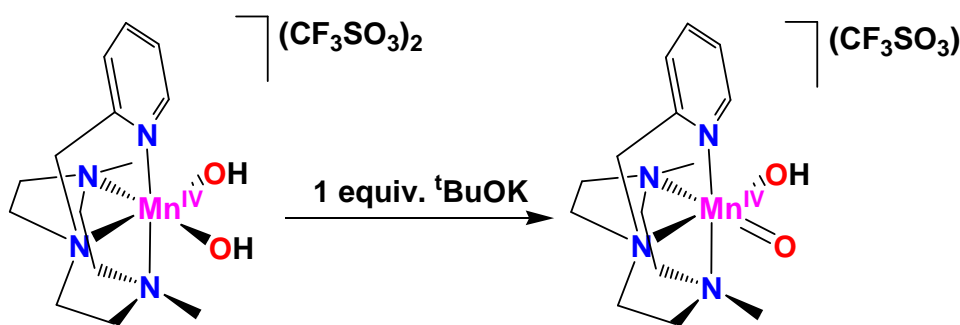
Complex [Mn(CF₃SO₃)₂(^{H,Me}Pytacn)], **1** was synthesized as previously described.²

3.1 Synthesis of complex [Mn(OH)₂(^{H,Me}Pytacn)](CF₃SO₃)₂ (**2**):



40 mg of complex [Mn^{II}(CF₃SO₃)₂(^{H,Me}Pytacn)] (0.067 mmols) were solved in 1 mL of CH₃CN in an ice bath. Then, 67 μL of commercially available H₂O₂ 33% (0.67 mmols) were added directly to the mixture, observing a color change from colorless to deep purple. After 1 hour of stirring, the solution was frozen in a liquid N₂ bath, and 100 mL of cold diethyl ether (-80°C) were added. The two-phase mixture was left overnight, and then 37 mg of complex **2** were obtained by removing the solvents by decantation and drying by vacuum (0.058 mmols, 88%). Crystalline material suitable for X-Ray diffraction analysis was obtained by recrystallization of the purple material solving some of the purple material in acetonitrile and adding diethyl ether forming two phases, and leaving the solutions in the freezer (-40 °C) for several days. Anal. Calcd for C₁₆H₂₆F₆MnN₄O₈S₂: C, 30.24; H, 4.12; N, 8.82; S, 10.09 %. Found: C, 30.00; H, 4.23; N, 8.73; S, 9.90 %.

3.2 Generation of complex $[\text{Mn}(\text{O})(\text{OH})(^{\text{H,Me}}\text{Pytacn})](\text{CF}_3\text{SO}_3)_2$ (**3**):



1.33 mg of complex **2** (0.002 mmols) were solved in 2 mL of a $\text{CH}_3\text{CN}:\text{water}$ 5:1 w:w ($[\mathbf{2}] = 1 \text{ mM}$) and then cooled to 0°C . Afterwards, $67 \mu\text{L}$ of an aqueous solution containing 1.0 equiv. of $t\text{BuOK}$ was added, generating the deprotonated species **3**. UV-Vis of the reaction showed an isosbestic point meaning of a full and clean transformation from **2** to **3** (Figure 2). Furthermore, the addition of 1 equivalent of $\text{CF}_3\text{SO}_3\text{H}$ takes us to a 95% recover of complex **2**, showing the reversibility of the protonation/deprotonation process.

4. Characterization of complexes **2** and **3**.

4.1 Characterization of complexes **2** and **3** by ESI-MS and their exchange with H_2^{18}O .

1.33 mg of complex **2** (0.002 mmols) were solved in 2 mL of a $\text{CH}_3\text{CN}:\text{water}$ 5:1 w:w ($[\mathbf{2}] = 1 \text{ mM}$) and the resultant solution was analyzed the ESI-MS (Figure S1, top left), observing the mass $m/z = 168.5$ which corresponds to the complex **2** without the counteranions. When the same solution was prepared using H_2^{18}O , the peak of 168.5 slowly disappeared (30 minutes) and a new peak with a mass of $m/z = 170.5$ appeared (Figure S1, bottom left) which corresponds to the complex $\mathbf{2}\text{-}^{18}\text{O}$.

Complex **3** was generated adding 1 equiv. of $t\text{BuOK}$ to a complex **2** solution. A peak at $m/z = 336$ was recorded, which corresponds to complex **3** after losing the triflate counteranion (Figure S1, top right). When the same solution was generated using H_2^{18}O , this peak slowly disappeared (30 minutes) and a new peak at $m/z = 340$ appeared, which corresponds to the substitution of the two oxygen atoms by the labelled ones (Figure S1, bottom right).

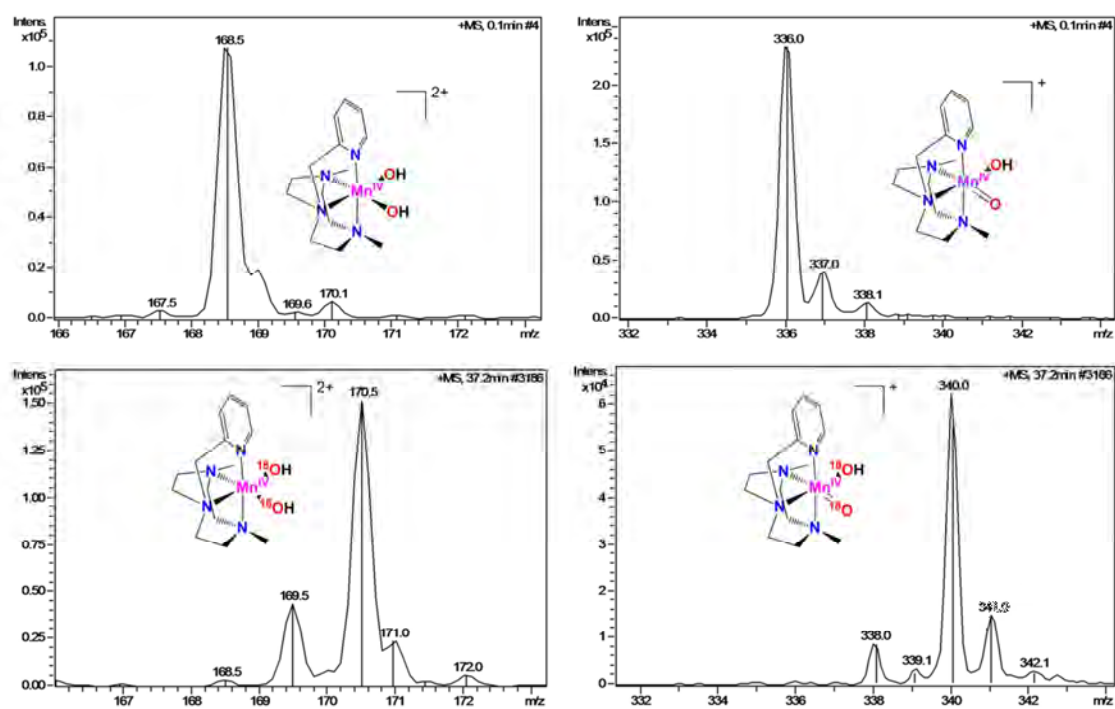


Figure S1. ESI-MS spectra of complexes **2** and **3** and their exchange with H_2^{18}O .

4.2 Characterization of complexes **2** and **3** by raman spectroscopy

6.6 mg of complex **2** (0.01 mmols) were dissolved in 0.1 mL of a CH_3CN :water 5:1 w:w ($[\text{2}] = 100\text{mM}$). Raman spectra were recorded with $\lambda_{\text{exc}} 785\text{ nm}$. A band is observed at 662 cm^{-1} that is absent in the spectrum of the manganese(II) complex **1** at the same concentration.

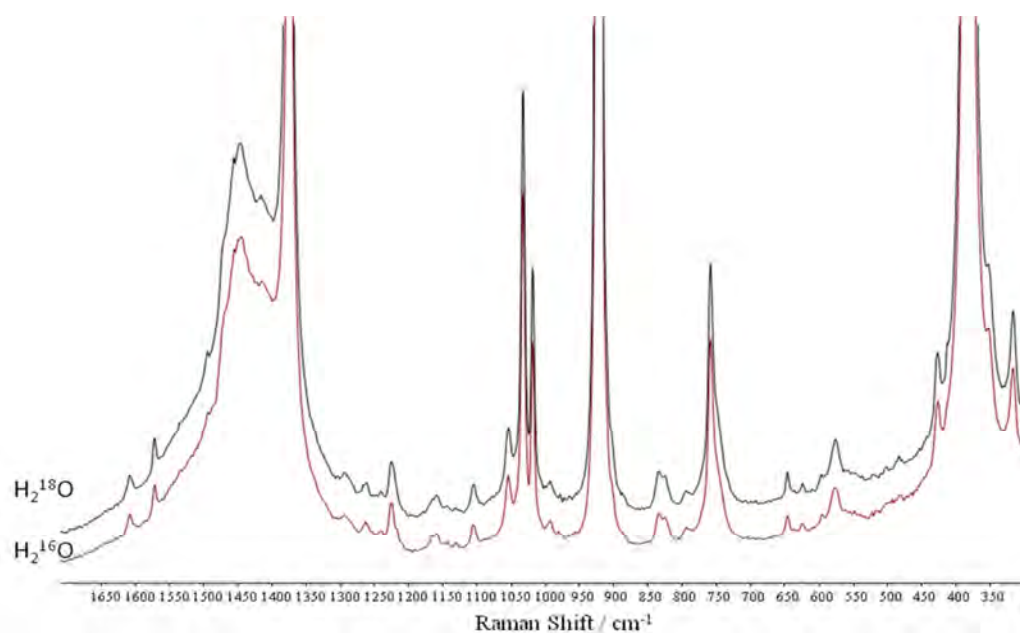


Figure S2. Raman Spectra of complex **1** ($[\text{LMn}^{\text{II}}\text{OTf}]_2$), 0.1 M) in CH_3CN at $\lambda_{\text{exc}} 785\text{ nm}$ with (red) H_2^{16}O and (black) H_2^{18}O .

Addition of H_2^{18}O instead of H_2^{16}O results in a shift of the 672 cm^{-1} band to 642 cm^{-1} with no other significant changes to the Raman spectrum being observed. The expected isotope shift based on the two atom (Mn-O) approximation is 29 cm^{-1} and hence the band is assigned to the manganese-oxygen vibration of the $\text{Mn}^{\text{IV}}\text{-(OH)}_2$ moiety (Figure 2).

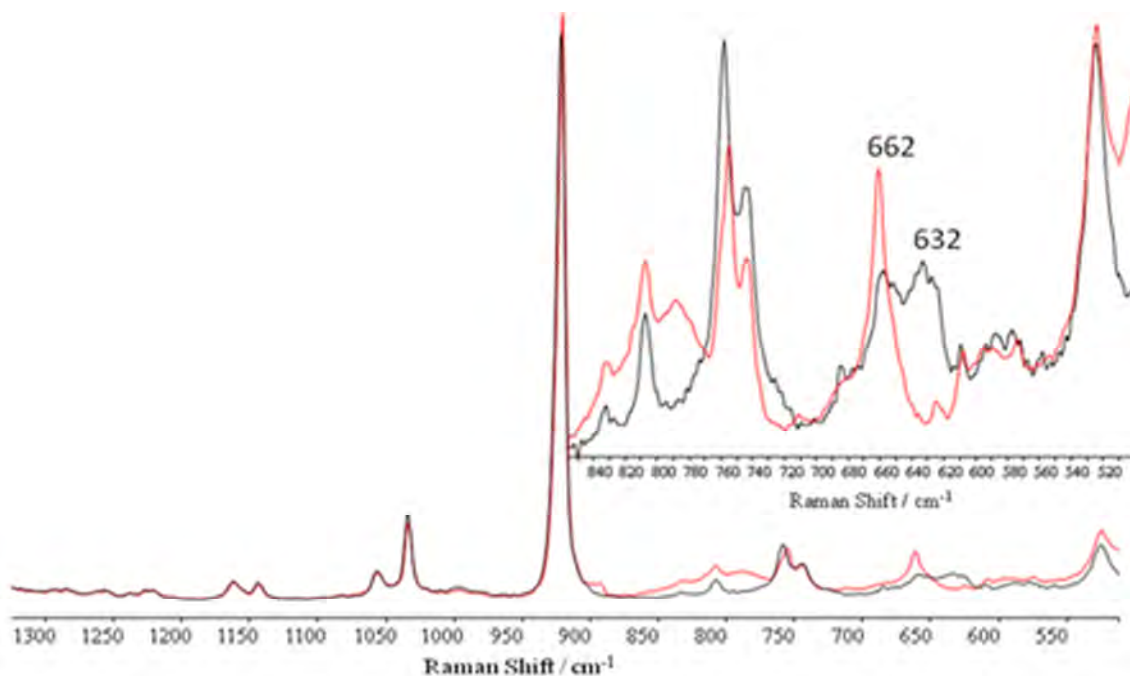


Figure S3. Raman Spectra of complex **2** (0.1 M) in CH_3CN at $\lambda_{\text{exc}} 785\text{ nm}$ with (red) H_2^{16}O and (black) H_2^{18}O .

Addition of 0.5 equivalents of base (e.g., tBuOK) to a solution of **2** results in the formation of **3** in situ and the concomitant disappearance of bands at 800 cm^{-1} (which is unaffected by addition of H_2^{18}O) and the Mn-O band of **2** at 662 cm^{-1} . Two new bands at 749 and 712 cm^{-1} are observed in the spectrum of **3**. Addition of H_2^{18}O results in the disappearance of the band at 749 cm^{-1} and the shift of the band at 712 cm^{-1} to 682 cm^{-1} . The shift expected for the manganese oxygen bond based on the two atom approximation is 31 cm^{-1} which is in agreement with the observed 30 cm^{-1} shift.

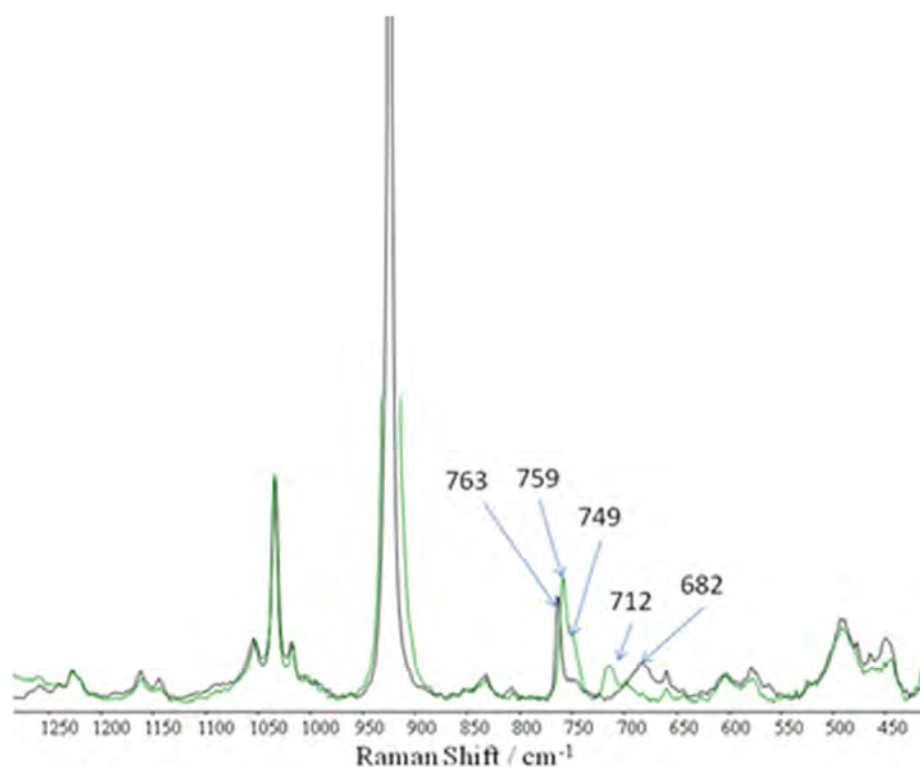


Figure S4. Raman Spectra of complex **3** (0.1 M) in CH₃CN at λ_{exc} 785 nm with (green) H₂¹⁶O and (black) H₂¹⁸O.

4.3 Characterization of complexes **2** and **3** by EPR

All EPR were run at 5K using a acetone:water 5:1 w:w solvent mixture. EPR of **1** (Figure S2 left, blue line) shows an interesting asymmetry which may be due to electron density localizing toward the solvent ligands rather than being spread evenly around the large multi dentate ligand. When oxidized to **2** the EPR (Figure S5 left, red line) shows a characteristic Mn(IV) signal with features at around $g = 4$ and 2. In addition to the characteristic Mn(IV) peak a small amount of multiline is located in the $g = 2$ region. The multiline signal can be assigned as a 16 line signal corresponding to a small amount of Mn(III,IV) dimer. EPR spectra of **2** after the addition of ^tBuOK show the transition between **2** and **3** (Figure S5, right). The broad feature at 1600 G can be seen to transition to the multiline feature at 1500 G. The multiline signal at 1500 G is most consistent with a slightly altered Mn(IV) monomer signal as stated and referenced in the text of the main article.

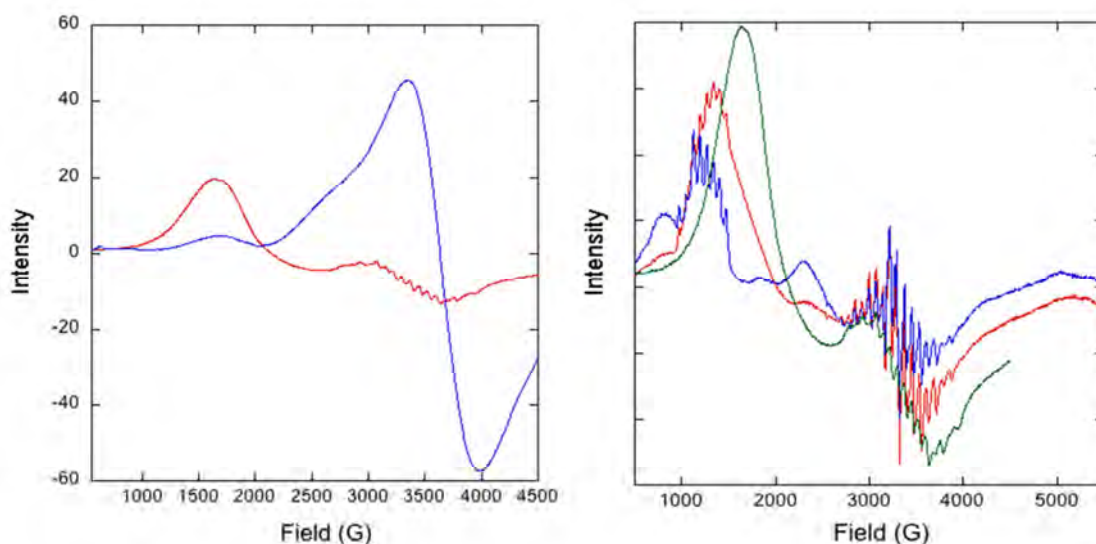


Figure S5. Left: EPR spectra (5K) of complexes **1** (blue line) and **2** (red line) a acetone:water 5:1 w:w solvent mixture. Right: EPR spectra of complexes **2** (green line), after addition of 0.5 equiv. of ^tBuOK (red line) and after addition of 1 equiv. of ^tBuOK (blue line) which corresponds to complex **3**.

4.4 Determination of μ_{eff} and unpaired electrons for complexes **2** and **3** by the Evans' method

To run the experiments, a special coaxial insert tube purchased from Wilmad Glass Co was used. An exact amount of complex **2** (2.66 mg) was solved in 0.4 mL of a mixture CD₃CN:D₂O 5:1 w:w which contained 8 μ L of CH₂Cl₂ and the resulting mixture was placed in the outer tube of the coaxial tube. The inner tube was filled with a reference solution which contained 4 μ L of CH₂Cl₂ in a 0.2 mL of a CD₃CN:D₂O 5:1 w:w. ¹H-NMR spectra of samples showed two different signals for CH₂Cl₂ corresponding to inner and outer tubes. The difference in the chemical shift between the two peaks was used to determine the μ_{eff} and the unpaired electrons of the metal center. For complex **3** the same procedure was followed, generating complex **3** by adding 1 equiv of ^tBuOK in the inner and the outer tubes of the sample used for complex **2**.

4.5 Determination of the redox potentials for complexes **2** and **3** by cyclic voltammetry

Cyclic voltammetry was employed to elucidate the electrochemical properties of complexes **2** and **3** (Figure S6). Complex **2** shows a reversible reduction (Mn(IV)/Mn(III)) at $E_{1/2} = 0.55$ V (vs SCE, 0.78 V vs SHE) in anhydrous acetonitrile (with 0.1 M NBu₄PF₆). Scanning from the open circuit potential initially to positive potentials shows that no oxidative redox processes (e.g. Mn(IV)/Mn(V)) occur within the potential window. When a mixture of acetonitrile:H₂O is used, the redox wave becomes irreversible, and a second reversible oxidation/reduction process is observed at $E_{1/2} = 0.86$ V (vs SCE) on the return scan indicating a change to the complexes ligand environment occurs upon reduction. When the pH is set to pH 6.1, the 1e⁻ reduction wave becomes reversible.

The cyclic voltammetry of complex **3**, obtained by in situ deprotonation of **2**, was performed at 0 °C in an acetonitrile:water mixture 5:1, at pH 9.1. In addition to the reduction wave at 0.55 V a second reduction was

observed at 0.05V (vs SCE) which is assigned tentatively to the reduction of the manganese(IV)(O)(OH) complex **3** to the related manganese(III)(O)(OH) complex which is rapidly protonated because of its higher basicity, and hence the redox processes of complex **2** are observed also.

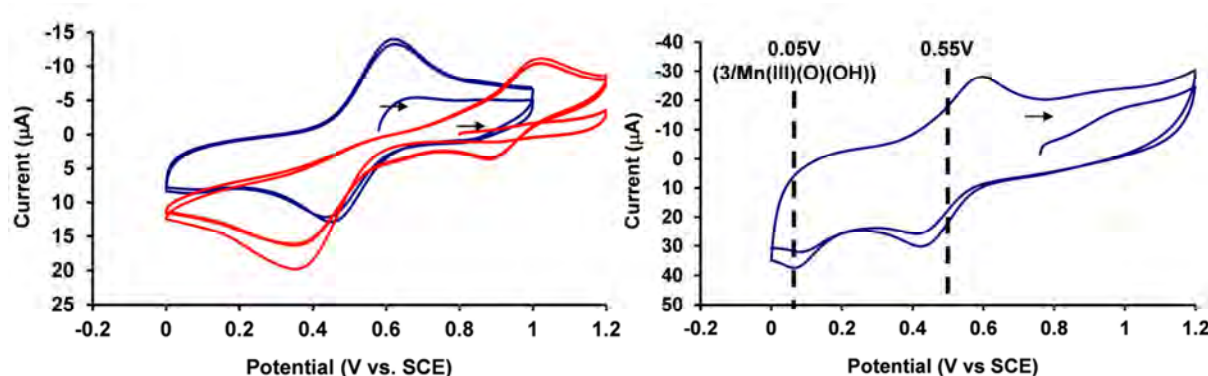


Figure S6. Cyclic voltammetry of complexes **2** (pH = 2.3 in red and pH = 6.1 in blue, left) and **3** (pH = 9.1, right).

4.6 Determination of the pK_a value for the deprotonation of complex **2** to **3**:

The pK_a value for the deprotonation process was obtained by a potentiometric titration. In a typical experiment, 3.3 mg of complex were solved in 0.5 mL of an CH_3CN :water 5:1 w:w ($[2] = 10\text{mM}$) and cooled to 0°C . After fixing the pH = 2 using a solution of $\text{CF}_3\text{SO}_3\text{H}$, several additions of a solution of ${}^t\text{BuOK}$ were done measuring the pH after each one. From the measurements, a plot of the added equivalents of base vs the pH allowed us to calculate the pK_a value for the deprotonation of complex **2** (Figure S7, right). The same experiment was also followed by UV-Vis measuring both, pH and UV-vis spectra, and an isobestic point was observed for the transformation between **2** and **3**, indicating the cleanliness of the deprotonation (Figure S7, left). Despite the fact that a second deprotonation process was observed at pH around 10-12, when this second reaction was followed by UV-Vis, a loss of the isobestic point was observed, and an increase of a band around 400 nm was observed, typical of a manganese(III) species, what can be understood as a decomposition of the manganese(IV) species at high pH.

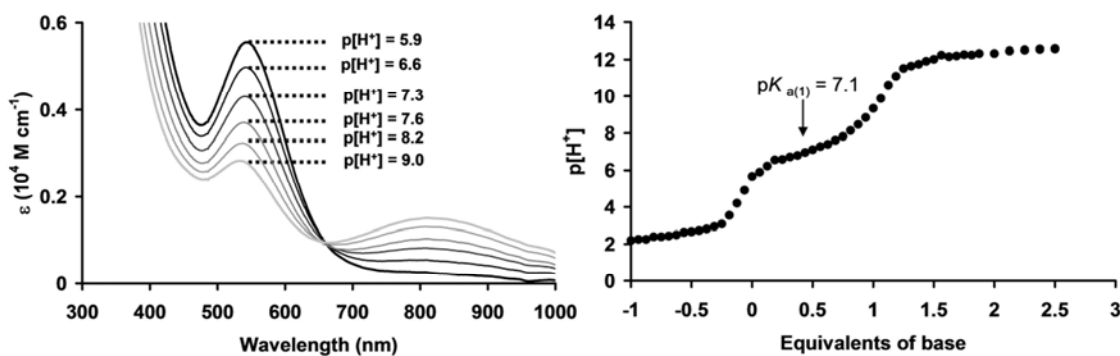


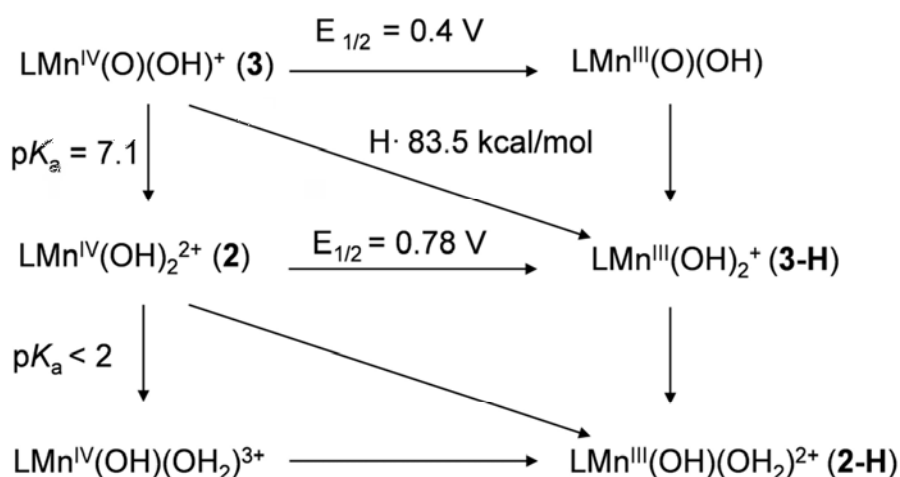
Figure S7. Potentiometric titration followed by UV-Vis (left) and plot of the equivalents of base added vs pH (right).

In order to corroborate the value obtained for the deprotonation, spectrophotometric titrations using soft bases such as 2,6-lutidine and 2-methylimidazole were performed. The reactions were followed by UV-vis monitoring the formation of complex **3** with the addition of several equivalents of the base. In order to calculate the pK_a of the deprotonation, the pK_a values for the two soft bases protonation in the reaction condition were also calculated using potentiometric titrations ($pK_a(2,6\text{-lutidine}) = 11.2$, $pK_a(2\text{-methylimidazole}) = 9.5$). A value of 7.4 using 2,6-lutidine and 7.0 using 2-methylimidazole were obtained, confirming the pK_a value of 7.1 ± 0.1 .

4.7 Calculation of the BDE_{C-H} as a driving force for the hydrogen atom abstraction ability.

The BDE of the complex **3-H** (Scheme S1) was calculated using the Bordwell equation $BDE = 1.37 pK_a + 23.06 E_{1/2} + C$ ($C = 55.7$ kcal) applying the pK_a found for the deprotonation between complexes **2** and **3**, and the $E_{1/2}$ value of the reduction of complex **2** ($BDE_{O-H}(\mathbf{3-H}) = 83.5$ kcal·mol⁻¹). However, we were not able to calculate this value for complex **2-H**.

Scheme S1. Redox potentials, pK_a values and BDE_{O-H} for manganese complexes ($L = \text{H,MePytacn}$).



5. Complexes reactivity towards C-H bonds.

5.1 Reactivity of complex **2** and **3** towards C-H bonds. Products analysis and final oxidation state of manganese.

2.66 mg of complex **2** were solved in 3.34 mL of a deoxygenated $\text{CH}_3\text{CN}:\text{H}_2\text{O}$ w:w 4:1 mixture ($[\mathbf{2}] = 1$ mM). Then, 0.66 mL of deoxygenated CH_3CN containing 10 equivalents of substrate (xanthene, 9,10-dihydroanthracene, fluorene) were added. The reaction was left for 2 days, and to the final solution, 80 μL of a solution containing 4×10^{-6} mols of biphenyl were added as internal standard to the crude. 2 mL of the solution were analyzed by HPLC-MS after passing the solution through basic alumina. After this analysis, the solution was evaporated and the obtained products and their respective yields were also confirmed by ¹H-NMR. The results are summarized in

Table 1, from which we can observe the inability of complex **2** to oxidize fluorene. The same experiments were carried out in the presence of oxygen, from which we observed the increase of the products in most of the cases. The other 2 mL of the reaction crude were used to determine the final oxidation state of the manganese: the crude solution was acidified using 0.2 mL of aqueous H₂SO₄ 0.5 M and 0.1 mL of aqueous KI 0.5M was added and the formation of the I₂ was observed (color changes to intense yellow). The I₂ produced was quantified using a solution of 0.002 M of Na₂S₂O₃ from which we calculated the final oxidation state of the manganese, 3.3 ± 0.1 (average of 4 different experiments). Both product yields and final oxidation state of manganese point out that complex **2** acts as a 1e⁻ oxidant.

For complex **3**, the same procedure was followed for both, products analysis and final oxidation state analysis. The final oxidation state of the complex is 3.2 ± 0.2 (average of 6 different experiments) and together with the quantification analysis pointed out that complex **3** was also acting as a 1e⁻ oxidant.

Table S1. Products quantification analysis of the oxidation of xanthene, 9,10-dihydroanthracene fluorine, xanthene-d₂ and 9,10-dyhydroanthracene-d₄ by complexes **2** and **3** by HPLC-MS and ¹H-NMR.

Substrate	Product	2 (N ₂)	2 (O ₂)	3 (N ₂)	3 (O ₂)
		Yield (yield e-)	Yield	Yield (yield e-)	Yield
Xanthene	9-xanthidrol	38 ± 5% (76%)	29%	25 ± 4% (50%)	30%
	Xanthone	6 ± 1% (24%)	26%	8 ± 2% (32%)	12%
	9,9'-bixanthyl	< 1%	< 1%	<1%	<1%
DHA	Anthracene	28 ± 5% (56%)	28%	26 ± 3% (52%)	29%
	Anthrone	< 1%	< 1%	<1%	< 1%
	Anthraquinone	6 ± 1% (48%)	3%	4 ± 1% (32%)	57%
Fluorene	9-hydroxyfluorene	< 1%	< 1%	6 ± 1% (12%)	13%
	Fluorenone	< 1%	< 1%	17 ± 1% (68%)	34%
	9,9'-bifluorenyl	< 1%	< 1%	< 1%	< 1%
Xanthene-d ₂	9-xanthidrol-d ₁	13 ± 5% (26%)	-	16 ± 5% (32%)	-
	Xanthone	10 ± 5% (40%)	-	10 ± 5% (40%)	-
	9,9'-bixanthyl-d ₂	< 1%	-	< 1%	-
DHA-d ₄	Anthracene-d ₂	30 ± 5% (60%)	-	25 ± 5% (50%)	-
	Anthrone-d ₂	< 1%	-	< 1%	-
	Anthraquinone	4 ± 5% (32%)	.	4 ± 5% (32%)	-

Furthermore, the quantification of the reaction products for the complex **3** was also carried out at different substrate concentrations, from we can observe that similar product ratios where obtained at non-saturated (2mM), intermediate (10mM) and saturated conditions (50mM) (Table S2).

Table S2. Products quantification analysis of the oxidation of xanthene, 9,10-dihydroanthracene fluorine, xanthene-d₂ and 9,10-dihydroanthracene-d₄ by complexes **3** by HPLC-MS and ¹H-NMR at different substrate concentrations (2mM, 10mM and 50mM).

		2mM	10mM	50mM
Substrate	Product	Yield (yield e-)	Yield (yield e-)	Yield (yield e-)
Xanthene	9-xanthidrol	10 ± 5% (20%)	25 ± 4% (50%)	24 ± 5% (48%)
	Xanthone	11 ± 5% (44%)	8 ± 2% (32%)	10 ± 5% (40%)
	9,9'-bixanthyl	< 1%	<1%	<1%
DHA	Anthracene	20 ± 5% (40%)	26 ± 3% (52%)	27 ± 5% (54%)
	Anthrone	< 1%	<1%	< 1%
	Anthraquinone	5 ± 5% (40%)	4 ± 1% (32%)	6 ± 5% (48%)
Fluorene	9-hydroxyfluorene	5 ± 5% (10%)	6 ± 1% (12%)	7 ± 5% (14%)
	Fluorenone	16 ± 5% (64%)	17 ± 1% (68%)	14 ± 5% (68%)
	9,9'-bifluorenyl	< 1%	< 1%	< 1%
Xanthene-d ₂	9-xanthidrol-d ₁	10 ± 5% (20%)	16 ± 5% (32%)	13 ± 5% (26%)
	Xanthone	13 ± 5% (52%)	10 ± 5% (40%)	12 ± 5% (48%)
	9,9'-bixanthyl-d ₂	< 1%	< 1%	< 1%
DHA-d ₄	Anthracene-d ₂	13 ± 5% (26%)	25 ± 5% (50%)	-
	Anthrone-d ₂	< 1%	< 1%	-
	Anthraquinone	6 ± 5% (48%)	4 ± 5% (32%)	-

In addition, we performed the reaction between complex **3** and toluene, and no presence of oxidized products were detected.

5.2 Reactivity of complex **2** towards C-H bonds. Kinetic analysis.

1.33 mg of complex **2** were solved in a 1.67 mL of a CH₃CN:H₂O w:w 4:1 mixture ([**2**] = 1 mM) in a UV-Vis cell at 25°C. 0.33 mL of CH₃CN containing the substrate was added, and the reaction was monitored by following the reaction at $\lambda = 545$ nm. The reaction rates were calculated applying the initial rates approximation (10% complex disappearance) in order to avoid the interference of secondary reactions. Complex **2** shows a pseudo-first order behavior for both substrate ([substrate] = 0.005-0.1 M) and complex ([**2**] = 0.0025-0.004 M) (Figure S8). We followed by UV-Vis the reactions between complex **2** and xanthene (BDE_{C-H} = 75.5 kcal·mol⁻¹), 1,4-cyclohexadiene (BDE_{C-H} = 77 kcal·mol⁻¹), 9,10-dihydroanthracene (BDE_{C-H} = 78 kcal·mol⁻¹) and fluorene (BDE_{C-H} = 80 kcal·mol⁻¹). For the complex with fluorene, or toluene we didn't observe decay of the complex band ($\lambda = 545$ nm) after several hours, precluding that complex **2** is unable to oxidize this substrate. For each substrate, a linear correlation between the substrate concentration and the rate observed was plotted (Figure 3) from where we calculate the second order reaction rate k_2' (which was corrected for the number of C-H reactive bonds).

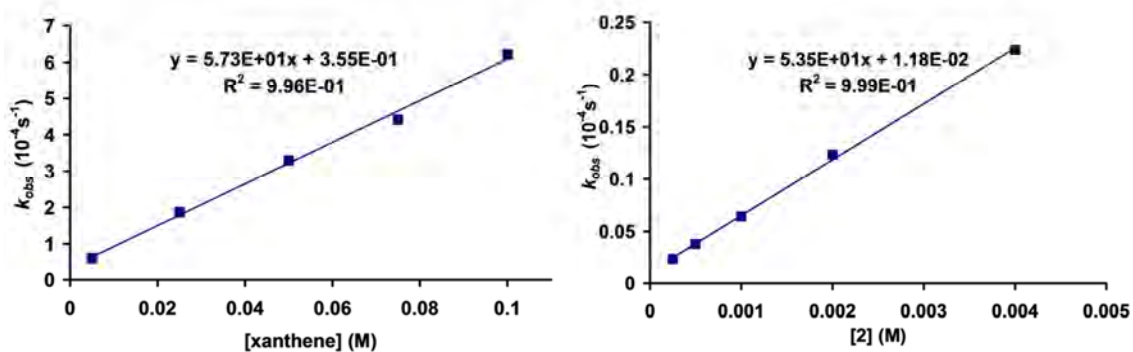


Figure S8. Pseudo-first order behavior for both substrate concentration (left) and complex concentration (right) in the reaction between complex **2** and xanthene.

In order to get the kinetic isotopic effect (KIE) we carried out the reaction for both xanthene- d_2 and DHA- d_4 . Comparing the k_2 values obtained from the linear plots, we calculate a KIE of 8.0 for xanthene and 6.6 for DHA (Figure S9).

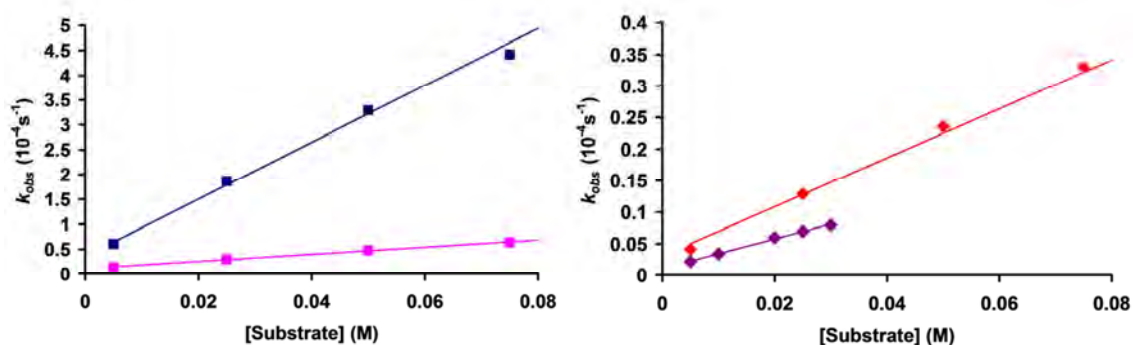


Figure S9. KIE experiments for the reactions between complex **2** and xanthenes/xanthenes- d_2 (left) and DHA/DHA- d_4 (right).

5.3 Reactivity of complex **3** towards C-H bonds. Kinetic analysis.

1.33 mg of complex **3** were solved in a 1.67 mL of a $\text{CH}_3\text{CN}:\text{H}_2\text{O}$ w:w 4:1 mixture ($[\mathbf{2}] = 1 \text{ mM}$) in a UV-Vis cell at 25°C . 66 μL of a solution containing 1 equiv. of $^t\text{BuOK}$ was added in order to generate complex **3**. After full the full formation of the complex, 0.33 mL of CH_3CN containing the substrate was added, and the reaction was monitored by following the reaction at $\lambda = 825 \text{ nm}$ (Figure S10). The reaction rates were calculated applying the initial rates approximation (10% complex disappearance) in order to avoid the interference of secondary reactions. In random cases we monitored the full decay of **3**, obtaining within error identical values to those obtained by the initial rate method. For the specific case of toluene, we didn't observe decay of the UV-vis spectroscopic features of **3** ($\lambda = 825 \text{ nm}$) after several hours. We conclude that complex **3** is unable to oxidize this substrate.

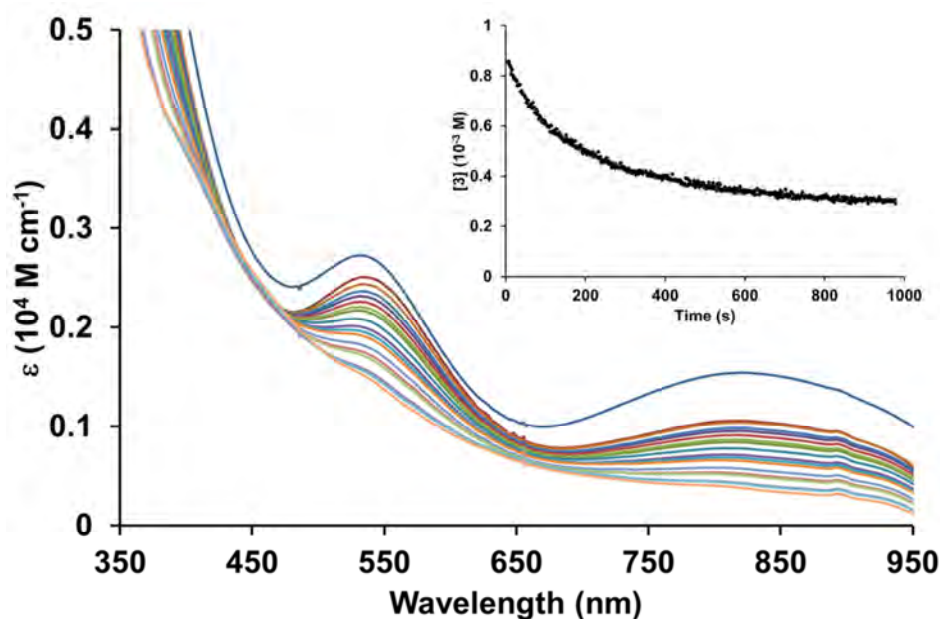


Figure S10. Reaction between complex **3** and 10 equiv. of xanthene.

Complex **3** shows a pseudo-first order for complex concentration ($[3] = 0.0025\text{-}0.004\text{ M}$). However, a saturation behavior was observed with an increase in the substrate concentration. Furthermore, these saturation curves were observed for all the substrates (xanthene, 1,4-CHD, DHA and fluorene) (Figure 3). These saturation plots are characteristic for reactions where an initial pre-equilibrium occurred previous to the rate determining step, and can be adjusted using the Equations 1 and 2, from where we can extract the equilibrium constant K_{eq} and the first order rate constant k_2 of the rate determining step (values summarized in Table 1) (Figure S11).

$$k_{obs} = \frac{k_2 K_{eq} [C - H]}{1 + K_{eq} [C - H]} \quad (\text{Equation 1})$$

$$\frac{1}{k_{obs}} = \frac{1}{k_2 K_{eq} [C - H]} + \frac{1}{k_2} \quad (\text{Equation 2})$$

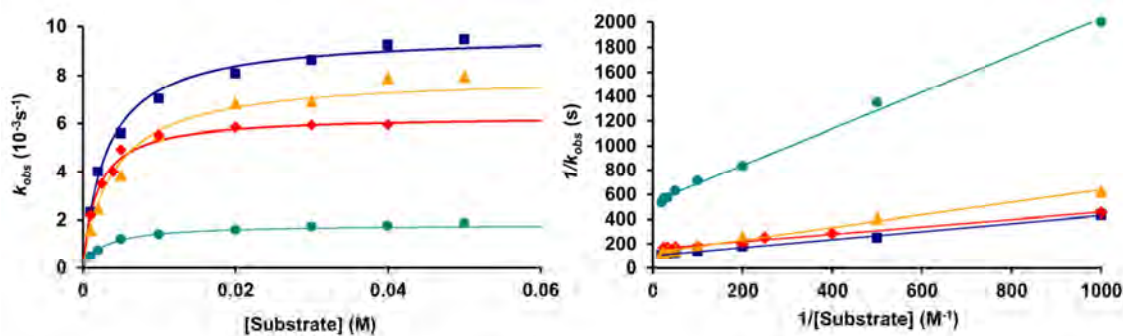


Figure S11. Saturation curves obtained for the reaction between complex **3** and substrates (left) and the adjust of the data using equation 2 (right) from where K_{eq} and k_2 were calculated.

The formation of the intermediate **I** was observed when complex **3** reacted with DHA under saturation conditions (10 equiv.). The band at 535 nm shifted to 539 nm (Figure S12).

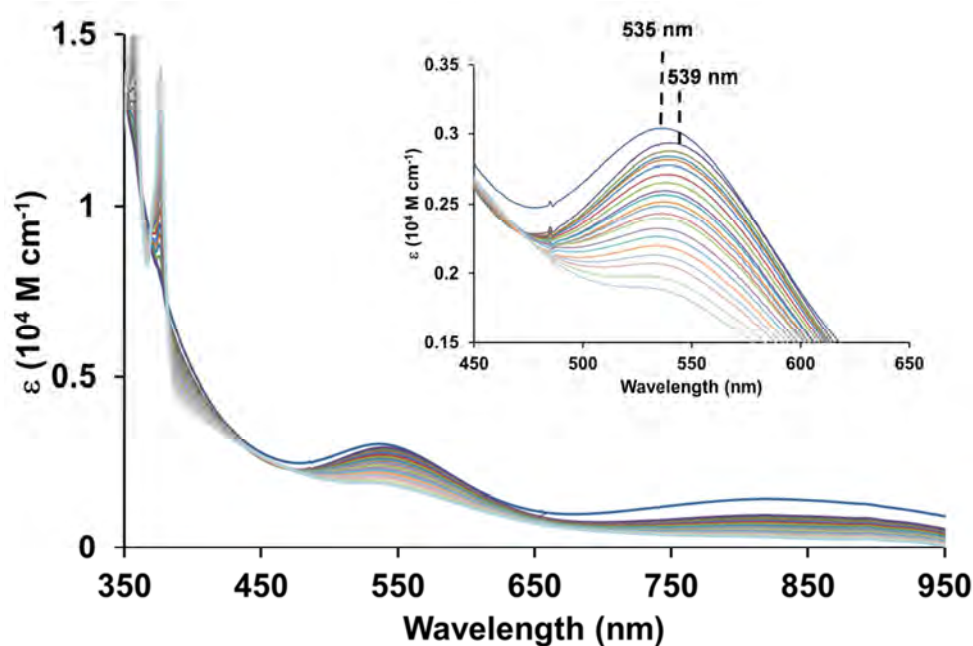


Figure S12. Reaction between complex **3** and 10 equiv. of DHA.

For the xanthene and the DHA, we also carried out kinetic isotopic effect experiments using their deuterated analogs (Figure S13). Curiously, while the pre-equilibrium constant K_{eq} was not effected for the deuteration (similar values for both xanthene/xanthene- d_2 and DHA/DHA- d_4 couples), k_2 presented a primary KIE for both xanthene (2.1) and DHA (3.1).

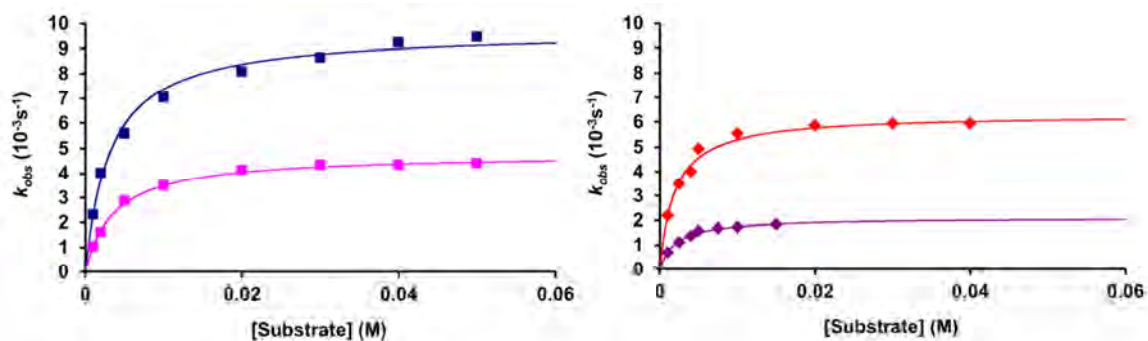


Figure S13. KIE experiments for the reactions between complex **3** and xanthenes/xanthenes- d_2 (left) and DHA/DHA- d_4 (right).

5.4 Reactivity of complex 2 and 3 towards C-H bonds. Kinetic analysis varying the temperature. Eyring and van't Hoff plots.

Table S3. Rate constants for the reaction of complexes 2 and 3 with 9,10-dihydroanthracene at different temperatures.

Substrate	T(K)	2		3	
		$k_2^{(\text{OH})}$ ($10^{-4} \text{ M}^{-1} \text{ s}^{-1}$)	K_{eq} (M^{-1})	$k_2^{(\text{O})}$ (10^{-4} s^{-1})	$K_{\text{eq}}k_2^{(\text{O})}$ ($\text{M}^{-1}\text{s}^{-1}$)
9,10-DHA	298	16 ± 1	523 ± 33	65 ± 4	3.40
	293	13 ± 1	583 ± 10	45 ± 1	2.62
	288	10 ± 1	680 ± 36	29 ± 1	1.97
	283	8.4 ± 1	713 ± 40	23 ± 1	1.64
	278	6.4 ± 1	838 ± 10	18 ± 1	1.51
	273	5.2 ± 1	923 ± 4	11 ± 1	1.01

The impact of the temperature in the kinetic experiments was evaluated for both complexes using DHA as substrate. The tests were carried out from 273-298K (6 different temperatures) and varying the concentration of the DHA was varied using at least 5 different concentrations (Figure S14). The values for complex 2 (k_2) and complex 3 (K_{eq} and k_2) were obtained for each temperature, from where we can construct the Eyring and van't Hoff plots.

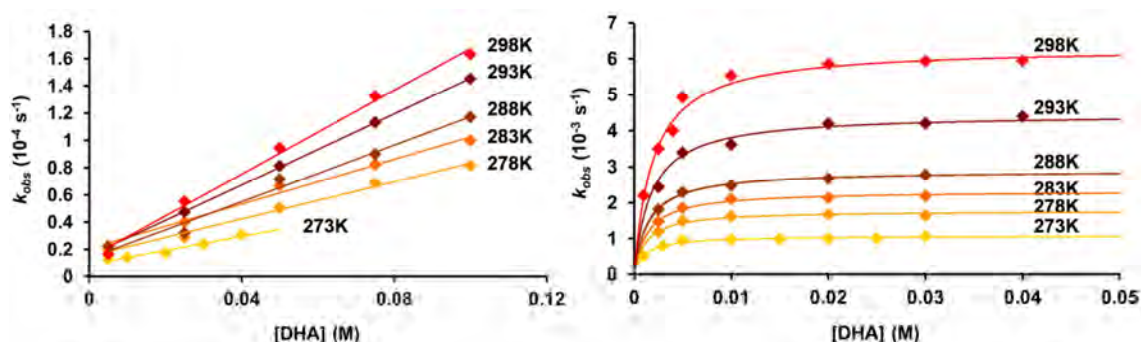


Figure S14. Reaction rates obtained for the hydrogen atom abstraction of DHA performed by complexes 2 and 3 at different temperatures.

From the Eyring plot (Figure S15, left), we can calculate the activation parameters ΔH^\ddagger , ΔS^\ddagger and ΔG^\ddagger (298K) of the rate determining step for both complexes 2 and 3. Furthermore, the construction of a van't Hoff plot (Figure S15, right) allows us to calculate the thermodynamic parameters for the first pre-equilibrium step occurred when complex 3 reacts with DHA (Table S4).

Table S4. Thermodynamic and activation parameters for the reaction of complexes 2 and 3 with DHA.

	ΔH	ΔS	ΔG^a	ΔH^\ddagger	ΔS^\ddagger	$\Delta G^{\ddagger a}$
Complex	(kcal/mol)	(cal/mol·K)	(kcal/mol)	(cal/mol)	(cal/mol·K)	(kcal/mol)
2	-	-	-	6.6 ± 0.1	-51.9 ± 0.4	22.1 ± 0.1
3	-3.6 ± 0.2	0.2 ± 0.4	-3.7 ± 0.2	10.3 ± 0.7	-37 ± 2	21.3 ± 0.7

^a Calculated at 298K.

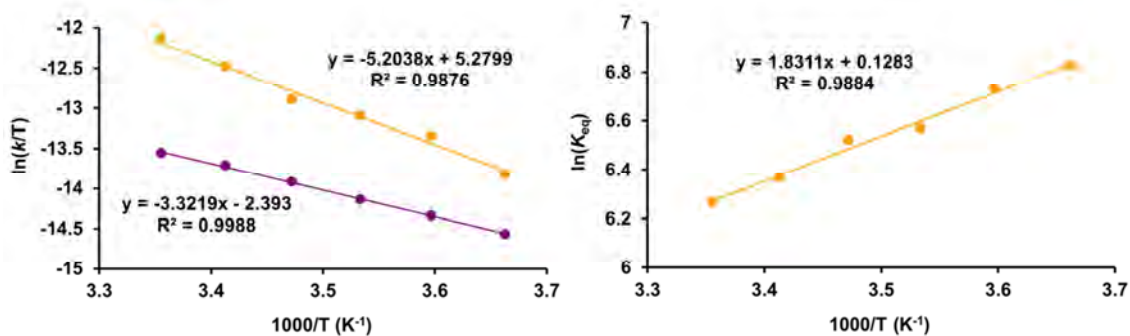


Figure S15. Eyring plots (left) and van't Hoff plot (right) for the hydrogen atom abstraction of DHA performed by complex 2 (●) and complex 3 (●).

5.5 Reactivity of complex 2 and 3 towards C-H bonds. Rate constants vs BDE_{C-H} .

The correlation between the observed rate constants ($\log k_2'$) vs the BDE_{C-H} of the different substrates was plotted. For both complexes, a linear correlation was observed, pointing out the fact that, the C-H bond cleavage occurred during the rate determining step. However, a major impact was observed for complex 2 (slope = -0.36) than for complex 3 (slope = -0.15).

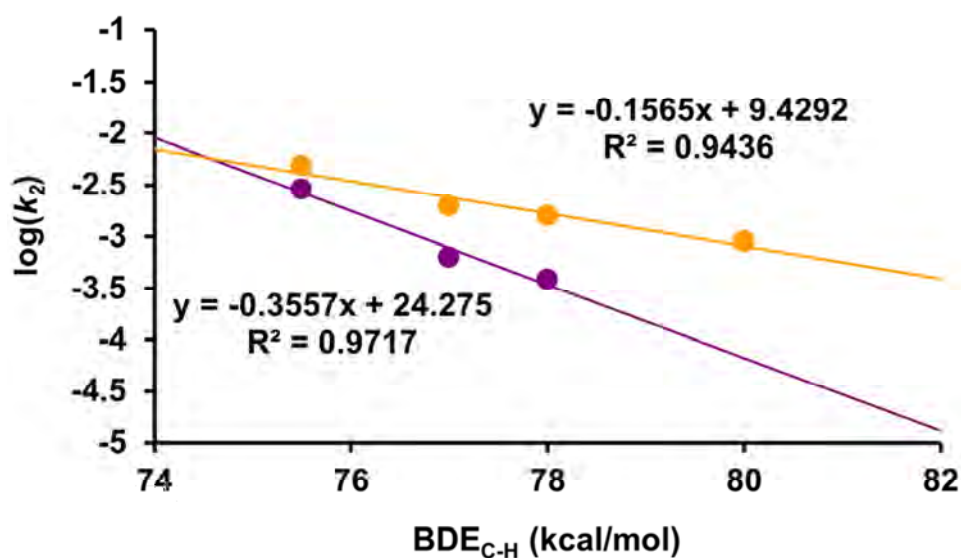


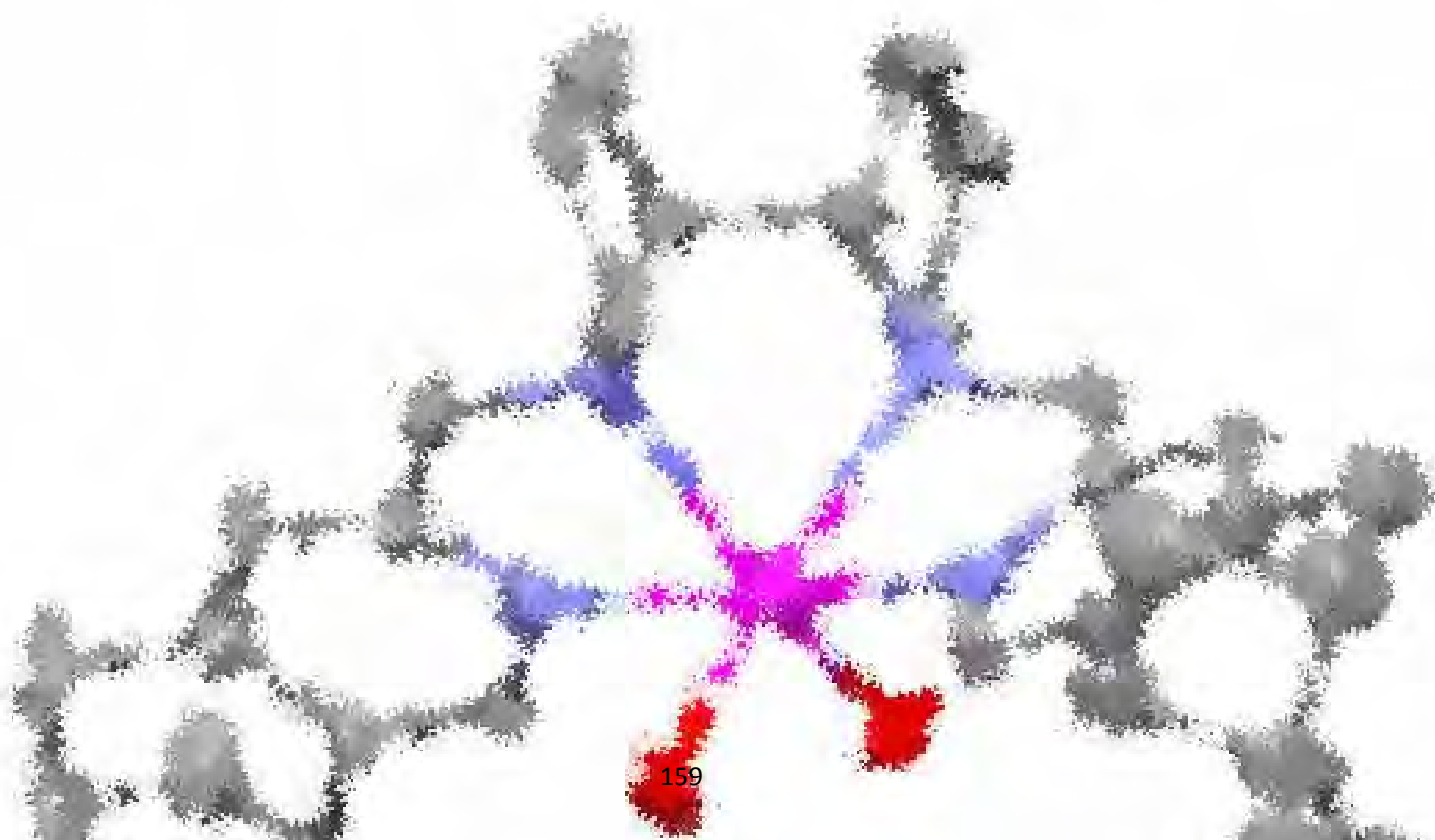
Figure S16. Dependence of the $\log(k_2')$ vs BDE_{C-H} for complex 2 (●) and complex 3 (●).

6. References

1. Prokop, K. A.; Visser, S. P.; Goldberg, D. P. *J. Am. Chem. Soc.* **2010**, *49*, 5091-5095.
2. Garcia-Bosch, I.; Company, A.; Fontrodona, X.; Ribas, X.; Costas, M. *Org. Lett.* **2008**, *10*, 2095-2098.

Chapter V

Alkene Epoxidation Catalyzed by Non-Porphyrinic Manganese Complexes.



Chapter V.1

Efficient and Selective Peracetic Acid Epoxidation Catalyzed by a Robust Manganese Catalyst.

Garcia-Bosch, I.; Company, A.; Fontrodona, X.; Ribas, X.; Costas, M. *Org. Lett.* **2008**, *10*, 2095-2098.

Isaac Garcia-Bosch, Anna Company, Xavier Fontrodona, Xavi Ribas and Miquel Costas. "Efficient and Selective Peracetic Acid Epoxidation Catalyzed by a Robust Manganese Catalyst". *Organic Letters*. Vol. 10, issue 11 (2008) : p. 2095–2098
Copyright © 2008 American Chemical Society

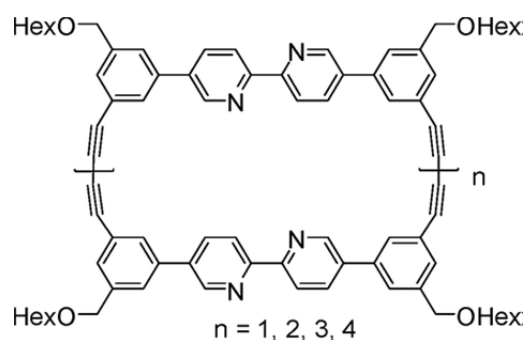
Publication Date (Web): April 25, 2008

<http://dx.doi.org/10.1021/ol800329m>

<http://pubs.acs.org/doi/abs/10.1021/ol800329m>

Abstract

A manganese catalyst containing a tetradentate ligand derived from triazacyclononane exhibits high catalytic activity in epoxidation reactions using peracetic acid as oxidant. The system exhibits broad substrate scope and requires small (0.1–0.15 mol %) catalyst loading. The catalyst is remarkably selective toward aliphatic *cis*-olefins. Mechanistic studies point toward an electrophilic oxidant delivering the oxygen atom in a concerted step.



Electronic Supporting Information

Experimental procedures and a CIF file for **1**. This material is available free of charge via the Internet at <http://pubs.acs.org>:

http://pubs.acs.org/doi/suppl/10.1021/ol800329m/suppl_file/ol800329m-file002.pdf

http://pubs.acs.org/doi/suppl/10.1021/ol800329m/suppl_file/ol800329m-file003.cif

Efficient and Selective Peracetic Acid Epoxidation Catalyzed by a Robust Manganese Catalyst

Isaac Garcia-Bosch,[†] Anna Company,[†] Xavier Fontrodona,[‡] Xavi Ribas,^{*,†} and Miquel Costas^{*,†}

Departament de Química, Campus de Montilivi, Universitat de Girona, E-17071 Girona, Catalonia, Spain and Serveis Tècnics de Recerca, Universitat de Girona

1) Experimental section	2
Materials	2
Instrumentation	2
Synthesis of ligands	2
Synthesis of complexes	3
2) Catalysis conditions	5
Optimization conditions	5
Reaction conditions (Table 1) and GC analysis.....	5
Reaction conditions (Table 1) and ¹ H-RMN analysis	5
Blank experiments	6
Reaction conditions for selectivity experiments	6
H ₂ O ¹⁸ Labeling conditions	7
3) References.....	8

1) Experimental section

Materials

Reagents and solvents used were of commercially available reagent quality unless stated otherwise. Solvents were purchased from SDS and Sharlab. Solvents were purified and dried by passing through an activated alumina purification system (M-Braun SPS-800) or by conventional distillation techniques. H₂¹⁸O (95% ¹⁸O-enriched) was received from ICON Isotopes

Instrumentation

IR spectra were taken in a Mattson-Galaxy Satellite FT-IR spectrophotometer using a MKII Golden Gate single reflection ATR system. UV-vis spectroscopy was performed on a Cary 50 Scan (Varian) UV-vis spectrophotometer with 1 cm or 0.2 cm quartz cells. NMR spectra were taken on Bruker DPX200 spectrometer using standard conditions. Elemental analyses were performed using a CHNS-O EA-1108 elemental analyzer from Fisons. The ESI-MS experiments were performed on a Navigator LC/MS chromatograph from Thermo Quest Finigan, using acetonitrile as the mobile phase. Product analyses were performed on a Shimadzu GC-2010 gas chromatography (AT-1701 column, 30 m) and a flame-ionization detector. GC mass spectral analyses were performed on a Thermoquest Trace GC 2000 Series (TRB-5MS column, 30 m) with a Finnigan Trace MS mass detector. The products were identified by comparison of their GC retention times and GC/MS with those of authentic compounds.

Synthesis of ligands

1,4-dimethyl-1,4,7-triazacyclononane trihydrobromide,¹ 2-chloromethyl-6-methylpyridine hydrochloride,³ 1,4-diisopropyl-7-(2-pyridylmethyl)-1,4,7-triazacyclononane (^{iPr,H}PyTACN),² 1,4-diisopropyl-7-(6-methyl-2-pyridylmethyl)-1,4,7-triazacyclononane (^{iPr,Me}PyTACN)³, 1-(2-pyridylmethyl)-4,7-dimethyl-1,4,7-triazacyclononane (^{Me,H}PyTACN)⁴ and Mn(CF₃SO₃)₂⁵ were synthesized as previously described.

1-(6-methyl-2-pyridylmethyl)-4,7-dimethyl-1,4,7-triazacyclononane (^{Me,Me}PyTACN).
2-Chloromethyl-6-methylpyridine hydrochloride (0.44 g, 2.5 mmols), 1,4-dimethyl-1,4,7-triazacyclononane trihydrobromide (1.00 g, 2.5 mmols) and anhydrous acetonitrile (30

mL) were mixed in a 50 mL flask. Na₂CO₃ (1.85 g) and tetrabutylammonium bromide, TBABr (0.04 g) were added directly as solids and the resulting mixture was heated at reflux under N₂ for 15 hours. After cooling to room temperature, the resulting yellow mixture was filtered and the filter cake was washed with CH₂Cl₂. The combined filtrates were evaporated under reduced pressure. To the resulting residue, 1M NaOH (30 mL) was added and the mixture was extracted with CH₂Cl₂ (3 x 20 mL). The combined organic layers were dried over anhydrous MgSO₄ and the solvent was removed under reduced pressure to yield 0.60 g of a pale yellow oil (2.3 mmols, 92 %). FT-IR (ATR) ν , cm⁻¹: 2960 – 2802(C-H)_{sp3}, 1578, 1456, 1358 (py). ¹H-NMR (CDCl₃, 200 MHz, 300K) δ , ppm: 7.54 (t, J = 7.6 Hz, 1H, pyH_γ), 7.29 (d, J = 7.4 Hz, 1H, pyH_β), 7.00 (d, J = 7.4 Hz, 1H, pyH_β), 3.82 (s, 2H, py-CH₂), 2.84 – 2.79 (m, 8H, N-CH₂-CH₂), 2.68 – 2.66 (m, 4H, N-CH₂-CH₂), 2.53 (s, 3H, py-CH₃), 2.36 (s, 6H, N-CH₃). ¹³C-NMR (CDCl₃, 50 MHz, 300K) δ , ppm: 159.85, 157.41 (pyC_q), 136.38 (pyC_γ), 121.16, 119.93 (pyC_β), 64.83 (py-CH₂-N), 57.20, 57.06, 56.28 (N-CH₂-C), 46.65 (N-CH₃), 24.38 (py-CH₃). ESI-MS (m/z): 263.1 [M+H]⁺.

Synthesis of complexes

[Mn(CF₃SO₃)₂(^{H,Me}PyTACN)] (1). A suspension of Mn(CF₃SO₃)₂ (82 mg, 0.23 mmols) in anhydrous THF (1 mL) was added dropwise to a vigorously stirred solution of ^{H,Me}PyTACN (58 mg, 0.23 mmols) in THF (1 mL). After a few seconds the solution became cloudy and a white precipitate appeared. After stirring for 1 hour the solution was filtered off and the resultant white solid dried under vacuum. The solid was dissolved in CH₂Cl₂ and filtered through Celite. Slow diethyl ether diffusion over the resultant solution afforded, in a few days, 119 mg of colorless crystals (0.20 mmols, 85 %). Anal. Calcd for C₁₆H₂₄F₆MnN₄O₆S₂ 1/4CH₂Cl₂: C, 31.34; H, 3.97; N, 9.00; S, 10.30 %. Found: C, 31.63; H, 4.19; N, 8.66; S, 10.10 %. FT-IR (ATR) ν , cm⁻¹: 2988 - 2948 (C-H)_{sp3}, 1365, 1312 (py), 1232, 1214, 1160, 1021, 629 (CF₃SO₃). ESI-MS (m/z): 452.1 [M-CF₃SO₃]⁺.

[Mn(CF₃SO₃)₂(^{Me,Me}PyTACN)] (2). A solution of Mn(CF₃SO₃)₂ (101 mg, 0.29 mmols) in anhydrous THF (1 mL) was added dropwise to a vigorously stirred solution of ^{Me,Me}PyTACN (75 mg, 0.29 mmols) in THF (1 mL). After a few seconds the solution became cloudy and a white precipitate appeared. After stirring for 1 hour the solution was filtered off and the resultant white solid dried under vacuum. The solid was dissolved in CH₂Cl₂ and filtered through Celite. Slow diethyl ether diffusion over this

solution afforded 100 mg of colorless crystals (0.17 mmols, 57 %). Anal. Calcd for $C_{17}H_{26}F_6MnN_4O_6S_2 \cdot 1/2THF$: C, 35.03; H, 4.64; N, 8.60; S, 9.84 %. Found: C, 34.77; H, 4.48; N, 8.87; S, 9.58 %. FT-IR (ATR) ν , cm^{-1} : 2992 - 2890 (C-H)_{sp3}, 1738, 1365, 1312 (py), 1232, 1214, 1033, 1022, 629 (CF₃SO₃). ESI-MS (m/z): 158.5 [M-2CF₃SO₃]²⁺, 466.0 [M-CF₃SO₃]⁺.

[Mn(CF₃SO₃)₂(^{H,iPr}PyTACN)] (3). A solution of Mn(CF₃SO₃)₂ (47 mg, 0.13 mmols) in anhydrous THF (2 mL) was added dropwise to a vigorously stirred solution of ^{H,iPr}PyTACN (40 mg, 0.13 mmols) in THF (1.5 mL). After a few seconds the solution became cloudy and a white powder appeared. After stirring for 1 hour the solution was filtered off and the resultant yellow solid was dried under vacuum. This solid was dissolved in CH₂Cl₂ and filtered through Celite. Slow diethyl ether diffusion over the resultant solution afforded, in a few days, 37 mg of colorless crystals (0.09 mmols, 68 %). Anal. Calcd for $C_{20}H_{32}F_6MnN_4O_6S_2$: C, 36.53; H, 4.91; N, 8.52; S, 9.75 %. Found: C, 36.31; H, 5.07; N, 8.83; S, 9.66 %. FT-IR (ATR) ν , cm^{-1} : 2982 - 2952 (C-H)_{sp3}, 1315 (py), 1213, 1171, 1024, 631 (CF₃SO₃). ESI-MS (m/z): 179.5 [M-2CF₃SO₃]²⁺, 508.1 [M-CF₃SO₃]⁺.

[Mn(CF₃SO₃)₂(^{Me,iPr}PyTACN)] (4). A solution of Mn(CF₃SO₃)₂ (107 mg, 0.24 mmols) in anhydrous THF (1 mL) was added dropwise to a vigorously stirred solution of ^{Me,iPr}PyTACN (75 mg, 0.24 mmols) in THF (1 mL). After a few seconds the solution became cloudy and a white powder appeared. After stirring for 1 hour the solution was filtered off and the resultant white solid was dried under vacuum. This solid was dissolved in CH₂Cl₂ and filtered through Celite. Slow diethyl ether diffusion over the resultant solution afforded 105 mg of colorless crystals (0.48 mmols, 72 %). Anal. Calcd for $C_{21}H_{34}F_6MnN_4O_6S_2$: C, 37.56; H, 5.10; N, 8.34; S, 9.55 %. Found: C, 37.23; H, 5.40; N, 8.21; S, 8.90 %. FT-IR (ATR) ν , cm^{-1} : 2981 - 2947 (C-H)_{sp3}, 1738, 1672, 1470, 1303 (py), 1222, 1157, 1024, 632 (CF₃SO₃). ESI-MS (m/z): 186.5 [M-2CF₃SO₃]²⁺, 522.1 [M-CF₃SO₃]⁺.

2) Catalysis conditions

Peracetic acid solutions employed in the reactions were prepared by diluting commercially available peracetic acid (32% $\text{CH}_3\text{CO}_3\text{H}$ solution in acetic acid) in acetonitrile (1:1 v:v).

Optimization conditions

An acetonitrile solution (3 mL) of 1-octene (50 mM) and the specific catalyst **1 - 4** (0.5 mM) was prepared in a vial equipped with a stir bar and cooled to 0 °C. 75 μL of a 1:1 v:v acetonitrile:peracetic acid solution 32% (1.0 equiv) were added by syringe pump over a period of 3 min. The solution was further stirred at 0°C for 30 minutes. At this point, the internal standard (biphenyl) was added and the solution was filtered through a basic alumina plug, which was subsequently rinsed with 2 x 1 mL AcOEt. GC analysis of the solution provided substrate conversion and product yield relative to the internal standard integration. The epoxide product was identified by comparison to the GC retention time of an authentic sample, and by its GC-MS spectrum.

Reaction conditions (Table 1) GC analysis

An acetonitrile solution (15 mL) of the specific olefin (0.11 M) and **1** (0.11 mM) was prepared in a 25 mL round bottom flask equipped with a stir bar. The solution was cooled in an ice bath and 0.98 mL of 1:1 v:v acetonitrile:peracetic acid solution 32% (1.4 equiv) were added by syringe pump over a period of 30 min. The solution was further stirred at 0 °C for 1 hour. At this point, the internal standard (biphenyl) was added and the solution was filtered through a basic alumina plug, which was subsequently rinsed with 2 x 1 mL AcOEt. GC analysis of the solution provided substrate conversions and product yields relative to the internal standard integration. Products were identified by comparison to the GC retention time of authentic samples, and by their GC-MS spectrum.

Reaction conditions (Table 1) $^1\text{H-RMN}$ analysis

An acetonitrile solution (15 mL) of the specific olefin (0.11 M) and **1** (0.11-0.18 mM) was prepared in a 25 mL round bottom flask equipped with a stir bar. The solution was cooled in an ice bath and 0.98 mL of an 1:1 v:v acetonitrile:peracetic acid solution 32%

(1.4 equiv) were added by syringe pump over a period of 30 min. The solution was further stirred at 0°C for 1 hour. At this point, 1.6 mL of the solution were extracted and solvents were removed under reduced pressure. The resultant product was dissolved in CDCl₃ and 20 mg of acetophenone (17 mmols) were added as internal standard. ¹H-RMN analysis provided olefin conversion and epoxide yield by relative integration to the internal standard. The olefin and epoxide signals were identified by comparison with those of authentic samples, with data from the literature⁷ and by GC-MS analysis.

Blank experiments

Blank experiments in the absence of catalyst were performed for cyclooctene, cis-2-heptene and styrene. After one hour, the non catalyzed reaction afforded only 17%, <2% and <1% respective epoxide yields demonstrating that it has a small or marginal contribution to the overall reaction.

Selectivity conditions

An acetonitrile solution (15 mL) of olefin A (0.11 M), olefin B (0.11 M) and **1** (0.12 mM) was prepared in a 25 mL round bottom flask equipped with a stir bar. The solution was cooled in an ice bath and 70 µl of an 1:1 v:v acetonitrile:peracetic acid solution 32% (0.1 equivalents) was added by syringe pump over a period of 3 minutes (the peracetic acid solution was diluted with acetonitrile from a commercially available 32% CH₃CO₃H solution in acetic acid). The solution was further stirred at 0 °C for 10 minutes. At this point, the internal standard (biphenyl) was added and the solution was filtered through a basic alumina plug and washed with 2 x 1 mL AcOEt. GC analysis of the solution provided the yields of the two different epoxide products relative to the internal standard integration.

Table S1. Competitive Epoxidations with catalysts **1** for the Hammett's plot

<i>p</i> - substituted styrene vs styrene	K _{obs}
<i>p</i> -NO ₂ -styrene	0.346
<i>p</i> -Cl-stryrene	1.028
<i>p</i> -Me-styrene	2.035

Table S2. Competitive Epoxidations of pairs of olefins with catalysts **1**.

Olefin A/Olefin B	Epoxide yields A:B(%), (A/B)
Cyclooctene/cis-2-heptene	2/1

Cis/trans-2-heptene	9/1
Cis/trans- β -Methylstyrene	1/1
Cyclooctene/styrene	1/13

H₂¹⁸O Labelling conditions

An acetonitrile solution (15 mL) of *cis*-2-heptene (11 mM), 33 μ l of H₂¹⁸O (110 mM) and **1** (0.11 mM) was prepared in a 25 mL round bottom flask equipped with a stir bar. The solution was cooled in an ice bath and 17.5 μ l of an 1:1 v:v acetonitrile:peracetic acid solution 32% (1 equivalent) was added by syringe pump over a period of 1 minute. The solution was further stirred at 0 °C for 30 minutes. At this point, the internal standard (biphenyl) was added and the solution was filtered through a basic alumina plug which was subsequently rinsed with 2 x 1 mL AcOEt. GC analysis of the solution provided the *cis*-2,3-epoxyheptane yield relative to the internal standard integration. GC-MS analysis of the solution showed no incorporation formation of ¹⁸O-labeled epoxide.

3) References

1. Flassbeck, C.; Wieghardt, K., *Z. Anorg. Allg. Chem.* **1992**, (608), 60-68.
2. Halfen, J. A.; Tolman, W. B., *Inorg. Synth.* **1998**, 34, 75-81.
3. Berreau, L. M.; Halfen, J. A.; Young Jr., V. G.; Tolman, W. B., *Inorg. Chim. Acta* **2000**, 297, 115-128.
4. Company, A.; Gómez, L.; Güell, M.; Ribas, X.; Luis, J.-M.; Que, L. Jr ; Costas. M. *J. Am. Chem. Soc.* **2007**, 129, 15766-15767
5. Murphy, A.; Dubois, G.; Stack, T. D. P., *J. Am. Chem. Soc.* **2003**, 125, 5250-5251.
6. Murphy, A.; Pace, A.; Stack, T. D. P. *Org. Lett.* **2004**, 6, 3119-312.

Chapter V.2

A Broad Substrate-Scope Method for Fast, Efficient and Selective Hydrogen Peroxide-Epoxidation.

García-Bosch, I.; Ribas, X.; Costas, M. *Adv. Synth. Catal.* **2009**, *351*, 348-352.

Isaac Garcia-Bosch, Xavi Ribas, Miquel Costas. "A Broad Substrate-Scope Method for Fast, Efficient and Selective Hydrogen Peroxide-Epoxidation". *Advanced synthesis & catalysis*. Vol. 351, issue 3 (February 2009) : p. 348-352
Copyright © 2009 WILEY-VCH Verlag GmbH & Co. KGaA

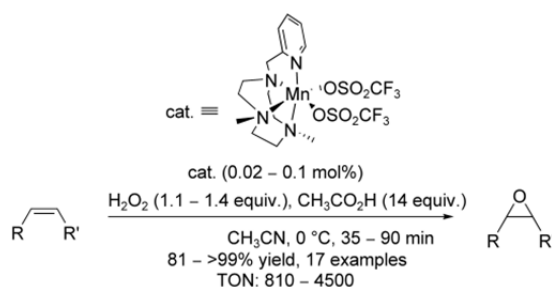
Article first published online: 6 FEB 2009

<http://dx.doi.org/10.1002/adsc.200800650>

<http://onlinelibrary.wiley.com/doi/10.1002/adsc.200800650/abstract>

Abstract

The efficient epoxidation of a broad range of olefins using hydrogen peroxide (H_2O_2) as the oxidant has been accomplished by a manganese catalyst that exhibits an uncommon chemoselectivity.



Keywords

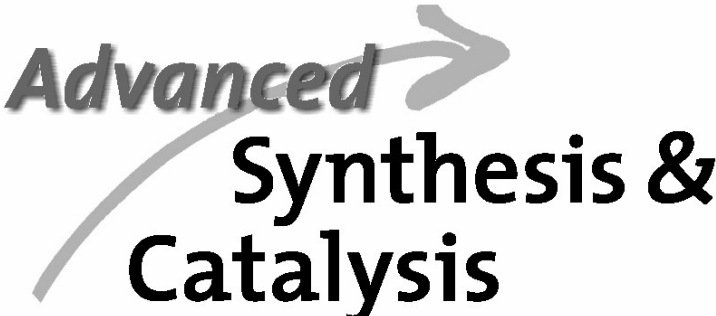
catalysis; chemoselectivity; epoxidation; hydrogen peroxide; manganese

Supporting information

Detailed facts of importance to specialist readers are published as "Supporting Information". Such documents are peer-reviewed, but not copy-edited or typeset. They are made available as submitted by the authors.

http://onlinelibrary.wiley.com/store/10.1002/adsc.200800650/asset/supinfo/adsc_200800650_sm_miscellaneous_information.pdf?v=1&s=fa7dbff7384c1831f8366c57419a6e949367e009

Please note: Wiley-Blackwell are not responsible for the content or functionality of any supporting materials supplied by the authors. Any queries (other than missing material) should be directed to the corresponding author for the article.



Advanced
**Synthesis &
Catalysis**

Supporting Information

© Copyright Wiley-VCH Verlag GmbH & Co. KGaA, 69451 Weinheim, 2009

Supporting Information for

A Broad-Scope Method for Fast, Efficient and Selective Hydrogen Peroxide-Epoxidation

Isaac Garcia, Xavi Ribas* and Miquel Costas*

Departament de Química, Universitat de Girona, Campus de Montilivi, E-17071, Girona, Spain

1) Experimental section	S2
Materials	S2
Instrumentation	S2
2) Catalysis conditions	S2
Optimization conditions, Acetic Acid Effect (Table 1).....	S2
Reaction conditions (Table 2) GC analysis	S3
Reaction conditions (Table 2- Entry 2) GC analysis.....	S3
Reaction conditions (Table 2) ¹ H-NMR analysis	S4
Reaction conditions (Table 2) Product isolation.....	S4
Selectivity conditions (Table S1).....	S5
H ₂ ¹⁸ O Labeling conditions.....	S6
H ₂ ¹⁸ O ₂ Labeling conditions	S6
3) References	S6

1. Experimental Section

Materials

Reagents and solvents used were of commercially available reagent quality unless stated otherwise. Solvents were purchased from SDS and Sharlab. Solvents were purified and dried by passing through an activated alumina purification system (M-Braun SPS-800) or by conventional distillation techniques. H_2^{18}O (95% ^{18}O -enriched) and $\text{H}_2^{18}\text{O}_2$ (90% ^{18}O -enriched in an aqueous solution (2.6%)) was received from ICON Isotopes.

Instrumentation

Product analyses were performed on a Shimadzu GC-2010 gas chromatography (AT-1701 column, 30 m) equipped with a flame-ionization detector. GC mass spectral analyses were performed on a Thermoquest Trace GC 2000 Series (TRB-5MS column, 30 m) with a Finnigan Trace MS mass detector. NMR spectra were taken on a Bruker DPX400 spectrometer using standard conditions. Oxidation products were identified by comparison of their GC retention times and GC/MS with those of authentic compounds, and/or by ^1H and ^{13}C -NMR analyses.

2. Catalysis conditions

Hydrogen peroxide solutions employed in the reactions were prepared by diluting commercially available hydrogen peroxide (32% H_2O_2 solution in water, Aldrich) in acetonitrile (1:1 v:v). Complexes (**1-3** and $[\text{Mn}(\text{bpy})_2]^{2+}$)¹⁻³ were synthesized as previously described. Commercially available glacial acetic acid (99-100%) from Riedel-de-Haën was employed. Olefin substrates were purchased from Aldrich, with the maximum purity available, and used as received.

Optimization conditions, Acetic Acid Effect (Table 1)

An acetonitrile solution (15 mL) of 1-octene (186 mg, 1.66 mmols, final reaction concentration 0.11 M) and **1** (1 mg, 1.66 μ mol, final reaction concentration 0.11 mM) was prepared in a 25 mL round bottom flask equipped with a stir bar and cooled to 0 °C. A variable number of equivalents (0.083 to 23.3 mmols, 0.05 to 14 equiv.) of acetic acid was directly added to the solution (from 5 μ L to 1.4 mL). Then, 0.35 mL of a 1:1 v:v acetonitrile: hydrogen peroxide solution 32% (1.83 mmols, 1.1 equiv.) was added by syringe pump over a period of 30 min. The solution was further stirred at 0 °C for 60 minutes. At this point, the internal standard (biphenyl) was added and the solution was filtered through a basic alumina plug, which was subsequently rinsed with 2 x 1 mL AcOEt. GC analysis of the solution provided substrate conversion and product yield relative to the internal standard integration. The epoxide product was identified by comparison to the GC retention time of an authentic sample, and by its GC-MS spectrum.

Reaction conditions (Table 2) GC analysis

An acetonitrile solution (15 mL) of the specific olefin (1.66 mmols, final reaction concentration 0.11 M), catalyst (**1** or **2**, 1.66 μ mol, final reaction concentration 0.11 mM) was prepared in a 25 mL round bottom flask equipped with a stir bar and cooled in an ice bath. 1.4 mL of acetic acid (23.3 mmols, 14 equiv.) was added directly to the solution. Then, 0.35-0.44 mL of 1:1 v:v acetonitrile:hydrogen peroxide solution 32% (1.83 to 2.33 mmols, 1.1-1.4 equiv) was added by syringe pump over a period of 30 min. The solution was further stirred at 0 °C for 5-60 minutes. At this point, the internal standard (biphenyl) was added and the solution was filtered through a basic alumina plug, which was subsequently rinsed with 2 x 1 mL AcOEt. GC analysis of the solution provided substrate conversions and product yields relative to the internal standard integration. Products were identified by comparison to the GC retention time of authentic samples, and by their GC-MS spectrum. Commercially not available epoxides were identified by a combination of ^1H , ^{13}C -NMR analyses, and GC-MS.

Reaction conditions (Table 2- Entry 2) GC analysis

An acetonitrile solution (15 mL) of styrene (8.32 mmols, final reaction concentration 0.60 M), **1** (1 mg, 1.66 μ mol, final reaction concentration 0.11 mM) was prepared in a 25 mL round bottom flask equipped with a stir bar and cooled in an ice bath. 1.4 mL of acetic acid (23.3 mmols, 14 equiv.) was added directly to the solution. Then, 1.9 mL of 1:1 v:v acetonitrile:hydrogen peroxide solution 32% (9.98 mmols, 1.2 equiv) was added by syringe pump over a period of 150 min. The solution was further stirred at 0 °C for 60 minutes. At this point, the internal standard (biphenyl) was added and the solution was filtered through a basic alumina plug, which was subsequently rinsed with 2 x 1 mL AcOEt. GC analysis of the solution provided substrate conversions and product yields relative to the internal standard integration. Products were identified by comparison to the GC retention time of authentic samples, and by their GC-MS spectrum.

Reaction conditions (Table 2) $^1\text{H-NMR}$ analysis

An acetonitrile solution (15 mL) of the specific olefin (1.66 mmols, final reaction concentration 0.11 M) and **1** (1 mg, 1.66 μ mol, 0.11 mM) was prepared in a 25 mL round bottom flask equipped with a stir bar and cooled in an ice bath. 1.4 mL of acetic acid was directly added (23.3 mmols, 14 equiv.) Then, 0.38-0.44 mL of an 1:1 v:v acetonitrile:hydrogen peroxide solution 32% (1.99-2.33 mmols, 1.2-1.4 equiv) was added by syringe pump over a period of 30 min. The solution was further stirred at 0°C for 5 minutes. At this point, 1.7 mL of the solution was extracted and solvents were removed under reduced pressure. The resultant product was dissolved in CDCl_3 and 20 mg of mesitylene (16 mmols) were added as internal standard. $^1\text{H-NMR}$ analysis provided olefin conversion and epoxide yield by relative integration to the internal standard. The epoxide signals were identified by a combination of ^1H , $^{13}\text{C-NMR}$ analyses, by comparison with those of authentic samples, with data from the literature²⁻³ and by GC-MS analysis.

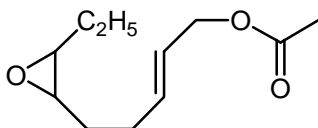
Reaction conditions (Table 2) Product isolation

General Procedure for epoxide isolation:

An acetonitrile solution (15 mL) of olefin (1.66 mmols, final reaction concentration 0.11 M) and **1** (1 mg, 1.66 μ mol, final reaction concentration 0.11 mM) was prepared in

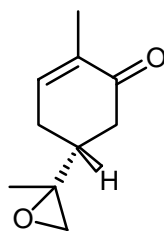
a 25 mL round bottom flask equipped with a stir bar and cooled in an ice bath. 1.4 mL of acetic acid was directly added (23.3 mmol, 14 equiv.). Then, 0.38 or 0.45 mL (depending on the olefin) of an 1:1 v:v acetonitrile:H₂O₂ solution 32% (1.99 or 2.33 mmols, 1.2 equiv or 1.4 equiv) was added by syringe pump over a period of 30 min. The solution was further stirred at 0°C for 5 minutes. At this point, 50 mL of an aqueous Na₂CO₃ saturated solution were added to the mixture. The resultant solution was extracted with diethyl ether (3 x 50 mL). Organic fractions were combined, dried over MgSO₄, filtered, and the solvent was removed under reduced pressure to afford the pure epoxide product.

2-*trans*-6-epoxide-nonenyl ester:



320 mg of *trans*-2-*cis*-6-nonadiethyl ester (97% pure, 1.66 mmols) were converted to 283 mg (1.43 mmols, 86% isolated yield, 95% NMR yield) of the corresponding monoepoxide using 1.99 mmols (1.2 equiv.) of H₂O₂. ¹H-NMR (400 MHz, CDCl₃, 300K) δ, ppm: 5.86 - 5.80 (m, 1H, CH=CH-CH₂-COOMe), 5.65 - 5.63 (m, 1H, CH=CH-CH₂-COOMe), 4.52 (d, J = 6.4 Hz, 2H, OCH₂-CH=CH), 2.96 - 2.84 (m, 2H, CH₃-CH₂-CHOCH-CH₂), 2.35 - 2.20 (m, 2H, CH₂-CH₂-CH=CH-), 2.05 (s, 3H, OCO-CH₃), 1.70 - 1.45 (m, 4H, CH₃-CH₂-CHOCH-CH₂-), 1.04 (t, J = 7.6 Hz, 3H, CH₃-CH₂). ¹³C-NMR (100 MHz, CDCl₃, 300K) δ, ppm: 170.81, 135.86, 127.88, 65.20, 58.38, 56.62, 29.34, 27.14, 21.26, 21.13, 10.66. GC-MS (EI) m/z (%): 57 (70) [C₂H₃O₂], 67 (100) [C₅H₇], 80 (70) [C₆H₈], 112 (50) [C₇H₁₂O], 155 (5) [C₉H₁₅O₂].

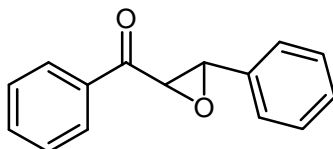
R-(-)-Carvone 8,9-epoxide:



252 mg of R-(-)-carvone (99% pure, 1.66 mmols) were converted to 256 mg of the corresponding 8,9-epoxide. (1.54 mmols, 92% isolated yield, NMR yield >99%) using 1.99 mmols (1.2 equiv.) of H₂O₂. ¹H-NMR (400 MHz, CDCl₃, 300K) δ, ppm:

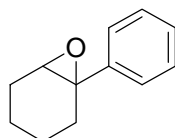
6.74 (m, 1H, C=CH), 2.70 - 2.02 (m, 7H), 1.78 (s, 3H, CH₃-C-O), 1.32 (d, J = 6.4 Hz, 3H, CH₃-C=CH). ¹³C-NMR (100 MHz, CDCl₃, 300K) δ, ppm: 198.88, 198.83, 144.17, 143.93, 135.63, 135.58, 57.97, 57.87, 52.94, 52.41, 41.35, 40.71, 40.36, 39.93, 27.90, 27.71, 19.00, 18.35, 15.70. GC-MS (EI) m/z (%): 82 (50) [C₅H₆O], 108 (100) [C₇H₈O], 121 (40) [C₈H₉O], 151 (20) [C₉H₁₁O₂].

***Trans*-chalcone epoxide:**



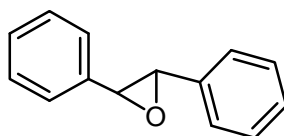
357 mg of *trans*-chalcone (97% pure, 1.66 mmol) were converted to 325 mg of the corresponding epoxide (1.45 mmols, 87% isolated yield, NMR yield 87%) using 2.33 mmols (1.4 equiv.) of H₂O₂. ¹H-NMR (400 MHz, CDCl₃, 300K) δ, ppm: 8.06 (m, 2H, Ar-H), 7.65 – 7.35 (m, 8H, Ar-H), 4.30 (d, J = 2 Hz, 1H, CH-O-CH), 4.07 (d, J = 2 Hz 1H, CH-O-CH). ¹³C-NMR (100 MHz, CDCl₃, 300K) δ, ppm: 193.11, 144.87, 135.50, 134.04, 132.83, 130.59, 129.10, 129.00, 128.92, 128.81, 128.49, 128.38 125.83, 61.04, 59.45. GC-MS (EI) m/z (%): 77 (90) [C₆H₅], 105 (100) [C₇H₅O], 208 (20) [C₁₅H₁₂O], 224.1 (20) [C₁₅H₁₂O₂].

1-phenyl-1-cyclohexane epoxide



277 mg of 1-phenyl-1-cyclohexene (95% pure, 1.66 mmols) were converted to 259 mg of the corresponding epoxide (1.49 mmol, 90% isolated yield, NMR yield 96%) using 2.33 mmols (1.4 equiv.) of H₂O₂. ¹H-NMR (400 MHz, CDCl₃, 300K) δ, ppm: 7.42 - 7.27 (m, 5H, Ar-H), 3.11 (t, J = 2 Hz, 1H, -CH-O-), 2.29 – 2.10 (m, 2H, CH₂-CH-O), 2.05 - 2.01 (m, 2H, CH₂-C-O), 1.70 – 1.30 (m, 4H, CH₂-CH₂). ¹³C-NMR (100 MHz, CDCl₃, 300K) δ, ppm: 142.53, 128.49, 127.17, 125.33, 61.95, 60.25, 29.28, 28.84, 20.12, 19.80. GC-MS (EI) m/z (%): 77 (80) [C₆H₅], 117 (60) [C₈H₅O], 173.4 (100) [C₁₂H₁₃O].

***Trans*-stilbene epoxide:**



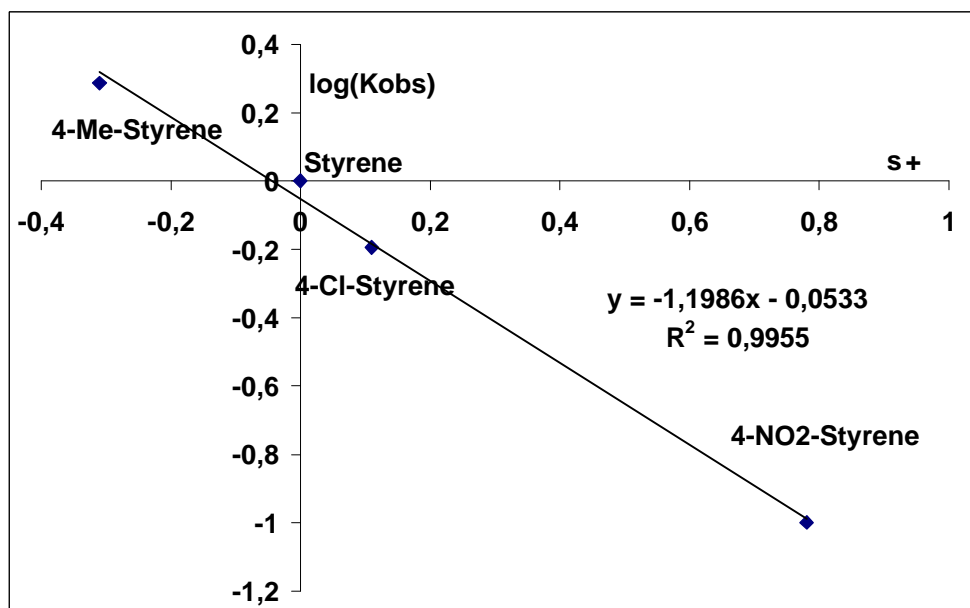
312 mg of *trans*-stilbene (96% pure, 1.66 mmol) were converted to 300 mg of the corresponding epoxide (1.53 mmols, 92% isolated yield, NMR yield 95%) using 2 mmols (1.2 equiv.) of H₂O₂. ¹H-NMR (200 MHz, CDCl₃, 300K) δ , ppm: 7.45 – 7.1 (m, 10H, Ar-H), 3.87 (s, 2H, CH-O-CH).

Selectivity conditions

An acetonitrile solution (15 mL) of olefin A (1.66 mmols, 0.11 M), olefin B (1.66 mmols, 0.11 M) and **1** (1 mg, 1.66 μ mol, 0.11 mM) was prepared in a 25 mL round bottom flask equipped with a stir bar and cooled in an ice bath. 1.4 mL of acetic acid (23.3 mmols, 14 equiv.) was directly added to the solution. Then, 32 μ l of an 1:1 v:v acetonitrile:hydrogen peroxide solution 32% (0.17 mmols, 0.1 equivalents) was added by syringe pump over a period of 3 minutes (the hydrogen peroxide solution was diluted with acetonitrile from a commercially available 32% H₂O₂ solution in H₂O). The solution was further stirred at 0 °C for 10 minutes. At this point, the internal standard (biphenyl) was added and the solution was filtered through a basic alumina plug and washed with 2 x 1 mL AcOEt. GC analysis of the solution provided the yields of the two different epoxide products relative to the internal standard integration (Table S1 and Scheme S1 shows the Hammett's plot details obtained for these competition experiments).

Table S1. Competitive Epoxidations with catalysts **1 for the Hammett's plot**

<i>p</i> - substituted styrene vs styrene	k _{obs}
4-NO ₂ -styrene	0.1
4-Cl-styrene	0.64
4-Me-styrene	1.93



Scheme S1. Hammett's plot of the competitive epoxidations

$H_2^{18}O$ Labeling conditions

An acetonitrile solution (15 mL) of styrene (1.66 mmols, final reaction concentration 0.11 M), 34 μ l of $H_2^{18}O$ (1.66 mmols, final reaction concentration 0.11 M) and **1** (1 mg, 1.66 μ mol, final reaction concentration 0.11 mM) was prepared in a 25 mL round bottom flask equipped with a stir bar. 1.4 mL of acetic acid (23.3 mmols, 14 equiv.) was directly added. The solution was cooled in an ice bath and 8 μ l of an 1:1 v:v acetonitrile:hydrogen peroxide solution 32% (0.42 mmols, 0.25 equivalents) was added by syringe pump over a period of 1 minute. The solution was further stirred at 0 °C for 10 minutes. At this point, the internal standard (biphenyl) was added and the solution was filtered through a basic alumina plug which was subsequently rinsed with 2 x 1 mL AcOEt. GC analysis of the solution provided the styrene oxide yield relative to the internal standard integration. GC-MS analysis of the solution showed no incorporation formation of ^{18}O -labeled epoxide.

$H_2^{18}O_2$ Labeling conditions

An acetonitrile solution (15 mL) of styrene (1.66 mmols, final reaction concentration 0.11 M) and **1** (1 mg, 1.66 μ mol, final reaction concentration 0.11 mM) was prepared

in a 25 mL round bottom flask equipped with a stir bar. 1.4 mL of acetic acid (23.3 mmols, 14 equiv.) was directly added to the solution. The mixture was cooled in an ice bath and 12.2 μl of $\text{H}_2^{18}\text{O}_2$ (2.6% H_2O_2 content, 16.6 μmols , 0.01 equivalent) was added by syringe pump over a period of 1 minute. The solution was further stirred at 0 °C for 10 minutes. At this point, the internal standard (biphenyl) was added and the solution was filtered through a basic alumina plug which was subsequently rinsed with 2 x 1 mL AcOEt. GC analysis of the solution provided the styrene oxide yield relative to the internal standard integration. GC-MS analysis of the solution showed formation of ^{18}O -labeled epoxide. The extent of the labelling was determined by computer simulation of the observed isotopic pattern.

3. References

1. I. Garcia-Bosch; A. Company; X. Fontrodona; X. Ribas; M. Costas, *Org. Lett.* **2008**, *10*, 2095-2098.
2. A. Murphy; G. Dubois; T. D. P. Stack, *J. Am. Chem. Soc.* **2003**, *125*, 5250-5251.
3. A. Murphy; A. Pace; T. D. P. Stack, *Org. Lett.* **2004**, *6*, 3119-3122

Chapter V.3

Stereoselective Epoxidation of Alkenes with Hydrogen Peroxide Using a Bipyrrolidine-Based Family of Manganese Complexes.

çGarcía-Bosch, I.; Gómez, L.; Polo, A.; Ribas, X.; Costas, M. Accepted in *Adv. Synth. Catal.* DOI: 10.1002/adsc.201100409.

Stereoselective epoxidation of alkenes with hydrogen peroxide using a bipyrrolidine-based family of manganese complexes

Isaac Garcia-Bosch, Laura Gómez, Alfonso Polo, Xavi Ribas* and Miquel Costas*

^a QBIS group. Departament de Química. Universitat de Girona. Campus Montilivi, E-17071 Girona, Catalonia (Spain).
E-mail: miquel.costas@udg.edu, xavi.ribas@udg.edu

Received: ((will be filled in by the editorial staff))



Supporting information for this article is available on the WWW under <http://dx.doi.org/10.1002/adsc.200#####>.

Abstract. Novel manganese complexes containing N4-tetradentate ligands derived from chiral bipyrrolidine diamines catalyse the stereoselective epoxidation of a wide array of alkenes using low catalyst loadings (0.1 mol%) and hydrogen peroxide (1.2 equiv.) as terminal oxidant. This family of catalysts affords good to excellent yields (80-100%) and moderate to good ee's (40-73%) in short reaction times (30 min.) making efficient use of hydrogen peroxide.

Keywords: Stereoselective; alkene epoxidation; manganese catalyst; hydrogen peroxide; green chemistry.

Epoxides play an important role as polyvalent building blocks in a wide range of chemical transformations.^[1, 2] Because of that, chemoselective and enantioselective epoxidations constitute important reactions for synthetic organic chemistry^[3, 4]. Extensive work has been done in order to obtain catalysts which could perform asymmetric epoxidations with high enantioselectivities.^[5] In this regard, Mn-Salen catalysts^[6-8] and Shi's ketone-based systems^[9] are excellent methods to epoxidize a wide range of olefins with high enantioselectivity (>90% ee), yet substantial room for improvement remains in terms of catalyst loadings, and use of oxidants with high atom economy. Because of environmental considerations, catalytic systems that use H₂O₂ as oxidant, and non-toxic first row transition metal ions catalysts are particularly appealing.^[5, 10] Katsuki and co-workers have developed a Ti-Salalen complex that catalyzes the epoxidation of alkenes with high enantioselectivities (>96%) using H₂O₂ as terminal oxidant.^[11] Beller and co-workers have also described an Fe-based methodology for asymmetric epoxidation of alkenes, which exhibits high stereoselectivities for stilbenes.^[12, 13] Therefore, the development of environmentally benign technologies capable of producing a wide range of enantiomerically pure epoxides, remains a challenge of interest and academic and technological significance. Selected

manganese complexes relying in N-rich ligands were first described by Stack and co-workers as very active catalyst in the epoxidation of a wide range of olefins using peracetic acid as oxidant.^[14, 15] The complex Λ -[Mn(CF₃SO₃)₂((S,S)-MCP)] **Λ -1** was particularly interesting because its chiral nature converted it in a promising candidate as stereoselective epoxidation catalysts (Scheme 1). Unfortunately, it affords very modest ee's, and structural modifications on catalyst structure resulted in loss of activity, which severely challenged further improvement. Following in these results, Mn-N₄ catalysts [Mn(CF₃SO₃)₂((S,S,R)-MCP)] **Λ -2**, and [Mn(CF₃SO₃)₂((S,S,S)-MCP)] **Λ -3**, containing pinene groups attached to positions 4,5 of the pyridine rings were designed. Introduction of these groups do not erase the catalytic activity, and the complex mediates the epoxidation of a wide range of olefins in moderate ee's (30-40%) using low catalyst loadings (0.5 mol%) and peracetic acid as oxidant.^[16] In parallel we also described a TACN-based complex [Mn(CF₃SO₃)₂(^{H,Me}PyTACN)] as an excellent catalyst for the selective and efficient epoxidation of a wide range of olefins using very low catalyst loadings (0.05-0.1 mol%). Our initial report made use of peracetic acid as oxidant,^[17] but in a subsequent work we indentified reaction conditions that allowed use of an small excess of H₂O₂ (1.2 equiv), in the presence of acetic acid (14 equiv.) as additive.^[18] These experimental conditions were then used by Xia, Sun and co-workers, who designed a novel MCP type of complex (Scheme 1, (R,R,R,R)-BPMCP) that epoxidizes α,β -enones with good enantiomeric excesses (70-80%).^[19] Very recently, Talsi and co-workers have also used the H₂O₂/AcOH conditions to epoxidize alkenes using complex [Mn(CF₃SO₃)₂((S,S)-BPBP)] (**Λ -4**) (Figure 1). Using this catalyst, the authors achieved high ee's (70-80%) for electron-deficient substrates, but more moderate ee's were measured with other substrates such as styrene (39% ee).^[20]

Supporting Information

for

Stereoselective epoxidation of alkenes with hydrogen peroxide using a bipyrrolidine-based family of manganese complexes

Isaac Garcia-Bosch, Laura Gómez, Alfonso Polo, Xavi Ribas* and Miquel Costas*

Contents:

S1. Instrumentation	S2
S2. Materials	S2
S.3 Synthesis of ligands	S2
S4. Synthesis of Complexes	S3
S5. Catalytic studies	S4
S6. References	S5

S1. Instrumentation

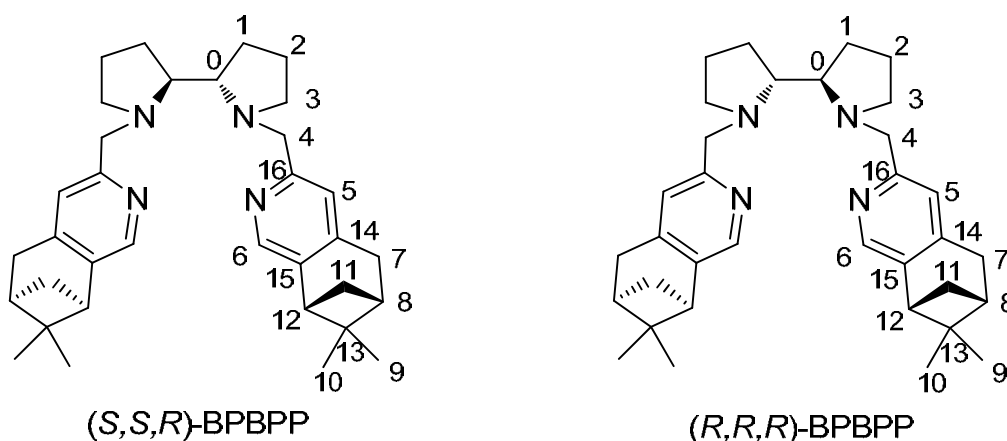
IR spectra were taken in a Mattson-Galaxy Satellite FT-IR spectrophotometer using a MKII Golden Gate single reflection ATR system. Elemental analyses were performed using a CHNS-O EA-1108 elemental analyzer from Fisons. NMR spectra were taken on Bruker Bruker DPX200 and DPX400 spectrometers using standard conditions. Electrospray ionization mass spectrometry (ESI-MS) experiments were performed on a Bruker Daltonics Esquire 3000 Spectrometer using a 1 μ M solution of the analyzed compound. Enantioselective chromatographic resolution was performed on an Agilent GC-7820-A chromatograph using a CHIRALCELDEX G-TA column.

S2. Materials

Reagents and solvents used were of commercially available reagent quality unless otherwise stated. Solvents were purchased from SDS and Scharlab. Acetonitrile, tetrahydrofuran and diethyl ether were purified and dried by passing through an activated alumina purification system (MBraun SPS-800) and stored into the glove box. Preparation and handling of air-sensitive materials were carried out in a N₂ drybox (MBraun) with O₂ and H₂O concentrations < 1 ppm.

S3. Synthesis of ligands:

(*S,S*)-2,2'-bipyrrolidine D-tartrate, (*R*)-pinene-PyCH₂Cl·HCl and (*S,S*)-BPBP were synthesized as previously reported.^[1]



Scheme S1. New N4-ligands synthesized. Numeric code used for NMR assignment.

(S,S,R)-BPBPP. A solution containing **(S,S)-2,2'-bipyrrolidine D-tartrate** (0.35 g, 1.2 mmol), H₂O (2.6 mL), CH₂Cl₂ (4 mL) was added to a 10 mL round bottom flask charged with a stir bar and **(R)-pinene-PyCH₂Cl·HCl**. The aqueous phase was extracted with CH₂Cl₂ (3 x 5 mL), the organic fractions were combined, dried over MgSO₄ and the solvent was removed under vacuum. The brown oil was purified over silica column (CH₂Cl₂:MeOH:NH₃ 97:2:1) and the collected fractions were combined and concentrated to 5 mL. This fraction was washed with 1M NaOH (1 mL), dried over MgSO₄ and the solvent was removed under reduced pressure to provide 230 mg (0.45 mmol, 37%) of a yellow oil that turns solid under vacuum. FT-IR (ATR) ν , cm⁻¹: 2921 – 2806 (C-H)_{sp³}, 1695, 1605, 1557, 1483, 1466, 1444, 1426, 1368, 1266, 1211, 1116, 1026, 948- 865. ¹H-NMR (400 MHz, CDCl₃, 300 K) δ , ppm: 8.02 (s, 2H, (6)); 7.17 (s, 2H, (5)); 4.10 (d, 2H, J = 14.0 Hz, (4)); 3.40 (d, 2H, J = 14.0 Hz, (4)); 3.04-3.00 (m, 2H, (3)); 2.94-2.92 (m, 4H, (7)); 2.80-2.76 (m, 2H, (12)); 2.71-2.63 (m, 4H, (11 exo and 0)); 2.30-2.18 (m, 4H, (3 and 8)); 1.84-1.67 (m, 8H, (1 and 2)); 1.39 (s, 6H, (10)); 1.15 (d, 2H J = 7.2 Hz, (11 endo)); 0.61 (s, 6H, (9)). ¹³C-NMR (75 MHz, CDCl₃, 300 K) δ , ppm: 145.1 (6); 158.2, 145.1, 140.8 (14, 15 and 16); 122.5 (5); 65.6 (0); 61.7 (4); 55.8 (3); 44.5 (12); 40.3 (8); 39.4 (13); 32.9 (7); 32.1 (11); 26.2 (9); 26.0, 23.6 (1 and 2); 21.6 (10). ESI-MS (m/z): 511.5 (100) [M+H]⁺.

(R,R,R)-BPBPP was prepared in analogous manner to **(S,S,R)-BPBPP** starting from **(R,R)-2,2'-bipyrrolidine L-tartrate**. (230 mg, 0.45 mmol, 37%). FT-IR (ATR) ν , cm⁻¹: 2968 - 2806 (C-H)_{sp³}. ¹H-NMR (400 MHz, CDCl₃, 300 K) δ , ppm: 8.02 (s, 2H, (6)); 7.15 (s, 2H, (5)); 4.13 (d, 2H, J = 14.0 Hz, (4)); 3.43 (d, 2H, J = 14.0 Hz, (4)); 3.03-2.99 (m, 2H, (3)); 2.92-2.91 (m, 4H, (7)); 2.78-2.71 (m, 4H, (12 and 0)); 2.68-2.63 (m, 2H, (11 exo)); 2.29-2.19 (m, 4H, (3 and 8)); 1.87-1.68 (m, 8H, (1 and 2)); 1.39 (s, 6H, (10)); 1.15 (d, 2H, J = 8.8 Hz, (11 endo)); 0.61 (s, 6H, (9)). ¹³C-NMR (75 MHz, CDCl₃, 300 K) δ , ppm: 144.9 (6), 158.1, 144.7, 140.5 (14, 15 and 16); 122.0 (5), 65.6 (0), 61.4 (4), 55.4 (3), 44.3 (12), 40.1 (8), 39.2 (13), 32.8 (7), 31.9 (11), 26.0 (9), 25.9, 23.4 (1 and 2); 21.4 (10). ESI-MS (m/z): 511.5 (100) [M+H]⁺.

S4. Synthesis of Complexes:

Λ -[Mn(CF₃SO₃)₂((*S,S*)-MCP)] (**Λ -1**), [Mn(CF₃SO₃)₂((*S,S,R*)-MCP)] (**Λ -2**) and [Mn(CF₃SO₃)₂((*R,R,R*)-MCP)] (**Λ -3**) were synthesised as previously described.^[2, 3] All manganese complexes were synthesized in the glovebox.

Λ -[Mn(CF₃SO₃)₂((*S,S*)-BPBP)] (**Λ -4):** A suspension of Mn(CF₃SO₃)₂ (50,2 mg, 0.14 mmols) in anhydrous THF (1 mL) was added dropwise to a vigorously stirred solution of (*S,S*)-BPBP (63,8 mg, 0.14 mmols) in THF (1 mL). After a few seconds the solution became cloudy and a white precipitate appeared. After stirring for 1 hour the solution was filtered off and the resultant white solid dried under vacuum. The solid was dissolved in CH₂Cl₂ and filtered through Celite. Slow diethyl ether diffusion over the resultant solution afforded, in a few days, 52 mg of colorless crystals (0.096 mmols, 54 %). Anal. Calcd for C₂₂H₂₆F₆MnN₄O₆S₂: C, 39.1; H, 3.9; N, 8.3; S, 9.5 %. Found: C, 39.5; H, 3.8; N, 8.6; S, 9.7 %. FT-IR (ATR) ν , cm⁻¹: 2990 - 2948 (C-H)_{sp3}, 1738, 1608, 1485-1444, 1307 (py), 1232, 1202, 1156, 1024, 899, 761, 633 (CF₃SO₃). ESI-MS (m/z): 526.1 [M-CF₃SO₃]⁺.

Λ -[Mn(CF₃SO₃)₂((*S,S,R*)-BPBP)] (**Λ -5):** Complex **5** was prepared in analogous manner to Λ -[Mn(OTf)₂((*S,S*)-BPBP)] (**Λ -4**) starting from Mn(CF₃SO₃)₂ (37 mg, 0.10 mmols) and (*S,S,R*)-BPBP (53,5 mg, 0.10 mmols). 60 mg of complex were obtained (0.07 mmols, 66 %). Anal. calcd for C₃₆H₄₂F₆MnN₄O₆S₂: C, 50.1; H, 5.4; N, 6.5; S, 7.4 %. Found: C, 50.3; H, 5.5; N, 6.3; S, 7.5 %. FT-IR (ATR) ν , cm⁻¹: 2990 - 2948 (C-H)_{sp3}, 1737, 1498, 1456, 1313 (py), 1232, 1211, 1161, 1027, 867, 820, 757, 633 (CF₃SO₃). ESI-MS (m/z): 714.3 (80) [M-CF₃SO₃]⁺, 282.6 (20) [M-(CF₃SO₃)₂]²⁺.

Λ -[Mn(CF₃SO₃)₂((*R,R,R*)-BPBP)] (**Λ -6):** Complex **6** was prepared in analogous manner to Λ -[Mn(OTf)₂((*S,S*)-BPBP)] (**Λ -4**) starting from Mn(CF₃SO₃)₂ (37 mg, 0.10 mmols) and (*S,S,R*)-BPBP (53.5 mg, 0.10 mmols). 70 mg of complex were obtained (0.081 mmols, 81 %). Anal. calcd for C₃₆H₄₂F₆MnN₄O₆S₂ (x 2 H₂O): C, 48.1; H, 5.6; N, 6.2; S, 7.1 %. Found: C, 47.7; H, 5.4; N, 6.3; S, 6.7 % FT-IR (ATR) ν , cm⁻¹: 2990 - 2948 (C-H)_{sp3}, 1738, 1608, 1485-1444, 1307 (py), 1232, 1202, 1156, 1024, 899, 761, 633 (CF₃SO₃). ESI-MS (m/z): 714.3 (80) [M-CF₃SO₃]⁺, 282.6 (20) [M-(CF₃SO₃)₂]²⁺.

S5. Catalytic studies:

Hydrogen peroxide solutions employed in the reactions were prepared by diluting commercially available hydrogen peroxide (32% H₂O₂ solution in water, Aldrich) in acetonitrile (1:1 v:v). Commercially available glacial acetic acid (99-100%) from Riedel-de-Haën was employed.

Reaction conditions for GC analysis

An acetonitrile solution (7.5 mL) of the specific olefin (0.12 M), complex **1-6** (0.12 mM) was prepared in a 25 mL round bottom flask equipped with a stir bar and cooled in an ice bath. 0.7 mL of acetic acid (14 equiv.) was added directly to the solution. Then, 0.19 mL of 1:1 v:v acetonitrile:hydrogen peroxide solution 32% (1.2 equiv.) was added by syringe pump over a period of 30 min. The solution was further stirred at 0 °C for 5 minutes. At this point, the internal standard (biphenyl) was added and the solution was filtered through a basic alumina plug, which was subsequently rinsed with 2 x 1 mL AcOEt. GC analysis of the solution provided substrate conversions and product yields relative to the internal standard integration. Products were identified by comparison to the GC retention time of authentic samples, and by their GC-MS spectrum.

Reaction conditions for ¹H-NMR analysis

An acetonitrile solution (7.5 mL) of the specific olefin (0.12 M), complex **1-6** (0.12 mM) was prepared in a 25 mL round bottom flask equipped with a stir bar and cooled in an ice bath. 0.7 mL of acetic acid (14 equiv.) was added directly to the solution. Then, 0.19 mL of 1:1 v:v acetonitrile:hydrogen peroxide solution 32% (1.2 equiv.) was added by syringe pump over a period of 30 min. The solution was further stirred at 0 °C for 5 minutes. At this point, 25 mL of a saturated aqueous solution of Na₂CO₃ was added, and the resulting mixture was extracted with 25 mL of CH₂Cl₂ (3 times). Then, organic layers were dried over MgSO₄ and the solvents were removed under reduced pressure. The resultant product was dissolved in CDCl₃ and analyzed by ¹H-NMR using Eu(hfc)₃ to quantify the enantiomeric excess.

S6. References

- [1] L. Gomez, I. Garcia-Bosch, A. Company, J. Benet-Buchholz, A. Polo, X. Sala, X. Ribas, M. Costas, *Angew. Chem. Int. Ed.* **2009**, *48*, 5720.

- [2] L. Gómez, I. Garcia-Bosch, A. Company, X. Sala, X. Fontrodona, X. Ribas, M. Costas, *Dalton Trans.* **2007**, 5539.
- [3] A. Murphy, G. Dubois, T. D. P. Stack, *J. Am. Chem. Soc.* **2003**, 125, 5250.

Chapter VI

Results and Discussion

VI. Results and discussion

Enzymes are considered as paradigm of ideal catalysts: they carry out chemical transformations very efficiently, usually with an exquisite selectivity and under mild conditions. Very often, enzymes contain one or more metal ions in their active center. Iron, copper, manganese, zinc and nickel are the most common transition metals of choice of biological systems.¹⁻³ Among them, metalloproteins capable of performing the activation of O₂ are particularly interesting because the relevance of the reaction in both biochemical and industrial transformations. Metalloenzymes use O₂ in several oxidative reactions by reducing molecular oxygen (which is inert under mild conditions) to more reactive species like superoxides, peroxides or even oxo forms.

Bioinorganic chemistry has used different approaches to understand the intriguing chemistry of living organisms. From these, discrete model complexes have arisen as very advantageous systems: the development of low-molecular weight complexes, which can reproduce either structural or chemical properties, has been used to elucidate mechanistic characteristics of natural enzymes. Moreover, these model complexes can be used in oxidative catalytic transformations in reactions of technological interest. In this thesis, we focus our attention on the preparation of bioinspired complexes of dinuclear copper centers and mononuclear manganese complexes and their implication in O₂ (and its reduced forms) activation and catalytic oxidative transformations.

Chapter III. O₂ Activation Mediated by Unsymmetric Dinuclear Copper Complexes

Metalloproteins which contain a coupled dicopper center in their active center have attracted our attention because their versatility in the activation of O₂ and further reactivity.^{4,5} Among them, hemocyanin and tyrosinase constitute an intriguing example of functionality, since both metalloenzymes have *iso*-structural active centers but their reactivity is different.^{6,7} While hemocyanin is used by some living systems as O₂-carrier, tyrosinase is capable of *ortho*-hydroxylating phenols to catechols and quinones. The use of model complexes to reproduce the reactivity of dinuclear copper systems has been widely pursued. Although hemocyanin reactivity has been reproduced in several systems, limited examples exist that have been capable of performing the oxidation of phenolic substrates to catechols, i.e. showing tyrosinase-like reactivity.⁸⁻¹¹

Chapter III.1. O₂ Activation and Selective Phenolate *ortho* Hydroxylation by an Unsymmetric Dicopper μ - η^1 : η^1 -Peroxo Complex.

In Chapter III.1, two novel dinucleating ligands are prepared. While ligand m -Xyl^{N⁴N⁴} contains two identical binding sites, ligand m -Xyl^{N³N⁴} has been designed with two distinct binding sites (Figure 1). The two corresponding dicopper(I) complexes have been synthesized and fully characterized. X-Ray analysis of [Cu^I₂(m -Xyl^{N³N⁴})]²⁺ (**1**) structure reveals that the copper ion bound at the tridentate site adopts a distorted T-shape geometry, whereas the copper metal bound at the tetradentate arm presents a distorted trigonal-pyramidal geometry. As expected, an identical distorted trigonal-pyramidal geometry is found for copper centers in the symmetric complex [Cu^I₂(m -Xyl^{N⁴N⁴})]²⁺ (**2**).

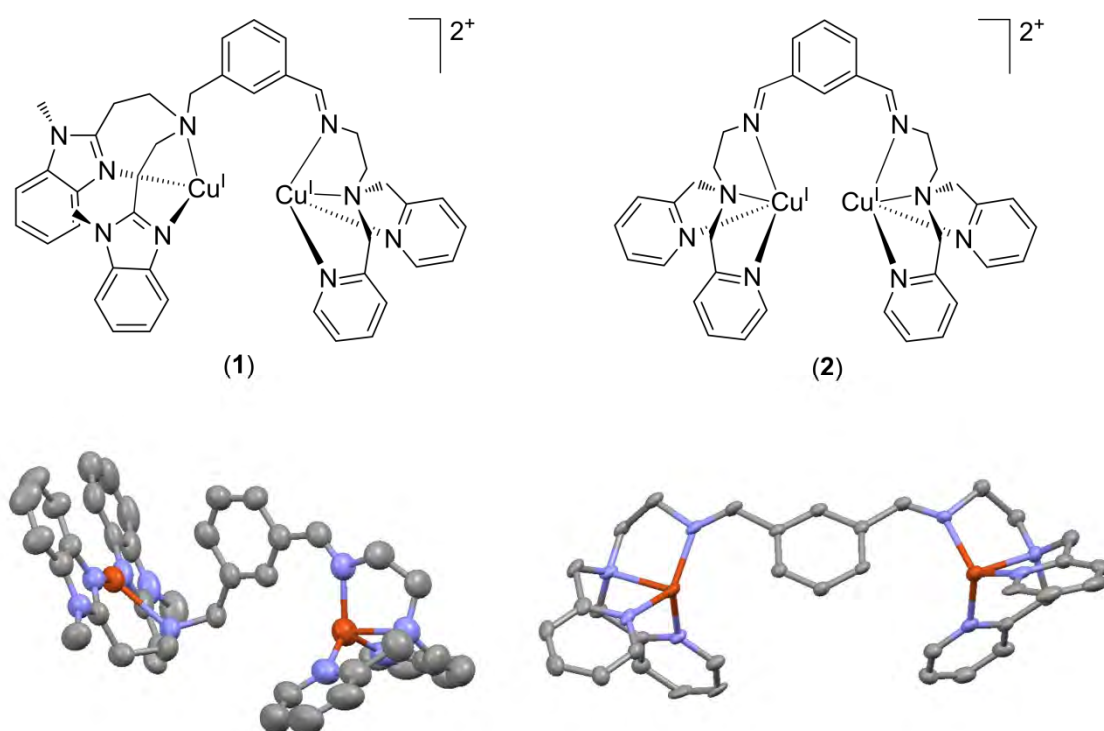


Figure 1. Dinuclear copper complexes (**1**) and (**2**) described in Chapter III.1 and their corresponding crystal structures.

The reaction of the dinuclear complexes (**1**) and (**2**) with O₂ in acetone at -90 °C leads to the formation of two metastable species (**1-O₂**) and (**2-O₂**), respectively. Complex (**1-O₂**) is characterized by UV-VIS, showing an intense visible band at $\lambda_{\text{max}} = 478 \text{ nm}$ ($\epsilon = 7800 \text{ M}^{-1} \text{ cm}^{-1}$), and by rRAMAN spectroscopy, showing two resonance-enhanced peaks at $\nu(\text{O-O}) = 832 \text{ cm}^{-1}$ ($\Delta[^{18}\text{O}_2] = 45 \text{ cm}^{-1}$) and $\nu(\text{Cu-O}) = 520 \text{ cm}^{-1}$ ($\Delta[^{18}\text{O}_2] = 22 \text{ cm}^{-1}$) (Figure 2). Both spectroscopic features are characteristic of a μ - η^1 : η^1 -peroxo dicopper(II) moiety.⁴ Complex (**2-O₂**) is also

characterized by UV-Vis showing two intense characteristic bands $\lambda_{\text{max}} = 500 \text{ nm}$ ($\epsilon = 5000 \text{ M}^{-1} \text{ cm}^{-1}$) and $\lambda_{\text{max}} = 635 \text{ nm}$ ($\epsilon = 3300 \text{ M}^{-1} \text{ cm}^{-1}$). rRaman spectroscopy shows a resonance-enhanced peak at $\nu(\text{O-O}) = 826 \text{ cm}^{-1}$ ($\Delta[^{18}\text{O}_2] = 44 \text{ cm}^{-1}$), which confirms the formulation of (**2-O₂**) as $\mu\text{-}\eta^1\text{:}\eta^1\text{-peroxo dicopper(II)}$ complex. The close related unsymmetric complex reported by Itoh and co-workers has been formulated as a $\mu\text{-}\eta^1\text{:}\eta^2\text{-peroxo dicopper(II)}$ complex (Figure 2).¹² However, we favor the formulation of complex (**1-O₂**) as *trans*-peroxo complex due to both UV-vis and rRaman features, which are in close agreement with complex $[\text{Cu}^{\text{II}}_2(\mu\text{-}\eta^1\text{:}\eta^1\text{-O}_2)(\text{tmpa})]^{2+}$ from which the crystal structure is known as well as other described *trans*-peroxo copper(II) systems.^{4,13}

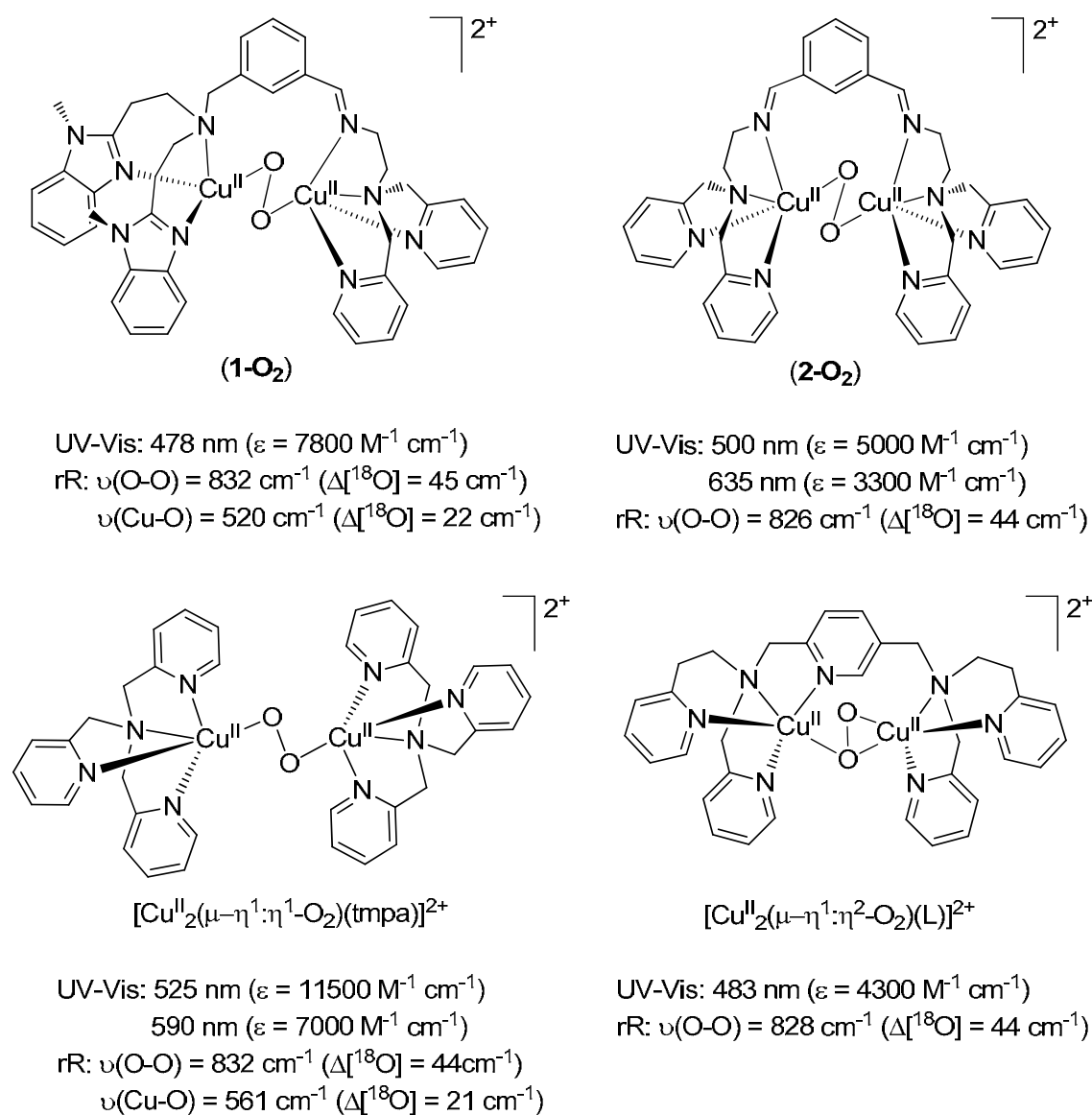
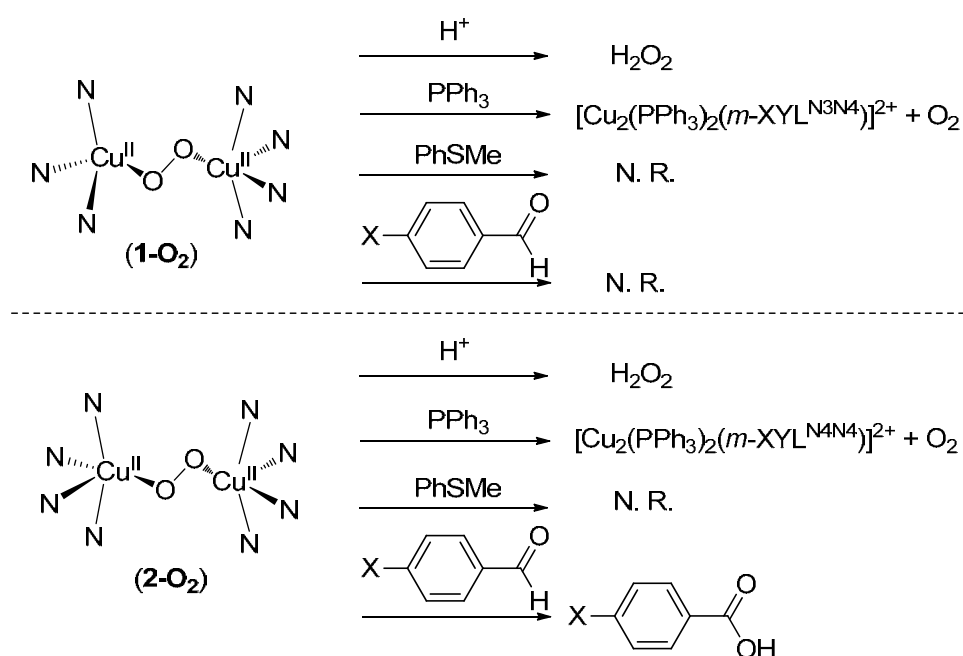


Figure 2. UV-Vis and rRaman features of complexes (**1-O₂**), (**2-O₂**), $[\text{Cu}^{\text{II}}_2(\mu\text{-}\eta^1\text{:}\eta^1\text{-O}_2)(\text{tmpa})]^{2+}$ and Itoh's unsymmetric complex $[\text{Cu}^{\text{II}}_2(\mu\text{-}\eta^1\text{:}\eta^2\text{-O}_2)(\text{L})]^{2+}$.

The reactivity of both complexes is tested using different substrates (Scheme 1). When complexes (**1-O₂**) and (**2-O₂**) react with 2 equiv. of strong acid, 1 equiv. of H₂O₂ is formed. Upon reaction with PPh₃, molecular oxygen is released and Cu^I-PPh₃ complexes are obtained. This reactivity is typical for μ - η^1 : η^1 -peroxo dicopper(II) complex, which has nucleophilic character.⁵ This behavior is also confirmed with the inability of (**1-O₂**) and (**2-O₂**) to perform the oxidation of thioanisole. The first difference in their reactivity is observed in the reaction with benzaldehydes. Complex (**2-O₂**) performs the quantitative oxidation of benzaldehyde to benzoic acid. The study of the reaction using *para*-substituted benzaldehydes is consistent with a nucleophilic attack of the Cu₂:O₂ center to the carbonyl. However, complex (**1-O₂**) was unable to perform the oxidation of benzaldehydes, being also unreactive in the oxo transfer reaction for electrophile substrates.



Scheme 1. Selected reactivity performed by complexes (**1-O₂**) and (**2-O₂**).

Remarkably, the reaction of (**1-O₂**) with *p*-X-phenolates (X = Cl, F, Me, H) causes the rapid transformation to a new species (**3^X**), which decomposes to form the correspondent catechol. On the other hand, reaction of complex (**2-O₂**) with phenolates doesn't conduct to their *ortho*-hydroxylation. Kinetic analysis of the reaction of (**1-O₂**) with *p*-X-phenolates indicates that an electrophilic species attacks the aromatic ring in the rate determining step (*r.d.s.*) (Figure 3). A two-step mechanism is proposed, where in a first step the coordination of the phenolate to the N₃Cu site gives rise to the formation of the intermediate (**3^X**). In the second step, the arene ring is oriented towards the peroxo moiety suffering an electrophilic attack. This is the first example of a Cu^{II}₂- μ - η^1 : η^1 -O₂ complex capable of performing electrophilic arene hydroxylation.

DFT calculations were conducted to elucidate the viability of the *trans*-peroxo copper(II) to perform the *ortho*-hydroxylation of phenolates (Figure 3). First of all, the formulation of (**1-O₂**) as $\mu\text{-}\eta^1\text{:}\eta^1\text{-peroxo}$ dicopper(II) is confirmed because other possible isomers are higher in energy. Secondly, the phenolate coordinates to the N₃Cu center and its binding doesn't cause the isomerization of the Cu₂:O₂ moiety, thus the $\mu\text{-}\eta^1\text{:}\eta^1\text{-peroxo}$ conformation is retained. Finally, DFT calculations showed proximity between the arene ring and one of the oxygens of the peroxide, suggesting a reasonable reaction through a σ^* pathway.¹⁴

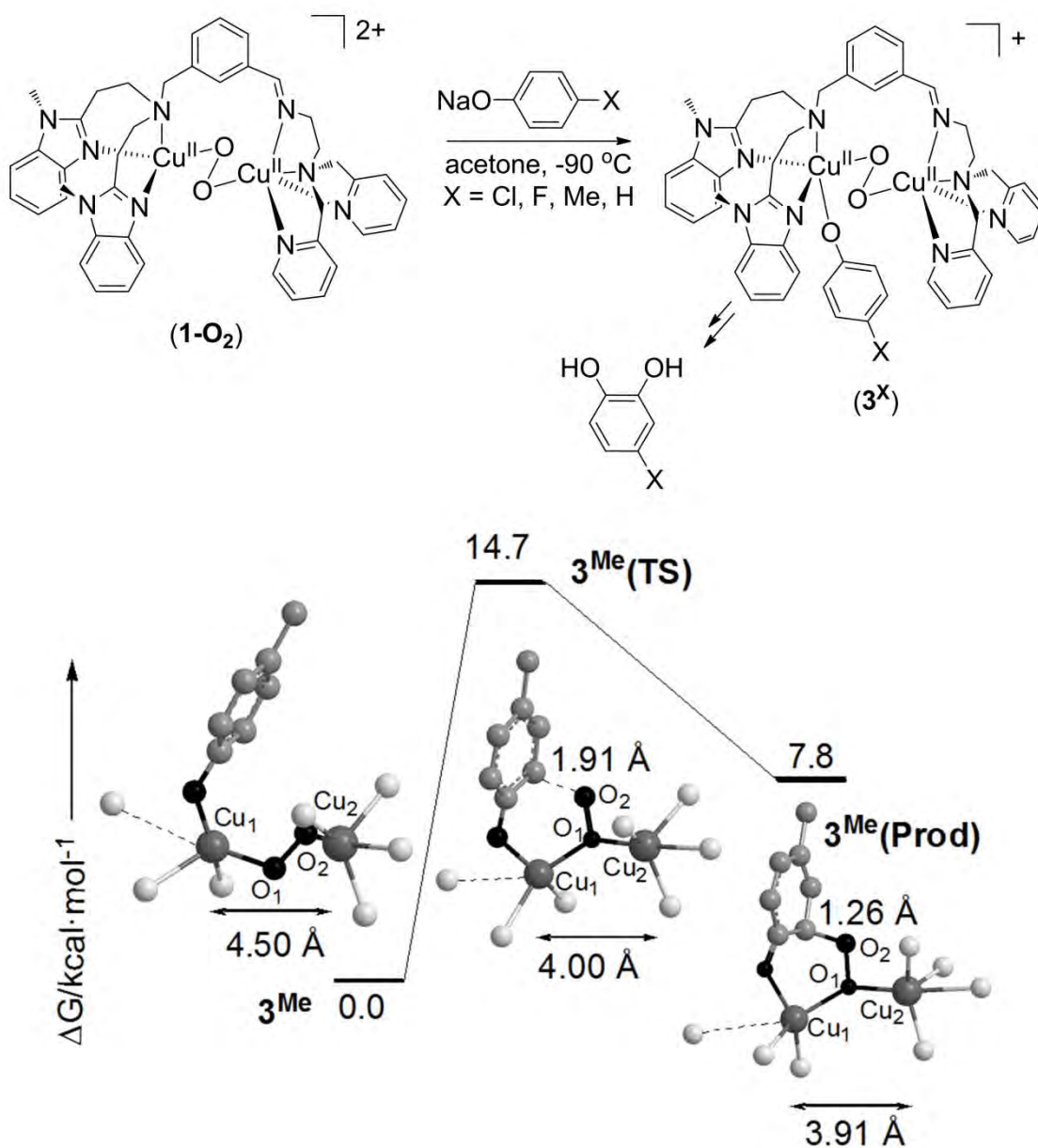


Figure 3. Stationary points along the reaction pathway of the *ortho*-hydroxylation of 4-methylphenolate into 4-methyl-catechol from (**3^{Me}**).

Summarizing, in Chapter III.1 it has been demonstrated that the available coordination site at the tetradentate N_3Cu center of (**1-O₂**) allows the coordination of the phenolic substrate, which is subsequently attacked by the peroxo moiety. Most important, this coordination event triggers the activation of the $Cu_2:O_2$ species, which is found to be unreactive in other electrophilic oxidations. This concept of activation has biological implications because in tyrosinase the coordination of the phenolate is directed by a specific channel to one of the copper centers which prompts the $Cu_2:O_2$ moiety to attack the arene ring.^{15,16} Like in tyrosinase, the asymmetry of the system plays a major role in the behavior of the intermediate species.

Chapter III.2. Electrophilic Arene Hydroxylation and Phenol O-H Oxidations Performed by an Unsymmetric μ - η^1 : η^1 -O₂-Peroxo-Dicopper(II) Complex.

In this chapter, the reactivity of the *trans*-peroxo dicopper(II) complex (**1-O₂**) towards phenolates and phenols is studied in detail.

Extending the mechanistic studies discussed in Chapter III.1, a detailed kinetic analysis of the *ortho*-hydroxylation performed by complex (**1-O₂**) in its reaction against *p*-substituted sodium phenolates is carried out. Firstly, the reaction rates at different phenolate concentrations are calculated ($[(\mathbf{1-O}_2)]=0.1\text{mM}$), observing saturation curves for all the tested substrates (Figure 4). As pointed in Chapter III.1, this behavior is consistent with a two-step mechanistic scenario where a substrate coordination event is previous to the rate determining step (*r.d.s.*). From the saturation curves and applying a Michaelis Menten's analysis, the equilibrium constants $K_{\text{eq(ONa)}}$ and $k_{2(\text{ONa})}$ for all the substrates are calculated. The equilibrium constants values ($K_{\text{eq(ONa)}} = 3000 - 6000 \text{ M}^{-1}$) are in close agreement with other systems capable of performing the *ortho*-hydroxylation of phenolates.⁹ Plotting the $k_{2(\text{ONa})}$ values against the corresponding Hammett constants σ^+ lead to a linear regression with a negative slope ($\rho = -2.7$) (Figure 4). This value is indicative of an electrophilic reaction and surprisingly, it resembles the value for the natural system Tyr ($\rho = -2.4$)¹⁷. Other Tyr-model systems exhibit lower ρ values, as for example Casella's ($\rho = -1.8$)¹⁰ and Itoh's systems ($\rho = -1.8$)⁹.

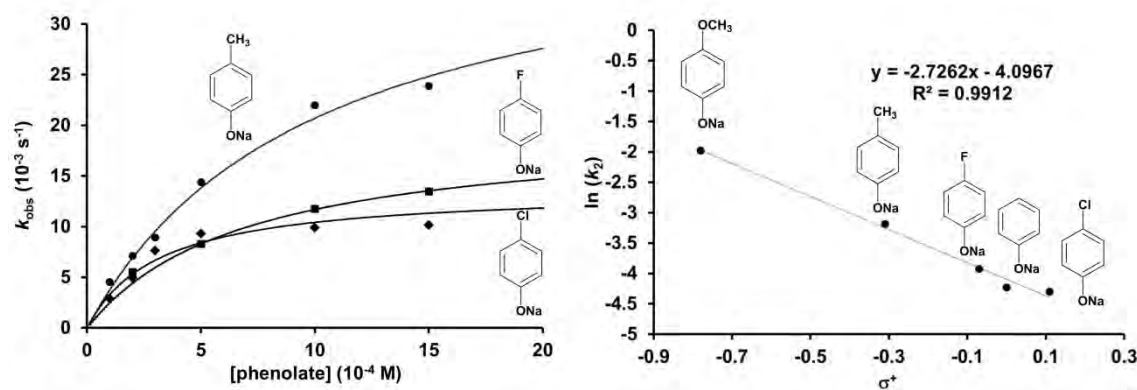


Figure 4. Kinetic experiment for the oxidation of *p*-substituted phenolates. Left: plot of k_{obs} vs $[p\text{-X-phenolate}]$. Right: plot of σ^+ vs $\ln(k_2)$ for the *ortho*-hydroxylation of *p*-X-phenolates.

A temperature dependent kinetic analysis is also carried out. From the saturation curves, the equilibrium constants $K_{\text{eq}(\text{ONa})}$ and $k_{2(\text{ONa})}$ calculated in a wide temperature range (178-203K) allow to build van't Hoff and Eyring plots, respectively (Figure 5). The thermodynamic parameters associated with the pre-equilibrium process are calculated, indicating that the process is enthalpically favored ($\Delta H^0 = -15.2 \pm 0.7 \text{ kJ}\cdot\text{mol}^{-1}$) and entropically disfavored ($\Delta S^0 = -17 \pm 4 \text{ J}\cdot\text{mol}^{-1}\cdot\text{K}^{-1}$), consistent with an associative step. However, the overall energetic contributions make the reaction energetically favorable ($\Delta G^0 = -12 \pm 2 \text{ kJ}\cdot\text{mol}^{-1}$ at 183K). The activation parameters of the *r.d.s.* are also calculated: $\Delta H^\ddagger = 42 \pm 2 \text{ kJ}\cdot\text{mol}^{-1}$, $\Delta S^\ddagger = -45 \pm 11 \text{ J}\cdot\text{mol}^{-1}\cdot\text{K}^{-1}$ and $\Delta G^\ddagger = 50 \pm 4 \text{ kJ}\cdot\text{mol}^{-1}$. These values are in close agreement with other related complexes^{8,11} and with the value obtained by DFT calculations for the *ortho*-hydroxylation of *p*-Me-phenolate by (**1-O₂**) (Chapter III.1).

Finally, the kinetic isotopic effect is determined by using sodium phenolate- d_5 . The saturation curve obtained (Figure 6) allows again to calculate the equilibrium constant $K_{\text{eq}(\text{ONa})}$ and $k_{2(\text{ONa})}$. The direct comparison with the values obtained for the non-deuterated substrate shows that the equilibrium is not altered by substrate deuteration ($K_{\text{eq}(\text{ONa})(\text{H})}/K_{\text{eq}(\text{ONa})(\text{D})} = 0.99$), and that an inverse isotopic effect is observed for the phenolate oxidation ($k_{2(\text{ONa})(\text{H})}/k_{2(\text{ONa})(\text{D})} = 0.88$), being consistent with a sp^2 to sp^3 isomerization.

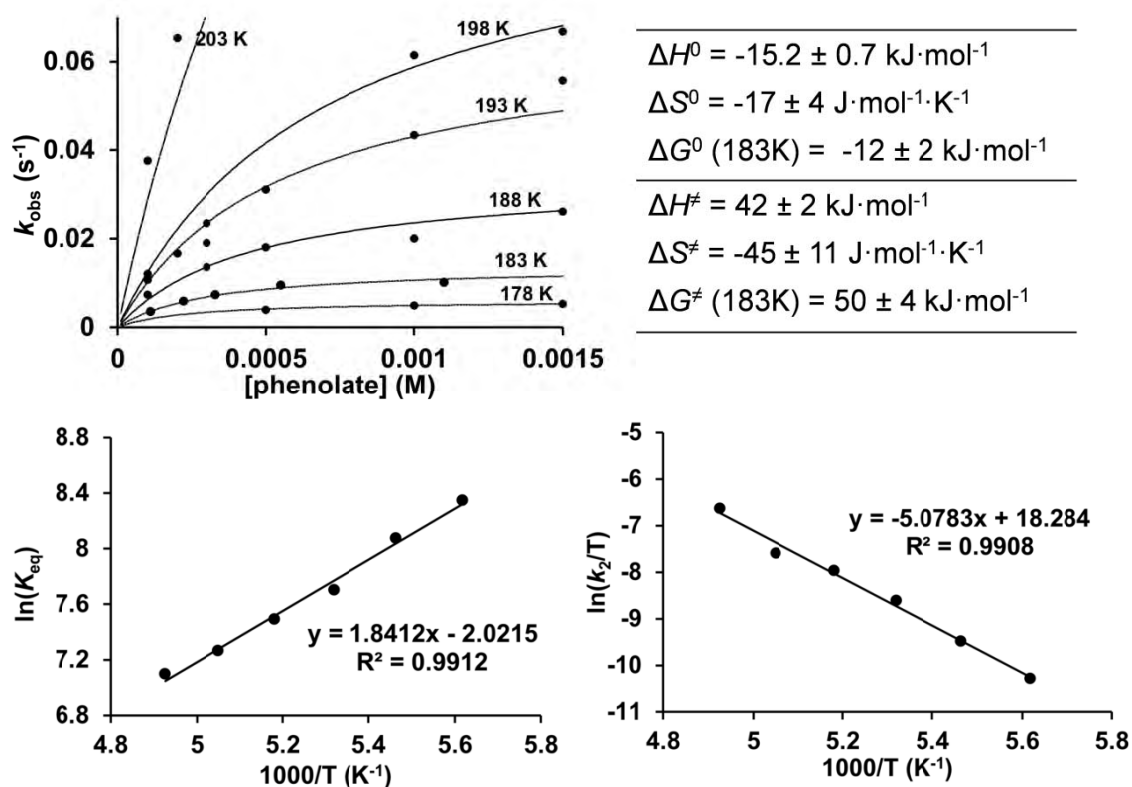


Figure 5. Temperature dependent kinetic experiments for the *ortho*-hydroxylation of sodium phenolates performed by (**1-O₂**). Top left: plot of k_{obs} vs [phenolate] at different temperatures. Top right: thermodynamic and activation parameters for the *ortho*-hydroxylation of sodium phenolate by complex (**1-O₂**). Van't Hoff (bottom left) and Eyring plots (bottom right) for the *ortho*-hydroxylation of sodium phenolate.

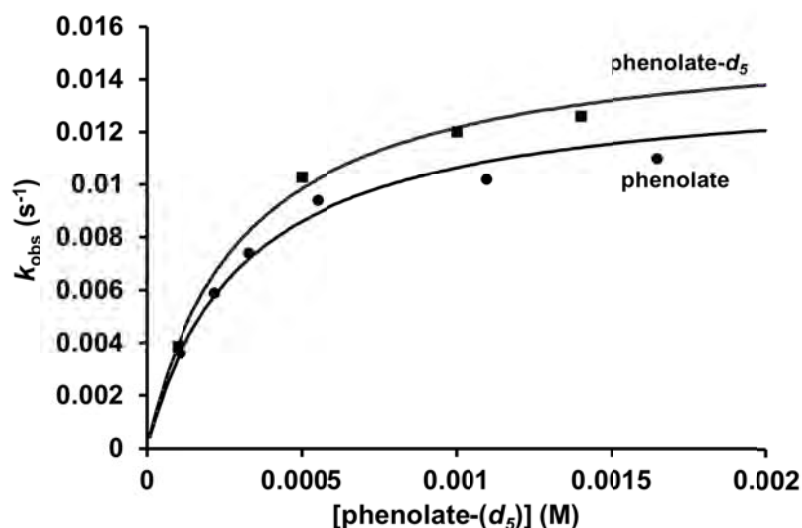
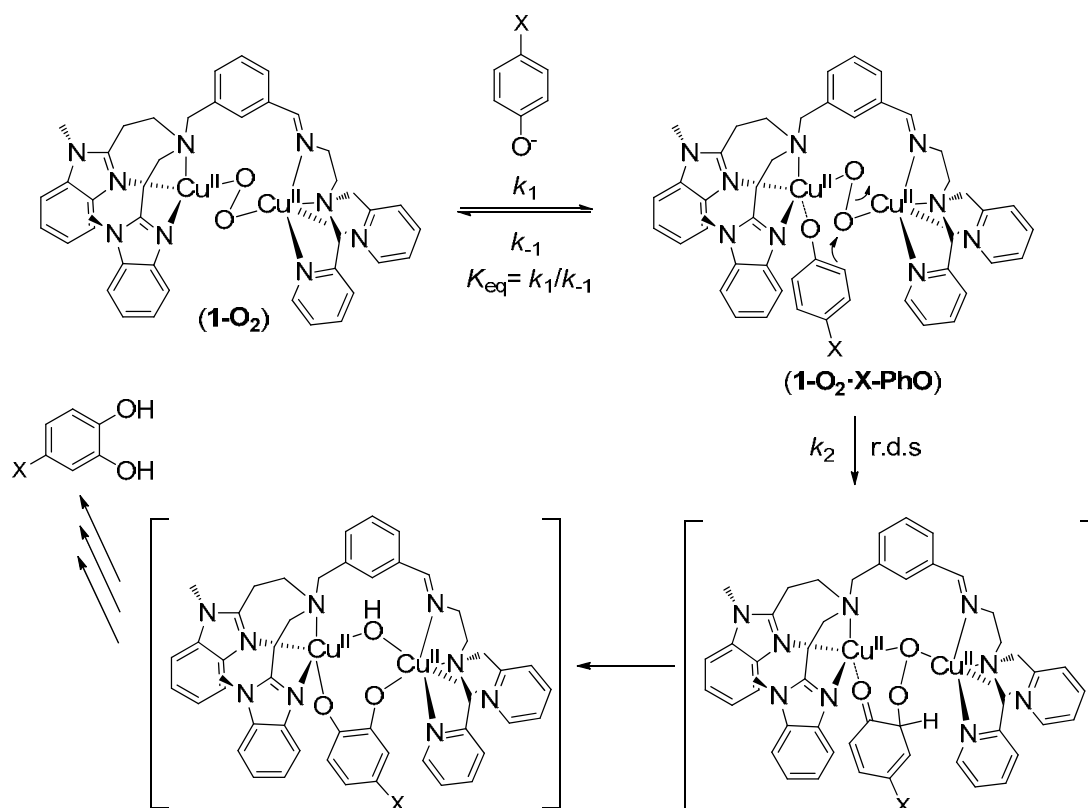


Figure 6. Kinetic experiments for the determination of the kinetic isotopic effect on the oxidation of sodium phenolate(d_5) by complex (**1-O₂**).

All these detailed studies allow us to build a mechanistic scenario where a reversible phenolate coordination event is followed by an electrophilic attack of the *trans*-peroxo moiety to the aromatic ring (Scheme 2).



Scheme 2. Mechanism proposed for the *ortho*-hydroxylation of sodium phenolates performed by **(1-O₂)**.

A detailed mechanistic study of the oxidation of phenols by **(1-O₂)** is also carried out in Chapter III.2. The reaction of the *trans*-peroxo complex **(1-O₂)** towards phenols leads to the formation of C-C coupling oxidation products in 25-50% yields. The products obtained and the yields indicate that **(1-O₂)** acts as a $1e^-$ oxidant, forming phenoxyl radicals that then evolve to form the final C-C coupling products. The reactions are followed by UV-Vis at -90°C and a bathochromic shift of the UV-Vis features of the *trans*-peroxo complex is observed. This shift is dependent of the phenol used, indicating that the UV-Vis band corresponds to an interaction between the **(1-O₂)** and the phenol (Figure 7).

A kinetic analysis of the oxidation of *p*-substituted phenols performed by **(1-O₂)** is carried out at -90°C . The reaction rates (k_{obs}) at different phenol concentrations are calculated and saturation curves are observed for all the phenols studied. Like in the case of phenolates, this kinetic behavior is consistent with a coordination pre-equilibrium step before the *r.d.s.*

Applying a Michaelis-Menten analysis, the equilibrium constants $K_{\text{eq(OH)}}$ and the $k_{2(\text{OH})}$ are calculated. The equilibrium constants show little influence on the substituent of the phenol. On the other hand, $k_{2(\text{OH})}$ increases as the $1e^-$ redox potential ($E^{\text{O}_{\text{ox}}}$) of the phenols decreases. A linear plot of the $(RT/F)\ln(k_{2(\text{OH})})$ vs. the $E^{\text{O}_{\text{ox}}}$ lead to a slope of -0.49. (Figure 7).

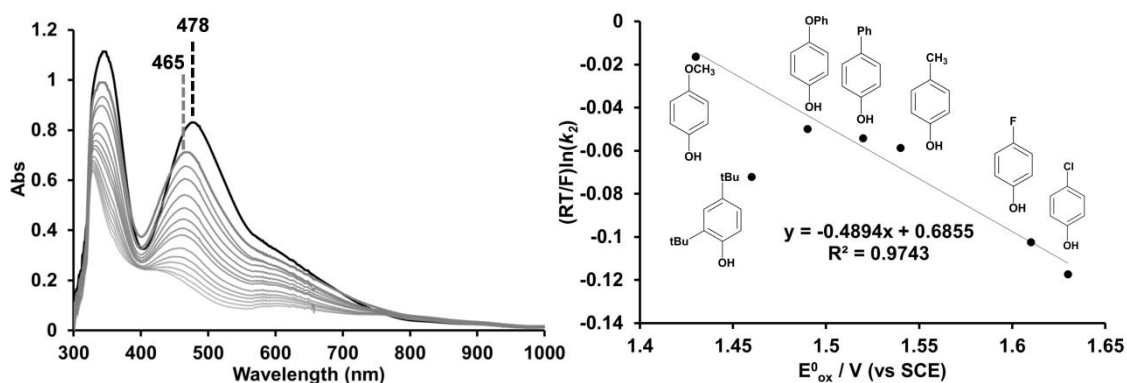


Figure 7. Left: UV-vis traces of the reaction between (1-O₂) and 4-Me-phenol. Right: plot of $(RT/F)\ln(k_{2(\text{OH})})$ vs the $1e^-$ oxidation potentials ($E^{\text{O}_{\text{ox}}}$) of selected phenols.

A temperature dependent kinetic analysis is also described from which the thermodynamic and activation parameters can be calculated (Figure 8). The variation on the equilibrium constants ($K_{\text{eq(OH)}}$) in a wide temperature range (183-203K) allows to build a van't Hoff plot from which the thermodynamic parameters $\Delta H^{\text{O}} = -8.9 \pm 0.7 \text{ kJ}\cdot\text{mol}^{-1}$ and $\Delta S^{\text{O}} = -26 \pm 4 \text{ J}\cdot\text{mol}^{-1}\cdot\text{K}^{-1}$ are obtained. The $\Delta G^{\text{O}} = -4.1 \pm 1 \text{ kJ}\cdot\text{mol}^{-1}$ calculated at 183K indicates that a small energetic gain is observed with the coordination of the phenol, reflecting the low binding constants observed ($K_{\text{eq(OH)}} \approx 10 \text{ M}^{-1}$). The activation parameters are obtained from the Eyring plot: $\Delta H^{\ddagger} = 52 \pm 10 \text{ kJ}\cdot\text{mol}^{-1}$ and $\Delta S^{\ddagger} = -15 \pm 6 \text{ J}\cdot\text{mol}^{-1}\cdot\text{K}^{-1}$. The negative ΔS^{\ddagger} is indicative of a more ordered transition state.

Finally, a primary isotopic effect for *the r.d.s.* is observed ($k_{2(\text{OH})}/k_{2(\text{OD})} = 1.53 - 2.00$) (Figure 9). These small values are close to those obtained by Itoh and co-workers for the proton-coupled electron transfer (PCET) for the oxidation of phenols by a dicopper(II) side-on peroxo complex and a dicopper(III) bis(μ -oxo) complex.¹⁸

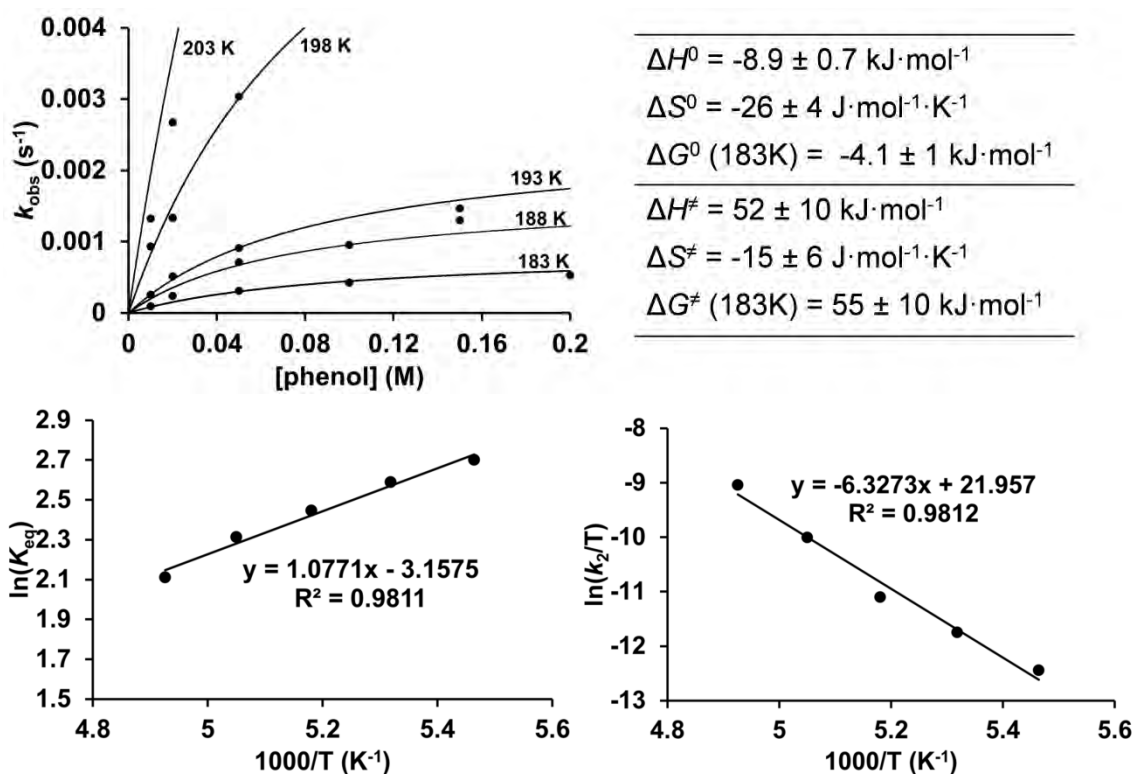


Figure 8. Temperature dependent kinetic experiments for the oxidation of phenol performed by complex (**1-O₂**). Top left: plot of k_{obs} vs [phenol] at different temperatures. Top right: thermodynamic and activation parameters for the phenol oxidation by complex (**1-O₂**). Van't Hoff (bottom left) and Eyring plots (bottom right) for oxidation of phenol.

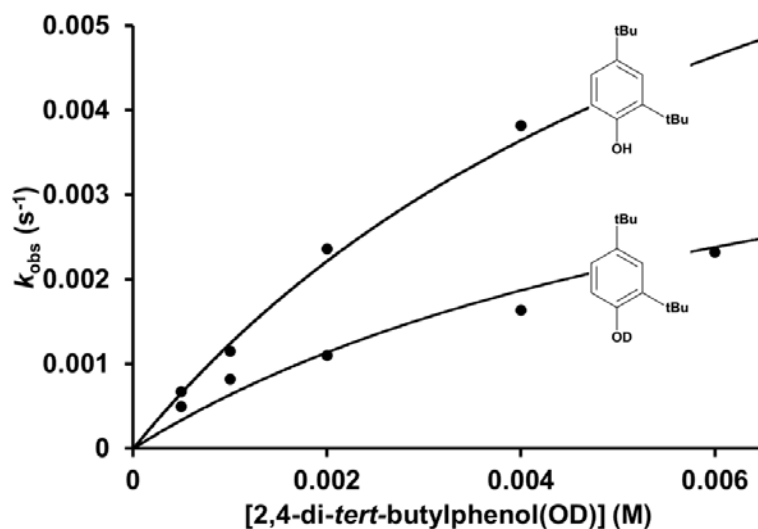
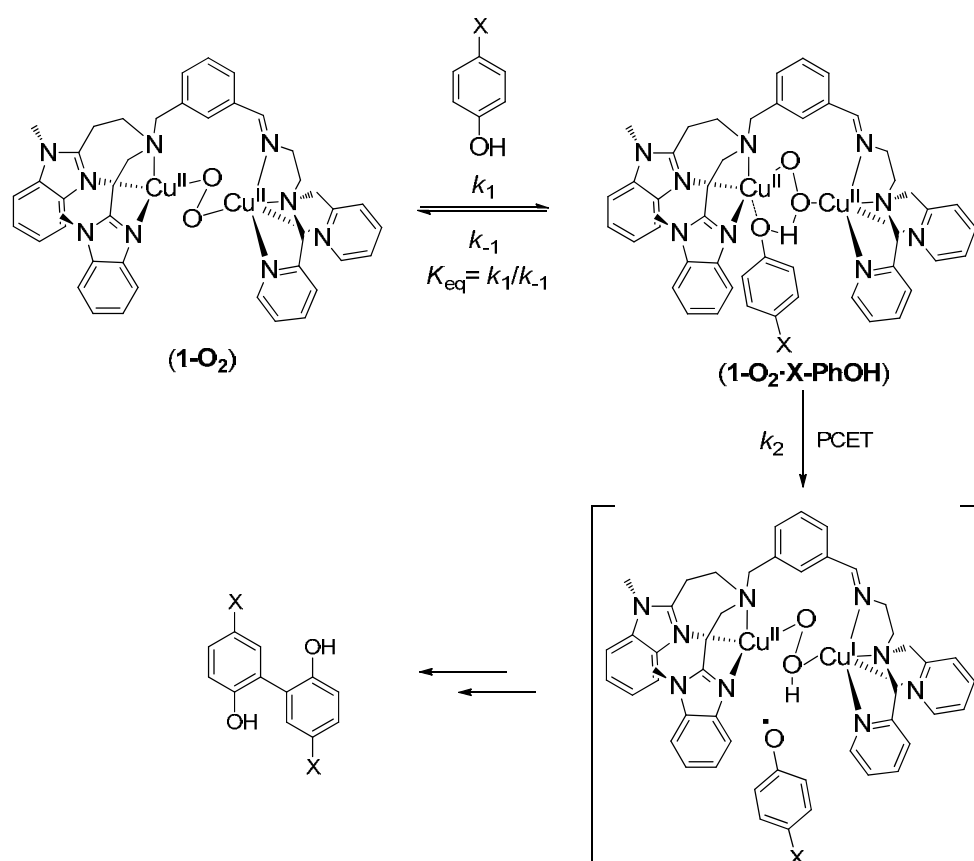


Figure 9. Kinetic experiments for the determination of the kinetic isotopic effect on the oxidation of 2,4-di-*tert*-butylphenol(d_1) by complex (**1-O₂**).

All the experimental data lead to draw a mechanistic scenario where a first reversible kinetic step involving phenol binding to the *trans*-peroxo complex (**1-O₂**) is proposed, followed by the 1e⁻ oxidation of the phenol to form the corresponding phenoxyl radical. Applying the Marcus formalism, the linear correlation obtained when plotting $(RT/F)\ln(k_{2(\text{OH})})$ vs. the redox potential of the phenols (slope = -0.49) is indicative of a proton-coupled electron transfer (PCET) during the *r.d.s.* (provided the reorganization barrier (λ) is larger than the driving force of the reaction (ΔG^0))¹⁹. So, the more reasonable mechanism proposed for the *r.d.s.* is a PCET, which is also in agreement with the K.I.E values obtained.²⁰⁻²²



Scheme 3. Mechanism proposed for oxidation of phenols performed by complex (**1-O₂**).

The reactivity shown by the *trans*-peroxo complex (**1-O₂**) towards phenolates and phenols has implications in the activity of the natural system Tyr. Despite the mechanistic details of the tyrosinase (Tyr) activity have been widely studied, some questions still arise from its unique reactivity:

i) **Substrate binding:** the first catalytic step in the oxidation of phenols performed by Tyr is the coordination of the phenol to one of the copper centers. Although it is known that the phenol is coordinated in its phenolate form, it is not clear which is the pathway of deprotonation of the

phenol. Although Tyr and complex (**1-O₂**) have a different Cu₂:O₂ core (side-on vs. *trans*-peroxo), complex (**1-O₂**) is able to coordinate both phenolates and phenols to one of the copper centers. It has been demonstrated that the ability to coordinate the substrate is related with the asymmetry of the complex: while the symmetric N₄Cu(II)-O₂-Cu(II)N₄ complex (**2-O₂**) is not able to carry out the oxidation of phenolates nor phenols, the presence of an available coordination site in the N₃Cu(II) center of (**1-O₂**) permits the binding of the substrate. Complex (**1-O₂**) binds more strongly phenolates than phenol ($\Delta\Delta G^0(183K) = \Delta G^0(\text{phenolate}) - \Delta G^0(\text{phenol}) = -8 \text{ kJ}\cdot\text{mol}^{-1}$) due to their anionic character. The kinetic analysis also shows a higher organization for the phenol binding ($\Delta\Delta S^0 = \Delta S^0(\text{phenolate}) - \Delta S^0(\text{phenol}) = -9 \text{ J}\cdot\text{mol}^{-1}\cdot\text{K}^{-1}$) which can be understood as a hydrogen bonding interaction between the phenol O-H bond and the peroxide oxygen atoms (Scheme 4). So, the binding process is dictating the reactivity toward phenols (O-H oxidation) and phenolates (arene oxidation), showing a reactivity without precedents for *trans*-peroxo Cu(II) complexes.

ii) **Phenolate *ortho*-hydroxylation vs. phenol (1H⁺/1e⁻) oxidation:** once the phenolate is coordinated to one of the copper centers of Tyr, a rotation of the Cu₂:O₂ core occurs in order to orientate the peroxide to the arene π orbitals, triggering the electrophilic attack. It has been shown that complex (**1-O₂**) is able to *ortho*-hydroxylate phenolates via electrophilic attack to the aromatic ring, orientating the arene ring toward the peroxo moiety of complex (**1-O₂**). A Hammett's plot analysis provides a ρ value of -2.7, in close agreement with the natural system ($\rho = -2.4$). On the other hand, complex (**1-O₂**) oxidizes phenols via PCET to form phenoxy radicals. This 1H⁺/1e⁻ process is one of the most common reactions in biological systems. So, the presence or absence of the proton plays a decisive role in the reaction pathways: the presence of the phenolate (absence of proton) triggers the rotation of the Cu₂:O₂ core avoiding the electron transfer which could generate a phenoxy radical, due to the higher oxidation state of phenolates. On the other hand, the presence of the proton in the coordination of the substrate as phenol directs the reaction towards the PCET pathway, possibly due to the hydrogen bonding of the phenol with the peroxide oxygen atoms, which disables the rotation of the Cu₂:O₂ core to attack electrophilically the arene.

Substrate	ΔH^\ddagger kJ·mol ⁻¹	ΔS^\ddagger J·mol ⁻¹ ·K ⁻¹	ΔG^\ddagger kJ·mol ⁻¹	ΔH^\ddagger kJ·mol ⁻¹	ΔS^\ddagger J·mol ⁻¹ ·K ⁻¹	ΔG^\ddagger J·mol ⁻¹
Phenolate	-15.2 ± 0.7	-17 ± 4	-12 ± 2	42 ± 2	-45 ± 11	50 ± 4
Phenol	-8.9 ± 0.7	-26 ± 4	-4.1 ± 1	52 ± 10	-15 ± 6	55 ± 10

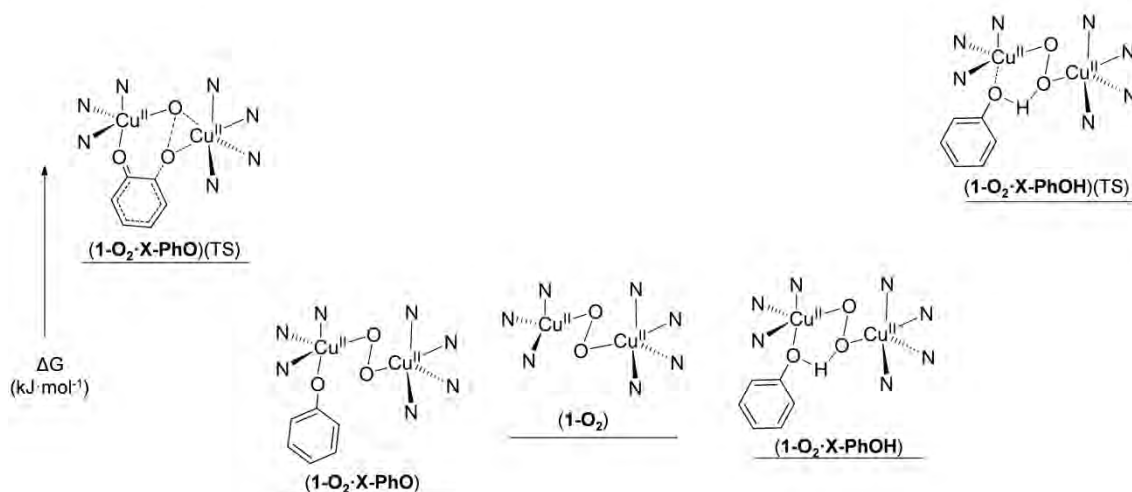


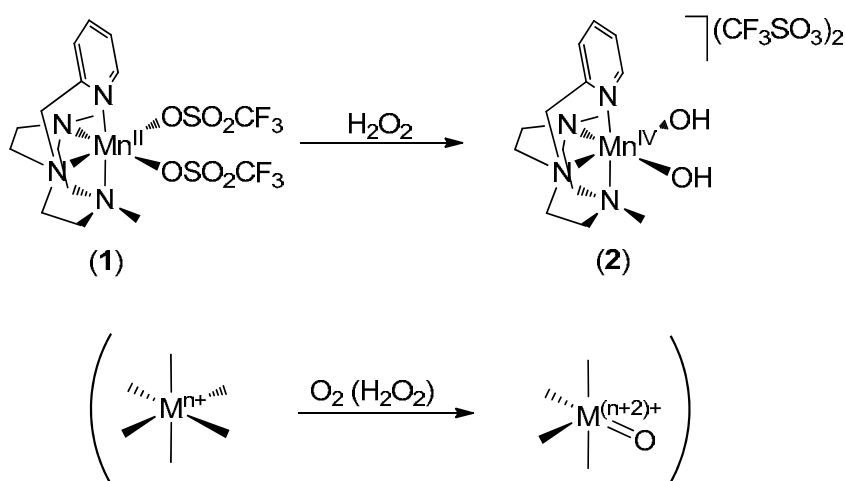
Figure 10. Comparison of the thermodynamic and activation parameters for the oxidation of phenols and phenolates by complex (1-O_2) and proposed reaction intermediates and transition states for both reactions (TS are taken from theoretical calculations for the *ortho*-hydroxylation of sodium phenolates and it is pure estimative for the oxidation of phenols).

Chapter IV. Non-Porphyrinic Manganese(IV) Complexes in C-H Hydrogen Atom Transfer Reactions

The oxidation of C-H bonds occurs in natural systems very efficiently using molecular oxygen as oxidant. These green processes (only water is obtained as residue) are catalyzed by metalloenzymes bearing one or more metals in the active site. It has been demonstrated that these metals use oxygen to reach high oxidation states, which are the responsible for the C-H activation, like in the paradigmatic cytochrome P450.^{23,24} It has also been observed that other non-heme systems like Rieske dioxygenases proceeds in an analog way, generating a putative Fe(V)(O) species that attacks the C-H bond.²⁵ For their relevance, several model systems centered in high-valence iron species have been developed to reproduce the oxidation of C-H bonds.²⁶⁻²⁹ Despite manganese is found in the active site of oxidative enzymes,³⁰⁻³² oxidation mechanisms mediated by manganese ions, especially in C-H oxidations remain poorly explored.

Chapter IV.1. Evidence for a Precursor Complex in C-H Hydrogen Atom Transfer Reactions Mediated by a Manganese(IV) Oxo Complex

Several oxidations found in natural or industrial processes involve one or more concerted proton-coupled electron transfer (PCET) in their reaction steps.²¹ A specific case of PCET is the hydrogen atom transfer (HAT), where the proton and the electron are transferred in a single kinetic step. This particular reaction has been observed in different natural processes such the oxidation of C-H bonds by compound I of cytochrome P450³³ or Rieske Dioxygenases²⁵. These HAT have been also observed in the model compounds which contain a high valent iron moiety in their structure.^{27,34} In Chapter IV.1., we describe the synthesis and characterization of two novel manganese(IV) complexes, which contain oxo and hydroxo moieties in their structure. Complex $[\text{Mn}^{\text{IV}}(\text{OH})_2(\text{}^{\text{H,Me}}\text{PyTACN})](\text{CF}_3\text{SO}_3)_2$ (**2**) is synthesized by the reaction of complex $[\text{Mn}^{\text{II}}(\text{}^{\text{H,Me}}\text{PyTACN})](\text{CF}_3\text{SO}_3)_2$ (**1**) with 10 equiv. of H_2O_2 (Scheme 4). This process can be understood as activation of H_2O_2 to generate a high valent species, the same strategy used by metalloenzymes.



Scheme 4. Synthesis of the high-valent manganese(IV) species and its analogy with the generation of high-valent metal species found in living systems.

X-Ray analysis of complex (**2**) confirms the $\text{Mn}^{\text{IV}}(\text{OH})_2$ moiety, which is protected against dimerization by the N-methyl groups and the pyridine. This is a rare example of Mn^{IV} complex with only one precedent reported by Busch and co-workers.³⁵ Curiously, complex (**2**) can be deprotonated using one equivalent of ${}^t\text{BuOK}$ to generate the manganese-oxo complex $[\text{Mn}^{\text{IV}}(\text{O})(\text{OH})(\text{}^{\text{H,Me}}\text{PyTACN})](\text{CF}_3\text{SO}_3)$ (**3**). Both manganese(IV) complexes were characterized using different spectroscopic methods such as UV-Vis, EPR and Raman spectroscopy (Figure 11).

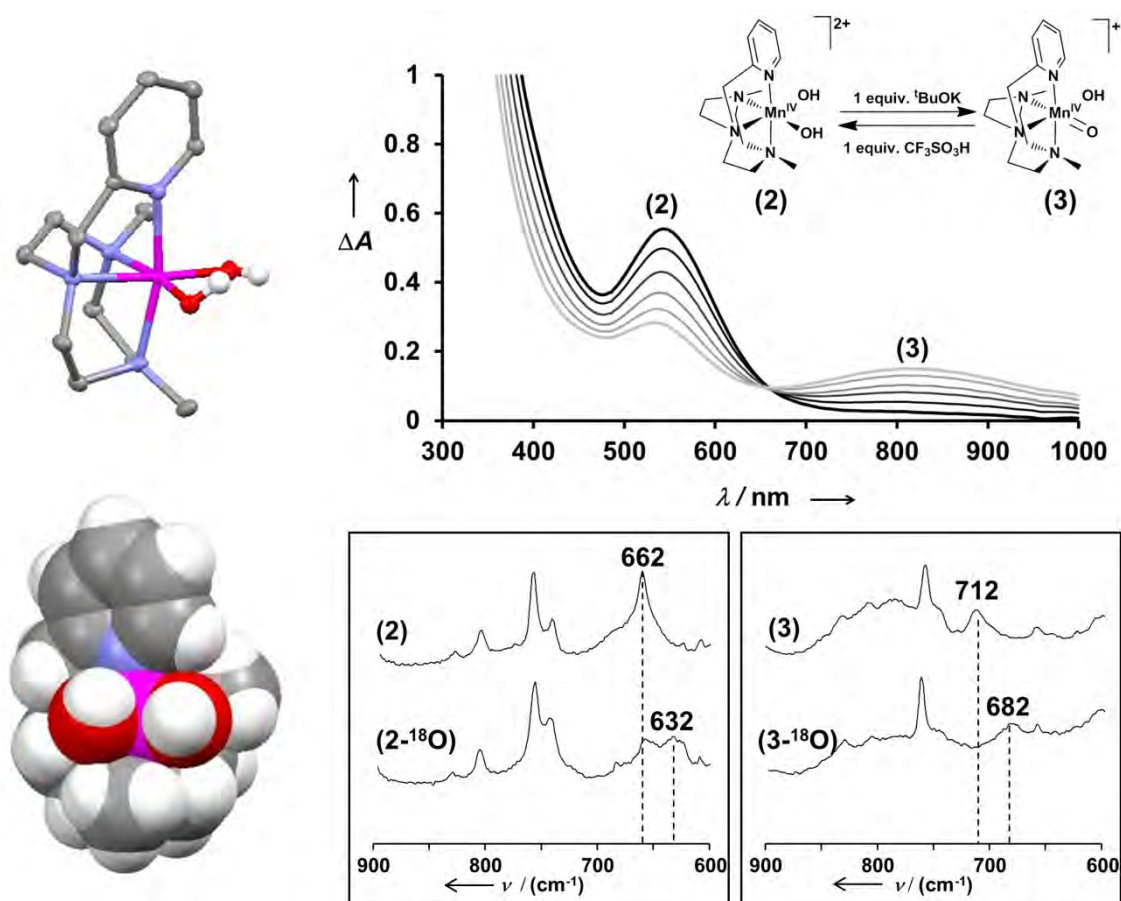


Figure 11. X-Ray characterization of complex (2) (left), UV-Vis characterization of the reaction to generate complex (3) (right, top) and Raman characterization of complexes (2) and (3).

In order to evaluate the ability of the manganese(IV) species in the oxidation of C-H bonds, the bond dissociation energy of the correspondent manganese(III) species is calculated by cyclic voltamperometry and acid/base titrations using the method widely developed by Mayer and coworkers (Figure 12).^{36,37} From the pK_a values and the redox potentials we are able to approximate a value of 83.4 kcal/mol for the O-H bond dissociation energy in complex (3-H).

The performance of complexes (2) and (3) in the HAT is evaluated for substrates with low C-H BDE such as xanthene (75.5 kcal/mol), 1,4-cyclohexadiene (77 kcal/mol), 9,10-dihydroanthracene (DHA, 78 kcal/mol) and fluorene (80 kcal/mol)^{38,39}. The product quantification supports that manganese(IV) species act as $1e^-$ oxidants, abstracting H \cdot to generate the carbon centered radical. The oxidation state of manganese is also determined by iodometric titration pointing to final manganese(III) complexes.

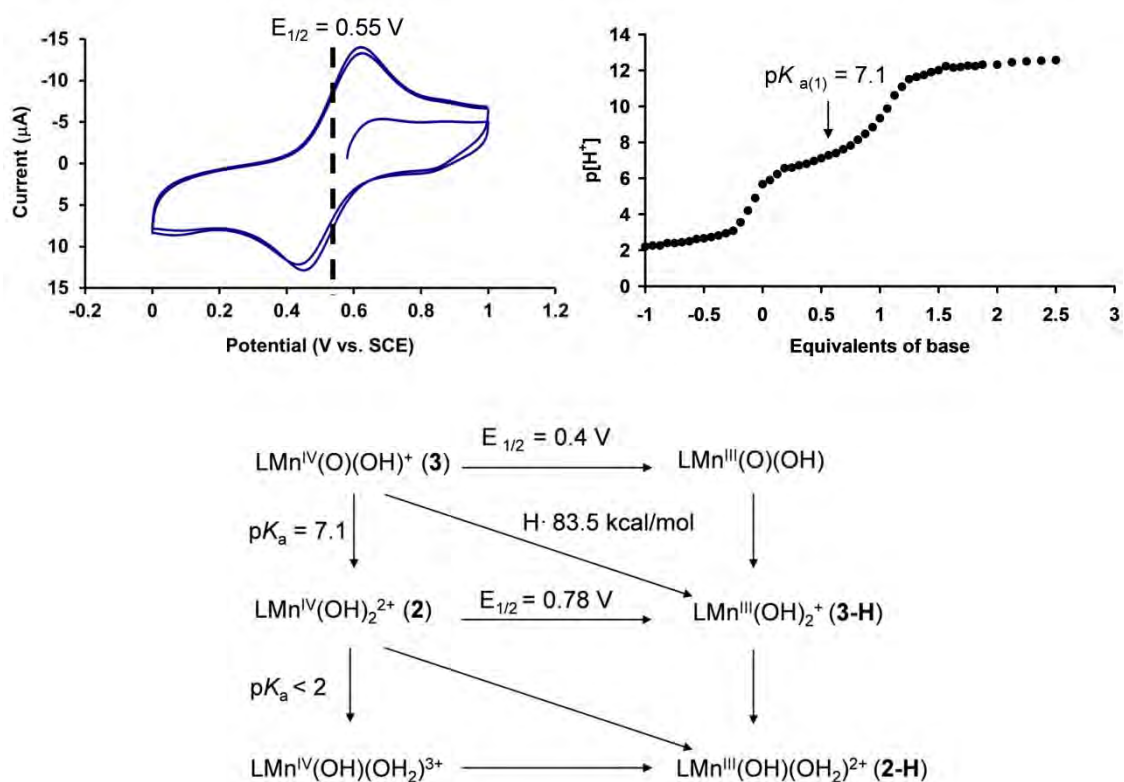


Figure 12. Top: cyclic voltamperometry for the reduction/oxidation of complex (2) (left), and titration for the deprotonation of complex (2) to generate complex (3) (right). Bottom: calculation of the thermodynamic parameters for the bond dissociation energy of complex (3-H).

Kinetic experiments are run to elucidate mechanistic details following the reaction towards C-H substrates by the UV-Vis decay of complexes (2) and (3) at $\lambda = 545$ nm and $\lambda = 825$ nm, respectively. Complex (2) reacts with substrates containing weak C-H bonds by a bi-molecular process with reaction rates that are first-order dependent on both complex and substrate concentrations (Figure 13). The second-order rate constants obtained ($k_2^{(OH)}$) are plotted against the BDE_{C-H} of each substrate from which results a linear plot, consisting of a hydrogen atom transfer during the rate determining step (*r.d.s.*). This hypothesis is further confirmed calculating the kinetic isotopic effect (KIE) for xanthene/xanthene- d_2 (6.6) and DHA/DHA- d_4 (8.0). These large values are also in agreement with a HAT process from the C-H bond to the manganese(IV) moiety.

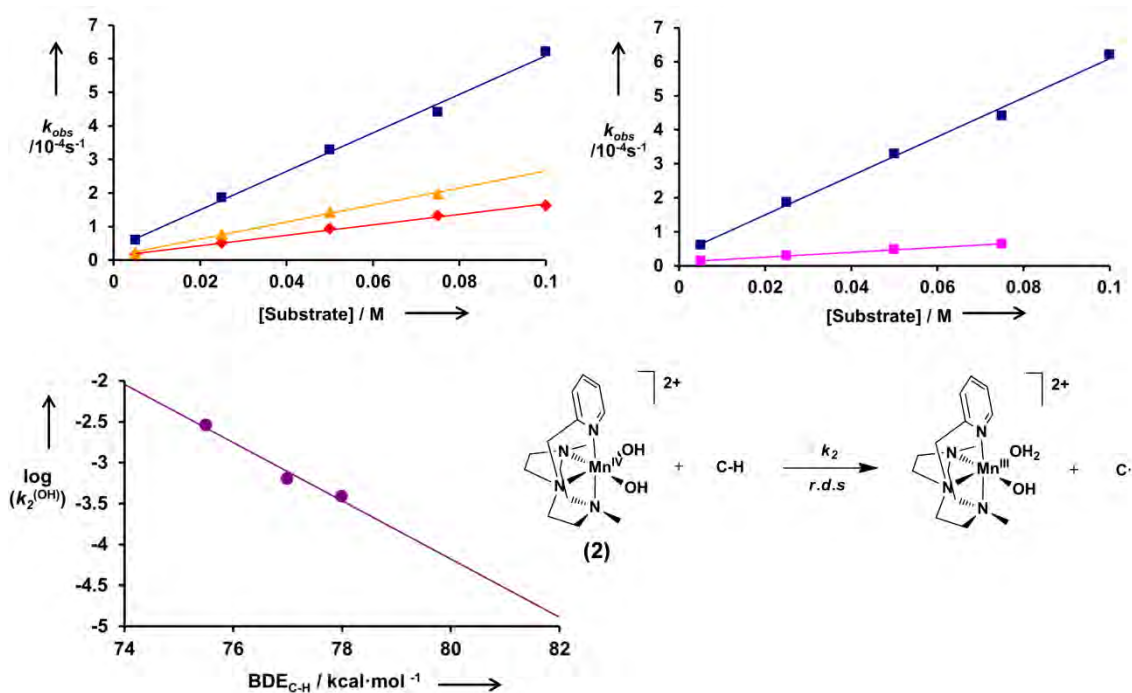


Figure 13. Kinetic experiments for the C-H oxidation performed by complex (2). Top left: plot of k_{obs} vs [substrate] for the reaction of complex (2) and xanthene (blue), 1,4-cyclohexadiene (yellow) and 9,10-dihydroanthracene (red). Top right: plot of k_{obs} vs [substrate] for the reaction of complex (2) and xanthene (blue) and xanthene- d_2 (pink). Bottom left: plot of $\log(k_2^{(OH)})$ vs BDE_{C-H} for the reaction between complex (2) and substrates with weak C-H bonds. Bottom right: proposed mechanism for the oxidation of C-H bonds performed by complex (2).

In contrast, complex (3) has a different behavior in its reaction with C-H bonds. Saturation plots are obtained when the concentration of substrate is increased (Figure 14). This scenario is typical of a fast equilibrium kinetic step before the *r.d.s.* The data obtained can be fitted by the equation $k_{obs} = k_2^{(0)} K_{eq} [\text{substrate}] / (1 + K_{eq} [\text{substrate}])$, which allows the calculation of the equilibrium constant K_{eq} and the first-order constant of the *r.d.s.*, $k_2^{(0)}$. Interestingly, the K_{eq} and $k_2^{(0)}$ values are dependent on the substrate, which involves the substrate in both kinetic steps. Moreover, while $k_2^{(0)}$ has a linear dependence on the BDE_{C-H} energies, the K_{eq} does not follow the same trend, supporting the C-H cleavage occurs during the second reaction step. Moreover, K_{eq} has no correlation with the pK_a and redox potential of the substrates, excluding a pre-equilibrium in which a proton or an electron transfer occur. On the basis of the kinetic analysis and the UV-Vis experiments, where a shift in the visible spectral features occurs ($\Delta\lambda < 4\text{nm}$), we propose the formation of an intermediate species (I) resulting from the weak non-covalent interaction between substrate and manganese(IV)-oxo complex. Kinetic isotopic effect experiments are carried out and we observe that K_{eq} is little affected by deuteration

(K.I.E = 1.1 and 1.2 for xantene(d_2) and DHA(d_4), respectively) but a primary kinetic isotopic effect is obtained for $k_2^{(0)}$, suggesting again that the C-H cleavage occurs in the rate determining step.

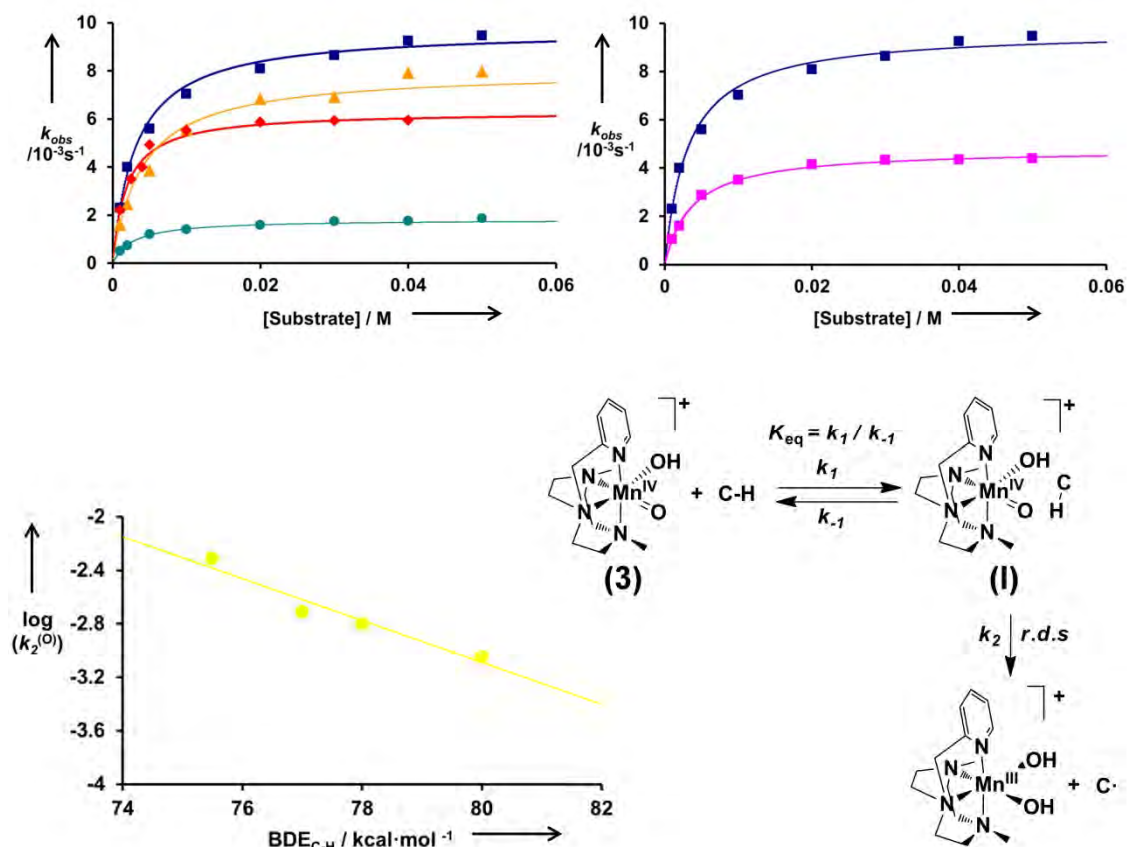


Figure 14. Kinetic experiments for the C-H oxidation performed by complex (3). Top left: plot of k_{obs} vs [substrate] for the reaction of complex (3) and xantene (blue), 1,4-cyclohexadiene (yellow), 9,10-dihydroanthracene (red) and fluorene (green). Top right: plot of k_{obs} vs [substrate] for the reaction of complex (3) and xantene (blue) and xantene- d_2 (pink). Bottom left: plot of $\log(k_2^{(0)})$ vs BDE_{C-H} for the reaction between complex (3) and substrates with weak C-H bonds. Bottom right: proposed mechanism for the oxidation of C-H bonds performed by complex (3).

Temperature dependent experiments are performed for the oxidation of DHA by complexes (2) and (3). Firstly, from a van't Hoff plot the thermodynamic parameters for the conversion from complex (3) to the intermediate (I) are calculated (Figure 15). Not surprisingly, the reaction is exothermic ($\Delta G^0 = -3.7 \pm 0.2$ kcal/mol, 298 K) and enthalpically driven ($\Delta H^0 = -3.6 \pm 0.2$ kcal/mol). Although a low entropic value for an associative process is obtained ($\Delta S^0 = -3.6 \pm 0.2$ cal/K·mol), it could be due to a desolvation process during the association event. Secondly, Eyring plots provide the activation parameters for the C-H cleavage during the rate-

determining step for both complexes (2) and intermediate (I). From the activation parameters calculated for complex (2) ($\Delta H^\ddagger = 6.6 \pm 0.1$ kcal/mol and $\Delta S^\ddagger = -51.9 \pm 0.3$ cal/K·mol) and complex (3) ($\Delta H^\ddagger = 10.3 \pm 0.7$ kcal/mol and $\Delta S^\ddagger = -37 \pm 2$ cal/K·mol), two main observations can be made: the difference in the ΔH^\ddagger reflects the difference in the manganese(III) species resulting from the abstraction of the hydrogen atom (complexes (2-H) and (3-H)); the ΔS^\ddagger values are consistent of a bimolecular encounter for complex (2) and a more organized transition state in the hydrogen atom abstraction in complex (3).

Complex	ΔH kcal·mol ⁻¹	ΔS cal·mol ⁻¹ ·K ⁻¹	ΔG kcal·mol ⁻¹	ΔH^\ddagger kcal·mol ⁻¹	ΔS^\ddagger cal·mol ⁻¹ ·K ⁻¹	ΔG^\ddagger kcal·mol ⁻¹
(2)	-	-	-	6.6 ± 0.1	-51.9 ± 0.4	22.1 ± 0.1
(3)	-3.6 ± 0.2	0.2 ± 0.4	-3.7 ± 0.2	10.3 ± 0.7	-37 ± 2	21.3 ± 0.7

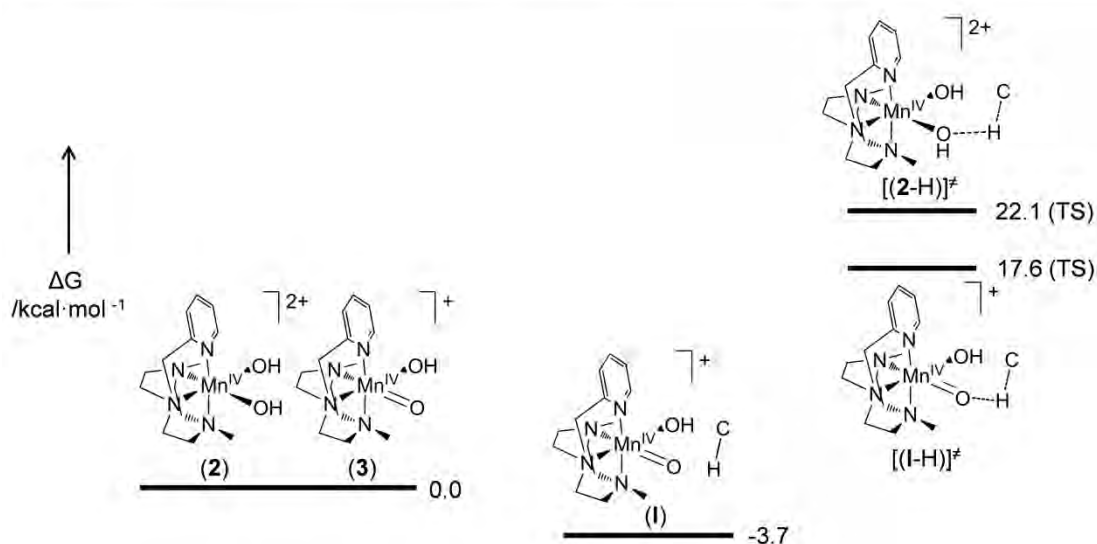


Figure 15. Thermodynamic and kinetic parameters for the C-H oxidation of DHA performed by complexes (2) and (3). In order to direct comparison, the energetic point zero is assumed arbitrarily for both complexes (2) and (3). TS are pure estimative.

Taking Marcus theory as a model framework to try to understand hydrogen transfer reactions, Mayer proposed that proton-coupled electron transfers (PCET) occurs by a formation of an initial H-donor/H-acceptor precursor previous to the hydrogen abstraction.^{22,37} Since in hydrogen atom transfer reactions (HAT) the electron and the proton are abstracted in one single step, the H-acceptor and H-donor are bound in very short distances, usually associated within hydrogen bonds. Despite this hypothesis, only two examples of metal-oxo systems show this association behavior and in both cases, the substrate contains an O-H unit that

directs the formation of hydrogen-bond interactions.^{40,41} In Chapter IV.1, the first example of a precursor species in HAT is described and it is explained on the basis of the basicity of the oxo moieties in complex **(3)** which stabilizes an encounter complex **(I)** by weak hydrogen bond-interactions. Two other main conclusions are also pointed. The first one is that complex **(3)** takes advantage of its higher basicity to carry out the HAT better than complex **(2)**. This is due to the energetic gain from the formation of the encounter complex **(I)**. Moreover, complex **(I)** has a kinetic preference over **(2)**, since a lower ΔG^\ddagger value for the rate-determining step is observed. The energetic preference of complex **(3)** for HAT due to its higher basicity it has been also observed by a pair of Mn-oxo complex described by Borovik and co-workers, where the higher basicity of the Mn(III)(O) complex provoked higher reactions rates in the oxidation of DHA.⁴² The authors proposed a change in the reaction mechanism, from hydrogen atom transfer for the Mn(IV)(O) to a separated proton and electron transfers for Mn(III)(O).

Last but not least, despite the relative reaction rates are in agreement with the BDE_{C-H} in the overall reaction between **(3)** and the different substrates, the difference in the K_{eq} makes that at low substrate concentrations where the reaction is dominated by the equilibrium step, stronger C-H bonds reacts faster than weaker ones. For instance, DHA (78 kcal/mol) reacts faster than 1,4-cyclohexadiene (77 kcal/mol) at low substrate concentrations (0 – 0.005M). These observations provide a new aspect that expands our understanding on the mechanism of C-H oxidation by high-valent metal oxo species (Figure 16).

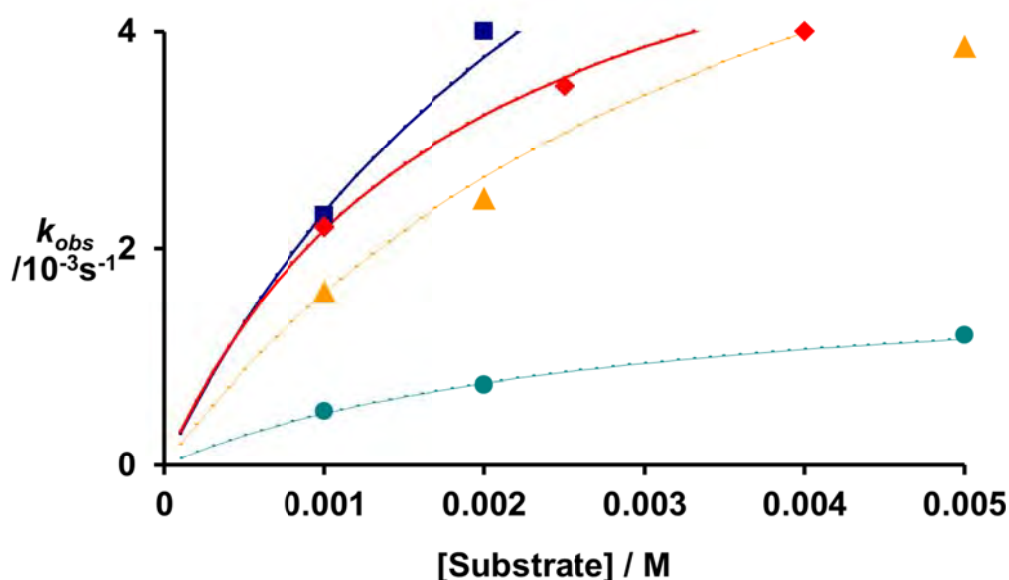


Figure 16. Plot of k_{obs} vs [substrate] for the reaction of complex **(3)** and xanthene (blue), 1,4-cyclohexadiene (yellow), 9,10-dihydroanthracene (red) and fluorene (green).

Chapter V. Alkene epoxidation catalyzed by non-porphyrinic manganese complexes.

Epoxides are valuable compounds used as intermediates to obtain value-added chemical products.⁴³ The development of a benign, broad, cheap and selective method for the epoxidation of alkenes has been extensively pursued. In this context, the combination of environmentally benign oxidants like O₂ or H₂O₂ with non-toxic first row metals such as Fe, Mn, Cu or Ni would be optimum.⁴⁴ However, the use of O₂ has been poorly achieved and the combination of H₂O₂ with Fe and Mn usually causes the formation of free-radical species and disproportionation processes. A milestone contribution was reported by Hage and co-workers by using complex [Mn₂(μ-O)₃(Me₃TACN)₂](PF₆)₂ as catalyst for the epoxidation of alkenes using H₂O₂.⁴⁵ However, the original method required high oxidant loadings (100 equiv.) because of extensive H₂O₂ decomposition. Methods to control this undesired side reaction were subsequently developed. Most significant was the discovery that acetic acid was particularly efficient in suppressing H₂O₂ destruction and therefore making the system particularly efficient.⁴⁶ Another major contribution was reported by Stack and coworkers where the use of non-porphyrinic manganese complexes with low peracetic acid loadings (1.2 equiv.) lead to the epoxidation of a wide scope of olefins.^{47,48} In Chapter V.1, we take advantage of these two precedents to design a Me₃TACN-based tetradentate ligand to synthesize a novel family of manganese complexes, which are tested as epoxidation catalysts in combination with peracetic acid. In Chapter V.2, we improve the epoxidation method described in Chapter V.1 by using H₂O₂ combined with acetic acid, which expands the substrate scope and also alters the chemoselectivity of the process. Finally, in Chapter V.3 it is described the design of chiral non-porphyrinic manganese complexes for the stereoselective epoxidation of alkenes using H₂O₂ as oxidant.

Chapter V.1. Efficient and Selective Peracetic Acid Epoxidation Catalyzed by a Robust Manganese Catalyst

Inspired by two reports where Hage's Me₃TACN and Stack's mcp systems were used as efficient epoxidation catalysts,^{45,47} the design of a novel family of N₄ manganese catalyst is reported. Complexes [Mn(CF₃SO₃)₂]^(R,R')(PyTACN)] (**1-4**) (Figure 17) are prepared by reaction of the corresponding ligand with Mn(CF₃SO₃), obtaining colorless crystalline compounds.

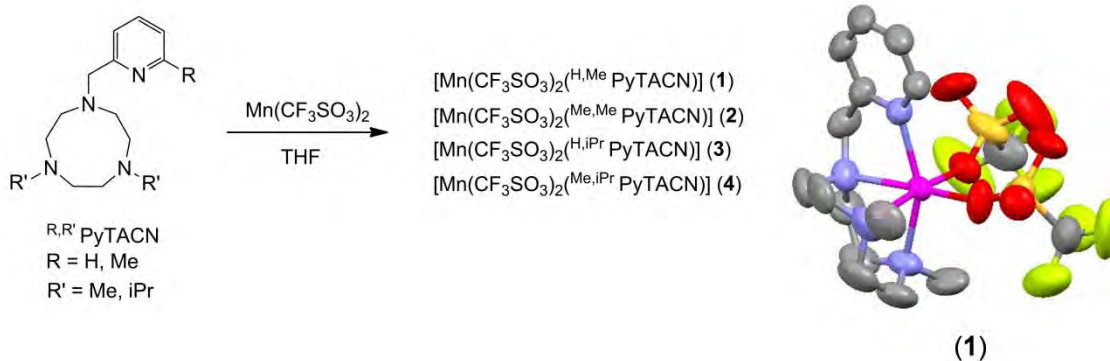


Figure 17. Manganese complexes synthesized in Chapter V.1. and X-ray structure of complex (1) (right).

In an initial trial, we test the ability of the complexes in the epoxidation of 1-octene using 1.4 equiv. of CH₃CO₃H. While complexes (3) and (4) (Figure 17) were almost inactive in the oxidation of 1-octene and complex (2) shows a moderate activity (27% epoxide yield), complex (1) reacts to an excellent yield (97%). Then, we focus our attention on complex (1) as catalyst in the epoxidation of a varied substrate scope using low catalyst loadings (0.1 – 0.15 mol%) and low oxidant loadings (1.4 equiv.) (Figure 18). Styrene and its derivatives are epoxidized with excellent yields (91-99%). Terminal aliphatic olefins like 1-octene or vinylcyclohexane are also converted with excellent yields (96 and 91%, respectively). When aliphatic *cis*-olefins are tested (cyclohexene, cyclooctene and *cis*-2-heptene) excellent yields are obtained (up to 99% in all cases). This method is also capable of epoxidizing trisubstituted olefins such as 2-methyl-2-heptene in good yields (86%), and electron-deficient substrates such as *trans*-chalcone (88%). However, the oxidation of *cis*- and *trans*-stilbene is achieved in modest yields (24 and 58%).

The chemoselectivity of the method is tested by the oxidation of substrates with two olefinic sites (Figure 19). Complex (1) allows the monoepoxidation of (*R*)-(-)-carvone (89%) and 4-vinylcyclohexene (78%). In a substrate containing a *cis*- and a *trans*-aliphatic olefin the *cis*-monoepoxide is only obtained (96% yield). The chemoselectivity of the system is further explored by competition experiments between pairs of olefins: styrene is oxidized 14 times faster than *cis*-2-heptene, and the latter is 9 times more reactive than *trans*-2-heptene. This selectivity towards *cis*-aliphatic olefins is one of the highest described to date.⁴⁹⁻⁵³ On the other hand, this *cis/trans* selectivity is radically switched when aromatic rings are involved: the epoxidation of *cis*- β -methylstyrene and *trans*- β -methylstyrene occurs at identical rates and in the competition between *cis*- and *trans*-stilbene, the *trans*- isomer reacts two times faster than the *cis*- one.

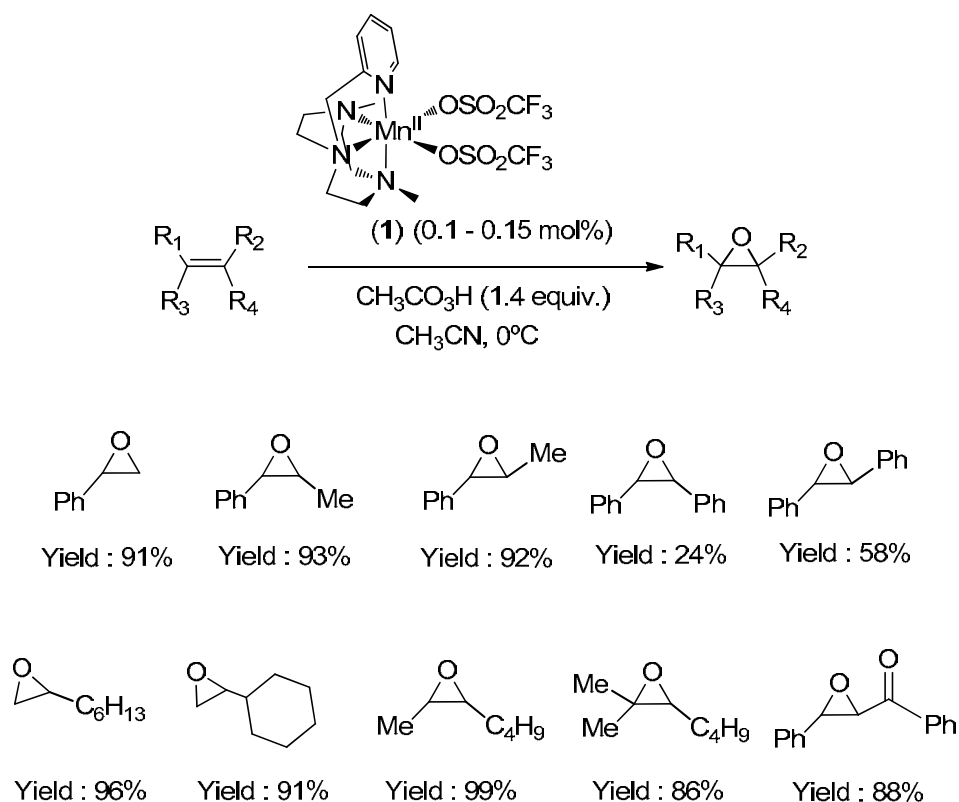


Figure 18. Selected examples of epoxidation performed by complex (1) with $\text{CH}_3\text{CO}_3\text{H}$.

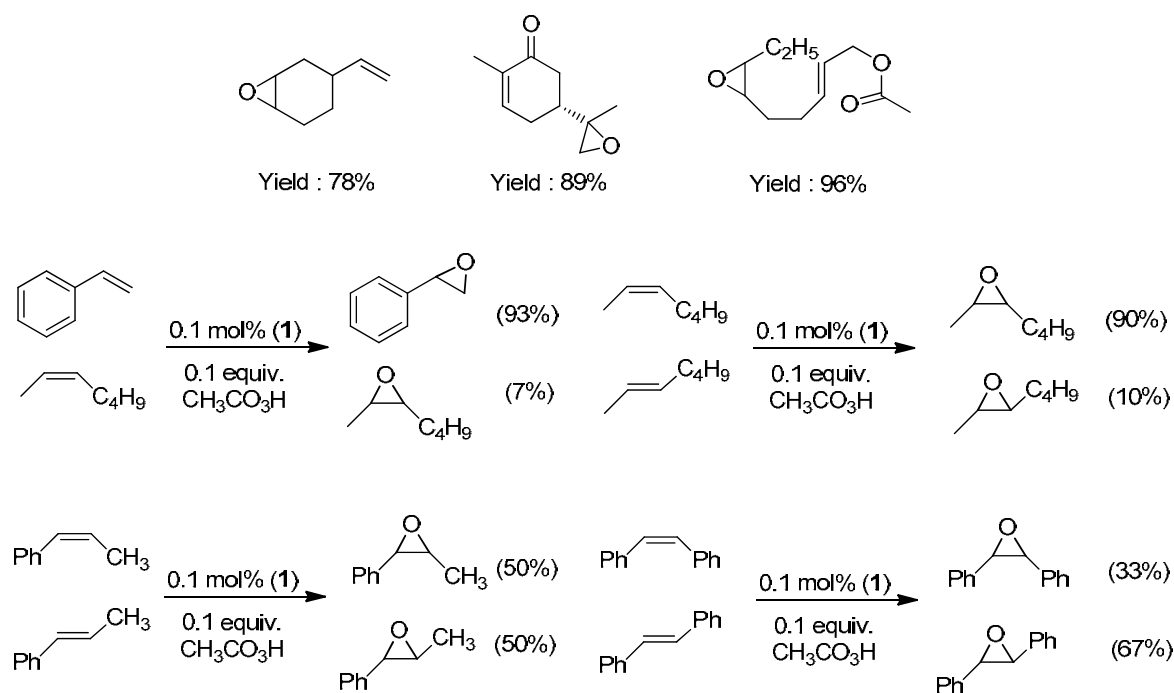


Figure 19. Top: chemoselective epoxidations performed by complex (1) with $\text{CH}_3\text{CO}_3\text{H}$. Bottom: competition experiments in the epoxidation of pairs of olefins.

Mechanistic studies aiming at understanding the species responsible for this chemistry are carried out (Figure 20). In first place, from a Hammett's plot constructed by competitive oxidation of *para*-substituted styrenes, a ρ value of -0.67 is obtained, indicative of an electrophilic type of oxidant. Secondly, the low presence of epimerized products in the oxidation of *cis*-olefins (traces in the *cis*-2-heptene and *cis*- β -methylstyrene, and 10% in *cis*-stilbene) suggest the no involvement of long-lived carbocationic species or radical intermediates commonly proposed in other epoxidations or that they are formed in minimum amounts. Finally, the epoxidation of *cis*-2-heptene in the presence of H_2^{18}O shows no incorporation of ^{18}O in the final product, indicating that the oxidant doesn't exchange with water or that this exchange is slower than the attack to the substrate. From these experimental evidences, two mechanistic scenarios are proposed: the first one is the involvement of a high-valent manganese-oxo species which transfer the oxygen directly to the substrate;⁵⁴ the second one has been also proposed for similar systems and implicates a high-valent manganese species act as a Lewis-acid in the activation of the oxidant.⁵⁵⁻⁵⁷ The absence of water exchange lead us to favor the latter mechanism, but no definitive evidences are reported.

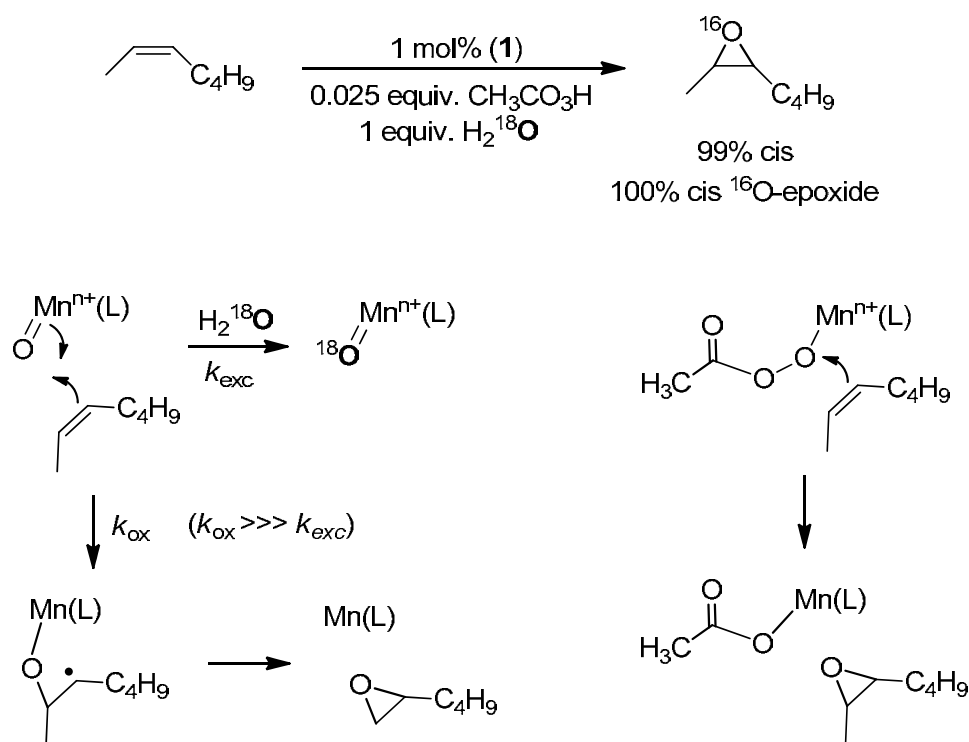


Figure 20. Mechanisms proposed for the oxidation of alkenes performed by (1) with $\text{CH}_3\text{CO}_3\text{H}$.

Chapter V.2. A Broad Substrate-Scope Method for Fast, Efficient and Selective Hydrogen Peroxide-Epoxidation

In Chapter V.2, a new method for the epoxidation of alkenes is described: like in Chapter V.1, complex $[\text{Mn}(\text{CF}_3\text{SO}_3)_2(\text{H}^i, \text{Me}^e \text{PyTACN})]$ (**1**) is used as catalyst (0.1 mol%) but this time it is combined with H_2O_2 as oxidant used in slight excess (1.1 – 1.4 equiv.). The propensity of manganese complexes to disproportionate H_2O_2 is herein avoided by using acetic acid as co-catalyst (14 equiv.). In comparison with the $\text{CH}_3\text{CO}_3\text{H}$ conditions, the $\text{H}_2\text{O}_2/\text{CH}_3\text{CO}_2\text{H}$ provides less acidic conditions with allows the preparation of acid-sensitive epoxides and it allows also to reduce the catalyst loadings to 0.02 mol%. Furthermore, reaction times are reduced (5 – 60 min).

In a first attempt, the use of complex (**1**) in the epoxidation of 1-octene with H_2O_2 causes the formation of O_2 from the H_2O_2 disproportion and low substrate conversions are obtained (<1%). Acetic acid is used to avoid the catalase activity: we optimize the conditions to use 14 equiv. of acetic acid to form the 1-octene epoxide with excellent yields (90%). The versatility of the conditions found is tested in the epoxidation of a wide array of substrates (Figure 21). Like in the peracetic acid conditions, epoxide formation is achieved with excellent yields: styrene (94% yield), *trans*- β -methylstyrene (91%), *cis*- β -methylstyrene (94%), *cis*-cyclooctene (95%), *cis*- and *trans*-2-heptene (83% and 81%), 1-octene (90%), vinylcyclohexane (84%), *trans*-chalcone (87%) and 2-methyl-2-heptene (89%). Most significantly, these $\text{H}_2\text{O}_2/\text{AcOH}$ conditions allow the epoxidation of acid-sensitive substrates such as *cis*-stilbene (88%), *trans*-stilbene (95%) and 1-phenyl-1-cyclohexene (90%). Furthermore, these mild conditions permit the epoxidation of styrene with very low catalyst loadings (0.02%, 90% yield, 4500 turnovers).

The chemoselectivity of the method is analyzed by the epoxidation of diolefinic substrates such as (*R*)-(-)-carvone (99% yield in the terminal site epoxidation), 4-vinylcyclohexene (83% yield in the internal site epoxidation) and *trans*-2-*cis*-nonadienyl ester (95% yield in the epoxidation of the *cis*- site) (Figure 22). Competition experiments between pair of olefins are carried out. Like in the $\text{CH}_3\text{CO}_3\text{H}$ conditions, a preference for the aliphatic *cis*-olefins is also observed, but with lower discrimination (5 to 1). Like in the $\text{CH}_3\text{CO}_3\text{H}$ conditions, *cis* and *trans*- β -methylstyrene are oxidized with similar rates (0.9 to 1). Interestingly, the preference for the epoxidation of *trans*-stilbene over *cis*-stilbene (6 to 1) is higher than in the peracetic acid conditions (2 to 1), which conforms one of the more selective systems found in the literature for aromatic *cis*-olefins.

To gain insight into the reaction mechanism, a Hammett's plot is constructed by competition experiments between *para*-substituted styrenes. A value of $\rho = -1.20$ is calculated from which the involvement of an electrophilic species as active oxidant is proposed. The difference with the ρ value found in the $\text{CH}_3\text{CO}_3\text{H}$ conditions ($\rho = -0.67$) suggests that important differences in the nature of the oxidizing species exists between the two processes. Like in the peracetic catalysis, no incorporation of ^{18}O into the product is observed when H_2^{18}O is present in the reaction (1.0 equiv.) (Figure 23). On the other hand, a 92% of incorporation of ^{18}O to the epoxide is observed when $\text{H}_2^{18}\text{O}_2$ is used (H_2O_2 contained 92% ^{18}O), indicating that the oxygen atom of the final product comes mostly from the oxidant. Stereoretention in the epoxidation of *cis*-olefins rules out the formation of free-diffusing radicals during the oxidation. Like in the $\text{CH}_3\text{CO}_3\text{H}$ conditions, two mechanistic scenarios can be proposed: the first one implies the formation of a high-valent manganese-oxo complex which reacts directly with alkenes and its exchange with labeled water is slower than the oxidation itself; the second one proposes the involvement of a high-valent manganese species that activates the oxidant acting as a Lewis acid.^{55,57} We favor the latter because the lack of water incorporation into products and the different selectivity observed in the $\text{CH}_3\text{CO}_3\text{H}$ and $\text{H}_2\text{O}_2/\text{AcOH}$ conditions, which implies different active species. The role of the acetic acid is not fully understood but two possible functions are proposed: it enhances the electrophilicity of the peroxo moiety, or it assists the heterolytic O-O bond cleavage to generate a high-valent manganese-oxo species, which would be the active species.⁵⁸

Importantly, these new conditions permit the epoxidation of a wider range of substrates using H_2O_2 in low loadings (1.1 – 1.4 equiv) with shorter time (5 – 60 min) and with lower catalyst loadings (0.02 – 0.1 mol%) than with peracetic acid. These methodology is applied for other manganese systems such as complex $[\text{Mn}(\text{CF}_3\text{SO}_3)_2(\text{bipy})_2]$, complex $[\text{Mn}(\text{CF}_3\text{SO}_3)_2((S,S)\text{-mcp})]$ and complex $[\text{Mn}(\text{CF}_3\text{SO}_3)_2(\text{mep})]$. Only complex $[\text{Mn}(\text{CF}_3\text{SO}_3)_2((S,S)\text{-mcp})]$ shows interesting results for specific substrates such as styrene (77%), *cis*-cyclooctene (97%) and 1-octene (89%) but it shows little activity for more challenging substrates such as *cis* and *trans*-stilbene (28% and 26%). Nevertheless, the encouraging results for complex $[\text{Mn}(\text{CF}_3\text{SO}_3)_2(\text{mcp})]$ opens up the use of more simple manganese complexes for fast, efficient and environmentally benign stereoselective epoxidation of alkenes.

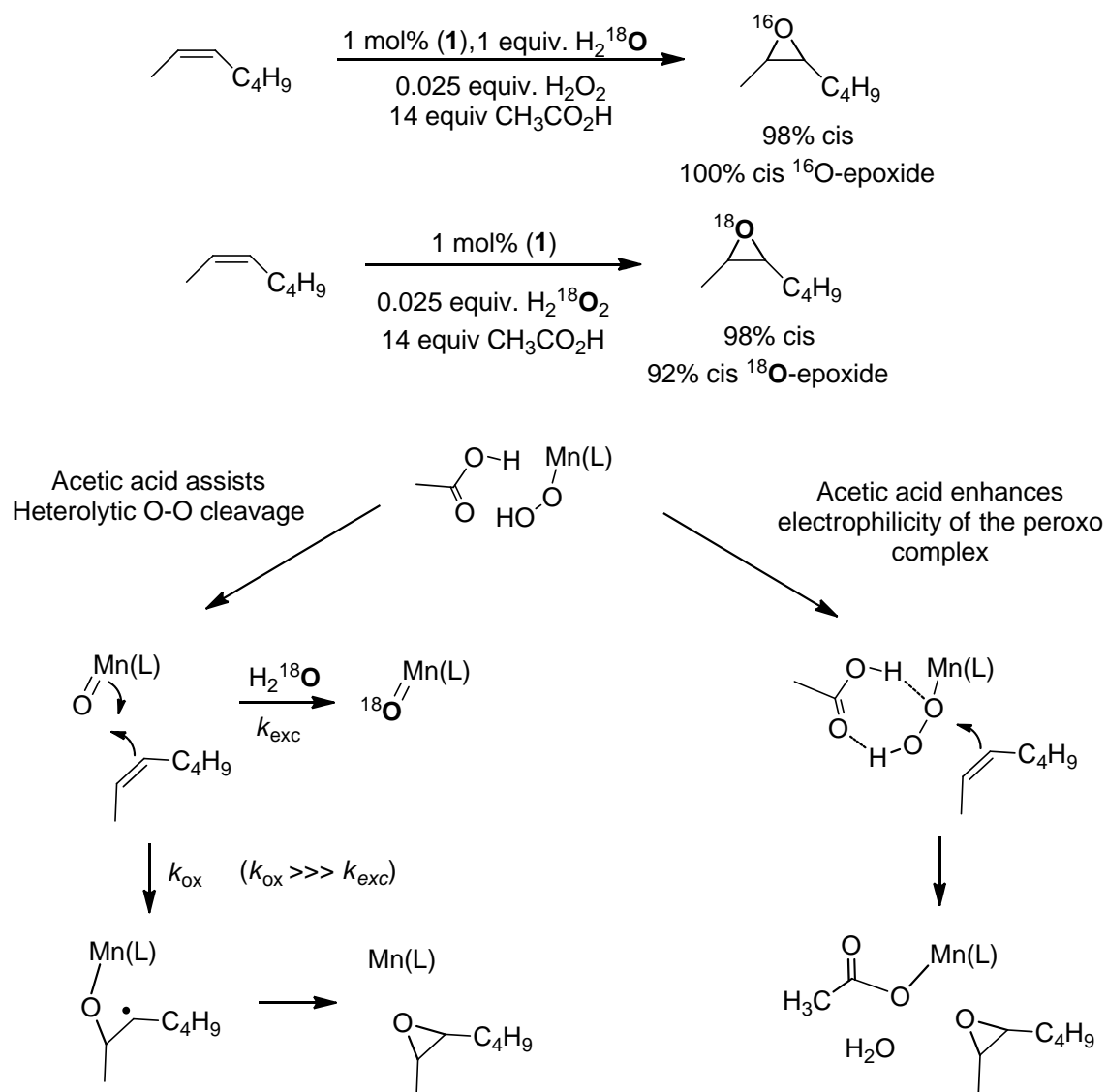


Figure 23. Top: mechanistic experiments on the epoxidation of alkenes by complex (1) with the $\text{H}_2\text{O}_2/\text{AcOH}$ conditions. Bottom: mechanistic scenarios proposed in the epoxidation of alkenes by complex (1) with the $\text{H}_2\text{O}_2/\text{AcOH}$ conditions.

Chapter V.3. Stereoselective Epoxidation of Alkenes with H₂O₂ Using a Bipyrrolidine-Based Family of Manganese Complexes.

Synthesis of enantiomerically pure epoxides is of great interest because they can be used as building blocks for a wide range of chemical transformations.^{43,59,60} Until the date, Mn-salen complexes^{61,62} and Ti-Salalen complexes⁶³ have been proved as the most efficient stereoselective epoxidation catalyst using H₂O₂ as oxidant. However, their relative limited substrate scope and high catalyst loadings used fuel the interest for novel catalytic methodologies. Following the precedent of Stack⁴⁷, our research group has developed manganese chiral complexes using mcpp ligands based in the mcp system by fusing a pinene ring in the 4,5-positions of the pyridine (Figure 24). Despite excellent yields were obtained for a wide variety of substrates, moderate ee's were achieved. Very recently, two new approaches have been reported by Xia and Sun and co-workers⁶⁴, and by Talsi and co-workers⁶⁵, where the mcp system is modified. In both cases, they took advantage of the H₂O₂/AcOH conditions reported by us in Chapter V.2.⁶⁶ to achieve excellent ee's for electron deficient substrates such as *trans*-chalcone (80-90%) but moderate yields were observed in most substrates. In Chapter V.3, we design a new catalyst based on the mcpp system where the chiral backbone is replaced by a bipyrrolidine moiety (Figure 24).

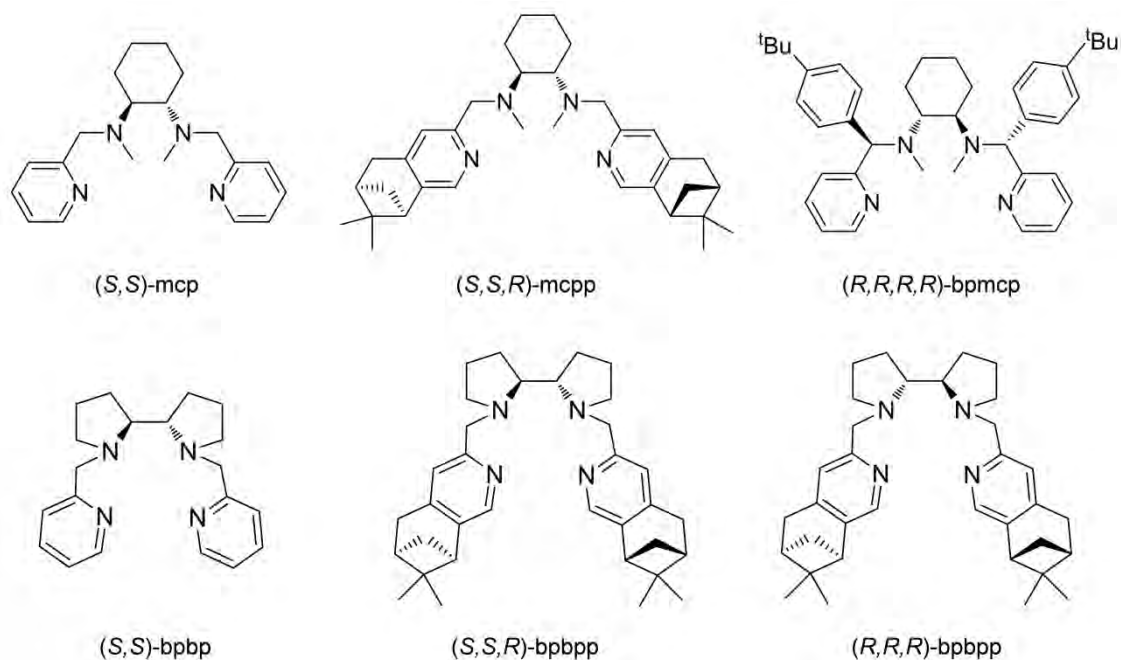


Figure 24. Chiral ligands described in Chapter V.3.

The two novel chiral ligands (*S,S,R*)-bpbpp and (*R,R,R*)-bpbpp are synthesized by the direct alkylation of the pinene-pyridine picoyl chloride with the desired 2,2'-bipyrrolidine

enantiomer. Complexes Λ -[Mn(CF₃SO₃)₂((*S,S,R*)-bpbpp)] (Λ -5) and Δ -[Mn(CF₃SO₃)₂((*S,S,R*)-bpbpp)] (Δ -6) are obtained by the direct reaction of 1 equiv. of Mn(CF₃SO₃)₂ with the corresponding ligand (Λ and Δ refer to the chiral coordination topology of the resulting complex, see Figure 25). Both complexes are analyzed by X-Ray diffraction (Figure 25) and ESI-MS, strongly suggesting their monomeric nature in solution.

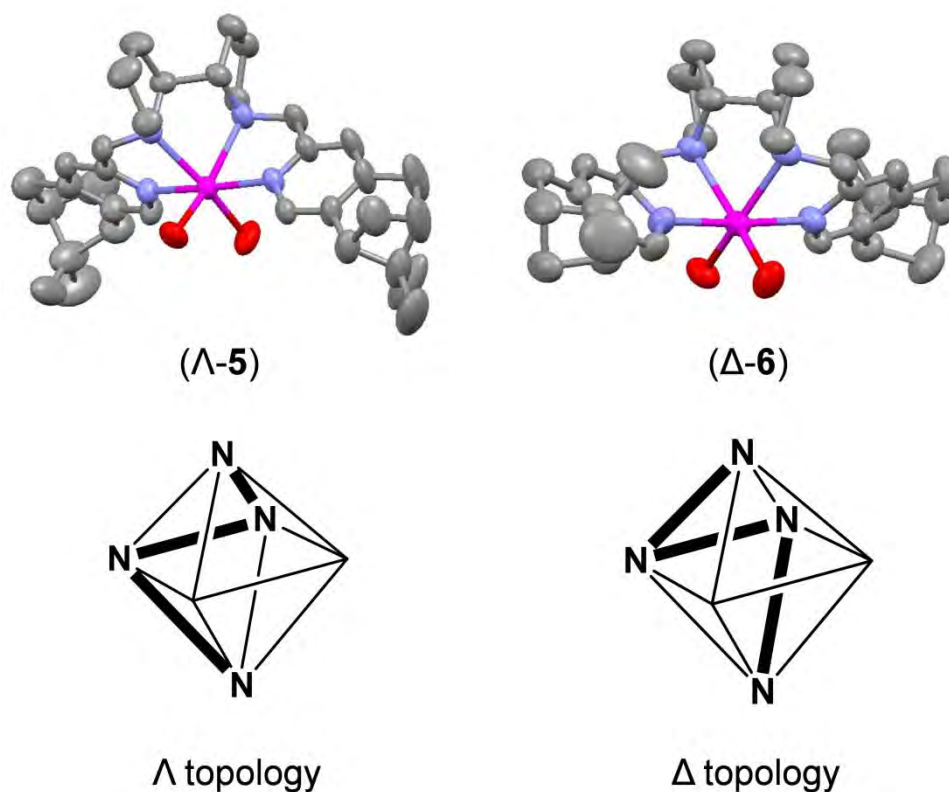


Figure 25. X-ray structures and topology of complexes (Λ -5) and (Δ -6).

In a first approach, complexes [Mn(CF₃SO₃)₂((*S,S*)-mcp)], Λ -[Mn(CF₃SO₃)₂((*S,S,R*)-mcpp)], Δ -[Mn(CF₃SO₃)₂((*R,R,R*)-mcpp)], Λ -[Mn(CF₃SO₃)₂((*S,S*)-bpbp)], Λ -[Mn(CF₃SO₃)₂((*S,S,R*)-bpbpp)] (Λ -5) and Δ -[Mn(CF₃SO₃)₂((*R,R,R*)-bpbpp)] (Δ -6) are tested in the epoxidation of styrene and *cis*- β -methylstyrene using 0.1 mol% of catalyst and H₂O₂ (1.2 equiv.) as oxidant combined with AcOH (14 equiv.). The best results are shown by complex (Δ -6), with 95% yield and 46% ee for the styrene and 87% yield and a 52% ee for *cis*- β -methylstyrene. Interestingly, the incorporation of the pinene moieties into the catalyst structure improves significantly the selectivity of the epoxidation reaction: in the epoxidation of styrene, while catalyst Λ -[Mn(CF₃SO₃)₂((*S,S*)-bpbp)] shows a 48% yield; complex (Λ -5) shows a 91% yield.

This methodology is extended to a varied array of substrates, using complexes (Λ -5) and (Δ -6) as catalyst (Figure 26). Complex (Δ -6) performs the stereoselective epoxidation of the

substrates with good to excellent product conversion (60-100%) and yields (49-100%). Furthermore, moderate enantioselectivities are observed for substrates such as styrene (46% ee), *cis*- β -methylstyrene (52% ee), 2-cyclohexen-1-one (53% ee), 6-cyano-2,2-dimethylchromene (64% ee) and *trans*-chalcone (66% ee); modest enantioselectivities for substrates such as *p*-substituted styrenes (38-43% ee's), coumarin (38%), *trans*- β -methylstyrene (23% ee) and low ee's for 1,2-dihydronaphthalene (4% ee), *trans*-stilbene (complex Δ -5, 8% ee) and 1-phenyl-1-cyclohexene (14% ee). When reactions are carried out at -40 °C, styrene is obtained in 54% ee, *cis*- β -methylstyrene in 60% ee, 2-cyclohexen-1-one in 66% ee, *trans*-chalcone in 72% ee and 6-cyano-2,2-dimethylchromene in 73% ee.

The regioselectivity of the epoxidation is also tested by using substrates with two olefin sites. 1-vinyl-1-cyclohexene is oxidized in the *cis*-internal position with a meritorious ee for an aliphatic substrate (48% ee). The selectivity for *cis*-olefins over *trans*-olefins is studied by using *trans-cis*-2,6-nonadienyl acetate, obtaining full conversion and yield for the epoxidation of the *cis*- moiety.

In conclusion, complex (Δ -6) catalyzes the stereoselective epoxidation of a wide array of substrates using only 1.2 equiv. of H₂O₂. Despite the stereoselectivities of the complexes reported by Xia and Sun⁶⁴ and by Talsi⁶⁵ for electron deficient substrates show slightly better results (ca. 80% ee), our system has been proved to act in lower catalyst loadings and good enantioselectivities can be extended to the synthesis of a wider range of substrates.

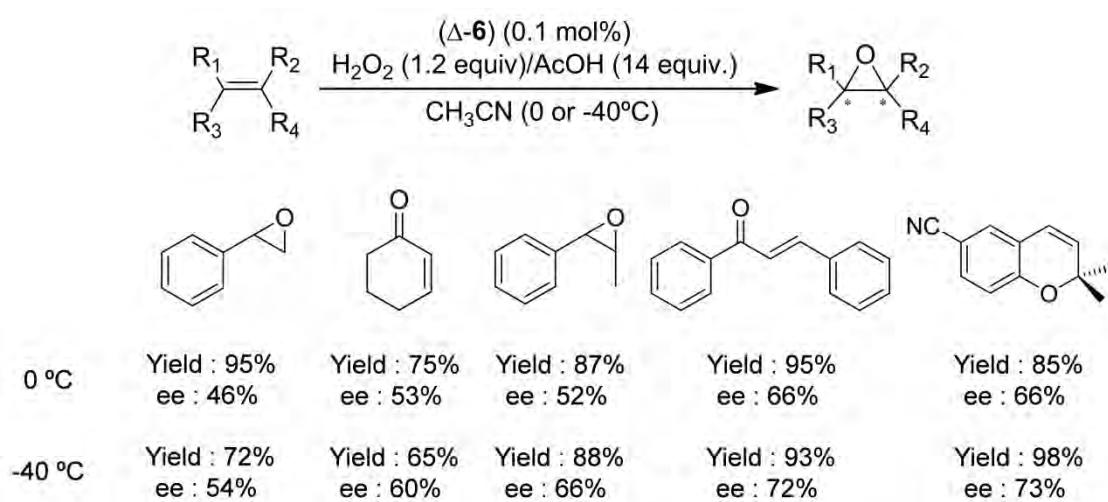


Figure 26. Stereoselective epoxidation of selected alkenes catalyzed by complex (Δ -6) using the H₂O₂/AcOH conditions.

REFERENCES

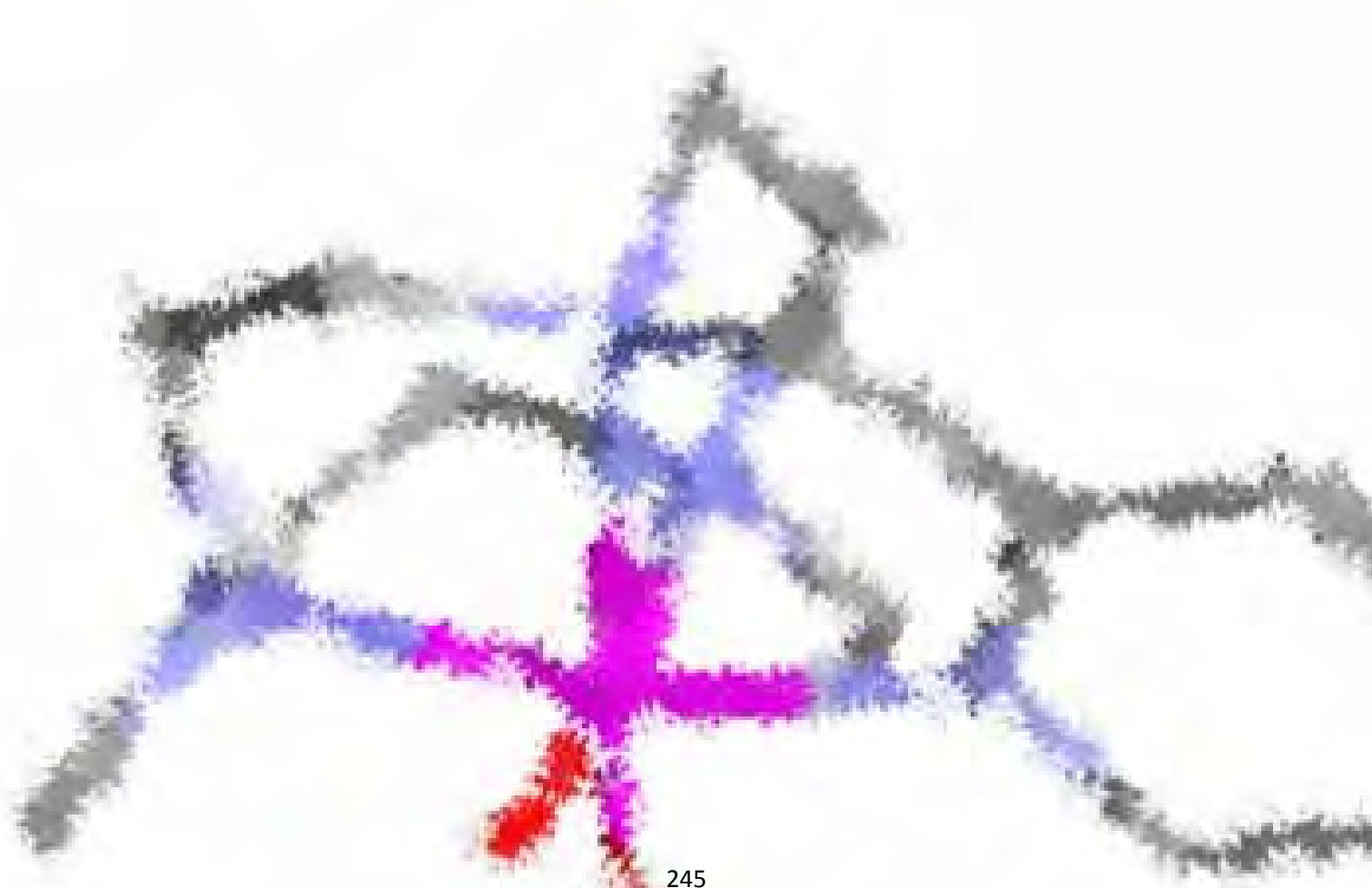
- (1) Bertini, I.; Gray, H. B.; Lippard, S. J.; Valentine, J. S. *Bioinorganic Chemistry*; University Science Books, 1994.
- (2) Holm, R. H.; Kennepohl, P.; Solomon, E. I. *Chem. Rev.* **1996**, *96*, 2239-2314.
- (3) Bertini, I.; Gray, H. B.; Stiefel, E. I.; Valentine, J. S. *Biological Inorganic Chemistry. Structure & Reactivity*; University Science Books, 2007.
- (4) Mirica, L. M.; Ottenwaelder, X.; Stack, T. D. P. *Chem. Rev.* **2004**, *114*, 1013-1046.
- (5) Lewis, E. A.; Tolman, W. B. *Chem. Rev.* **2004**, *114*, 1047-1076.
- (6) Cuff, M. E.; Miller, K. I.; Holde, K. E. v.; Hendrickson, W. A. *J. Mol. Biol.* **1998**, *278*, 855-870.
- (7) Matoba, Y.; Kumagai, T.; Yamamoto, A.; Yoshitsu, H.; Sugiyama, M. *J. Biol. Chem.* **2006**, *281*, 8981-8990.
- (8) Company, A.; Palavicini, S.; Garcia-Bosch, I.; Mas-Ballesté, R.; Que, L., Jr.; Rybak-Akimova, E. V.; Casella, L.; Ribas, X.; Costas, M. *Chem. Eur. J.* **2008**, *14*, 3535-3538.
- (9) Itoh, S.; Kumei, H.; Taki, M.; Nagatomo, S.; Kitagawa, T.; Fukuzumi, S. *J. Am. Chem. Soc.* **2001**, *123*, 6708-6709.
- (10) Palavicini, S.; Granata, A.; Monzani, E.; Casella, L. *J. Am. Chem. Soc.* **2005**, *127*, 18031-18036.
- (11) Mirica, L. M.; Vance, M.; Rudd, D. J.; Hedman, B.; Hodgson, K. O.; Solomon, E. I.; Stack, T. D. P. *Science* **2005**, *308*, 1890-1892.
- (12) Tachi, Y.; Aita, K.; Teramae, S.; Tani, F.; Naruta, Y.; Fukuzumi, S.; Itoh, S. *Inorg. Chem.* **2004**, *43*, 4558-4560.
- (13) Tyeklár, Z.; Jacobson, R. R.; Wei, N.; Murthy, N. N.; Zubieta, J.; Karlin, K. D. *J. Am. Chem. Soc.* **1993**, *115*, 2677-2689.
- (14) Rolffe, M.; Schottenheim, J.; Decker, H.; Tuczek, F. *Chem. Soc. Rev.* **2011**, *40*, 4077-4098.
- (15) Decker, H.; Dillinger, R.; Tuczek, F. *Angew. Chem. Int. Ed.* **2000**, *39*, 1591-1595.
- (16) Decker, H.; Schweikardt, T.; Tuczek, F. *Angew. Chem. Int. Ed.* **2006**, *45*, 4546-4550.
- (17) Granata, A.; Monzani, E.; Bubacco, L.; Casella, L. *Chem. Eur. J.* **2006**, *12*, 2504-2514.
- (18) Osako, T.; Ohkubo, K.; Taki, M.; Tachi, Y.; Fukuzumi, S.; Itoh, S. *J. Am. Chem. Soc.* **2003**, *125*, 11027-11033.
- (19) Marcus, R. A.; Sutin, N. *Biochim. Biophys. Acta* **1985**, *811*, 265-322.
- (20) Mayer, J. M.; Hrovat, D. A.; Thomas, J. L.; Borden, W. T. *J. Am. Chem. Soc.* **2002**, *124*, 11142-11147.
- (21) Warren, J. J.; Tronic, T. A.; Mayer, J. M. *Chem. Rev.* **2010**, *110*, 6961-7001.
- (22) Mayer, J. M. *Acc. Chem. Res.* **2011**, *44*, 36-46.

- (23) Shaik, S.; Kumar, D.; de Visser, S. P.; Altun, A.; Thiel, W. *Chem. Rev.* **2005**, *105*, 2279-2328.
- (24) Atkison, J. K.; Hollenberg, P. F.; Ingold, K. U.; Johnson, C. C.; LeTadic, M.-H.; Newcomb, M.; Putt, D. A. *Biochemistry* **1994**, *33*, 10630-10637.
- (25) Costas, M.; Mehn, M. P.; Jensen, M. P.; Que, L., Jr. *Chem. Rev.* **2004**, *104*, 939-986.
- (26) Nam, W.; Lim, M. H.; Moon, S. K.; Kim, C. *J. Am. Chem. Soc.* **2000**, *122*, 10805-10809.
- (27) Kaizer, J.; Klinker, E. J.; Oh, N. Y.; Rohde, J.-U.; Song, W. J.; Stubna, A.; Kim, J.; Munck, E.; Nam, W.; Que, L., Jr. *J. Am. Chem. Soc.* **2004**, *126*, 472-473.
- (28) Company, A.; Gómez, L.; Güell, M.; Ribas, X.; Luis, J. M.; Que, L., Jr; Costas, M. *J. Am. Chem. Soc.* **2007**, *129*, 15766-15767.
- (29) Costas, M.; Chen, K.; Que, L., Jr. *Coord. Chem. Rev.* **2000**, *200-202*, 517-544.
- (30) Sundaramoorthy, M.; Kishi, K.; Gold, M. H.; Poulos, T. L. *J. Biol. Chem.* **1994**, *269*, 32759-32767.
- (31) Su, C.; Sahlin, M.; Oliw, E. H. *J. Biol. Chem.* **2000**, *275*, 18830-18835.
- (32) Emerson, J. P.; Kovaleva, E. G.; Farquhar, E. R.; Lipscomb, J. D.; Que, L., Jr. *Proc. Natl. Acad. Sci. USA* **2008**, *105*, 7347-7352.
- (33) Meunier, B.; de Visser, S. P.; Shaik, S. *Chem. Rev.* **2004**, *104*, 3947-3980.
- (34) Gupta, R.; Borovik, A. S. *J. Am. Chem. Soc.* **2003**, *125*, 13234-13242.
- (35) Yin, G.; McCormick, J. M.; Buchalova, M.; Danby, A. M.; Rodgers, K.; Day, V. W.; Smith, K.; Perkins, C. M.; Kitko, D.; Carter, J. D.; Scheper, W. M.; Busch, D. H. *Inorg. Chem.* **2006**, *45*, 8052-8061.
- (36) Mayer, J. M. *Acc. Chem. Res.* **1998**, *31*, 441-450.
- (37) Roth, J. P.; Yoder, J. C.; Won, T.-J.; Mayer, J. M. *Science* **2001**, *294*, 2524-2526.
- (38) Bordwell, F. G.; Cheng, J. P.; Harrelson, J. A. *J. Am. Chem. Soc.* **1988**, *110*, 1229-1231.
- (39) Luo, Y.-R. *Comprehensive Handbook of Chemical Bond Energies*; CRC Press, 2007.
- (40) Kojima, T.; Hirai, Y.; Ishizuka, T.; Shiota, Y.; Yoshizawa, K.; Ikemura, K.; Ogura, T.; Fukuzumi, S. *Angew. Chem. Int. Ed.* **2010**, *49*, 8449-8453.
- (41) Mader, E. A.; Mayer, J. M. *Inorg. Chem.* **2010**, *49*, 3685-3687.
- (42) Parsell, T. H.; Yang, M.-Y.; Borovik, A. S. *J. Am. Chem. Soc.* **2009**, *131*, 2762-2763.
- (43) Sundermeier, U.; Döbler, C.; Beller, M. In *Modern Oxidation Methods*; Bäckvall, J.-E., Ed.; Wiley-VCH: Weinheim, 2004.
- (44) Lane, B. S.; Burgess, K. *Chem. Rev.* **2003**, *103*, 2457-2474.
- (45) Hage, R.; Iburg, J. E.; Kerschner, J.; Koek, J. H.; Lempers, E. L. M.; Martens, R. J.; Racherla, U. S.; Russell, S. W.; Swarthoff, T.; Vliet, M. R. P. v.; Warnaar, J. B.; Wolf, L. v. d.; Krijnen, B. *Nature* **1994**, *369*, 637-639

- (46) Shul'pin, G. B.; Siiss-Fink, G.; Smith, J. R. L. *Tetrahedron* **1999**, *55*, 5345-5358.
- (47) Murphy, A.; Dubois, G.; Stack, T. D. P. *J. Am. Chem. Soc.* **2003**, *125*, 5250-5251.
- (48) Murphy, A.; Pace, A.; Stack, T. D. P. *Org. Lett.* **2004**, *6*, 3119-3122.
- (49) Sato, K.; Aoki, M.; Ogawa, M.; Hashimoto, T.; Panyella, D.; Noyori, R. *Bull. Chem. Soc. Jpn.* **1997**, *70*.
- (50) Baumstark, A. L.; Vasquez, P. C. *J. Org. Chem.* **1988**, *53*, 3437-3439
- (51) Groves, J. T.; Nemo, T. E. *J. Am. Chem. Soc.* **1983**, *115*, 5786 - 5791.
- (52) Meunier, B.; Guilmet, E.; Carvalho, M.-E. D.; Poilblanc, R. *J. Am. Chem. Soc.* **1984**, *106*, 6668-6676.
- (53) Kamata, K.; Yonehara, K.; Sumida, Y.; Yamaguchi, K.; Hikichi, S.; Mizuno, N. *Science* **2003**, *300*, 964-966.
- (54) McGarrigle, E. M.; Gilheany, D. G. *Chem. Rev.* **2005**, *105*, 1563-1602.
- (55) Yin, G.; Buchalova, M.; Danby, A. M.; Perkins, C. M.; Kitko, D.; Carter, J. D.; Scheper, W. M.; Busch, D. H. *J. Am. Chem. Soc.* **2005**, *127*, 17170-17171.
- (56) Wang, S. H.; Mandimutsira, B. S.; Todd, R.; Ramdhanie, B.; Fox, J. P.; Goldberg, D. P. *J. Am. Chem. Soc.* **2004**, *126*, 18-19.
- (57) Ottenbacher, R. V.; Bryliakov, K. P.; Talsi, E. P. *Inorg. Chem.* **2010**, *49*, 8620-8628.
- (58) Mas-Ballesté, R.; Que, L. J. *J. Am. Chem. Soc.* **2007**, *129*, 15964-15972.
- (59) Lei, X.; John A. Porco, J. *J. Am. Chem. Soc.* **2006**, *128*, 14790-14791.
- (60) Faveri, G. D.; Ilyashenko, G.; Watkinson, M. *Chem. Soc. Rev.* **2011**, *40*, 1722-1760.
- (61) Zhang, W.; Loebach, J. L.; Wilson, S. R.; Jacobsen, E. N. *J. Am. Chem. Soc.* **1990**, *112*, 2801-2803.
- (62) Katsuki, T. *Coord. Chem. Rev.* **1995**, *140*, 189-214.
- (63) Sawada, Y.; Matsumoto, K.; Kondo, S.; Watanabe, H.; Ozawa, T.; Suzuki, K.; Saito, B.; Katsuki, T. *Angew. Chem. Int. Ed.* **2006**, *45*, 3478-3480.
- (64) Wu, M.; Wang, B.; Wang, S.; Xia, C.; Sun, W. *Org. Lett.* **2009**, *11*, 3622-3625.
- (65) Ottenbacher, R. V.; Bryliakov, K. P.; Talsi, E. P. *Adv. Synth. Catal.* **2011**, *353*, 885-889.
- (66) Garcia-Bosch, I.; Ribas, X.; Costas, M. *Adv. Synth. Catal.* **2009**, *351*, 348-352.

Chapter VII

Conclusions



VII. Conclusions

- In Chapter III, a novel dinuclear Cu(I) unsymmetric complex and its analogous symmetric complex have been designed as model for O₂-activation proteins.
- In Chapter III.1, the reaction of both Cu(I)₂ complexes with O₂ led to the formation of Cu₂:O₂ species which have been spectroscopically characterized using UV-Vis and rRaman, both being formulated as *trans*-peroxo copper(II) centers. No oxidation of oxophilic substrates such as PPh₃ and PhSMe was accomplished, but both Cu₂:O₂ complexes reacted with H⁺ and CO₂. These observations suggest that both complexes have a nucleophilic character. Surprisingly, when their reaction with sodium phenolates was tested two different behaviors were observed: while the symmetric complex was unable to oxidize the substrate, the unsymmetric complex performed the *ortho*-hydroxylation of the phenolate. This is the first example of a *trans*-peroxo copper(II) species capable of performing this type of oxidation. Mechanistic studies and DFT calculations were carried out suggesting an electrophilic attack of the Cu₂-peroxo moiety to the arene ring. This reaction has biological implication because the unsymmetric complex is mimicking the oxidation of phenols found in tyrosinase. Like in the living system, the coordination of the phenolate to one of the copper centers activates the Cu₂:O₂ core to perform the electrophilic oxidation of the substrate.
- In Chapter III.2, the reactions of the dinuclear Cu₂:O₂ complexes with phenolates and phenols have been studied in detail. The *ortho*-hydroxylation of phenolates performed by the unsymmetric *trans*-peroxo-Cu^{II}₂ complex occurs via reversible coordination of the substrate previous to the electrophilic attack of the peroxide to the arene. On the other hand, the oxidation of phenols performed by the unsymmetric complex occurs via formation of phenoxy radical formation. Mechanistic studies show that the reaction proceeds via a reversible coordination of the phenol to the N₃Cu(II) center previous to a one electron oxidation by a proton-coupled electron transfer (PCET). In both cases, the ability of the asymmetric complex to coordinate the substrate to one of the metal sites triggers the electrophilic reactivity of the Cu₂:O₂ center. Thermodynamic and activation parameters of both oxidation reactions (*ortho*-hydroxylation of phenolates and 1H⁺/1e⁻ oxidation of phenols) indicate that the presence or absence of the H⁺ in the substrate (phenol/phenolate) determines the oxidation reaction pathway.

- In Chapter IV, the synthesis and characterization of two novel non-porphyrinic manganese(IV) complexes has been accomplished. In the reaction of the manganese(IV) bis(hydroxide) complex with C-H bonds, a one-step hydrogen atom transfer has been proposed as mechanism of oxidation. On the other hand, the manganese(IV) oxo complex has shown a different behavior in C-H oxidations. A two-step mechanism has been proposed: in a first step, an association between complex and substrate is explained due to weak hydrogen interactions between the C-H and the manganese-oxo moiety. Then, this association precursor has been proposed to evolve via hydrogen atom transfer. This is the first example of a metal-oxo complex acting via an association intermediate in C-H oxidation reactions. Mechanistic studies also have revealed that the precursor complex not only affects the overall C-H oxidation rate but also alters the relative C-H reactivity of the different substrates in the hydrogen atom transfer.
- In Chapter V, manganese(II) complexes have been developed as catalysts for efficient, environmentally benign and selective epoxidation of a broad range of alkenes.
- In Chapter V.1, a novel family of manganese(II) complexes based on the PyTACN have been synthesized and fully characterized. From preliminary catalytic studies, complex $[\text{Mn}(\text{CF}_3\text{SO}_3)_2(\text{H,MePyTACN})]$ has emerged as a very robust catalyst for the epoxidation of 1-octene using $\text{CH}_3\text{CO}_3\text{H}$ as oxidant. The use of this catalyst in low catalyst (0.1 mol%) and oxidant loadings (1.4 equiv.) has been expanded to a wide range of catalytic epoxidations where high selectivity and efficiency has been observed. The system has shown excellent selectivity for the epoxidation of aliphatic *cis*-olefins, which shifted to a *trans*-selectivity for aromatic olefins. Despite the involvement of a high-valent manganese-oxo species have not been ruled out, mechanistic studies suggest that the epoxidation occurs via Lewis-acid activation of the peracetic acid in a concerted mechanism.
- In Chapter V.2, complex $[\text{Mn}(\text{CF}_3\text{SO}_3)_2(\text{H,MePyTACN})]$ has been used in the catalytic epoxidation of alkenes using hydrogen peroxide as oxidant combined with acetic acid as co-catalyst. These soft conditions compared with the peracetic system (lower pH) have allowed the epoxidation of a wider range of substrates, and in selected examples they have also allowed the reduction of catalyst loadings (0.02 mol%). The chemoselectivity of the system has also been evaluated showing a lower affinity towards aliphatic *cis*-olefins than the peracetic acid system. However, the selectivity for aromatic *trans*-olefins has been increased: the system affords the highest selectivity for *trans*-aromatic olefins

reported to date. Mechanistic studies have suggested that the epoxidation of alkenes proceeds via Lewis-acid activation of the hydrogen peroxide in a concerted step where acetic acid could enhance the electrophilicity of the active species. However, the participation of a high-valent manganese(oxo) species cannot be ruled out.

- In Chapter V.3, we have developed a novel family of chiral mononuclear manganese complexes for the stereoselective epoxidation of alkenes. The catalyst $[\text{Mn}(\text{CF}_3\text{SO}_3)_2((R,R,R)\text{-mcpp})]$ has emerged as a very selective and efficient catalyst in the epoxidation of a wide range of olefins using environmentally benign conditions. The system has been capable to stereoselectively epoxidize substrates such as styrene (54% ee), *cis*- β -methylstyrene (66% ee), 2-cyclohexenone (60% ee), *trans*-chalcone (72% ee) and DBPCN (73% ee) with excellent yields (60 – 100%). This is a remarkable system for the enantioselective epoxidation of substrate because of low catalyst loadings used (0.1 mol%), the use of cheap and environmentally benign oxidant (H_2O_2 , 1.1 - 1.4 equiv.) and the possibility to expand the range of epoxides obtained in excellent yields (60-100%) and notable enantioselectivities (up to 76% ee's).

